INDIAN INSTITUTE OF TECHNOLOGY ROORKEE
ROORKEE

CANDIDATE'S DECLARATION

I hereby declare that the work which is being presented in this thesis entitled "**FINITE ELEMENT ANALYSIS OF AIRCRAFT CRASH ON NUCLEAR CONTAINMENT STRUCTURE**", in partial fulfilment of the requirements for the award of the Degree of Doctor of Philosophy and submitted in the Department of Civil Engineering of Indian Institute of Technology Roorkee, Roorkee, is an authentic record of my own work carried out at Department of Civil Engineering during the period from July, 2010 to March, 2014, under the supervision of **Dr. M. A. Iqbal**, Assistant Professor and **Dr. P. Bhargava**, Professor, Department of Civil Engineering, Indian Institute of Technology Roorkee, Roorkee, India.

The matter presented in this thesis has not been submitted by me for the award of any other degree of this or any other Institute/University.

(**MD. REHAN SADIQUE**)

This is to certify that the above statement made by the candidate is correct to the best of our knowledge.

(P. BHARGAVA)
Supervisor

(M. A. IQBAL)
Supervisor

Date: /03/2014

The Ph.D. Viva-Voce Examination of **Md. Rehan Sadique**, Research Scholar, has been held on _____

Signature of Supervisor(s) Chairman, SRC External Examiner

Head of the Department/Chairman, ODC

ABSTRACT

In view of the previous missile and aircraft attacks on important structures and the associated very high risk of failure the present study has been designed to evaluate response of nuclear containment structure against aircraft crash. The numerical simulations have been carried out using the implicit and explicit integration schemes of ABAQUS finite element code. The Concrete Damaged Plasticity model has been employed to predict the behavior of concrete. The model is based upon the concept of isotropic damaged elasticity in conjunction with isotropic tensile and compressive plasticity to represent the post elastic behaviour of concrete. The material behavior of the steel reinforcement as well as the aircraft was incorporated using the Johnson-Cook elasto-viscoplastic material model that is capable to predict the flow and fracture behavior of the ductile materials.

The outer containment of the BWR Mark III nuclear power plant has been impacted by commercial and fighter planes in order to identify the most vulnerable location and the most damaging aircraft. The preliminary studies led to the conclusion that the reaction-time curve of aircraft can be efficiently employed to accurately predict the response of the containment. However, the present approach for estimating the reaction-time response of aircraft against flat and rigid target is unrealistic and hence requires careful investigation. Thus the geometric models of Boeing 707-320 and Boeing 747-400 aircrafts have been developed and the corresponding reaction-time curves were obtained assuming deformable and non-deformable targets of varying curvature. The curvature and deformability of the target has been found to have significant influence on the reaction-time response of the aircraft. A decrement in the peak reaction force has been noticed with increase in target curvature. Further, the arrival of the peak has also been found to have delayed with an increase in the curvature radius. The magnitude of the reaction offered by the deformable target was lower than that of the rigid target of equivalent curvature radius. The reaction-time curves thus obtained have been compared with those obtained through the available analytical expressions.

The area of containment in contact with that of the aircraft has also been found to vary with respect to time and the striking velocity. The effect of contact area on the response of containment has been studied employing two different approaches for the application of reaction-time curve. In the first approach an average of the total contact area of aircraft was considered

for the application of curve. In the second approach the contact area was trifurcated representing fuselage, first set of engines and second set of engines and the reaction was assigned with respect to location and the time of the respective component. The response of containment obtained through the average and trifurcated surface areas was then compared with that obtained against geometric models of aircraft. It has been observed that the average area approach for the application of loading overestimated the local deformation while underestimated the global deformation of the containment. However, the magnitude of deformations predicted by the area trifurcation approach and the geometric model of the aircraft are comparatively low and in close agreement. The trifurcation approach is therefore more accurate and hence represents a more realistic estimate of the contact area of the aircraft.

The reaction-time curves and the corresponding contact area thus obtained have been idealized and employed to seek the response of the containment. The geometric models of the aircrafts, developed numerically, have also been employed to hit the containment structure at the most vulnerable location. The response of the containment has been obtained in terms of local and global deformation, stresses induced in the concrete and reinforcement and the corresponding material degradation. The results thus obtained corresponding to the geometric model and the reaction-time curve have been compared and discussed.

The effect of fire induced due to aircraft crash has also been studied against Boeing 707-320 and Boeing 747-400 aircrafts. The reaction-time response curve obtained against curved flexible target was applied on the surface of containment based on the average area approach. The impact of aircraft was considered to occur up to the point the engines came in contact. Thereafter the fire was assumed to have spread since the majority of the aircraft fuel is stored in and around the wings. The fire effect was considered to be most severe at the bottom of containment up to 10 m height from the base. This is due to the fact that most of the fuel will immediately flow down to the bottom of containment. In the impact region, moderate fire effect has been considered since some of the fuel will also burn in this region immediately after the breach of the fuel tank. The heat transfer analysis has been carried out to obtain the nodal temperature in the concrete as well as reinforcement elements. The fire duration has been considered to be 2hrs for Boeing 707-320 and 3hrs for Boeing 747-400. Thereafter, thermal stress analysis has been performed considering the deformed geometry of the containment due to aircraft impact as the initial state. The stresses due the induced fire have been found to cause the

local scabbing of concrete leading to exposure of reinforcement. However, the induced fire has not been found to affect the global behavior of the containment structure.

ACKNOWLEDGEMENT

In the name of ALLAH the most beneficent and merciful. At the outset I am grateful to the Almighty **ALLAH** for giving me strength to carry out this work. As I approach the end of my Ph.D., I am left with profound feelings of accomplishment, excitement, and gratitude to a number of people whose support has been significant in completing this thesis.

My supervisors **Dr. Mohd. Ashraf Iqbal** and **Dr. Predeep Bhargava** have been a constant source of inspiration, motivation and guidance throughout the past three and half years. I have learned so much from their keen insight, their research and problem solving abilities and their amazing energy. What I learned from them is not only the knowledge, but also the way to be a positive and energetic person. I am most grateful to my supervisors for their valuable advices, interests and encouragements throughout the period of this research work, right from the inception of the problem to the final preparation of the manuscript.

My sincere thanks go to **Dr. A. K. Jain** and **Dr. D. Kashyap**, the Heads of the Civil Engineering Department, for extending the computational and other facilities of the department.

I would like to take this opportunity to thank the members of the Doctoral Scrutiny Committee viz**. Dr. R. R. Bhargava**, Department of Mathematics, **Dr. V. Prakash**, **Dr. N.K. Samadhiya** and **Dr. A. Upadhyay** of the Department of Civil Engineering for their valuable suggestions. I sincerely acknowledge other faculty members of the department especially **Dr. N. M. Bhandari, Dr. M. N. Viladkar** and **Dr. Sanjay Chikermane** for their technical suggestions as well as friendly interactions.

Special thanks are due for my co-scholars in the Civil Engineering Department **Ajmal Hussain, Gaurav Tiwari, Praveen Kamat, Ravi Khandelwal** and Junior M. Tech students

Maj. S. Rai, Hitesh Lakhani, Imran Ahmad, Shiva Thouta, and **Ankit Aggarwal** for extending all sorts of helps without any hesitation and making my stay a very pleasant and memorable one during my tenure at IIT, Roorkee. I would like to mention an individual thanks to **Alim Rawsan** for his rigorous help in making the final format of this thesis.

I would like to thank all my well-wishers from my preceding institute, **Aligarh Muslim University,** especially **Dr. Javed Arif, Dr. Masroor Alam, Dr. Sarfraz Ansari** and **Dr. Sabeeh Akhtar** for their initial motivations towards research.

My sincerest gratitude goes to my beloved parents and in-laws for their encouragements shown during this period. I am indebted particularly to my parents, **Dr. Md. Sharfuddin** and **Dr. Raziya Ajazi** who relieved me of all family responsibilities throughout the research period. I would like to express my regards to my sisters and brother-in-laws. Their benediction, motivation and inspiration have always provided me a formidable mental support.

I would like to express my warmest thanks to my wife **Zeenat**, my little doll **Hamna**, and the cutie pie **Abdullah** who were standing by me and endured all the sufferings silently and looked forward to this day.

Finally I am thankful to the authorities of **Indian Institute of Technology Roorkee**, Roorkee for providing me all necessary assistance in the form of research and guidance.

(MD REHAN SADIQUE)

CONTENTS PAGE NO.

List of Figures

List of Tables

Chapter-1

INTRODUCTION

1.1 GENERAL

The population growth and industrial development stipulated a significant increase in the global energy consumption in last few decades. In spite of the controversial nature, the nuclear power is considered to be an efficient, reliable and cheapest source of energy (NEI, 2014) satisfying more than 20% global electricity demand. As an advantageous physical characteristic, nuclear fuel has extremely high energy density compared to fossil fuels (IAEA, 1997). The share of nuclear energy has increased rapidly throughout the globe. Particularly, the developing Asian countries emerged as the most vibrant consumers (WNA, 2013). However, the endorsement of safety standard for the production of nuclear energy remains an important concern. There is no scope for any discrepancy, noncompliance or negligence. Mitigating the environment exposure of the nuclear radiation remains the highest challenge for the proliferation of nuclear energy. The nuclear containment structure provides biological and nuclear shielding to barricade the radiation dose to the atmosphere. It also protects the reactor from an external threat and extends perfect enclosure for the controlled chain reaction process. The breach of nuclear containment would result an uncontrolled radiological release in the environment causing short as well as long term disastrous aftereffects for the living beings and extensive radiological contamination over a vast area. Keeping in view the associated vulnerability, the nuclear containment structures are generally designed in two layers. The inner containment is made up of either high strength reinforced concrete or steel to prevent the leakage of radiation in case of any internal failure. The outer containment is a thick reinforced concrete structure to protect the inner containment from any external threat. In addition, it provides a final protective layer to prevent the environment exposure of the nuclear radiation. Earlier, there was a practice to design the nuclear power plants to withstand the event of severe internal or external accident, such as large fires, earthquakes, hurricanes that might be expected during the plant lifetime.

The consequence of failure of a containment building and the leakage of nuclear radiation are going to be far reaching and hazardous and may be so enormous that the energy production may even have to be abandoned. Majority of nuclear power plants are situated in countries with heavy air traffic and military base. As a result of which the risk of accidental and intentional crash of commercial and fighter aircrafts are very high. Apart from the accidental crash, several deliberate attacks have also been conducted on the nuclear containment structures.

Keeping in view the present circumstances the design criteria of nuclear power reactor buildings has been reconsidered by many countries in order to withstand the deliberate aircraft crash. The Nuclear Regulatory Commission (NRC) has also recommended modification in the structural design of the containment. As per the latest recommendations of the commission the applicants for NPP need to perform a design specific assessment in order to evaluate the performance of the containment against the direct impact of large commercial aircrafts, (Federal Register notice, 2009).

The aircraft crash on nuclear containment structure is a highly complex process involving large strains, high strain rate, high temperature, and multiple failure mechanisms. This problem involves both type of nonlinearity i.e. material as well as geometric nonlinearity. The material nonlinearity occurs when stress-strain behavior in the constitutive model is nonlinear, while geometric nonlinearity means significant effect on load deformation behavior with change in geometry, (Bonet and Wood, 2008, Lahiri et al., 2010, Gupta 2013). It is highly uneconomical to conduct such experiments even at low scale. Due to very limited scope of experimentation, the research in this area streamlined towards numerical and analytical methods to obtain the solution of such a complex but important problem. Moreover, in order to simplify the complexity, some assumptions have also been proposed in the numerical/analytical approaches. The coupled analysis of aircraft crash on the containment need exact modeling of an aircraft and the containment structure that is quite challenging and time consuming. In addition, coupled analysis needs excessive manual as well as CPU time and storage requirement. The intricacy of coupled analysis compelled investigators to switch towards an uncoupled analysis. In case of uncoupled analysis only the nuclear containment is modeled and the loading of aircraft is assigned through an impact load curve. The problem is therefore segregated in two parts i.e., determination of load versus time curve and application of the curve on the geometry of the containment. The loading of aircraft is obtained through the impact energy and the crushing strength of the aircraft and recorded in the form of force-time history curves. The force time history curves for various aircrafts at different incidence velocities are available in literature. These curves can be employed to predict a fairly accurate response of the containment structure against a given aircraft. However, the uncoupled analysis of aircraft crash problem has certain limitations with respect to the determination of force-time history curve as well as its application. These have been discussed in the forthcoming chapters.

1.2 REVIEW OF LITERATURE

A number of countries depend on nuclear energy to supply at least one-quarter of their total electricity. APS-1 was the first nuclear power plant connected to the power grid and started generating electricity for commercial use on June 26, 1954, at Obninsk, Russia. As of February 2012, 435 nuclear power plant units are in operation in 31 countries while 63 more plants are under construction in 15 countries (ENS, 2013). The majority of nuclear containment structures in world are doubly shell envelope consisting of a primary inner pre-stressed concrete or steel containment shell and an outer reinforced concrete shell. There are several types of these power reactors as described in Fig. 1.1. Out of these, only the Pressurized Water Reactors (PWRs) and Boiling Water Reactors (BWRs) are in commercial operation. An illustrative diagram of BWR Mark III type containment has been shown in Fig. 1.2.

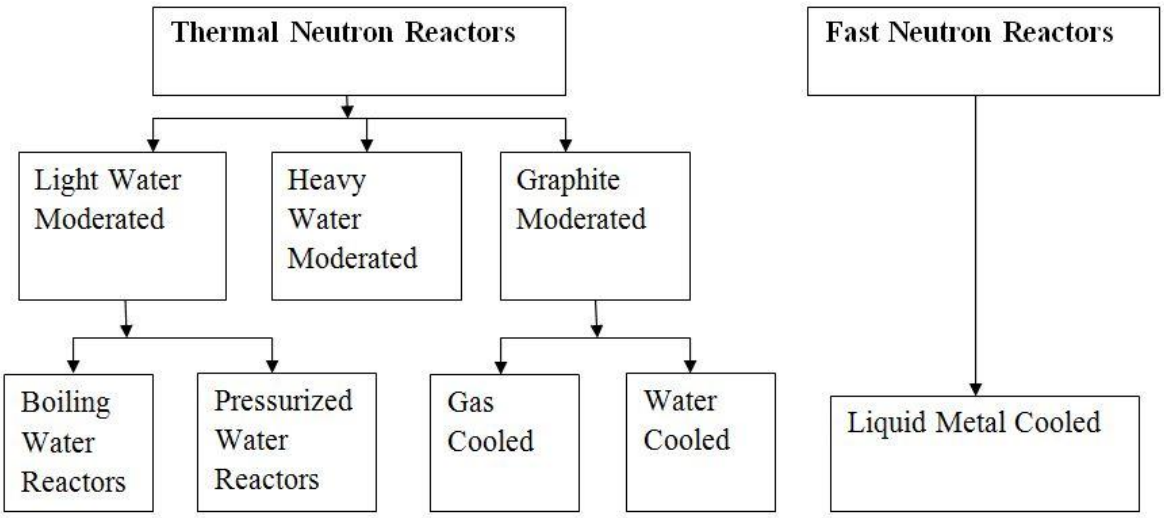

Fig. 1.1 Different type of nuclear power plant

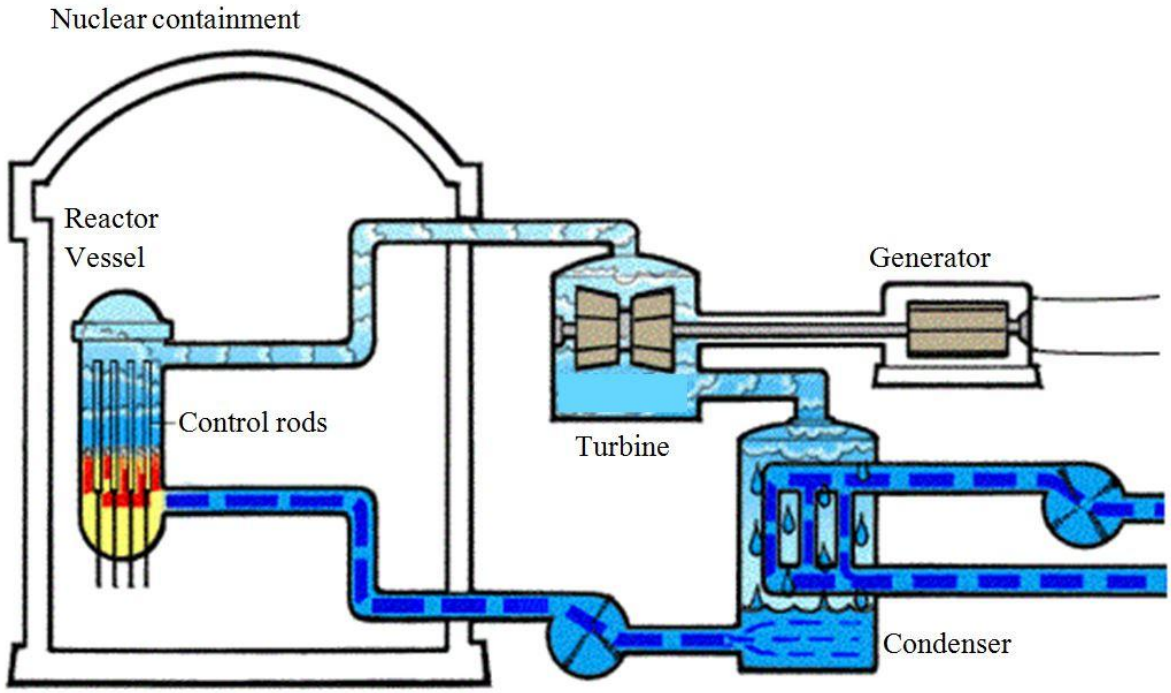

Fig. 1.2 Schematic diagram of BWR nuclear power plant

In the second half of twentieth century significant development in missile and aircraft technology has been attained. Consequently, researchers started to study the safety of important structures including storage facilities (above and underground), nuclear power plants, dams and other military and civil installations against aircraft crash.

The impact process may be classified as hard or soft depending on the projectile deformability relative to that of the target. However, the structure of an aircraft is a combination of soft (fuselage) as well as hard (engines, landing gears, stiffeners) components, (Heckotter and Sievers, 2013). A reinforced concrete structure like nuclear containment may experience flexural failure against a soft missile while punching shear failure against a hard missile. The failure mechanism of a target has also been found to be dependent on its stiffness and incidence velocity of the impacting projectile. The stiff target is more susceptible to shear failure while thin target to flexural failure. Similarly, at lower incidence velocity, the target may experience predominant bending while at high velocities the failure will be localized and shear dominant, (Martin O., 2010).

As such the problem of aircraft crash on the containment structure is highly complex due to geometric and material nonlinearity, associated large deformations, high rate of deformation and possible adiabatic effects. There are several approaches and methodologies which have been adopted to evaluate the target response. The studies in this area can be categorized according to their mode espoused for the execution of the problem. Thus, the available literature on aircraft crash problem has been categorised in four major groups i.e., analytical studies, experimental work, probabilistic approach and numerical simulations. The studies dealing with the constitutive modelling of concrete and its behaviour under high strain rate and elevated temperature are discussed separately.

1.2.1 Analytical Studies

The uncoupling of aircraft and target structure converts the impact load to impulse load. The work carried out by Riera (1968) to uncouple the problem of aircraft crash is considered to be the benchmark in this area. The total reaction of Boeing 802-320 against a rigid target with respect to time was obtained with the help of inertial and stiffness characteristics of the aircraft. An impact velocity of 200 knots (102.8 m/s) was assumed in the calculation and the incidence angle was considered normal to the surface. The total reaction F(t) at the interface between the collapsing aircraft and rigid body, see Fig. 1.3, is calculated by applying the concepts of conservation of momentum with some justified assumptions;

$$F[x(t)] = P_c[x(t)] - \mu[x(t)]V^2 - m_c \frac{dV_t}{dt} \quad (1.1)$$

Where F[x(t)] is the obtained reaction force from the structure (target);

μ is mass distribution per unit length at a distance x(t) for nose of aircraft;

$P_c[x(t)]$ is the crushing strength or buckling load of the aircraft;

V = velocity of the uncrushed portion of the aircraft at time t;

V_t = velocity of the structure at time t;

m_c = crushed mass of the projectile and mass of the target.

It can be noticed from Eqn. 1 that mass density and crushing strength of aircraft are variable depending on both x (distance) and t (Time). The variation of linear mass density and

crushing strength with respect to length of aircraft has been plotted in Fig. 1.4. As the engines are located at the wings, both of these curves have been found to have their peak close to the mid of the total length of aircraft.

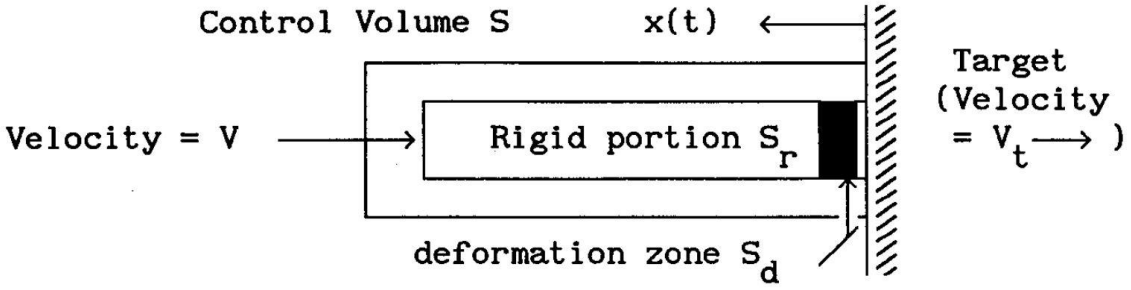

Fig. 1.3 Soft projectile striking a rigid target, (Abbas et al., 1996)

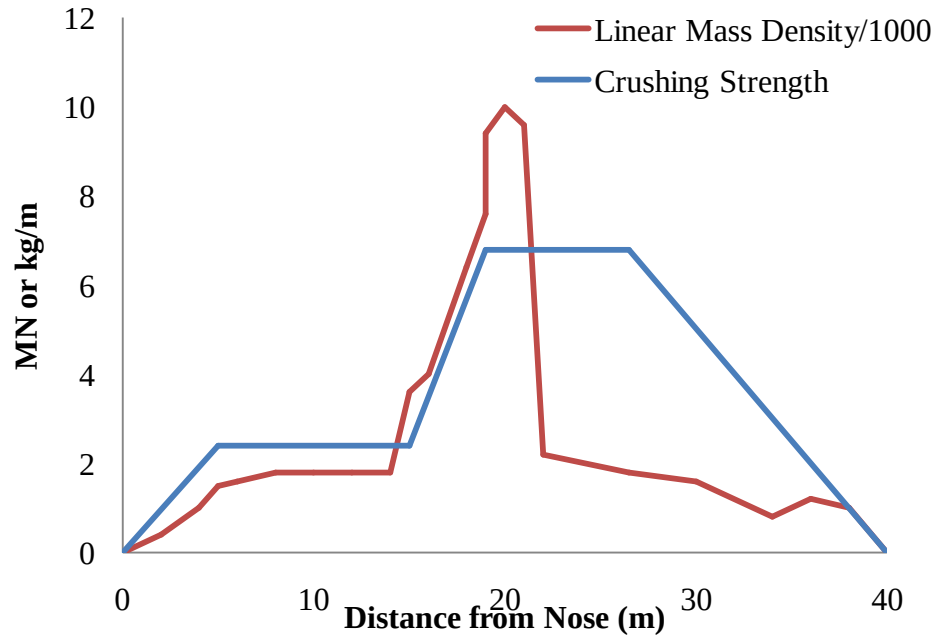

Fig. 1.4 Variation of mass density (linear) and crushing strength along the length of Boeing

An alternative derivation to obtain the reaction-time response curve was presented by Rice and Bahar (1978). The shortcoming in this derivation is the assumption that velocity distribution is continuous throughout the control volume. There will be a finite jump of velocity at the projectile-target interface due to the assumption of deformation zone to be mathematically zero. In actual sense, the thickness of deformation zone is negligible in comparison to the total

un-deformed length, but mathematically not to be zero. Hence, with these assumptions, we found lower limit of the function described in Eqn. 1. In an attempt to upgrade the Riera's formulation, Hornyik (1977) calculated energy balance with the assumption of rigid perfectly plastic behavior of the projectile. In another comprehensive study, Wolf et al., (1978) used lumped masses interconnected through elasto-plastic springs as the aircraft model to obtain the Riera's reaction-time curve. Authors found that for a range of impact velocities the two models agree extremely well.

During the analysis of containment through application of force- history curve, damping is neglected as it does not affect the maximum response for the impact loading (Rebora et. al., 1976). It was observed that the effect of gravitational forces upon the reaction is negligible and also stresses due to gravity were quite low, (Gardner, 1984 and Abbas, 1992). For soft missiles, such as aircraft moving at standard speeds, the elastic stiffness of aircraft body does not play any significant role in the reaction-time curve. However, a correct evaluation of the crushing strength and buckling behavior is of much importance (Bignon and Riera, 1980). Riera et al. (1982) concluded that in case of aircraft impact against nuclear structures, the engines should be considered as independent projectiles, and if necessary, their effect be superimposed to the fuselage.

In order to withstand the aircraft crash, deliberations were also made for the improvement in the structural design of the containment. Paul et al., (1993) studied the impact of the Boeing 707-320 aircraft at three locations of a BWR nuclear containment building, Fig. 1.5. It was concluded that 1.2 m thick cylindrical wall and 0.61 m thick dome is sufficient to resist the horizontal crash near the junction of dome and cylinder, however, unsafe for either of these locations. Zerna et al., (1976) suggested that steel fibers and cables can enable new design solutions for aircraft-impact resistant structures. The use of steel fibers and cables as longitudinal reinforcement will increase allowable deformation of the structure. Hence, the thickness of the structure can be decreased as it provides only on the protection from penetration and is independent of the requirements for bending and shear. Further, Krutzik (1988) concluded that steel-fiber-reinforced concrete shells with thicknesses greater than or equal to 0.8 m have sufficient nonlinear capacity to resist crash of a military airplane such as the Phantom jet. In a

recent study, Koechlin and Potapov (2009) confirmed that an aircraft crash is a soft impact and if perforation occurs, it would be a shear cone failure mode.

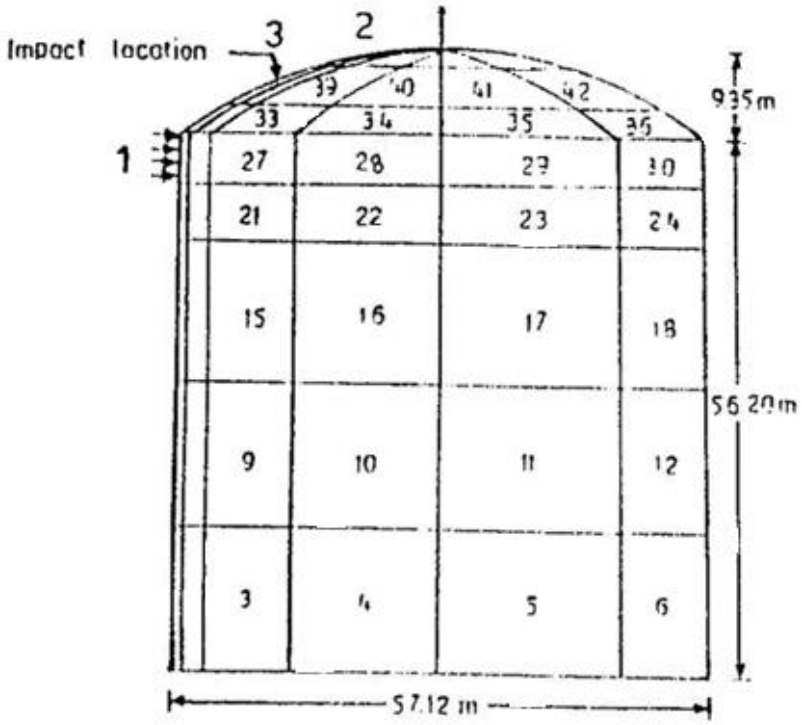

Fig. 1.5 Impact location on containment building (Paul et al., 1993)

The effect of target yielding had also been studied and led to the conclusion that the target flexibility does not have significant effect on the reaction-time curves, (Drittler et. al., 1976, Nabold and Schildknecht, 1977 Wolf et al., 1978, and Riera, 1980). Abbas et al., (1995a, 1995b) on the other hand noticed that the reaction-time response obtained on the basis of a rigid target is not only unrealistic but also un-conservative. It was also concluded that effect of target yielding is dependent upon the characteristics of the target as well as missile. Hence, it is undesirable to use the reaction-time response obtained on the basis of a rigid target concept. This is an new conclusion made by the author of this thesis. Abbas et al., (1995a, 1995b), though commented about the target yielding however they could not obtain any distinct effect of target yielding on the reaction time response of Boeing 707-320, FB-111 Fighter Jet and Phantom F4 aircrafts, see Fig. 1.6.

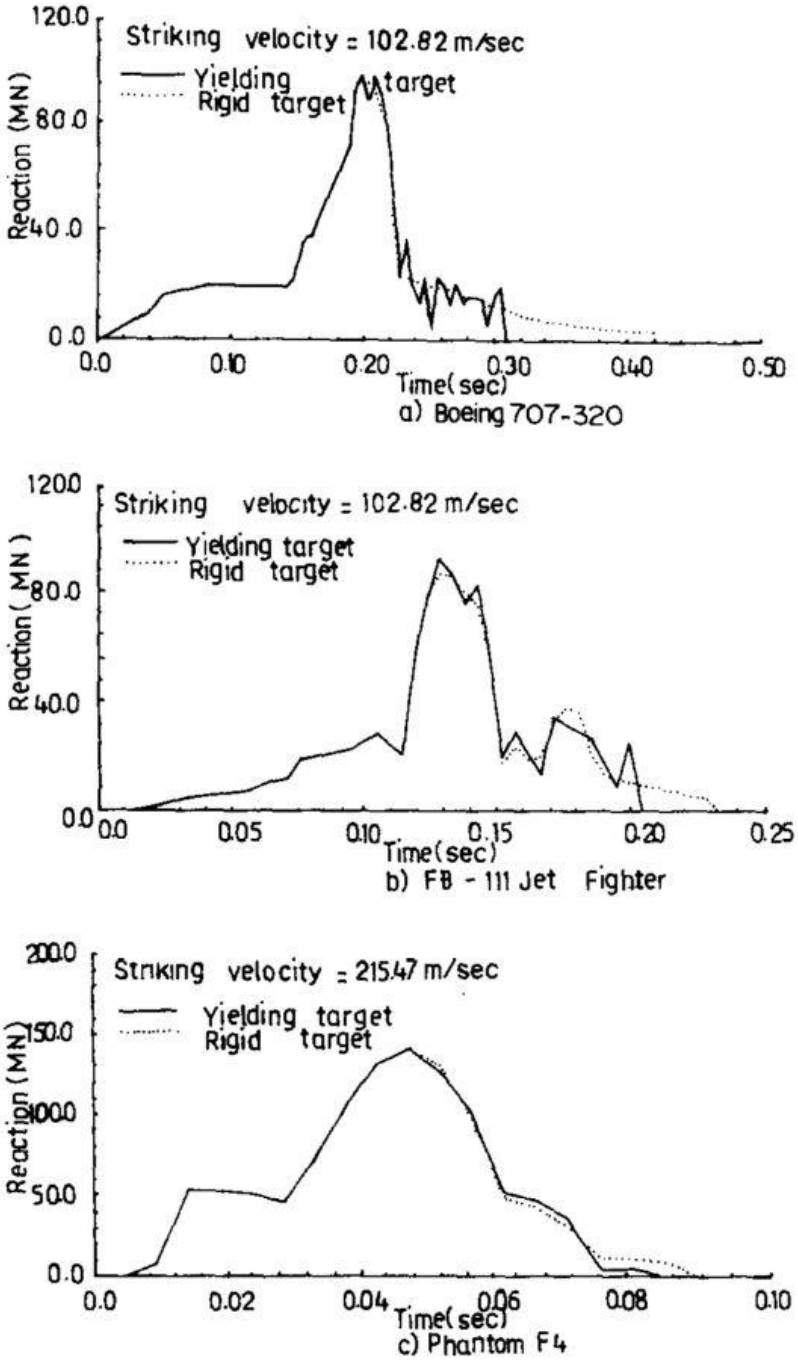

Fig. 1.6 Effect of target yielding upon reaction time response (Abbas et al., 1995)

Thereafter, many researchers proposed the reaction time response of different fighter and commercial aircrafts based on Riera's approach (Gomathinayagam et al., 1994, Abbas et al., 1995 & 1996, Iliev et al., 2011, Lo Forano and Forasassi, 2011). The reaction time response curves of a few aircrafts have been provided in Fig. 1.7 for comparison. It can be seen that the

modern commercial aircrafts have higher peak impact force and their impact duration is also longer due to their huge length and high crushing strength.

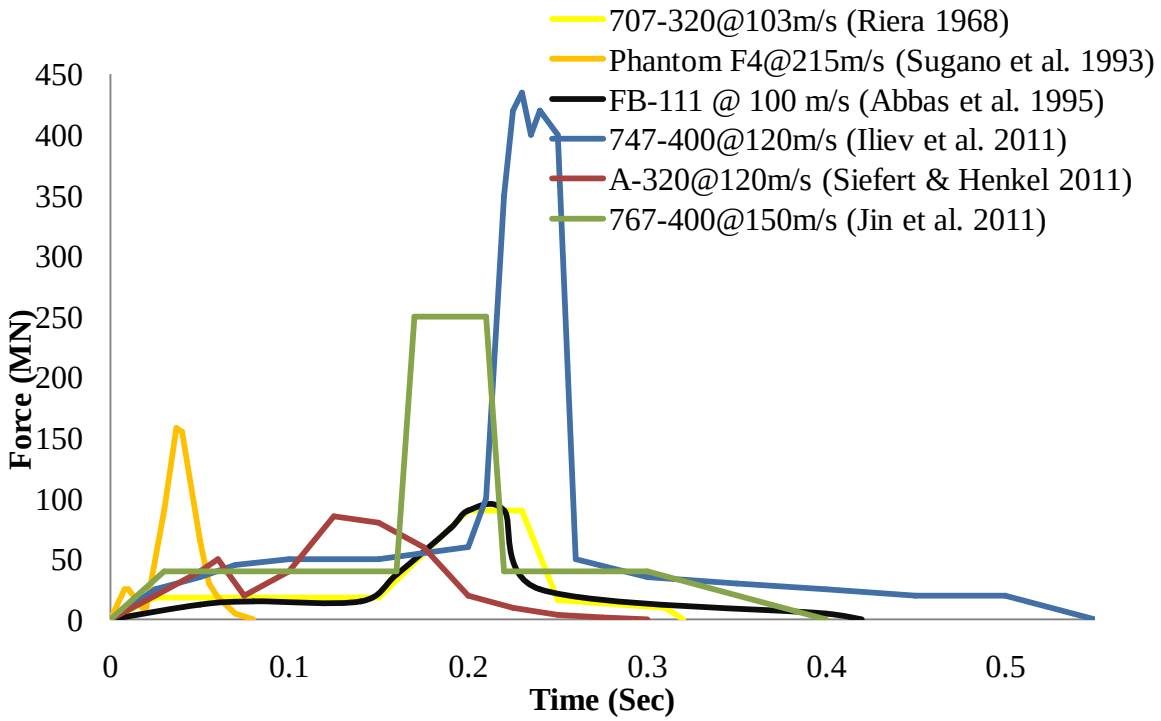

Fig. 1.7 Reaction time response curves of different aircrafts

1.2.2 Experimental Studies

The experimentation of this problem is highly expensive, complicated and risky such that that it is almost impossible for individuals and academic institutions to perform such experiments. In spite of this however, one experiment has been conducted by Sugano et al., (1993a, b and c) wherein the fighter jet Phantom F-4 had been crashed on a heavy concrete wall at Sandiya laboratory, USA. Sugano et al., (1993a) performed a full-scale impact test of aircraft against a heavy, reinforced concrete target. The total weight of the aircraft was 17000 kg including the weight of attachments as well as 4350 kg of water that was filled to simulate the fuel and attain mass distribution. The target consisted of a reinforced concrete wall of horizontal and vertical span of 7 m and thickness 3.66 m. The weight of the wall was 425000 kg (almost 25 times the weight of the Phantom F-4) and it was mounted on a platform. The orientation of the aircraft was considered normal with respect to target while the incidence velocity 215 m/s, see Fig. 1.8.

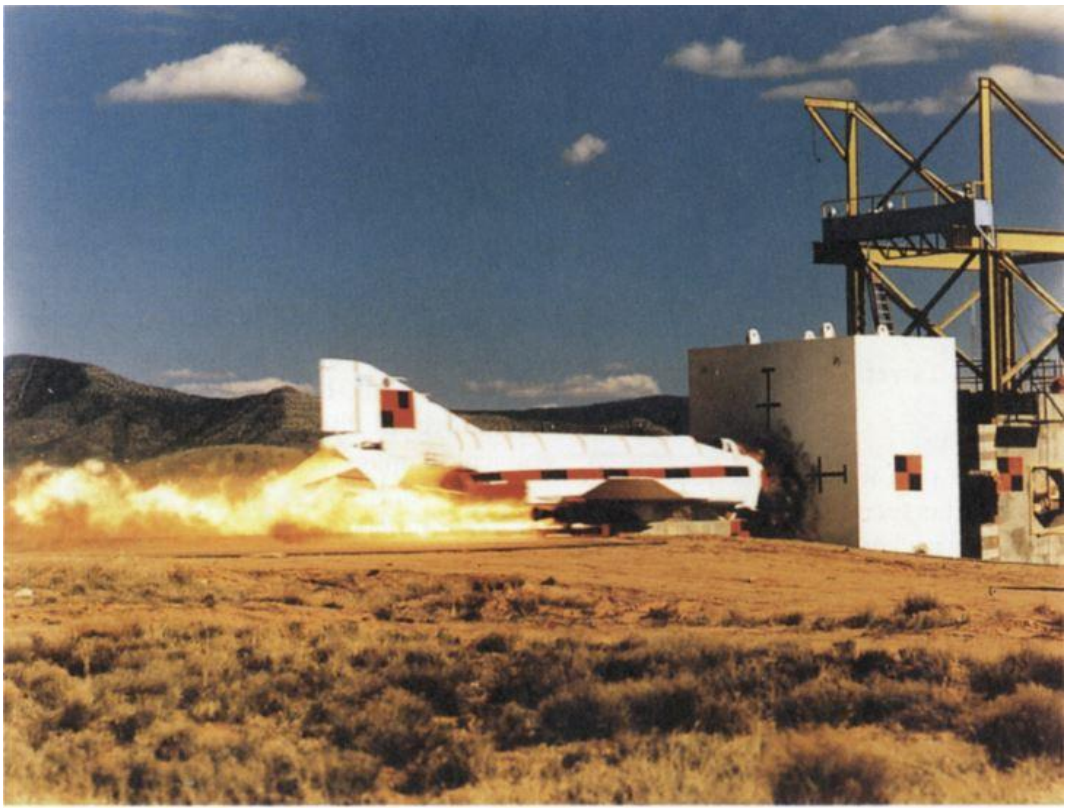

Fig. 1.8 Phantom F4 striking reinforced concrete wall (Sugano et al. 1993a)

The maximum penetration of concrete caused by engines was 60 mm and that caused by fuselage was 20 mm. The RCC wall experienced a displacement of 1.83 m against the back-up structure and rebounded back. For kinematic measurements, sensors were mounted on the aircraft and the target. The total impact force, F, was evaluated independently from the change in momentum of the target and the aircraft, see Fig. 1.9. The experimentally predicted impact force-time curve confirmed that the existing "Riera approach", can be used for evaluating the impact force.

Motivated by a full scale aircraft impact test (Sugano et al., 1993a), the authors systematically performed the impact of engines separately. As they noticed during the full scale test that the engines caused deeper local penetration than aircraft fuselage in the massive concrete target. In order to establish low cost feasible testing pattern, an extensive series of engine impact tests was conducted in scales 1:2.5 and 1:7.5 in addition to full scale tests. It was concluded that précised physical scaling laws lead to better quantitative results. This important

finding enabled the researchers to extend their studies on smaller testing facilities in laboratories to vary different parameters in aircraft impact study.

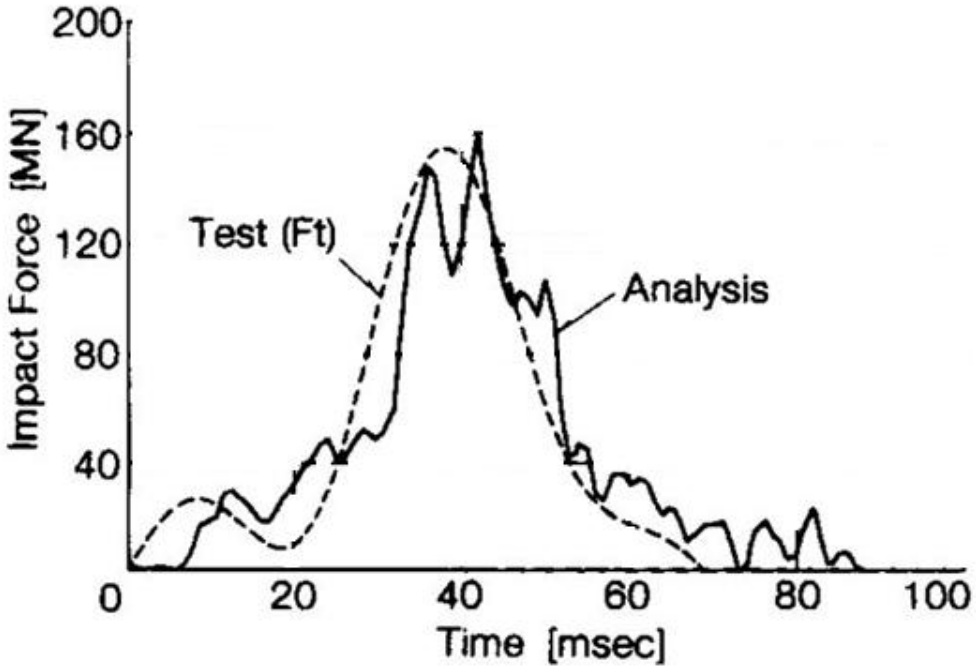

Fig. 1.9 Impact force versus time curve (Sugano et al. 1993a)

An experimental series on Ultra High Performance Concrete (UHPC) panels subjected to aircraft engine impact has been studied by Riedel et al., (2010) with reference to a test series on normal strength concrete. A small scale laboratory configuration was developed and the experimentation was carried out at a scale factor of 1/10, Fig. 1.10. The fiber reinforced UHPC is a concrete based material which combines ultra-high strength, high packing density and an improved ductility. It also possesses significant energy dissipation capacity due to the presence of fiber reinforcement. The above characteristics rendered the penetrations depth to a mere footprint and controlled spalling of concrete. On the rear side of the concrete panel the fibers remained connected till the crack width equals half of its length and thus prevented the matrix from scabbing.

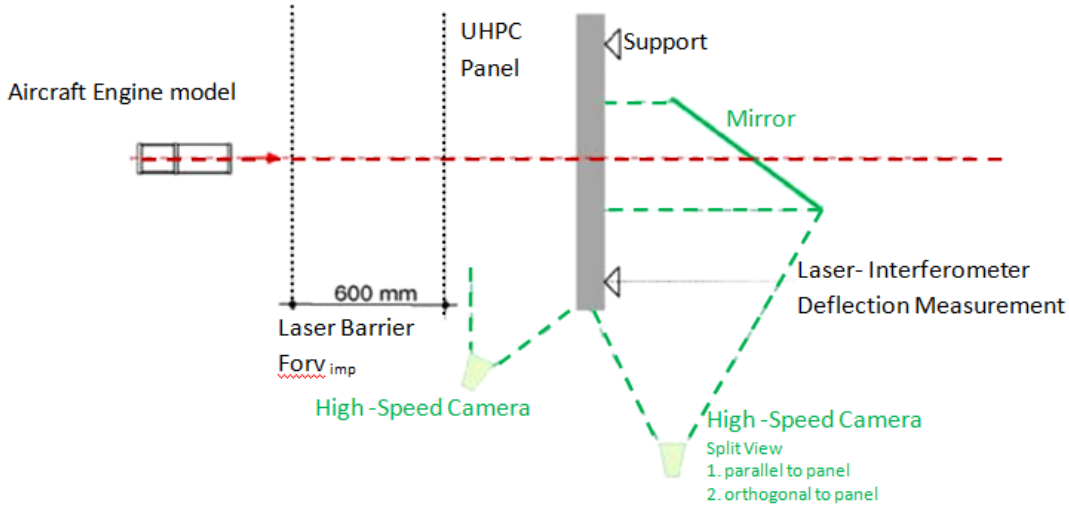

Fig. 1.10 Experimental configuration (Werner et al. 2010)

1.2.3 Probabilistic Approaches

Probabilistic methods address the uncertainty issues associated with a problem. Probabilistic approaches to the design and safety analysis of nuclear power plants have been proposed by Farmer (1967) and Wall (1969). They established a limit-line which demarcates between acceptable and unacceptable risks. Before September 2001, WTC attack, the usual practice was to evaluate the probability of aircraft crash on the nuclear power plant. If the probability was estimated to be lesser than a given allowable limit, the possibility of strike was neglected as the design basis criterion. Otherwise adequate measures were taken to reduce the possibility of strike.

Chelapati and Kennedy (1972) estimated the conditional and absolute probability of failure of reinforced concrete walls of nuclear power plant due to the accidental strike of an aircraft. It was shown that if an aircraft hits a reactor building the response of the entire building is negligible but significant damage occurs to its specific structural components. The probabilistic approaches and yield line theory was employed to evaluate the conditional probability of local collapse of the wall panel. It was concluded that the probabilities of damage under the perforation and collapse mode were approximately of the same order of magnitude. Under the impact of an aircraft, the cracking mode of damage has been estimated using elastic analyses. It was predicted that the cracking mode of damage occurs much earlier than the other

two modes of damage i.e. perforation or collapse. It has also shown that the impact load level predicted for cracking mode of damage was very conservative.

Hornyik et al., (1973) estimated the probability of crashes onto the plant site by a military aircraft on a racetrack pattern flight. Zorn and Schueller (1986) and Kobayashi (1988) evaluated the probability of a crash onto a plant located near the flight zone assuming that the flight density in the zone as well as the flying direction is uniform. Based on an extensive analysis of aircraft crash incidents Zorn and Schueller (1986) concluded that the engines detach shortly after impact from the fuselage. It was emphasized that the superposition of the hard engine and the soft fuselage impact is a time and spatial problem where the geometry of the target should not be neglected.

In a reliability study, Siddiqui et al., (2003) observed that the reliability of containment increases sharply with the increase in takeoff point distance from NPP. However, the rate of increment in reliability slows down as the distance becomes longer. Aircraft mass and its velocity have been found to have remarkable effect on the containment reliability. A containment, which is reliable against one aircraft strike, may be highly unreliable for another aircraft having the same velocity but higher mass and vice versa.

In the nutshell it may be pointed out that majority of the probabilistic studies are concerned to the accidental crash. However, the vulnerability against intentional attacks has been seen to increase significantly in the recent years.

1.2.4 Numerical Studies

Analysis of nuclear containment structures against aircraft impact needs a non-linear transient analysis involving thousands of time steps to study the impact response (Gomathinayagam et al., 1994). Non-linear finite element analysis of aircraft crash on important concrete structures like nuclear containments and military installations has been studied through high speed computational facilities and sophisticated finite element codes.

Abbas et al., (1995, 1996) observed that the junction of dome and cylinder is most critical location and Phantom F4 is more destructive than Boeing 707-320 and FB-111 jet fighter. Katayama et al., (2004) conducted a three-dimensional computer simulation of the impact of a Boeing 747 passenger jet using the AUTODYN-3D computer program. The targets were

reinforced and non-reinforced concrete walls with three different thicknesses. It was concluded that the reinforced concrete of 3 m thickness was not severely damaged when impacted by the aircraft at 300 km/h incidence velocity. However, in order to improve the accuracy of the simulation the assumption adopted in the Katayama (2004) need to be reviewed. For example, the weight of the fuel has been distributed uniformly to all the elements of jetliner because of the lack of information about its exact location.

Arros and Doumbalski (2007) employed reaction-time curve as well as geometric model of Boeing 747-400 aircraft to compare the response of a fictitious nuclear building. The numerical model of Boeing-747 was made with wing load distributed over entire length. It was also mentioned that if the wing area is slightly reduced, the displacement obtained by reaction-time curve will exactly match to that of the geometric model. Kukreja (2005) described that the outer layer of Mark III BWR and PHWR containments will absorb significant energy of Boeing 707-320 and Airbus 300B4 by undergoing local damage and perforation, while the inner layer will experience insignificant deformation. Lo Frano and Forasassi (2011) found that Boeing-747 has the highest damaging potential (with penetration depth 1.0 m) followed by Boeing-707, Boeing-720 and Phantom F4 when impacted on IRIS containment building. Moreover, if the thickness of containment is less than 1 m, significant deformation and penetration will occur against large commercial aircrafts.

Almost all of these numerical studies employed finite element method in different manners. Finite element technique is extremely versatile and powerful, the correct employment of this technique enables the solution of highly sophisticated phenomena. The accuracy of the finite element simulation depends on various factors such as type of analysis, size of increment, contact and boundary conditions, size of element and its aspect ratio. The size of element depends on the problem and the specific results to be extracted. Therefore, in order to obtained accurate results through a finite element simulation, one has to perform the mesh convergence study. Abbas et al., (1996) adopted 52, 20-noded isoparametric brick elements with a total number of 342 nodes to discretize the BWR containment. For a similar simulation, Kukreja (2005) considered a few hundred elements and more recently Iqbal et. al., (2012) obtained a total number of elements in the containment to be 514,640. The effect of element size is clearly visible in their findings. The maximum penetration depth (deformation) of the containment

observed by Abbas et al., (1996) at the junction of dome and cylinder was 34.2 mm, while Kukreja (2005) validated his material model with Abbas et al., (1996) and reported that the maximum deformation was 46 mm at the same location. However, Iqbal et al. (2012) found a maximum deformation of 66.9 mm at the same location. In an another study on a cantilever beam in plane stress condition, Ciria et al., (2008) reported that relative error had been reduced from 10.5% to 0.066 % with increase in total number of element from 34 to 5506. Therefore, it can be concluded that for any regions of highly concentrated stress, such as around loading points and supports, an optimum element size must be carefully selected keeping in view the accuracy of the solution and the availability of the computation setup.

The numerical simulation of aircraft crash problem has two basic approaches related to the application of load i.e., either to model the geometry of aircraft for hitting the target structure or apply its loading through the reaction time response curve. The development of an accurate geometric model of aircraft and its discretization is very complex in a finite element code. The latest commercial aircrafts possess complex structure with nonlinear geometry and varying stiffness. The fuselage of an aircraft is a semi-monocoque structure made up of aluminum alloy skin to carry cabin pressure (tension) and shear loads. The longitudinal stringers (longerons) are provided to resist the longitudinal tension and compression. In order to maintain the fuselage shape and distribute the skin load, circumferential frames are employed. In case of standard military aircrafts, thick bulkheads are used in place of frames (Starke Jr. and Staley, 1996).

The selection of a proper constitutive model and characterization of the material is essential. The determination of an equivalent stiffness for fuselage, wings and intermediate stiffener is also important. In actual practice the thickness of wings varies from the junction of fuselage to the extreme end of the wing. Hence, preparation of the geometric model which identically replicates all the characteristics of an aircraft is nearly impossible. Material characteristics of many aluminum alloy had been discussed in literature.(Xue and Wierzbicki, 2008, Borvik et al., 2010, Luo et al., 2011)

On the other hand, in the reaction time response approach, it is the area of impact that should be determined precisely along with reaction-time curve. Riera (1968) schematically calculated the probable interface between a Boeing 707-320 aircraft crushing normally on a spherical surface of diameter 67 m. It was concluded that if the impact is considered at the dome

the impact area may be assumed to be 20.43 m^2 while for a flat surface it may be around 37.16 m^2. In another study, Yang and Godfrey (1970) concluded that the area of interface between the aircraft and the structure would be about 10 to 15% greater than the cross-sectional area of the aircraft.

For the strike of Phantom F4 on a rigid target, Riera (1980) assumed the impact area to be 7 m^2. On the other hand, Sugano et al., (1993a) found through experimentation the projected area of fuselage to be 4.6 m^2 while the impact area to be 10 m^2 against a flat concrete target. It should be noted that the impact area has been considered to be approximately circular and the effect of wings has been neglected, see Fig. 1.11. Furthermore, Abbas et al., (1995, 1996) assumed area of impact to be 28 m^2 for Boeing 707-320, Phantom F4 and FB 111 aircrafts impacting the BWR Nuclear Power Plant containment of diameter 42 m. Gomathinayagam et al., (1994) and Kukreja (2005) also assumed impact area to be 28 m^2 for all the aircraft considered in his study.

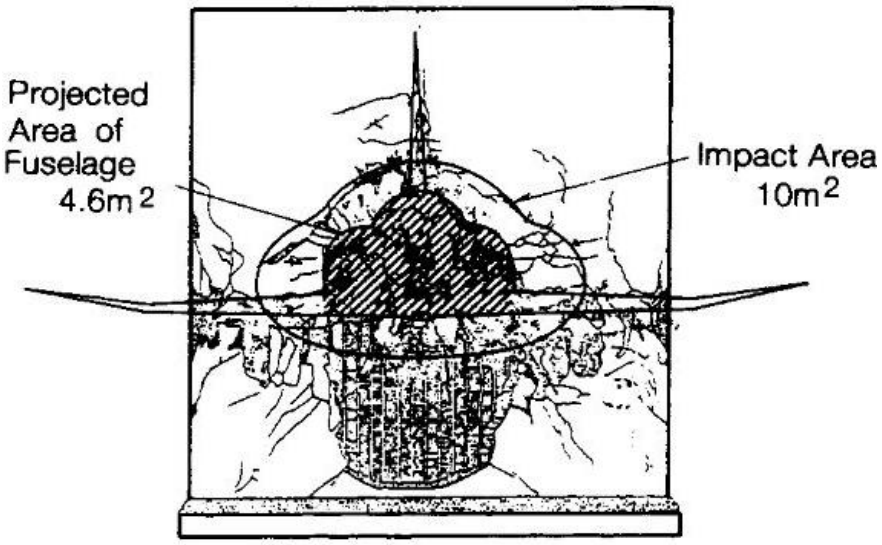

Fig. 1.11 Area of impact (Sugano et al., 1993a)

Aross and Doumbalski (2007), while studying the impact of Boeing 747-400, concluded that the outcome of the Riera time history method may be quite sensitive to the assumptions associated with loading area and timing of load application (e.g., consideration of wing sweep angle, etc.). Iliev et al., (2011) assumed the impact area of fuselage to be circular with diameter 8 m while the wing area to be rectangular, 33 m x 2 m, for Boeing 747-400. Jin et al., (2011)

separated the impact area of fuselage and wings for Boeing 767-400 and observed that the engine contributes largely to the total impact load. Siefert and Henkel (2011) applied the reaction-time response curve of fuselage, wings and engines separately on their corresponding area of contact calculated by authors. It was concluded that for the simulation of an Airbus A320 the load-time-function shows lower values of dispalcements than for the geometric model approach. This contradicts the general assumption that the results obtained through the load-time-function are in general conservative.

A clear cut demarcation of impact area for fuselage, engines or wings of the aircraft and its corresponding reaction curve cannot be obtained, as the influence of one part of aircraft on the force-reaction curve of other part cannot be nullified. Hence, in order to establish standard design code the subject of effective area of impact needs further investigation.

1.2.5 Behavior of Concrete under High Rate of Loading

The dynamic behavior of concrete is highly non-linear and dependent on the confining pressure or boundary conditions. The study on the fracture mechanics of concrete, initiated by Kalpan in (1961), progressed for more than half a century. The most recent study on this subject has been reported by Hao et al., (2013). A major contribution towards the advancement of fracture mechanics of concrete was made Hillerborg et al. (1976), Bazant and Cedolin (1983), Dharmaraju et al., (2004), Matsagar and Jangid, (2002, 2007).

The failure of a target structure is governed by many factors such as geometry, material parameters and impact conditions. The failure of concrete target can be predicted through a proper understanding of fracture energy and strain softening behavior. The fracture energy may be defined as the energy required to open unit area of crack surface. The fictitious crack model (FCM) originally developed by Hillerborg et al., (1976) is a powerful tool to predict crack formation in the concrete. The fracture energy is a unique material property, independent of specimen size, shape and type of loading, (Bazant and Pfeiffer, 1987). Fracture energies were generally estimated in laboratories using standard size specimens, the valid range of specimen sizes were yet under discussion. However, to measure a size independent value of fracture energy large specimens need to be tested, (Muralidhara et al., 2011, 2013; Murthy et al., 2013)

The failure mechanism of reinforced concrete target impacted by a projectile will be either flexure dominant or shear dominant (punching failure). Both of these failure modes are the

resultant of the elastic-plastic response of the reinforced concrete target. In case of flexural failure, the front surface of the target is subjected to compression and the distal surface is subjected to tension. This condition leads to the formation of cracks along the thickness of the target. Hence, Abbas et al., (2004) reported the cracking strain as a sensitive parameter thus its requires accurate estimation for the purpose of precise analysis. In case of punching shear failure, a shear cone forms inside the target. Under the worst condition the shear cone is punched out of the target. The material undergoes failure due to the excessive shear stresses in contrast to that of the flexural failure wherein the compression/tension is predominant (Martin, 2010).

The modes of failure also depend upon the shape of projectile, strength of concrete and the quantity of reinforcement. The over reinforced target as well as the target subjected to soft impact or low velocity impact is susceptible to flexural failure. On the other hand, the under reinforced target as well as the target subjected to hard impact or high velocity impact are more likely to undergo punching failure. The spacing of the reinforcement and the diameter of the missile may also affect the failure mechanism.

Li et al., (2005) described in detail the failure mechanism of concrete as penetration, cone cracking, radial cracking, spalling and perforation, see Fig.1.12. The punching failure was subcategorized into four different local failure modes viz. surface failure, spalling, scabbing and perforation;

a) Penetration is defined as the tunneling into the concrete target by the projectile. The length of the tunnel is called penetration depth.
b) Cone cracking and plugging is defined as the formation of a cone-like crack under the projectile and the subsequent shear plugging.
c) Spalling is the expulsion of target material from the proximal face of the target.
d) Radial cracking is defined as propagation of cracks from the impact point towards the proximal or distal face or both.
e) Scabbing is the eviction of fragments from the distal face of the target.
f) Perforation is the complete passage of the projectile through the target with or without a residual velocity.

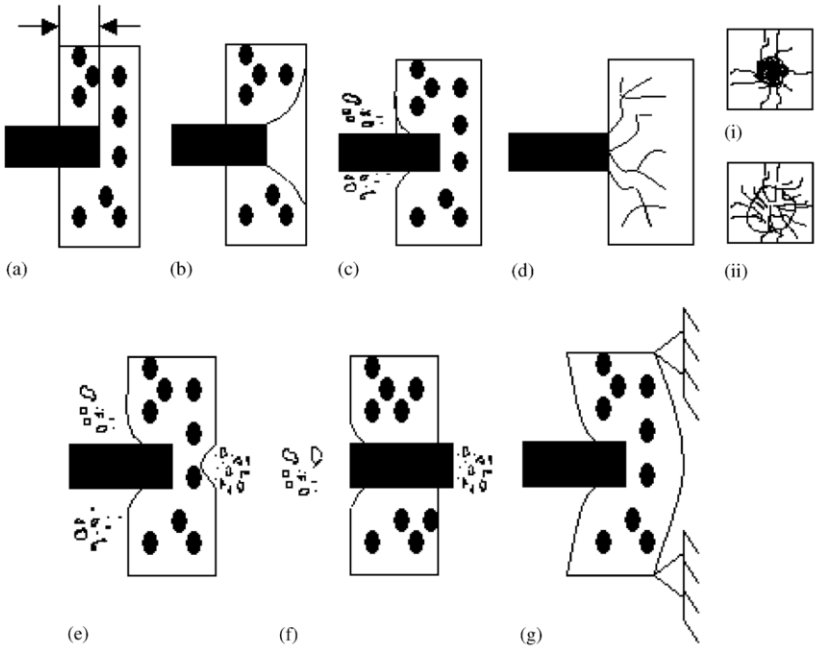

Fig. 1.12 Effect of rigid projectile impact on brittle target (a) Penetration (b) Cone cracking (c) Spalling (d) Cracks on (i) proximal face and (ii) distal face (e) Scabbing (f) Perforation (g) overall target response (Li et al., 2005)

The local punching or shear failure generally depends upon the thickness of the target to projectile diameter ratio (x/d) as well the stress wave response of the structure. When the thickness of target is large and velocity of projectile is low, the target offers adequate resistance to projectile motion and the damage is restricted to the top surface. However, if the velocity of projectile is higher, the material from the front surface ejects out and a small pit is created. This phenomenon is known as spalling. When the x/d ratio is small and the velocity of the projectile is high, the stress waves reach the rear surface of the target (not the projectile itself) and the material from the rear surface is chipped out. This phenomenon is known as scabbing.

A lots of material model has been developed to define the behavior of concrete under extreme loading conditions. several fracture model used for high dynamic simulation of concrete structures had been studied (Wierzbicki et al., 2005; Lu and Tu, 2009; Trivedi and Singh, 2013). They had concluded that the concrete damage model is sufficiently capable of modeling concrete behavior at a range of stress conditions. However, no single modelling approach of material model can exactly model the impact, shock blast or fire simultaneously (Lu Y., 2009).

1.2.6 Behavior of Concrete at Elevated Temperature

Concrete is most widely used construction material and inherently fire resistant. It has excellent fire retarding characteristics and good thermal properties like non-combustibility, non-emission of any toxic fumes/smoke and non-dripping of any molten particles when exposed to fire. In general, the required reinforcement cover is the main aspect of the design criteria. However, the standard laboratory test condition are entirely different from real-world fires. Particularly cooling phase of all real fire is different from each other, however, initial heating rates may not also be the same. Basically, the behaviour of concrete under fire is dependent on the temperature-dependent material properties. With an increase in temperature the strength and elastic properties of concrete decrease and at the same time the expansion of the material leads to the development of stresses in the members in addition to the stresses developed due to loads. At high temperature the influence of type of aggregate is higher on the properties of concrete. Carbonate, siliceous and lightweight aggregate are three most used aggregates. Limestone and dolomite comes under carbonate aggregates while granite and sandstone under siliceous aggregate. After thermal treatment of shale, slate, or clay, light weight aggregates are usually produced.

The literature on the behavior of concrete under elevated temperature can be broadly classified into three categories;

(i) The studies based on the fire parameters for example fire duration and its intensity
(ii) Effect of elevated temperature on the mechanical and thermal properties of concrete
(iii) Effect of fire on the whole structural and individual components

The major damage mechanism responsible for deterioration in properties of concrete exposed to high temperatures may be categories as below.

- phase transformations taking place in cement paste (Malhotra 1956, Khoury 2000).
- Phase transformation taking place in aggregate (Fletcher et al., 2007),
- Thermal incompatibility between the cement paste and aggregate (Fletcher et al., 2007),
- Spalling of concrete (Khoury and Adenburg, 2000).

However, Usmani et al., (2001) emphasized that the structural response in fire is more governed by the induced stresses and displacements rather than material degradation. Law and

Gillie (2010) had also proposed the interaction diagrams for sections of structure at ambient and elevated temperature. Roben at al., (2010) suggested to consider different rate of spread of fire in tall and complicated structures. Table 1.1 shows the effect of fire on RCC structures during heating phase. The cooling phase is considered equally important due to the fact that the peak temperature in a member is attained during the cooling phase. Hence, the structural elements are more vulnerable to failure during the cooling phase. Fig. 1.13 shows the change in surface texture of concrete on exposure to high temperature up to 1200 ^{0}C (Arioz, 2007).

Table 1.1 Various stages of heating phase

Heating stage		Probable effects
i.	Rise in surface temperature	Surface cracking
ii.	Heat transfer from surface to the interior of concrete	Loss of strength, cracking and spalling
iii.	Heat transfer from concrete to reinforcement	Reduction of yield strength, possible buckling and deflection increases.

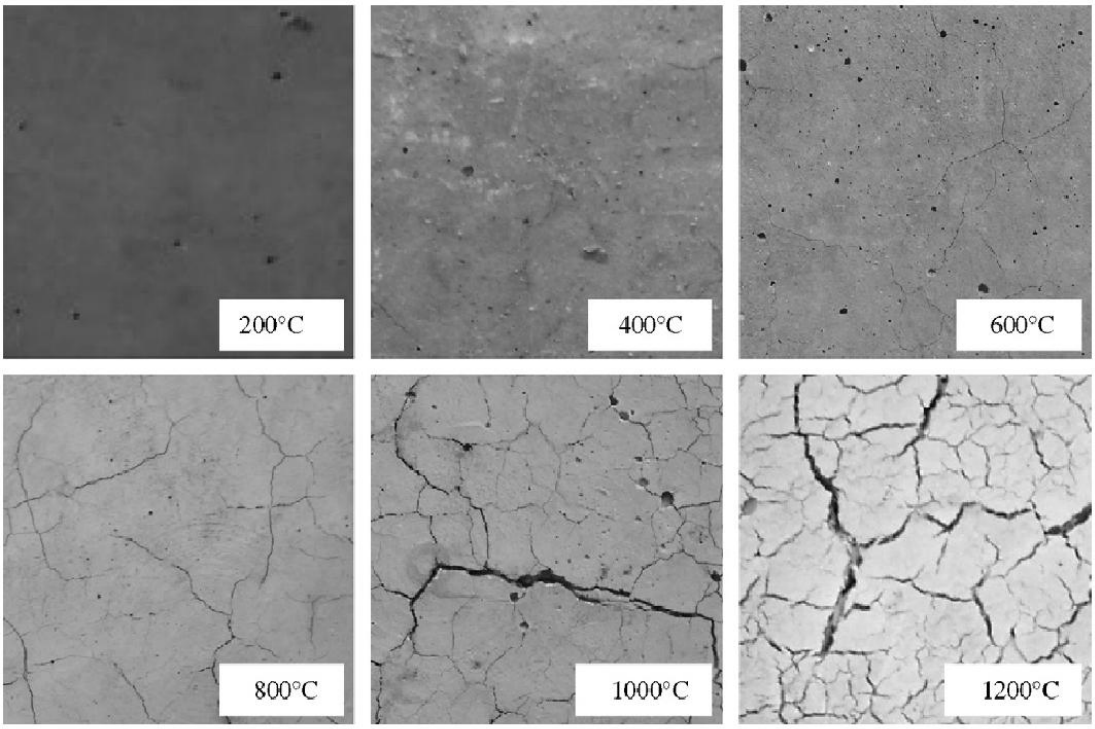

Fig. 1.13 Surface texture of the concrete sample exposed to elevated temperatures (Arioz, 2007)

The compressive strength of concrete reduces with increase in temperature, Fig. 1.14. Till the attainment of designated temperature the specimens were stressed to 40% of their compressive strength. Thereafter load were increased up to the failure of the specimen. At 1200°F the residual strength of concrete containing siliceous aggregate was approximately 50%, however, the significant reduction started even at 800°F. Moreover, negligible loss of strength had been noticed in concrete containing lightweight and carbonate aggregate up 1200 °F temperature. The fire resistance properties of lightweight concrete has been found to better than normal weight concrete of same. The modulus of elasticity of concrete is also significantly affected by temperature elevation, Fig. 1.15. The modulus of elasticity for the concrete obtained through different types of aggregates has been found to reduce with an increase in temperature. Further, the creep and relaxation has also been found to amplify significantly due to temperature elevation.

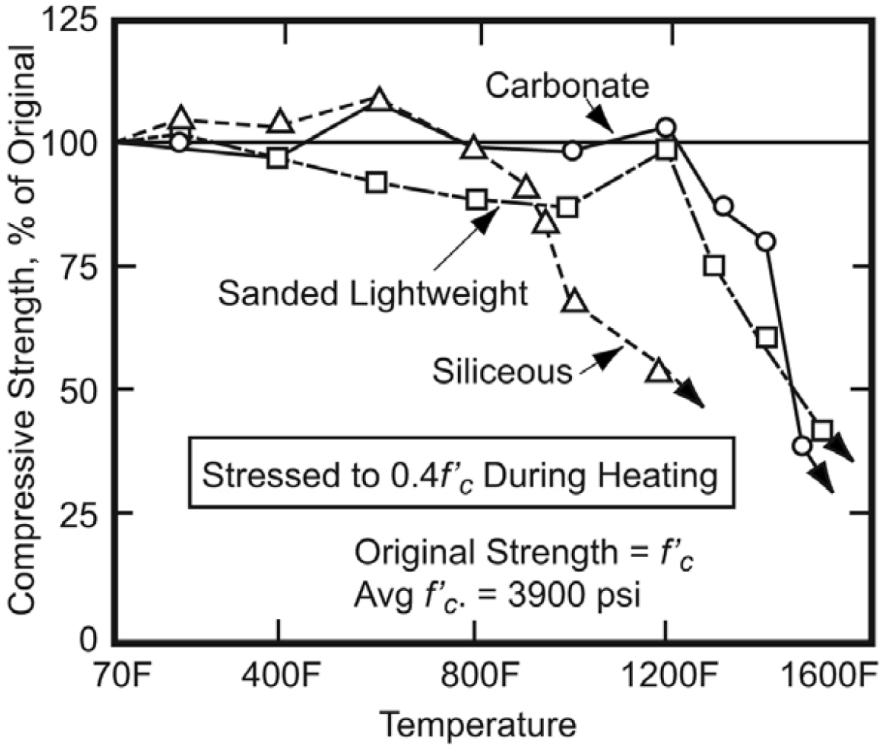

Fig. 1.14 Effect of high temperature on the compressive strength of concrete, (Bilow and Kamara, 2008)

The strength loss of concrete under high temperature depends upon the following conditions: (Kodur et al., 2010)

i. Type of exposure (duration, no. of faces and percentage of exposure)
ii. Type of concrete (strength, aggregate type etc.)
iii. Loading (level of initial load before and during exposure to fire)

The behavior of a fire exposed RC element depends on the following:

i. Internal temperature experienced,
ii. Load level during the fire,
iii. Cooling regime, rate of cooling,
iv. Strength recovery duration following cooling.

Following conclusions can be drawn after a detailed study of experimental results available in the literature [Kumar and Kumar (2003), Abrams (1977), Carvel (2005), Lie and Irwin (1993), Lie and Kodur (1995), Liu et al. (2010), Ayman (2006)]

- High strength concrete (HSC) beams have lower fire resistance Normal strength concrete(NSC) beams,
- Type of fire scenario, axial restraints and load level have significant influence on the overall fire resistance of RC beams,
- HSC has faster degradation of strength and stiffness at the elevated temperature,
- Permeability and load ratio plays significant role in spalling of concrete,
- Lower load level leads to higher fire resistance,
- Maximum temperature within the RC elements is not necessarily found during the heating phase i.e., temperature inside an element keep rising for some time even after the furnace temperature starts to fall.

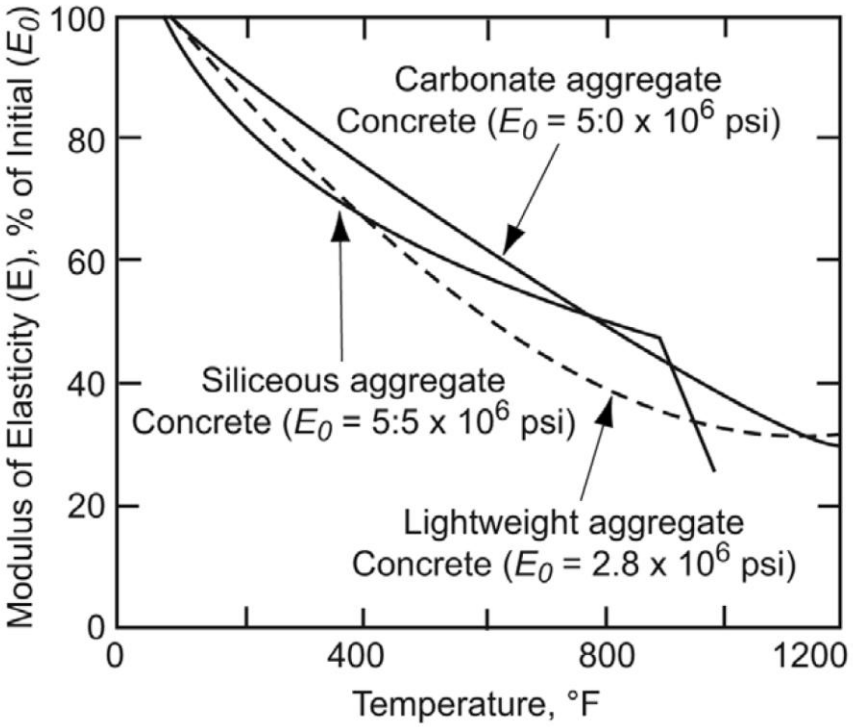

Fig. 1.15 Change in the modulus of elasticity of concrete due to high temperature, (Bilow and Kamara, 2008)

1.2.7 Spalling of Concrete at Elevated Temperature

Spalling may be regarded as one of the most complex and least known behavior of concrete under elevated temperature (Khoury, 2000). Canisius et al., (2003) conclude that spalling is not only restricted to higher temperature, it may occurs at 200°C. In case of severe spalling, reinforcement may also get exposed leading to enhanced rate of heating it. Hence, it may lead to the decline of reinforcement strength and a deterioration of the mechanical properties of the whole. Moreover, spalling also reduced the strength of the structure against imposed loading due to reduce in the cross-section. Thus spalling may affect the overall behavior of structure before start of any other fire induced effect.

The mechanism of spalling is built-up of high pressure within the concrete due to evaporation of moisture content. Hence, with sudden formation of cracks and chunks concrete begins to dissipate the stress leading to spalling. High strength and high performance concrete is more prone to spalling due to lesser porosity and moisture absorbance capacity, Khoury (2000).

1.2.8 Behavior of Reinforcing Steel under High Rate of Loading

The steel bars used as the reinforcement (generally abbreviated as rebar) may be classified in the different groups, Cadoni et al., (2012, 2013);

a) cold drawn rebar (used as mesh and/or as stirrups),
b) hot rolled rebar (used as rebar),
c) stainless-steel rebar (used in harsh environmental conditions),
d) quenched and self-tempered rebar (generally used as principal reinforcement).

Due to high strength and efficient ductility the quenched and self-tempered rebar is extensively used in reinforced structures. The experimental and numerical studies of the structural steel Weldox 460 E has been studied in literatures, (Børvik et al., 2001, 2002 and 2003; Hopperstad et al., 2003). In the present study material parameters for constitutive modeling has been considered from Borvik et al., 2002. In order to study the collective effects of strain rate as well as stress triaxiality on Weldox 460 E, Hopperstad et al., 2003 conducted tests at high strain rates in a Split Hopkinson Tension Bar. They reported that the strength of material increase with increasing strain rate, while on the ductility, effect of strain rate could be ascertained significantly . Effect of tempering temperature, plate thickness and presence of holes on ballistic impact behavior and ASB formation of a high strength steel had been studied by Mishra et al., (2012).

Experimental investigation of Weldox 460 E steel at high strain rates and elevated temperatures with high stress triaxiality using Split Hopkinson Tension Bar has been performed by Borvik et al., 2005. The strain rates were varied between 500 and 1500 s^{-1}, while the initial temperature were varied between 100 and 500 °C. The influence of temperature on the stress–strain behavior were significant at high strain rates compared with quasi-static loading conditions. Engineering stress–strain curves obtained with smooth specimens at different initial temperatures and initial loading condition are presented in Fig. 1.16. It has been reported that initial loading equal to 20 kN gives nominal strain-rate between 450 and 550 s^{-1}, while a 40 kN initial loading results in nominal strain-rate between 1300 and 1400 1/s. It has been concluded that strength as well as elongation to fracture decrease with increase in temperature, while the strain hardening increases slightly, Fig. 1.16.

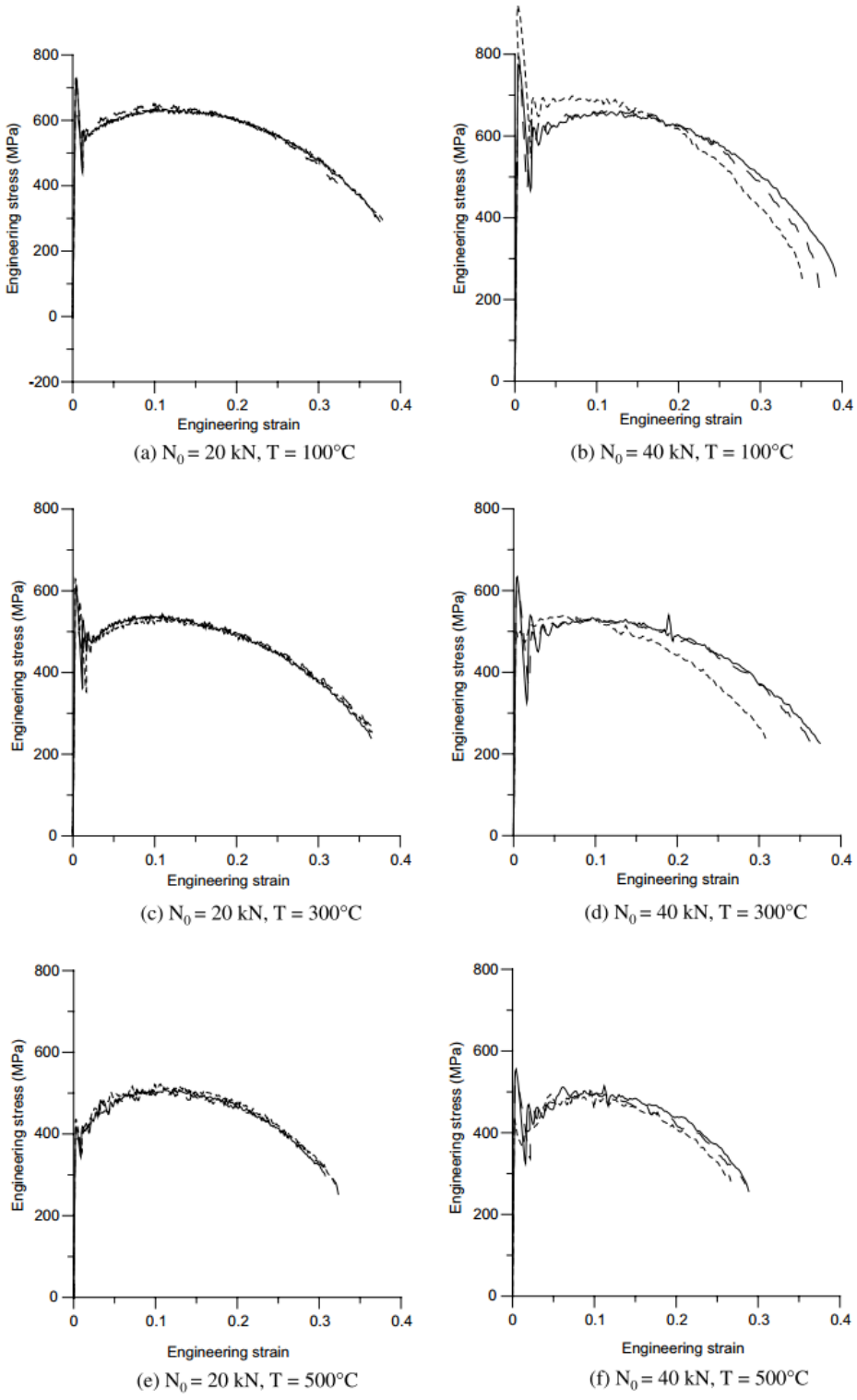

Fig. 1.16 Engineering stress–strain curves for smooth specimens, (Borvik et al., 2005).

1.2.9 Behavior of Reinforcing Steel at Elevated Temperature

Under high temperatures strength and stiffness of steel deteriorate in a manner similar to that of the concrete (Freskakis, 1980). Topcu and Karakurt (2008) have reported that the deterioration of yield strength and modulus of elasticity of steel bars is considered as the primary element affecting the performance of RC structures in fire. They have suggested that the protective cover thickness should be higher for increasing the fire safety of RC members. There is one third reduction in the yield strength of the conventional steel at 600°C, (Unluoglu et al., 2007). Reduction in the stiffness and strength of steel at elevated temperature depends on their manufacturing process (Anderberg 1978, Buchanan 2001, Eurocode-2 2004). Felicetti et al., (2009) experimentally found that above 600°C quenched and self-tempered bars are more sensitive than carbon-steel bars. Elghazouli et al., (2009) performed experimental investigation on steel reinforcement at ambient temperature as well as under steady-state and transient elevated temperature conditions. After exposure to higher temperature levels, there is a reduction in strength reaching 10-15% in the case of cold-worked bars for 600°C.

The bond characteristics between steel reinforcement and concrete are important when modeling global behavior and predicting reinforcement fracture at ultimate failure (Giroldo and Bailley, 2008). However, Bingo and Gul (2009) investigated that bond strength between concrete and steel increases up to 150°C and then decrease with further increase in the temperature. The yield strength of the steel reinforcement is also reported to be reduced at elevated temperature. The change in the yield strength of steel with respect to temperature has been shown in Fig. 1.17. The degradation of modulus of elasticity with temperature was plotted in Fig. 1.18.

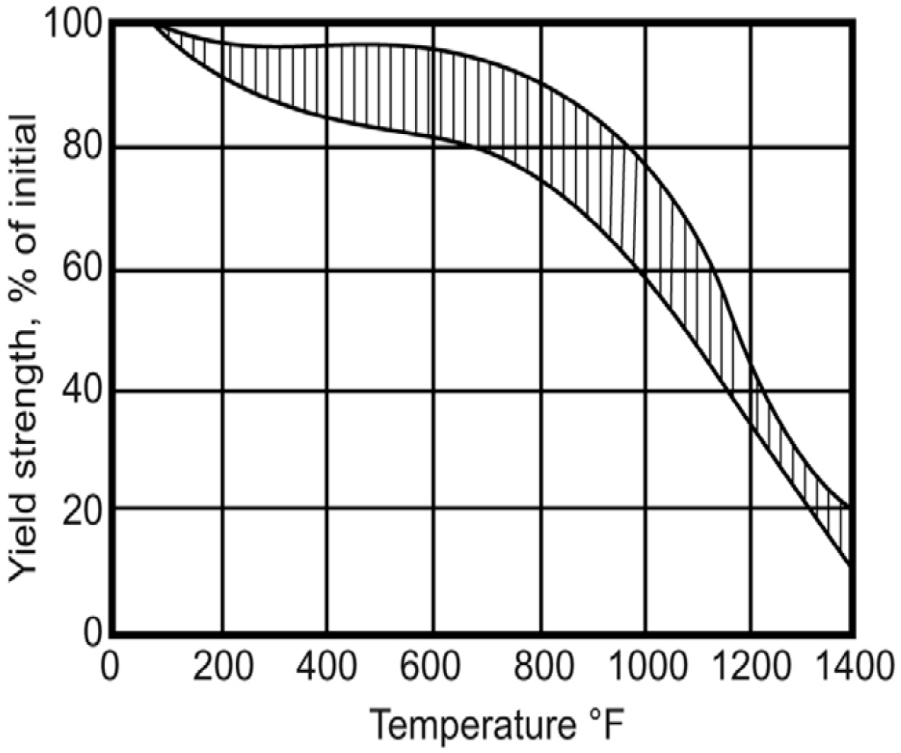

Fig. 1.17 yield strength versus temperature elevation for steel reinforcement, (Bilow and Kamara, 2008)

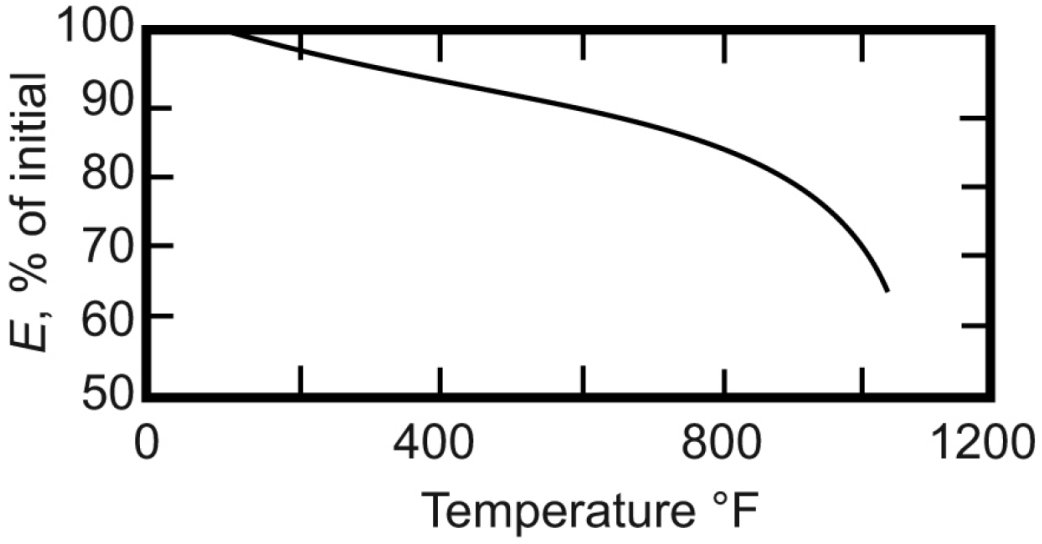

Fig. 1.18 modulus of elasticity versus temperature elevation for steel, (Bilow and Kamara, 2008)

1.3 GAPS IDENTIFIED

The studies mentioned above lead to the conclusion that the subject of nuclear containment under aircraft crash has been significantly studied in the last few decades in order to comprehend the response of nuclear containment structure. The researchers have adopted different approaches to study the performance of the existing containment structures against the deliberate and accidental crash. They have also suggested the section adequacy to avoid the breach of the containment. The probabilistic approaches have been used to estimate the possibility of aircraft crash. The numerical modelling and simulation of the problem has been refined over a period of time.

As such the reaction-time approach is well established for the design and analysis of nuclear containment structures against aircraft crash. However, the accuracy of the available reaction-time responses has to be reconsidered keeping in view the deformability, curvature and material of the target. Further, the surface area for the application of the reaction-time curve has to be evaluated systematically. As per the recent practice the average cross-sectional area of the aircraft is considered to be the contact area. However, the contact area is actually a time dependent variable, averaging it to obtain a constant circular impact region will result in the overestimation of the damage intensity and underestimation of the damage vicinity. Therefore the area of impact for the fuselage and wings shall have to be segregated in order to accurately determine the intensity and proximity of the damage.

It is a general opinion that aircraft-crash-induced fires involve very high uncertainty and complexity from fire scenario to fire analysis and assessment. The methodology for measuring the endurance of nuclear structures against large fire scenario has not been established yet. Presently, the fire induced by aircraft crash has not been considered a design criterion (Jeon et al, 2012). Therefore extensive research is required in the field of fire and blast induced due to aircraft crash to follow up the standard safety requirements.

1.4 OBJECTIVE AND SCOPE OF PRESENT STUDY

The safety of the nuclear containment structure against various kinds of threats has always been a topic of research. The studies addressing the aircraft crash problem have also been attempted from the beginning of nineteenth century. However, the intentional aircraft crash had

not been considered to have occurred before September 2001 attack on World Trade Centre and hence, the seriousness of this subject was realized after this incidence.

The studies have also been carried out to understand the material behavior of concrete as well as other ductile materials under varying strain rate and temperature. Various constitutive models were developed and validated through small scale experimentation. They have also been employed in studying the response of nuclear containment structures against aircraft crash. However, the coupled analysis of such structures remains a complex issue due to the fact that the exact modeling of aircraft geometry and material is essentially impossible. Thus the problem can be evaluated using the uncoupled analysis approach which is simpler and computationally inexpensive.

The present research problem has been identified as the impact of aircraft over the outer containment of a BWR Mark III nuclear power plant. The finite element simulations have been carried out to study the response of containment structure against commercial and fighter aircrafts. The containment was modeled as a three-dimensional deformable reinforced concrete structure. For the initial investigation the loading of aircraft was applied using the available reaction-time response curves. The effect of strike location on the containment structure has been studied. The most vulnerable location has been identified and selected for further investigation with different types of aircrafts. These studies led to the conclusion that the reaction time approach to obtain the containment response is simpler and effective. However, the current methodology for the evaluation of reaction time curve is unrealistic and needs careful investigation.

Thus the basic assumption of flat and rigid target has been reevaluated by studying the influence of target curvature and flexibility on the reaction-time response. The geometric model of aircraft Boeing 707-320 and Boeing 747-400 was developed using ABAQUS/CAE and the reaction-time response has been obtained against flat rigid target. The reaction-time response thus obtained has been validated through the analytical expressions available in literature. The geometric model of aircrafts was also impacted on the rigid targets of varying curvature. The reaction-time response obtained against the curved rigid and flexible targets has been compared.

The effect of contact area of the aircraft on the response of containment has also been studied. The contact area versus time curve was obtained by hitting the geometric model of aircraft on the flat rigid target. The response of containment was obtained by two different approaches. In the first approach the average of the total contact area was considered for the application of load. In the second approach the contact area was trifurcated i.e., fuselage, first set of engines and second set of engines, and the loading was applied at the corresponding location. The response of containment obtained through the average and trifurcated surface areas was then compared with that obtained against geometric model of aircrafts. All the above simulations were carried out in using the explicit solution technique available in ABAQUS finite element code.

The effect of fire induced due to aircraft crash has also been studied against Boeing 707-320 and Boeing 747-400 aircrafts. The reaction-time response curve obtained against curved flexible target was applied on the surface area of the containment based on the average area method discussed above. The impact of aircraft was considered to occur up to the point the engines came in contact. Thereafter the fire was assumed to have spread since the majority of the aircraft fuel is stored in and around the wings. The fire effect was considered to be most severe at at the bottom of containment up to 10 m height from the base. This is due to the fact that most of the fuel will flow down to the bottom of containment. Between these two extreme regions however, moderate fire effect was considered. The heat transfer analysis has been carried out to obtain the nodal temperature in the concrete as well as reinforcement elements. The fire duration has been considered to be 2hrs for Boeing 707-320 and 3hrs for Boeing 747-400.Thereafter, thermal stress analysis has been performed considering the deformed geometry of the containment due to aircraft impact as the initial state. The simulations to study the induced fire effects were carried out using implicit technique of ABAQUS finite element code since the heat transfer analysis was not supported by the explicit solution technique available in ABAQUS.

1.5 ORGANISATION OF THESEIS

The thesis has been organized in six chapters

In the present chapter; a general introduction of the problem has been given. Complexity and importance of different issues related to the problem have been discussed. The review of

literature is divided in three zones i.e., analytical, experimental and numerical studies. The different methodologies adopted for the analysis of the problem have been categorized. The assumptions and limitations of the available studies have also been discussed. The literature pertaining to the behavior of reinforced concrete under high strain and temperature has also been discussed. The research gaps have been identified and scope of the present study has been provided.

Chapter 2 describes the geometric modeling and finite element discretization of aircrafts as well as containment structure. The characteristics of aircrafts and containment were presented. Issues related to type and size of mesh has been discussed. Detailing of interaction and boundary conditions were provided in this chapter.

Chapter 3; This chapter deals with the constitutive modeling of aircrafts and containment structure. The basic concepts of constitutive models for concrete, reinforcement and aircraft were discussed. The detail regarding material properties under high stain rate loading and elevated temperature has been described.

The results and discussion part has been divided in three sections.

Chapter 4; This chapter describes the response of the BWR Mark III type nuclear containment against reaction curve of the aircrafts. The influence of strain rate and strike location on the response of containment structure has been studied. Observations of comparative studies of strain rate, strike location and different aircrafts has been discussed in detail.

Chapter 5; In this chapter the reaction time response curve was re-evaluated with incorporating the target characteristics. Validation of geometric models of aircrafts has been performed. The effect of target curvature and flexibility has also been studied. The response of containment has been compared against geometric model of aircraft and reaction time response curves. Effect of area of impact on the response of containment has also been assessed.

Chapter 6; This chapter elaborates the effects of crash induced fire. The detail of the heat transfer and thermal stress analysis has been discussed. Fire effects due to both Boeing 707-320 and Boeing 747-400 has been presented.

Chapter 7; This chapter summaries the entire work of this thesis in a concise form. The summary is followed by the conclusions of the present study and the scope of future research.

The last part of this thesis consists of bibliography and list of publication.

Chapter 2

GEOMETRIC AND FINITE ELEMENT MODELLING

2.1 GENERAL

The nuclear containment and aircraft are huge and complex structures. The detailed geometric and finite element modeling of each of their components are highly complex however it governs the accuracy of the finite element simulation. It is therefore pertinent to discuss the critical aspects of the problem related to modeling, interaction and discretization. The present study addresses a detailed investigation of the nuclear containment structure subjected to aircraft crash. Thus the problem includes the modeling of some deformable and non-deformable structures. The deformable structures include Boeing 707-320, Boeing 747-400 aircrafts and the nuclear containment structure. The aircrafts have been modeled as a three dimensional deformable shell, the concrete structure of the nuclear containment as three dimensional deformable solid whereas the reinforcement as three dimensional deformable wire. The non-deformable structures include rigid surfaces employed to evaluate the reaction time response of aircrafts that was subsequently applied on the containment structure in order to terminate the coupled analysis. The modeling and meshing of the problem was carried out using ABAQUS/CAE.

2.2 BOEING 707-320 AIRCRAFT

The Boeing 707-320 aircrafts are comparatively old, however, they have been considered to be the bench mark in the literature to study the crash response of the nuclear containment structures. Thus in order to validate the preliminary simulations the present problem was also initiated from the study of Boeing 707-320 aircraft. However, there are issues discussed in the present study pertaining to this aircraft which have not been dealt earlier.

The commercial aircrafts of 707 series of Boeing was introduced in service in 1958. Its introduction to aviation industry revolutionized the air voyage with jet speed, long range and high seating capacity. The 707 series also laid the foundation for Boeing's dominance in the commercial airliner market. The Boeing 707-320 is one of the few variants of 707 series. A brief geometric description of Boeing 707-320 aircraft has been presented in Table 2.1 and the detailed drawings are shown in Fig. 2.1 (*Boeing, 2013*).

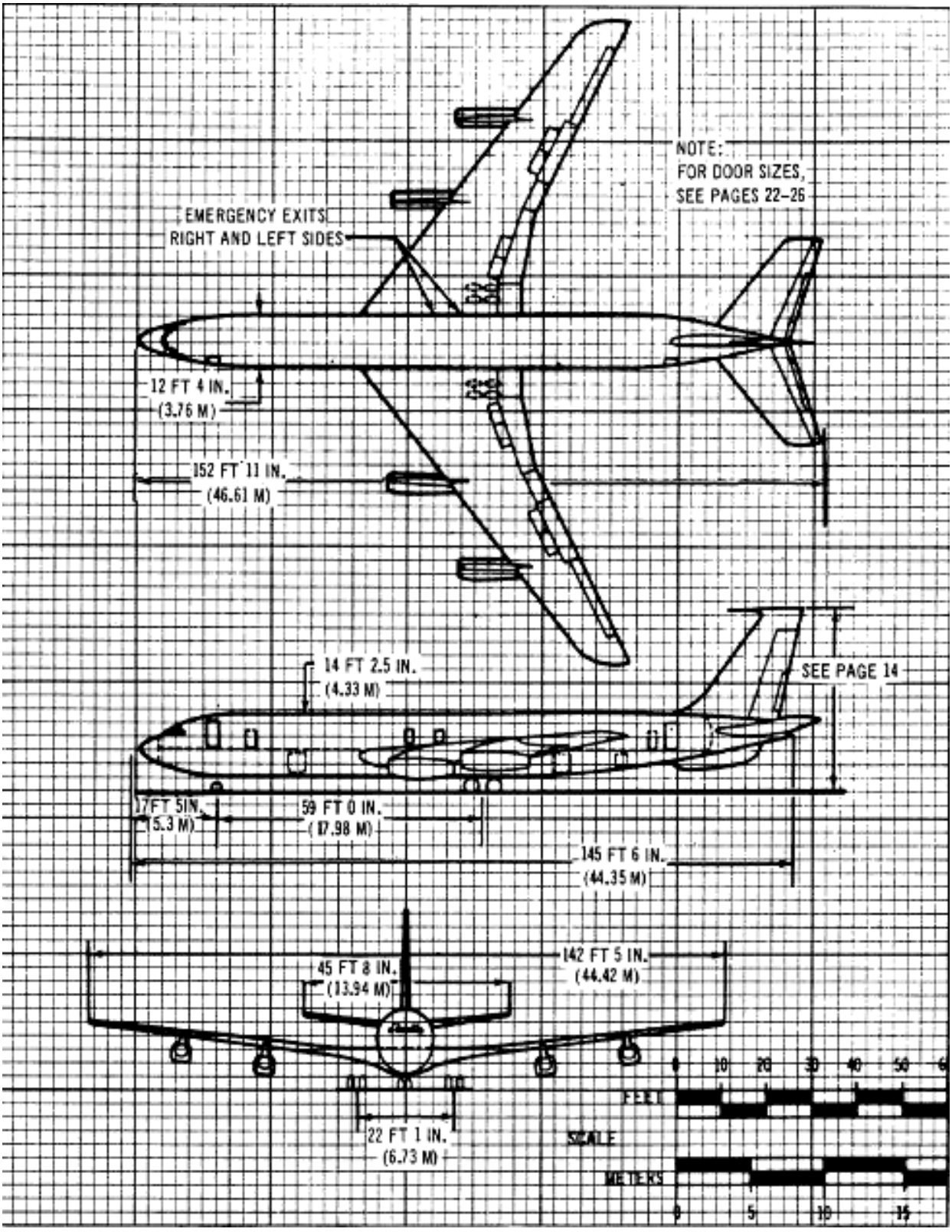

Fig. 2.1 Geometric detail of Boeing 707-320

Table 2.1 Boeing 707-320 Specification

Wingspan	145 feet 9 inches (44.42 m)
Length	152 feet 11 inches (46.6 m)
Wing Area	3,010 square feet (280 m^2)
Gross Weight	336,000 pounds (152,400 kg)
Cruising Speed	607 mph (977 km/h)
Range	6,160 miles (9,913 km)
Passenger Cabin	141 passengers mixed class/ 189 economy

2.2.1 Modeling of Boeing 707-320

The Boeing 707-320 has approximately 46 m length and two engines at each wing as shown in Fig. 2.2. The fuselage, wings, engines and tails of the aircraft are modeled separately with the help of Fig. 2.1 and Fig. 2.2. Finally all these parts were assembled at their respective co-ordinates. The aircraft body was subsequently partitioned into small regions to enable appropriate meshing. The components of aircrafts comprising of simple geometry have been meshed with structured elements, highlighted in green in Fig. 2.3. However, those comprising of complex geometry for example engines and nose have been meshed with a combination of structured and non-structured elements highlighted in pink, Fig. 2.3. Some parts of the wings and fuselage being in the vicinity of other complex regions could also not be meshed with structured elements.

Fig. 2.2 Boeing 707-320

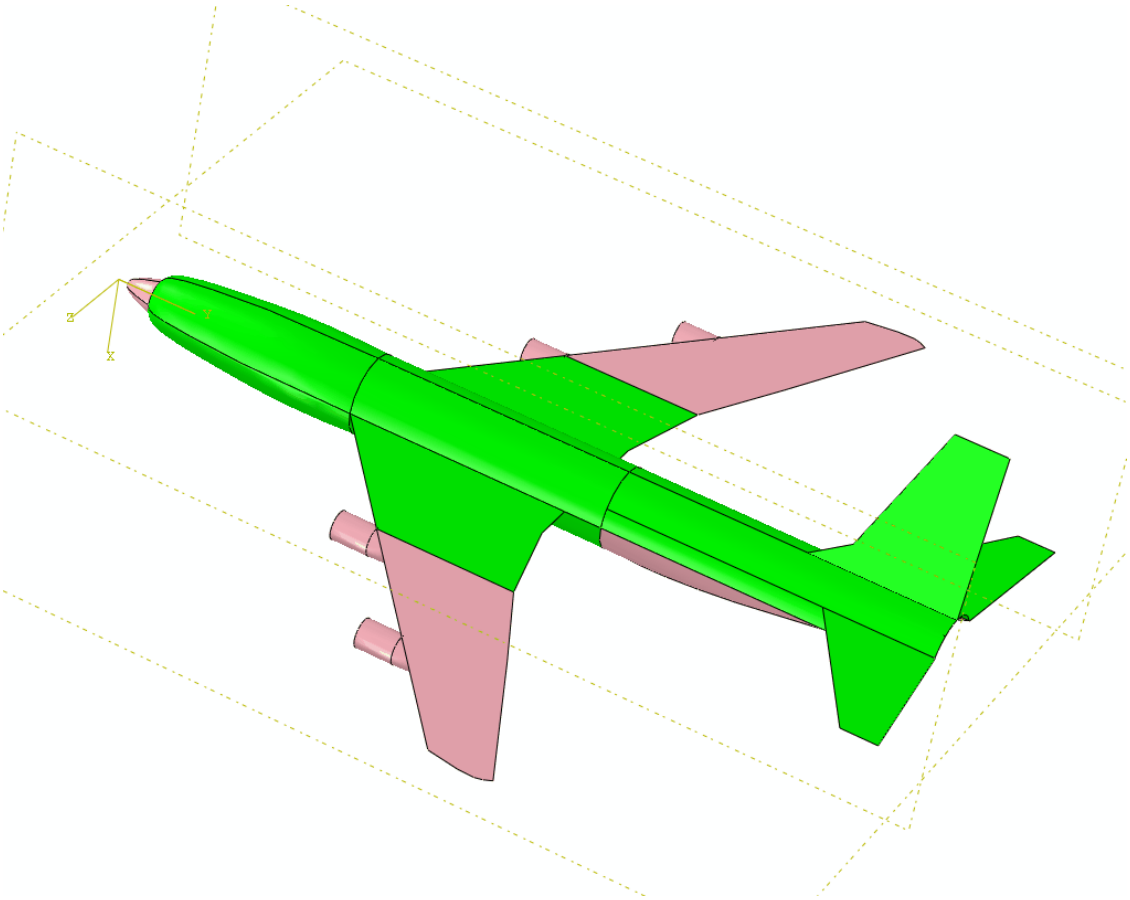

Fig. 2.3 Partition for meshing of Boeing 707-320 geometric model

2.2.2 Meshing of Boeing 707-320

As the finite element solver uses a large memory to run the simulation and store the numerical data, significant efforts were made to restrict the number of elements within the efficiency of available computational facility. The size and shape of the elements has been decided after properly studying the mesh convergence. The warping and distortion of the elements has been reduced to minimum. In general the size of element was considered to be 20 cm^2 for all the components of aircraft except engines. The engines were meshed with comparatively finer elements, 2.5 mm^2, in order to avoid warping of elements due to their highly nonlinear geometry. A total number of 157950 elements were assigned to the aircraft with a total number of 157127 nodes. Most of these elements were linear quadrilateral elements of type S4. However, the nose, engines and some other transition regions have been meshed with a combination of S4 and S3R due to nonlinear geometry and compatibility problems. The detailed meshing of Boeing 707-320 aircraft is highlighted in in Fig 2.4.

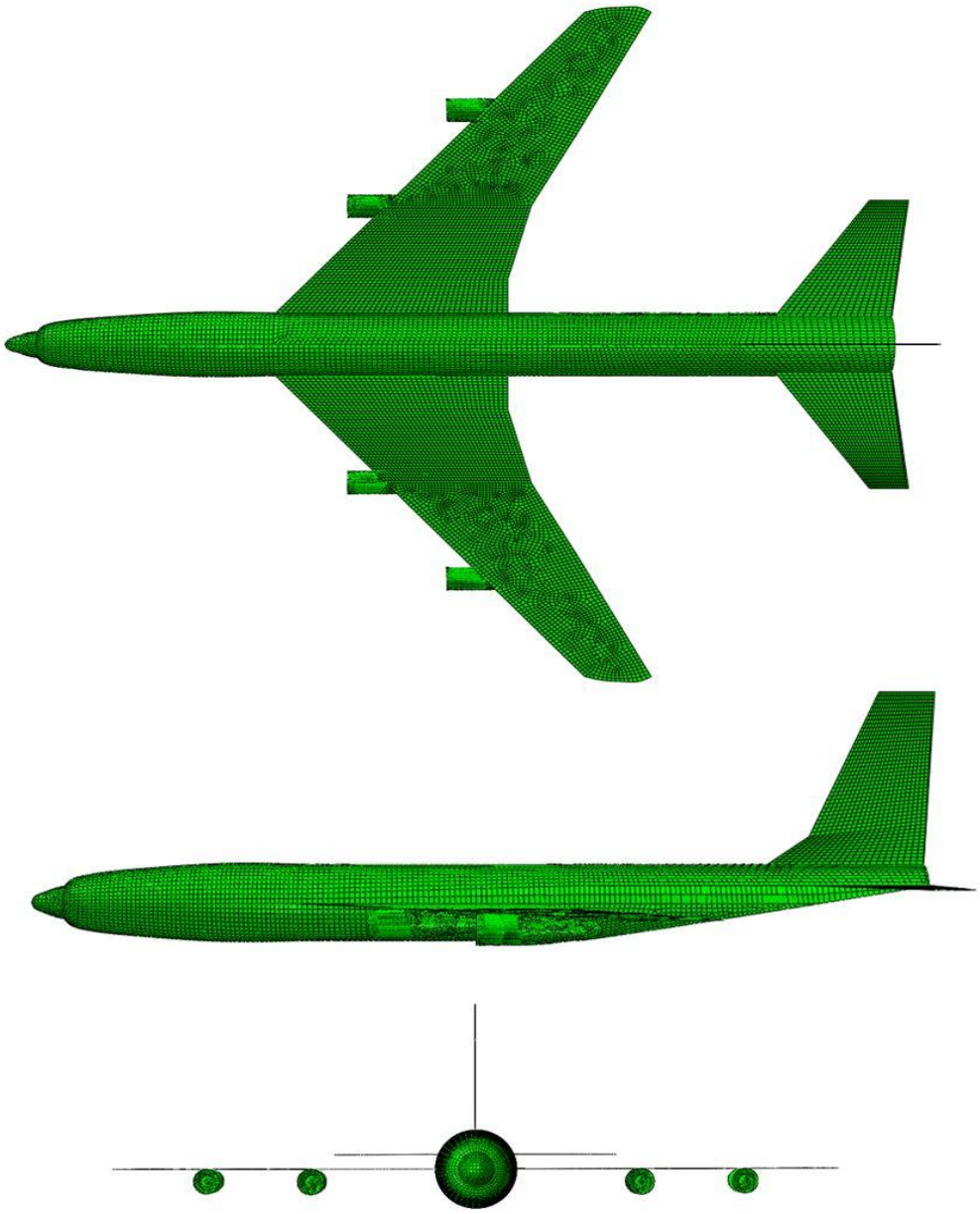

Fig. 2.4 Mesh detail of Boeing 707-320

2.3 BOEING 747-400 AIRCRAFT

The airplane Boeing 747-400 is one of the latest aircraft with longest range and highest sold model of Boeing 747 family. The Boeing launched 747-400 in April, 1988. While retaining the four-engine wide-body layout of its predecessors, the 747-400 embodies numerous technological and structural changes to produce a more efficient airframe. Its most distinguished

features are 6-foot (1.8 m) winglets mounted on 6-foot (1.8 m) wing tip extensions. The Boeing 747-400 is equipped with a two-crew glass cockpit, along with more fuel-efficient engines, a horizontal stabilizer fuel tank, and revised fuselage/wing fairings. The aircraft also features an all-new light weighted interior with upgraded in-flight entertainment architecture. The model has a maximum capacity of 660 passengers and can fly non-stop for up to 7,670 nautical miles (14,200 km). A brief geometric specification of the Boeing 747-400 has been tabulated below, see Table 2.2.

Table 2.2 Boeing 747-400 geometric specifications

Wingspan	64.4m
Length	70.7m
Height	19.4m
Seating	365 seats
Gross Weight	394,600kg
Maximum Speed	910km/h (M0.85)
Altitude capability	13,700 m
Range	12,370 km
Take off Distance	3,580 m
Landing Distance	2,300 m
Fuel Capacity	56,940 U.S.G.
Engine Horsepower	26,310 kg x 4

2.3.1 Modeling of Boeing 747 -400

The Boeing 747-400 was modeled using three dimensional deformable shell. Different parts of the aircraft such as nose, front wing, main fuselage, engine, rear wing etc., were modeled with exact geometric description provided at Boeing website, Fig. 2.5, and then assembled together using ABAQUS/CAE. The geometry of the aircraft was partitioned subsequently for proper discretization, see Fig. 2.6.

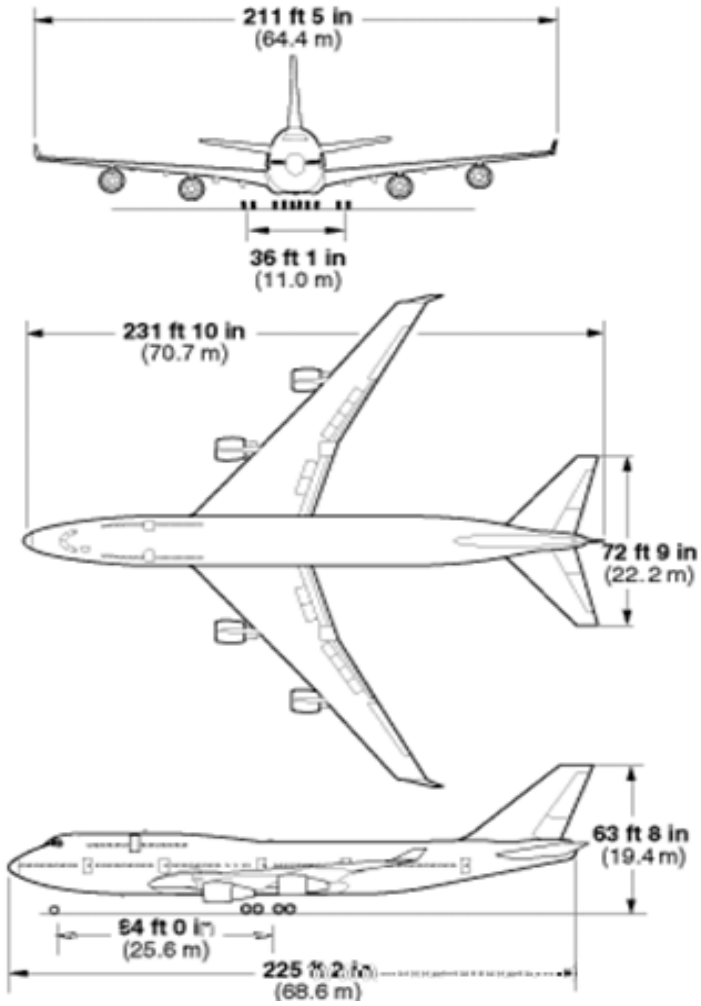

Fig. 2.5 Boeing 747 -400 Geometrical Dimensions and its model made in Abaqus/CAE

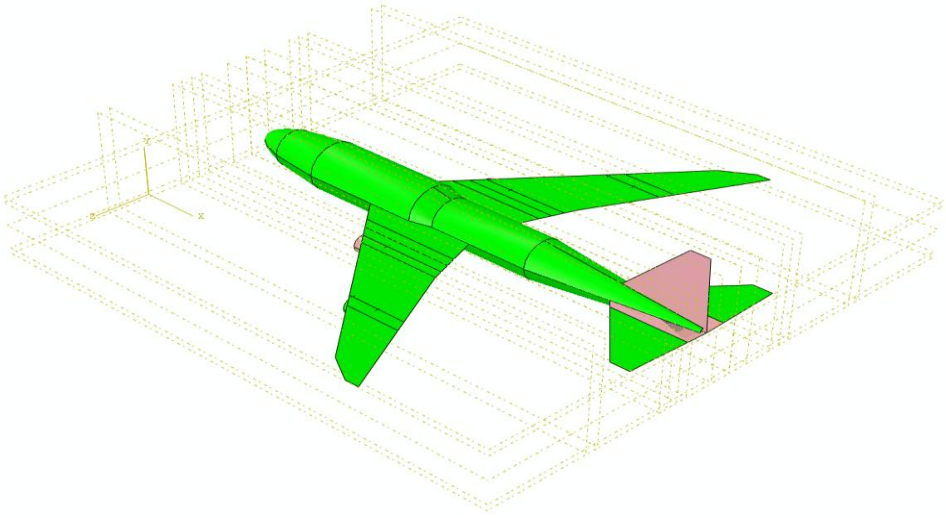

Fig. 2.6 Partition for meshing of Boeing 707-320 geometric model

2.3.2 Meshing of Boeing 747 -400

The structured meshing was preferred in general, however, in a few regions due to complex geometry non-structured meshing has been done. The number of elements has been kept within efficiency of the available machines, however, the mesh convergence has been performed and the number of warped and distorted elements has been reduced to minimum. After a number of trials the overall size of element was considered to be 20 cm^2. A total number of elements adopted in the body of aircraft were 190689 with a total number of 187127 nodes. Most of these elements were linear quadrilateral of type S4, however, in the transition and complex regions S3 elements were also assigned. A detailed meshing of aircraft Boeing 747-400 is highlighted in Fig. 2.7.

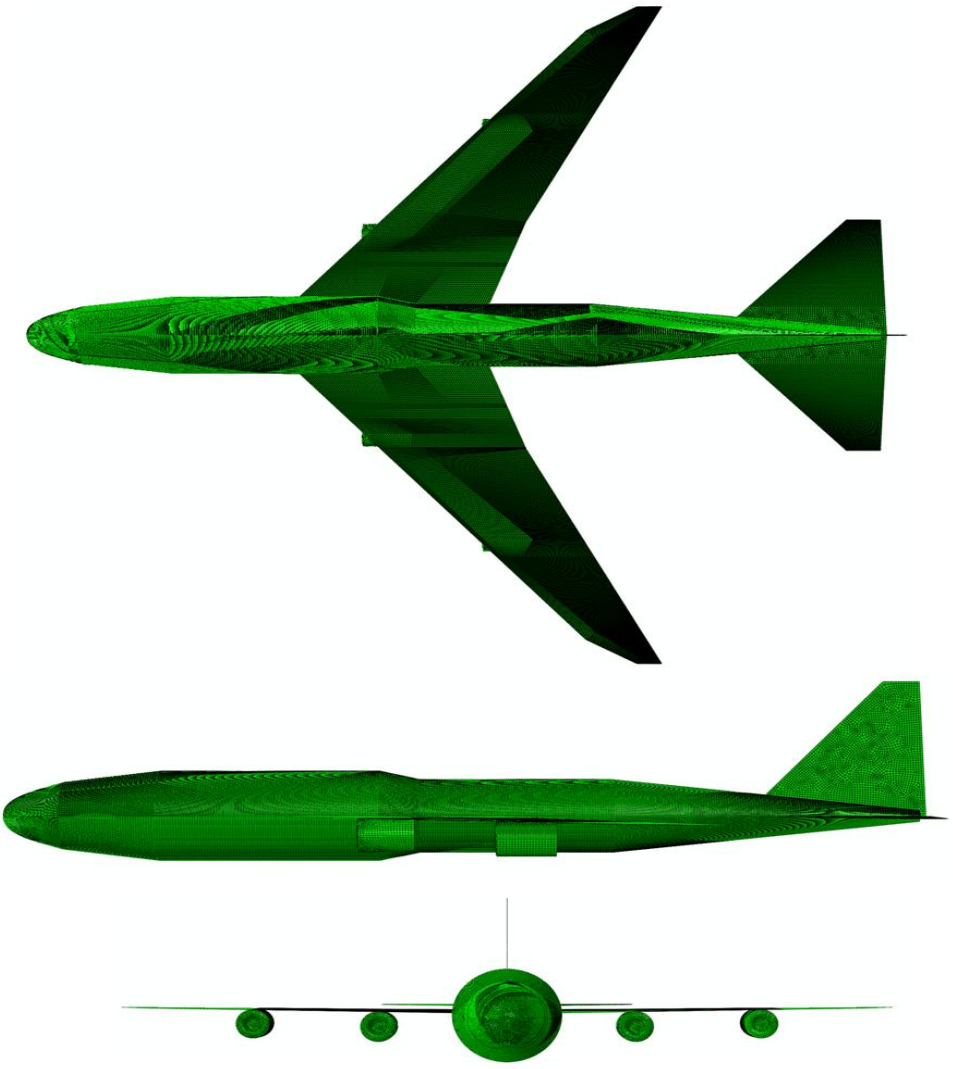

Fig. 2.7 Mesh detail of Boeing 747-400

2.4 NUCLEAR CONTAINMNET BWR MARK III

In nuclear power reactors, containment systems have variation in size, shape, materials and suppression systems. The kind of containment used is determined by the class of reactor and the specific plant requirements. The outer containment of a typical BWR Mark III type containment has been considered in the present study. The BWR Mark III is a modern evolved model of Boiling Water Reactors Nuclear Power Plants.

2.4.1 Modeling of Outer Containment

A three-dimensional model of the containment was made using preprocessing module of ABAQUS. The outer containment of a typical nuclear power plant BWR Mark-III type, has been considered in the present study. The geometric model of the containment has been considered identical to that of the Abbas et al. (1996). The containment has a semi-spherical dome supported on circular cylindrical wall of inner diameter 42 m and thickness 1.2 m. The wall thickness has been assumed to be constant throughout the containment building in accordance with Abbas et al. (1996). The total height of the containment was 67 m while that of the cylindrical wall 46 m. The containment has been modeled half along its circumference when the loading of aircraft has been assigned through reaction time curve, Fig. 2.8(a). This is due to the fact that the loading and geometry both are symmetric in this case. The containment has therefore been assigned symmetric boundary conditions. However, when the geometric model of the aircraft has been hit on the containment, the problem may not remain symmetric and therefore the whole containment has been modeled along with the aircraft. However, due to the geometric modeling of aircraft as well as containment the problem became computationally very expensive. Thus, in order to make it feasible for simulation the dome has been replaced with that of the flattened surface, Fig. 2.8(b). The base of the containment has been assumed to be fixed with respect to all degrees of freedom.

2.4.2 Modeling of Reinforcement

The containment structure is doubly reinforced with Ø 40 mm bars placed at 80 mm c/c both ways at the inner and outer faces of the cylindrical wall as well as the spherical dome. The

effective cover to concrete was assumed to be 100 mm. The reinforcement modeled as 3D wire was placed in the structure using linear/radial pattern option available in ABAQUS/CAE. The modeling of reinforcement in the outer face of the containment structure is shown in Fig. 2.9 for both the containment with dome and flattened top.

The contact between the concrete and the reinforcement was modeled using embedded element technique available in the ABAQUS finite element code. This technique enables the user to model the constraint between a group of elements embedded inside a group of host elements. The response of host element was used to constrain the translational degree of freedom of the embedded elements and a perfect bonding between the host and embedded element is assumed. The various constraints and interactions have been discussed in detail in section 2.5 of the present chapter.

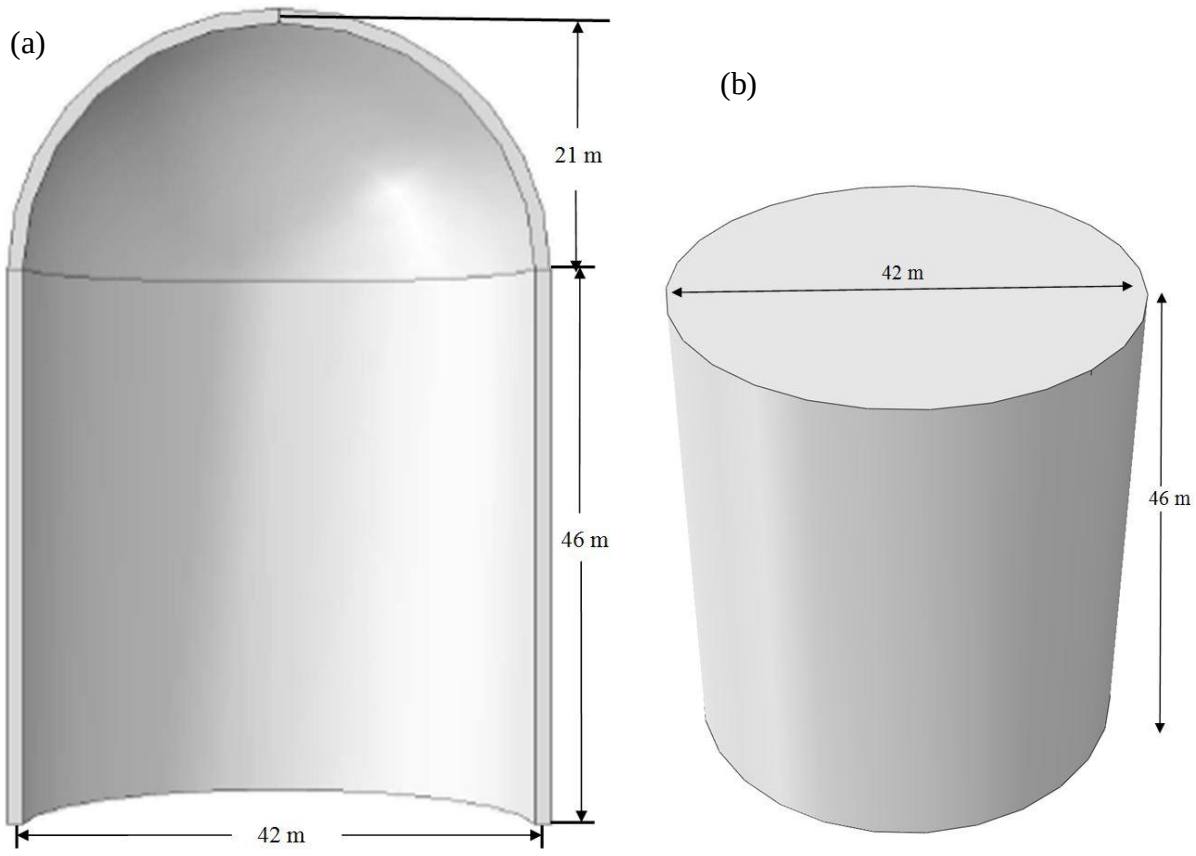

Fig. 2.8 outer containment of BWR Mark III type NPP (a) with dome (b) without dome

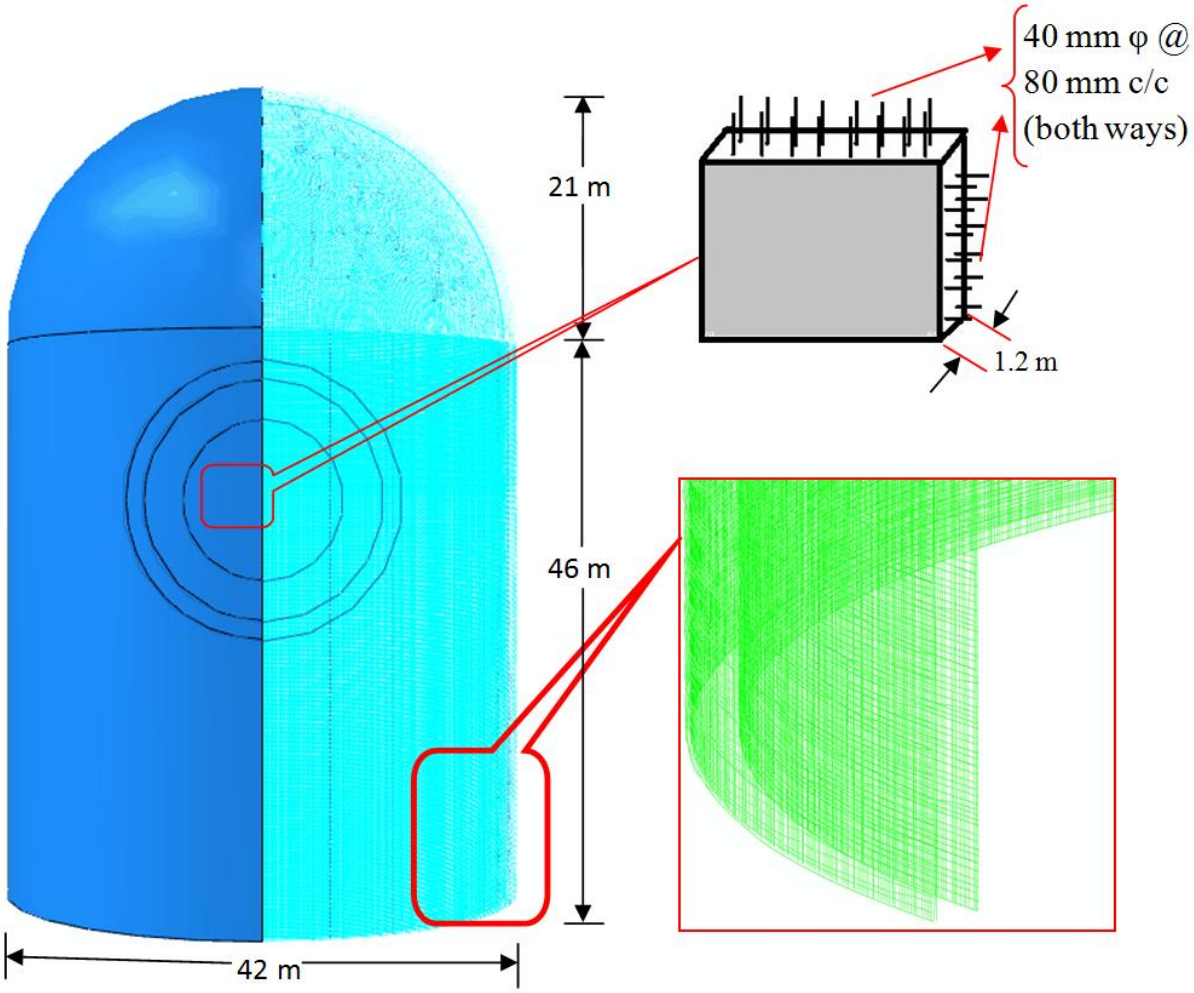

Fig. 2.9 Reinforcement details of outer containment structure of NPP

2.4.3 Meshing of Containment with Dome

The geometry of the containment was divided into various regions for an appropriate meshing. The meshing was carefully done in order to achieve accurate results within optimum time as well as to avoid the excessive distortion of the elements. The detail of meshing for the containment with dome is shown in Fig. 2.10-2.12.

The containment with dome has been meshed in two distinct manner based on the size of aircraft. The central circular region of the containment subjected to aircraft loading, identified as

"R-I" [Figs. 2.10 and 2.11] was meshed with three-dimensional, reduced integration, 8 node brick elements. The size of element was 120 mm x 120 mm x 120 mm giving 10 elements at the containment thickness with unity aspect ratio. The diameter of R-I was considered 6 m for Boeing 707-320, Phantom F4 and Airbus A-320 aircrafts, Fig. 2.10. For Boeing 747-400 and Boeing 767-400 aircrafts however, the diameter of R-I was considered 12 m due to the larger cross-section of their fuselage, Fig. 2.11.

The next region R-II, in Fig. 2.10, was considered as a transition region in order to vary the size of elements between region R-I (120 mm x 120 mm x 120 mm) and R-III (600 mm x 600 mm x 600 mm) without affecting their aspect ratio. As a result of which the region "R-II" was meshed with tetrahedral elements of edge size varying from 120 mm (at the inner periphery) to 600 mm (at the outer periphery). The region R-III comprising of the whole body of the containment, except R-I and R-II, was meshed with the three-dimensional 8 node brick elements of size 600 mm x 600 mm x 600 mm.

In Fig. 2.11 there is a region between R-I and R-II, designated as R-IB, the elements of this region are identical to those of R-I with slightly larger size (300 mm x 180 mm x 120 mm). This region was considered in order to avoid the excessive distortion of the elements that was prominent in this case at the interface of R-I and R-II as well as R-II and R-III. Except this, the meshing in Fig. 2.11 is almost identical to that of Fig. 2.10.

The meshing of the reinforcement of the containment with dome has been described in Fig. 2.12. The reinforcing bars were discretized with 2 node three dimensional truss element of 600 mm length throughout the containment along the circumferential and meridonial directions.

A mesh convergence study was carried out wherein the size of concrete element was varied as 150 mm x 150 mm x 150 mm, 120 mm x 120 mm x 120 mm and 100 mm x 100 mm x 100 mm in the impact region (R-I), Fig. 2.10, and hitting the containment by Boeing 707-320 aircraft. The maximum nodal deformation in the impact region was found to be 90.82 mm, 89.96 mm and 89.6 mm respectively. For reinforcement however, the element size was finally selected to be 600 mm based on the convergence of results and the efficiency of the available computational facility.

The total number of elements employed for the discretization of concrete was 78838 for the containment shown in Fig. 2.10. Among them, 39072 elements were C3D8R (three dimensional eight node linear brick) and 39766 elements were C3D4 (linear tetrahedral). However, for containment shown in Fig. 2.11 the total number of elements employed for the discretization of concrete was 110854 including 90574 C3D8R elements (linear hexahedral brick) and 20280 C3D4 (linear tetrahedral). The reinforcement was discretized in to a total number of 435802 linear wire elements, T3D2. The total number of elements for the reinforcement was identical for the containments shown in Fig. 2.10 and 2.11.

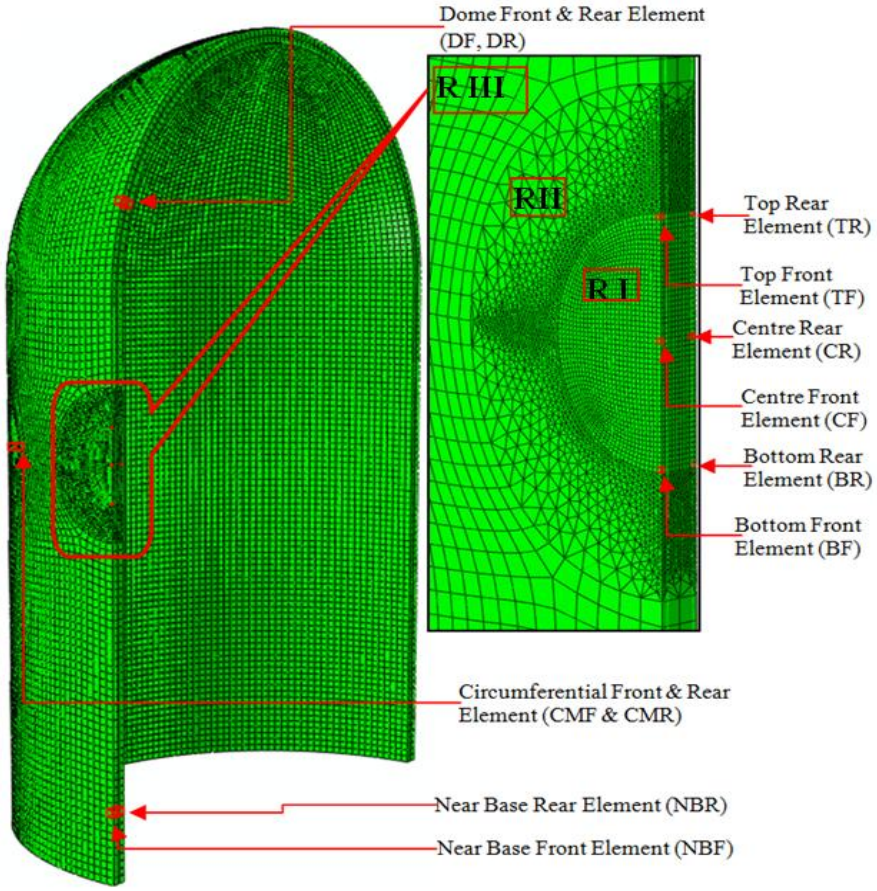

Fig. 2.10 Discretization of the containment subjected to impact by Boeing 707-320, Airbus A320 and Phantom F4

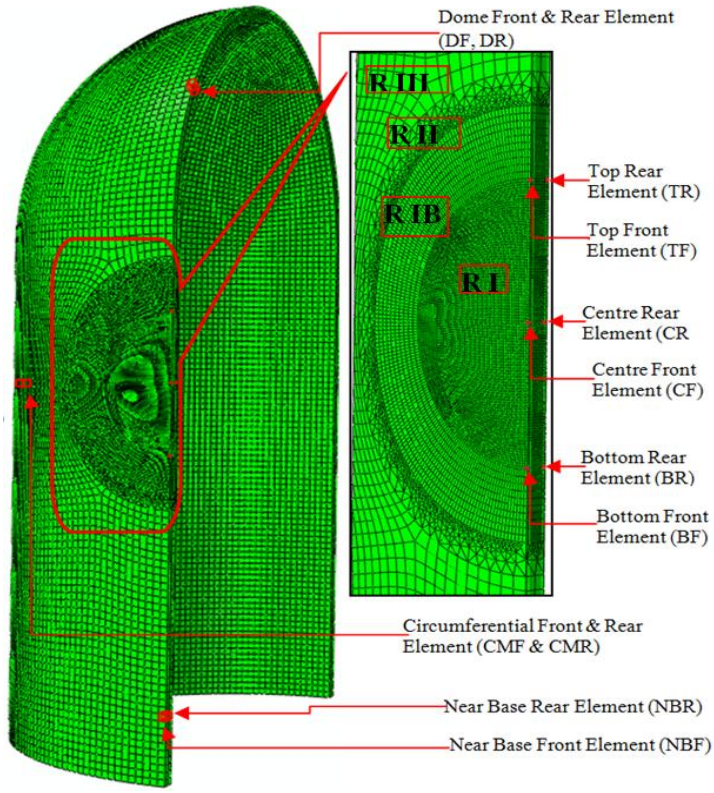

Fig. 2.11 Discretization of the containment subjected to impact by Boeing 747-400 and Boeing 767-400

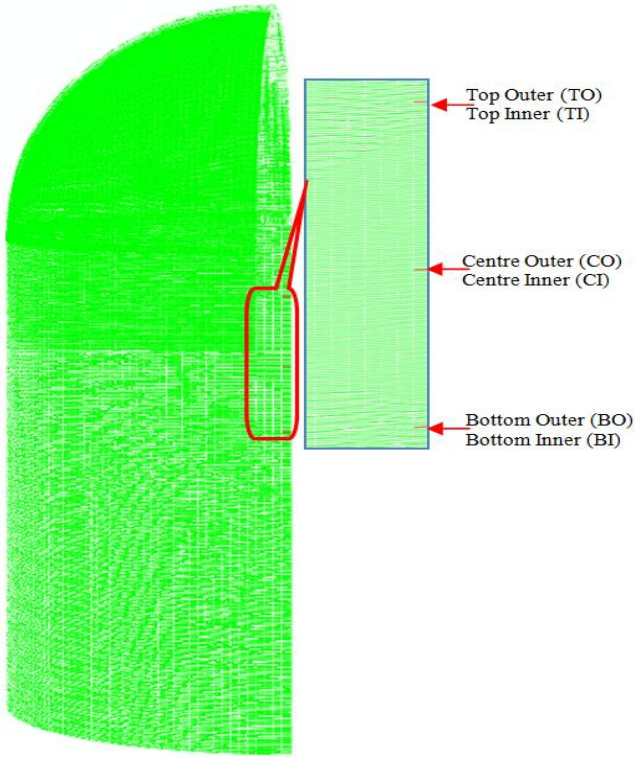

Fig. 2.12 Discretization of the reinforcement

The containment with dome has also been employed for studying the effect of fire induced due to aircraft crash. The meshing is almost same to what has been discussed above however there is minor modification in the bottom region of containment up to 10 m height from the base. The size of concrete elements was considered to be 200 mm x 200 mm x 200 mm in this region giving 6 elements across the thickness. The mesh convergence was studied for the heat transfer analysis. It was presumed that the fire will not spread throughout the containment wall hence a square reinforced concrete wall of size 6 m x 6 m was studied under fire in order to perform the mesh convergence. The size of element was varied as 600 mm x 600 mm x 600 mm, 300 mm x 300 mm x 300 mm, 200 mm x 200 mm x 200 mm, 150 mm x 150 mm x 150 mm, 75 mm x 75 mm, 75 mm and 37.5 mm x 37.5 mm x 37.5 mm giving 2, 4, 6 and 8, 16 and 32 eight node brick elements at the thickness, Fig. 2.13. The results obtained are shown in Fig. 2.14 in the form of temperature variation contours. The temperature gradient across the containment thickness has been plotted in Fig. 2.15. It was found that the temperature gradient varied up to 6 elements across the thickness and thereafter became almost constant, indicating no further influence of element size. Hence 6 elements across the thickness have been considered for the region under the application of fire for all the simulations of heat transfer and thermal stress analysis. The detail of elements have been highlighted in Table 2.3. The size of reinforcement elements however, was kept unchanged.

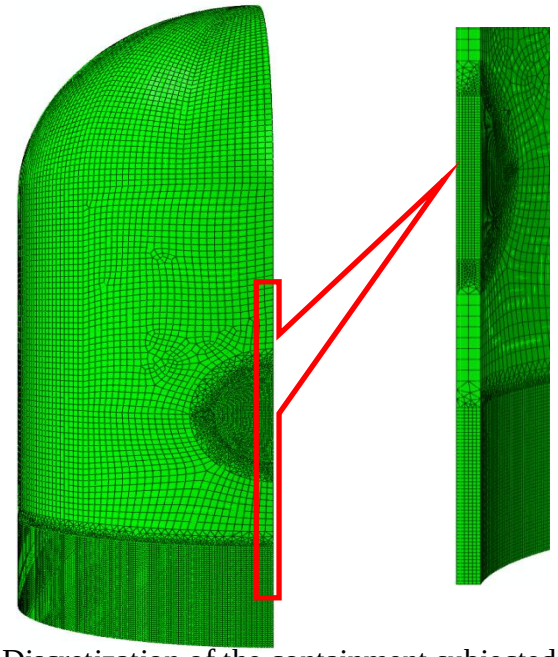

Fig. 2.13 Discretization of the containment subjected to crash induced fire

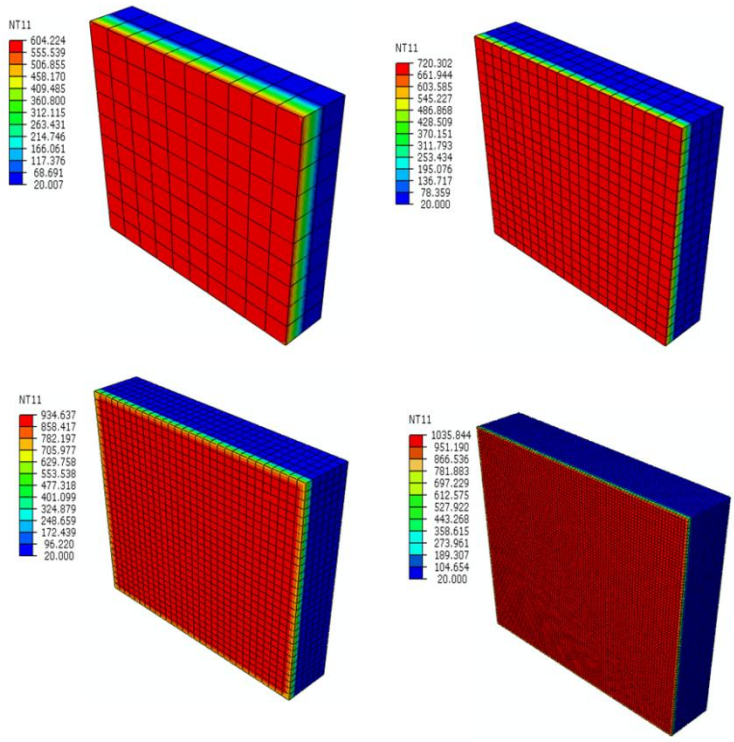

Fig. 2.14 Variation of temperature along the thickness with different number of elements (a) 2 element (b) 4element(c) 6 element (d) 8 element

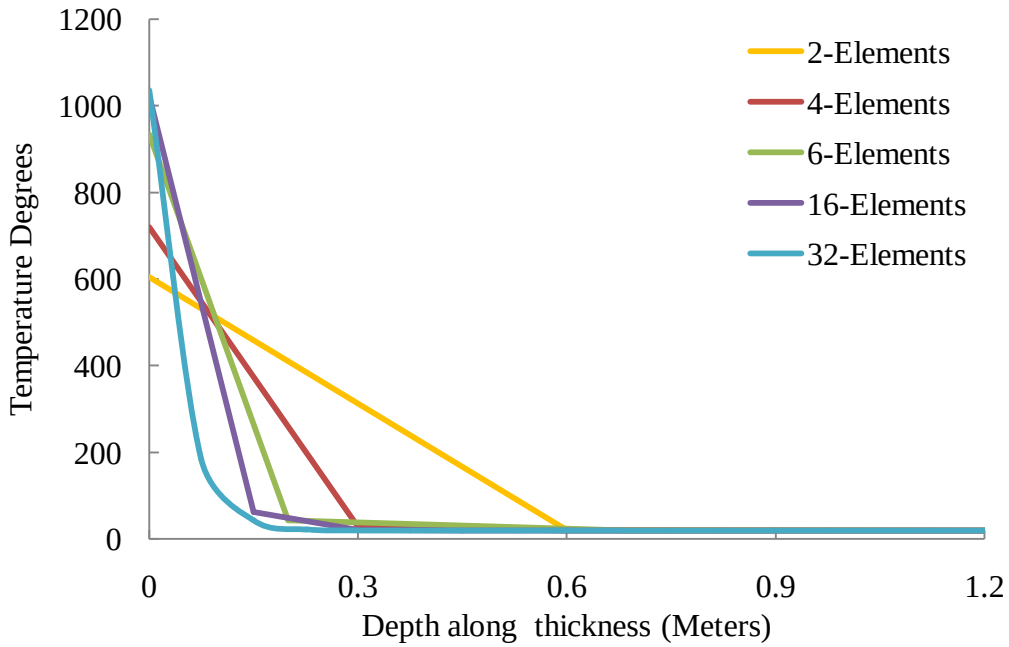

Fig. 2.15 Variation of temperature along the thickness with different no. of elements

Table 2.3 Number of element in containment for heat transfer analysis

	Boeing 707-320	Boeing 747-400
Total number of elements	536687	559219
linear hexahedral elements of type DC3D8	75234	86140
linear tetrahedral elements of type DC3D4	25651	37277
linear line elements of type DC1D2	435802	435802

2.4.4 Meshing of Containment with Flattened Top

For the containment with flattened top, the size of elements has been considered almost identical to what has been adopted for the containment with dome. However, the area and the shape of the impact region have been modified in accordance with the requirement of the problem. Initially the geometric model of aircraft has been impacted on the containment and hence the application area has been chosen according to the size of aircraft, see Fig. 2.16(a). Subsequent to obtaining the response against the geometric model of aircraft, the resultant reaction time curve has been further applied on the same geometry of containment. However, there are two distinct manners through which the reaction time curve has been applied on the containment. In the first case, the reaction time curve was divided in three parts representing the fuselage, first set of engines and second set of engines and thus applied at respective locations and corresponding equivalent area, see Fig. 2.16(b). In the second case, the total reaction time curve has been applied on an average circular area, see Fig. 2.16(c). Hence, the meshing of the containment with flattened top has been carried out in three different manners. Moreover, the size of impact zones has also been affected by the size of aircrafts i.e., Boeing 707-320 and Boeing 747-400. The detailed description of the size and shape of impact region and the meshing of different regions of the containment is illustrated in Table 2.4

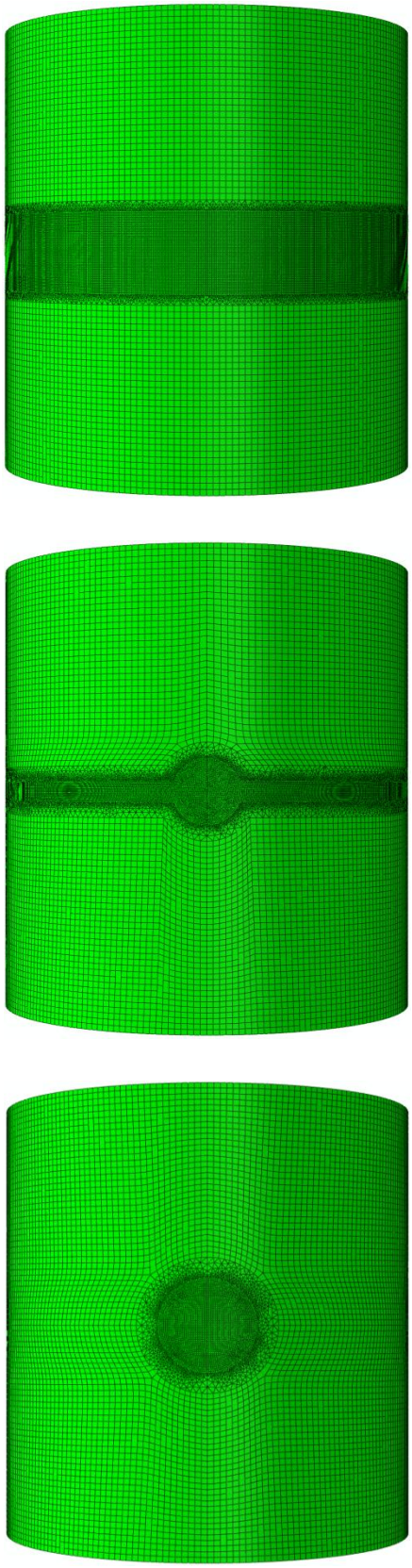

Fig. 2.16 Discretization of the containment analyzed with (a) geometric model of aircraft (b) area trifurcation scheme (c) average area scheme

Table 2.4 Number of element in containment for strike of geometric model analysis and comparison

	Boeing 707-320	Boeing 747-400
Geometric model	128962	284736
Area trifurcation scheme	168857	328433
Average area scheme	80542	100322

The impact region has been meshed with three-dimensional, reduced integration, 8 node brick elements of size 120 mm x 120 mm x120 mm. In the outer region however, the size of element has been increased to 600 mm x 600 mm x 600 mm. The intermediate regions (between the impact and outer region) have been meshed with tetrahedral elements of varying size. The reinforcement was meshed with two node three-dimensional truss element of size 600 mm. The size of reinforcement was considered same throughout the containment. The total number of elements in the containment was 393359 including 218029 linear hexahedral elements (C3D8R) and 77666 linear tetrahedral elements (C3D4) of concrete, and 97664 linear line elements (T3D2) of reinforcement. Further, as discussed in section 2.3 the total number of elements in the geometric model of Boeing 707-320 and Boeing 747-400 were 157950 and 190689 respectively. Therefore a total number of elements in the whole problem of coupled analysis reached approximately 600 thousands.

The mesh convergence has already been performed for the containment with dome. Keeping in view that the characteristic of meshing is almost same to what has been adopted for the containment with dome, the mesh convergence has not been further studied.

2.5 INTERACTIONS AND BOUNDARY CONDITIONS

ABAQUS does not recognize mechanical contact between the interacting bodies unless the appropriate contact definition has been specified. The mere physical proximity of two surfaces in an assembly is not enough to indicate any type of interaction between the surfaces. Interaction is step dependent process, hence it must be indicated that in which step it will remain active.

2.5.1 For Containment Structure

In the present study the interaction between the truss elements of the reinforcement and solid elements the concrete has been assigned through embedded constraint option for impact and thermal stress analysis. The reinforcement was considered as the embedded and the concrete as the host element. In the embedded element technique the translational degrees of freedom of the embedded nodes is governed by the degree of freedom of the nearest node of the host element i.e., the reinforcing steel is assumed to have perfect bonding with concrete.

However, embedded constraint are not employed for heat transfer analysis. A surface-based tie constraint was used in coupled temperature-displacement, coupled thermal-electrical-structural, coupled thermal-electrical, or heat transfer simulations. The tie constraint works on master-slave formulation and allows to fuse together two regions even though the meshes on the surfaces of these regions may be dissimilar. It constrains each of the nodes on the slave surface to have the same motion and the same value of temperature, pore pressure, acoustic pressure, or electrical potential as the point on the master surface to which it is closest. The constraint prevents slave nodes from separating or sliding relative to the master surface.

By default, embedded/slave nodes must lie within a distance calculated by multiplying the average size of all non-embedded/non-slave elements in the model by 0.05. If these node is located outside the specified geometric tolerance zone, an error message will be issued. The geometric tolerance is defined as a limit that how far embedded/slave node can lie outside the regions of the host/master elements in the model. The geometric tolerance can be defined either as a fraction of the average size of all non-embedded elements in the model or as an absolute distance in the length units chosen for the model. If both exterior tolerances are specified, ABAQUS uses the tighter tolerance of the two. The average size of all the non-embedded elements is calculated and multiplied by the fractional exterior, which is then compared to the absolute exterior tolerance to determine the tighter tolerance of the two. In the present analysis the option of both tolerance methods have been selected. However, the values of absolute and fractional tolerance have been modified according to the requirements of simulations.

Also the base of the containment structure is assumed to be rigid i.e. all degrees of freedom have been restrained and thus assigned fixed boundary conditions. The partial or half

model was provided with symmetric boundary conditions on the face normal to the plane of loading. Hence motion across this symmetric plane has been restricted.

2.5.2 For Aircrafts and Rigid Targets

ABAQUS/Explicit provides two algorithms for modeling contact and interaction problems i.e. the general contact algorithm and contact pair algorithm. The general contact algorithm can be used only with three dimensional surfaces. While contact pairs can be formed using a pair of rigid or deformable surfaces or a single deformable surface. It does not require surfaces with matching meshes. The order in which the surfaces are specified is important only when a non-default weighing factor is specified.

Surface-to-surface contact interactions describe contact between two deformable surfaces or between a deformable and a rigid surface. The self-contact interactions describe contact between different areas on a single surface. Self-contact will be recognized between any node on a self-contact surface and any other point on the same surface, including either side of shells or membranes. In the present study a self contact has been defined for the aircrafts body, with an assumption that during deformation different parts of aircraft may come in contact.

For surface forming contact pair, the rigid surface must always be the master surface. A node base surface can be used only as a slave surface. Hence, in present study geometric model of aircrafts were assumed as the slave surface. The orientation of surface normal could be critical for the proper detection of contact between two contacting surfaces. At the point of closest proximity the normal of a single sided master surface forming the contact pair should always point toward the slave surface. As the two bodies come in contact, the penetrations are detected and the contact constraints are applied according to the constraint enforcement method (kinematic or penalty). Penetrations of master nodes into the slave surface can go undetected see Fig. 2.17, unless the mesh on the slave surface is adequately refined.

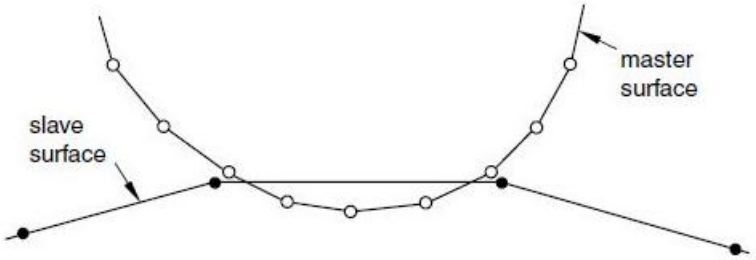

Fig. 2.17 Penetration of master nodes into slave surface with pure master-slave contact

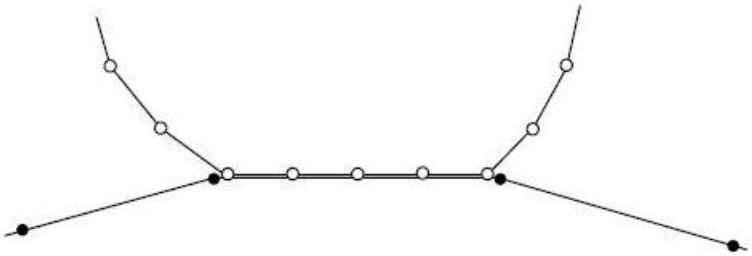

Fig. 2.18 Balanced master-slave contact constraint with kinematic compliance.

The balanced master-slave contact constraint is used as illustrated in Fig 2.18. The balanced approach minimizes the penetration of the contacting bodies and, thus, provides more accurate results. There are two tracking approaches for the contact pair algorithm in ABAQUS/Explicit, finite sliding and small sliding. The finite sliding is the most general algorithm which allows arbitrary motion of the surfaces forming the contact pair. The small sliding assumes that although the body may undergo large motions, there will be relatively little sliding of one surface over the other. Only the finite sliding approach is available for self-contact or contact involving analytical rigid surfaces.

Moreover, a set of data has also been defined that was referred to an interaction called interaction properties. A contact interaction property can define tangential behavior (friction and elastic slip) and normal behavior (hard, soft, or damped contact and separation). In the present study mechanical constraint formulation has been done through Kinematic contact algorithm. The kinematic contact algorithm uses a kinematic predictor/corrector contact algorithm to strictly enforce contact constraints (for example, no penetrations are allowed).

Chapter 3

CONSTITUTIVE MODELLING

3.1 GENERAL

The selection of a proper constitutive model is important for the finite element analysis of any problem. The accuracy of the numerical results directly corresponds to the precision of the material model. The aircraft crash on the nuclear containment structure is a highly nonlinear phenomenon with respect to the material behavior. The complexity of the problem further exaggerates due to the involvement of high strain rate and temperature. There are material models of different degree of complexity for predicting the behavior of concrete and metals under high rate of loading (Lu and Tu, 2009; Wierzbicki et al., 2005). However, due to the problems associated with the calibration process and identification of material parameters generally simpler models are preferred.

Johnson and Cook (1983, 1985) proposed a constitutive model for predicting the flow and fracture behavior of ductile materials. The model is most suitable for predicting the high strain rate and temperature behavior of metals. It involves easy calibration process and lesser number of material parameters. The equivalent stress proposed by the model includes the effect of isotropic strain hardening, strain rate hardening and temperature softening. The equivalent fracture strain is a function of stress triaxiality, strain rate and temperature.

Concrete being a brittle material shows entirely different characteristics in tension and compression. Thus the behavior of concrete under high rate of loading becomes more complex than that of the reinforcement. Martin (2010) compared the results of three different models for predicting damage of concrete under high strain rate viz. (i) concrete smeared cracking model, (ii) concrete damaged plasticity model and (iii) concrete brittle cracking model. It was concluded that the concrete damaged plasticity (CDP) model includes hardening as well as softening in the post elastic response of concrete and has been found to be most suitable for impact problems. The CDP model available in ABAQUS is actually a modification of the Drucker–Prager strength hypothesis wherein the scalar isotropic damage has been introduced later by several researchers (Kachanov 1958; Rabotnov 1969; Lubliner et al., 1989; Lee and Fenves 1998).

In the present study the material behavior of aircraft has been incorporated in the numerical simulations through the Johnson-Cook elasto-viscoplastic material model.

The material behavior of concrete under impact loading has been incorporated using the concrete damaged plasticity model wherein the stress-strain relationship has been defined as a function of strain rate. The same model has been employed for predicting the behavior of concrete under the influence of fire. However, the stress-strain relationship in this case has been defined as a function of temperature.

In order to predict the behavior of reinforcement under impact loading the Johnson-Cook (1985) flow and fracture material model has been employed. However, in order to predict the behavior of reinforcement under the influence of fire, the stress-strain relationship was defined as a function of temperature. The degradation of modulus of elasticity has also been considered as a function of temperature as per the recommendation of Eurocode 2.

3.2 CONSTITUTIVE MODELLING OF CONCRETE FOR IMPACT LOADING

The Concrete Damaged Plasticity (CDP) model available in finite element code ABAQUS was employed in order to predict the behavior of concrete in the numerical simulations. It can be executed both in Abaqus/Standard as well as Abaqus/Explicit analysis schemes. The CDP model incorporates the plastic behaviour of the concrete both in compression as well as in tension. Even though this model has been intended primarily for the analysis of reinforced concrete structures subjected to monotonic, cyclic and dynamic loading under low confining pressures however, it can efficiently be used for plain concrete also. The model used the concept of isotropic damaged elasticity in combination with isotropic tensile and compressive plasticity to represent the post-elastic behaviour of concrete. Hence, due to these characteristics, the model has been effectively used in investigating the perforation resistance of the plain and reinforced concrete structure. The CDP model has the option to use strain rate as well as temperature dependent behavior of the concrete.

3.2.1 Stress-Strain Relationship

The cracking in tension and crushing in compression were assumed to be two main failure mechanism of concrete in any plasticity based damage model. The evolution of the yield (or failure) surfaces is controlled by two hardening variables, $\bar{\varepsilon}_t^{pl}$ and $\widetilde{\bar{\varepsilon}}_c^{pl}$ linked to failure mechanism under tension and compression loading, respectively. $\tilde{\varepsilon}_t^{pl}$ and $\tilde{\varepsilon}_c^{pl}$ are referred to tension and compression equivalent plastic strains, respectively. Generally under the uniaxial

tension the stress-strain response of the concrete material follows a linear elastic relationship until the value of the failure stress, σ_{to} is reached. The failure stress corresponds to the onset of micro-cracking in the concrete material. If unloading of concrete specimen has done from any position on the strain softening branch of the stress-strain curves, the elastic stiffening of the material appears to be damaged due to the weakened unloading response. The degradation of the elastic stiffness is described by two damage variables, d_t and d_c, which are assumed to be the functions of the plastic strains, temperature, and field variables:

$$d_t = d_t(\tilde{\varepsilon}_t^{pl}, \theta, f_i)i \qquad 0 \le d_t \le 1,$$

$$d_c = d_c(\tilde{\varepsilon}_c^{pl}, \theta, f_i)i \qquad 0 \le d_c \le 1.$$

The damage variables can take values from zero to one, where zero representing undamaged material and one representing total loss of strength. Fig 3.1(a) and (b) shows the stress-strain curves for the concrete material under uniaxial loading in tension and compression respectively. The stress-strain relationship under uniaxial tension and compression loading are, respectively;

$$\sigma_t = (1-d_t)E_0(\varepsilon_t - \tilde{\varepsilon}_t^{pl}), \qquad (3.1)$$

$$\sigma_c = (1-d_c)E_0(\varepsilon_c - \tilde{\varepsilon}_c^{pl}). \qquad (3.2)$$

Under the uniaxial cyclic loading the model presumes the decrease of the elastic modulus in term of a scalar degradation variable *d* as;

$$E = (1-d)\,E_0, \qquad (3.3)$$

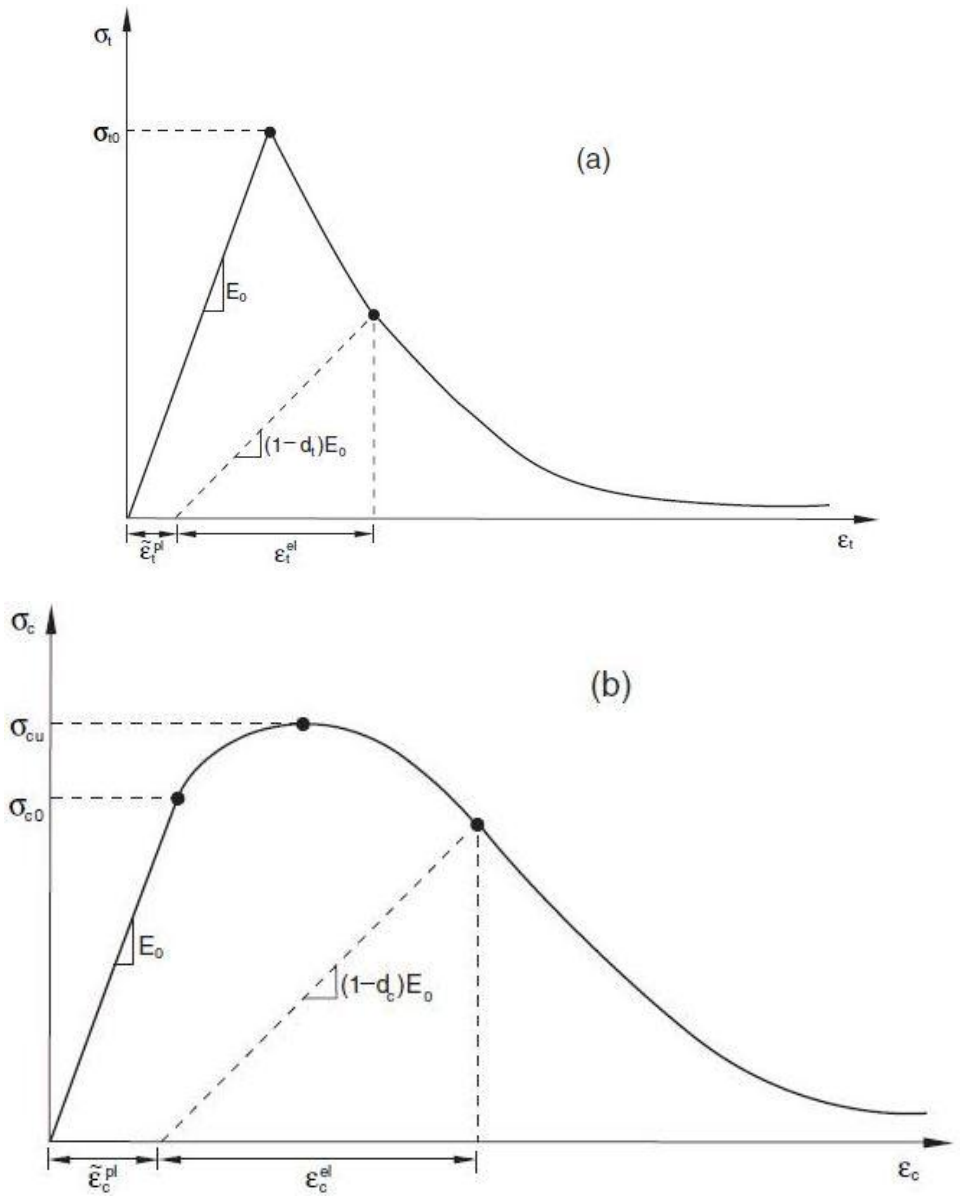

Fig 3.1 Response of concrete to uniaxial loading under (a) tension, (b) compression

Fig 3.2 and Fig. 3.3 shows the use of cracking strain in defining the tensile and compressive data for the concrete respectively.

In the multi-axial behaviour the stress-strain relationship for the general three-dimensional multi-axial condition are given by the scalar damage elasticity equation:

$$\sigma = (1\text{-}d)\, D_0^{el}(\varepsilon\text{-}\varepsilon^{pl}) \qquad (3.4)$$

Where D_0^{el} is the initial (undamaged) elasticity matrix

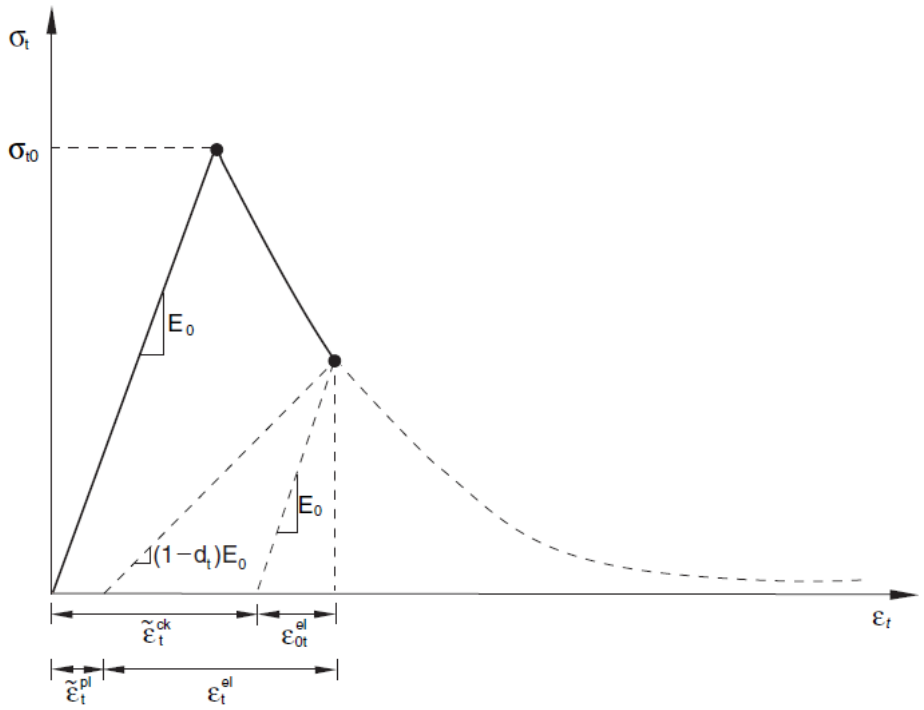

Fig 3.2 Cracking strain behavior under tension

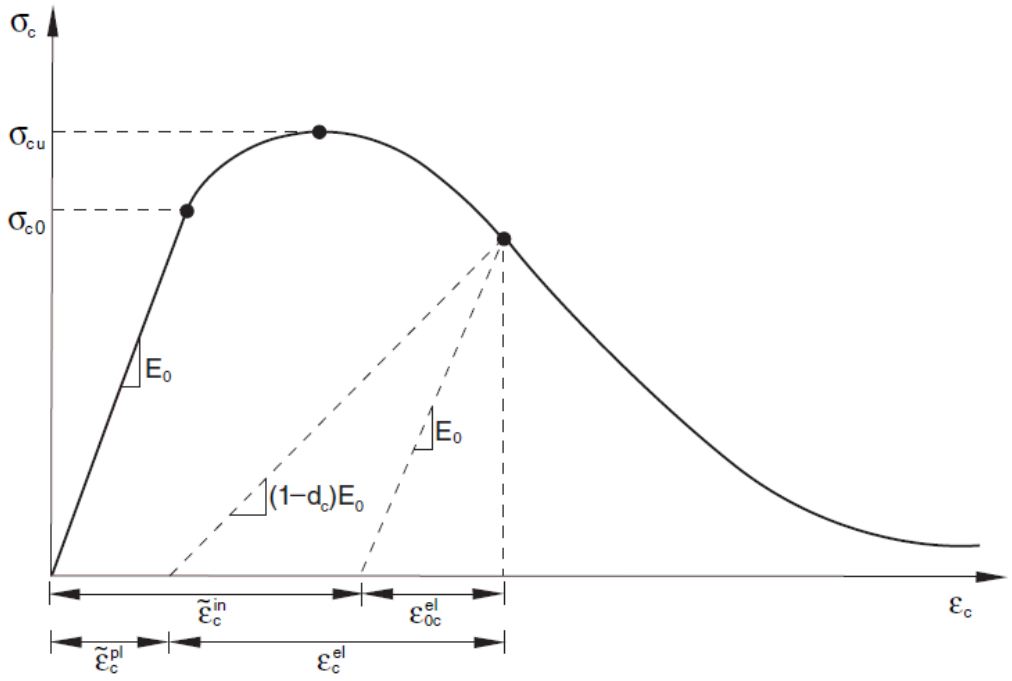

Fig 3.3 Cracking strain behavior under compression

3.2.2 Fracture Energy Cracking Criterion

The response of concrete in tension has been described using Hillerborg's (1976) fracture energy criterion. Hillerborg (1976) used the brittle fracture concept to define the energy required to open a unit area of crack, G_f, as a material parameter. With this approach the concrete's brittle behavior is characterized by a stress-displacement response rather than a stress-strain response. In this model the value of fracture energy, G_f, can be specified directly as a material property and a linear loss of strength is assumed after cracking, Fig. 3.4.

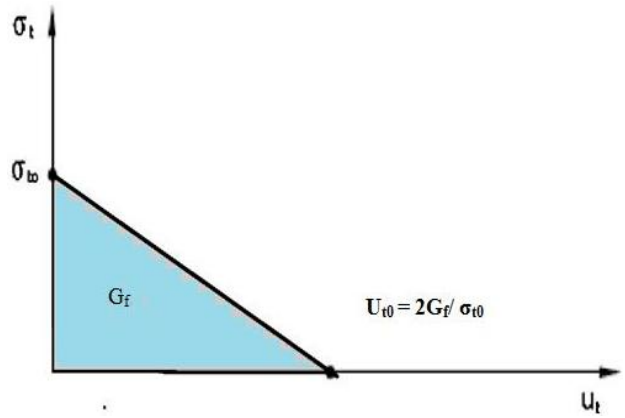

Fig 3.4 Post-failure fracture energy curve.

3.2.3 Material Properties Under Compression

If the damage is not considered in the concrete damage plasticity model, the plastic strain equals the inelastic strain however, the material still follows the actual envelope path. In the present study the response of concrete under compression was incorporated using the stress-strain curve of Sinha et al., (1964) and Grote et al., (2001). Sinha et al., (1964) carried out cyclic loading tests on 25.8 MPa cylinders at very low strain rate, Fig. 3.5. While Grote et al., (2001) carried out experiments at varying strain rates. They tested cylindrical specimens (Ø 3 in. and length 6 in.) of compressive strength 30 MPa under quasi-static loading. At high strain rate however (250 s^{-1}- 1700 s^{-1}), the material tests were carried out on split Hopkinson pressure bar (SHPB), Fig. 3.6. The stress and inelastic strains were obtained from these curves and their values were tabulated corresponding to the very low strain rate and 290 s^{-1}, 620 s^{-1}, 1050 s^{-1} and 1500 s^{-1} strain rate. In each simulation therefore five stress-strain curves were incorporated to

include the effect of varying strain rate. It is pertinent to mention here that the compressive strength of concrete in the numerical simulations performed by Abbas et al., (1996) was 35 MPa. Table 3.1 represents the basic properties of the concrete opted in the present study.

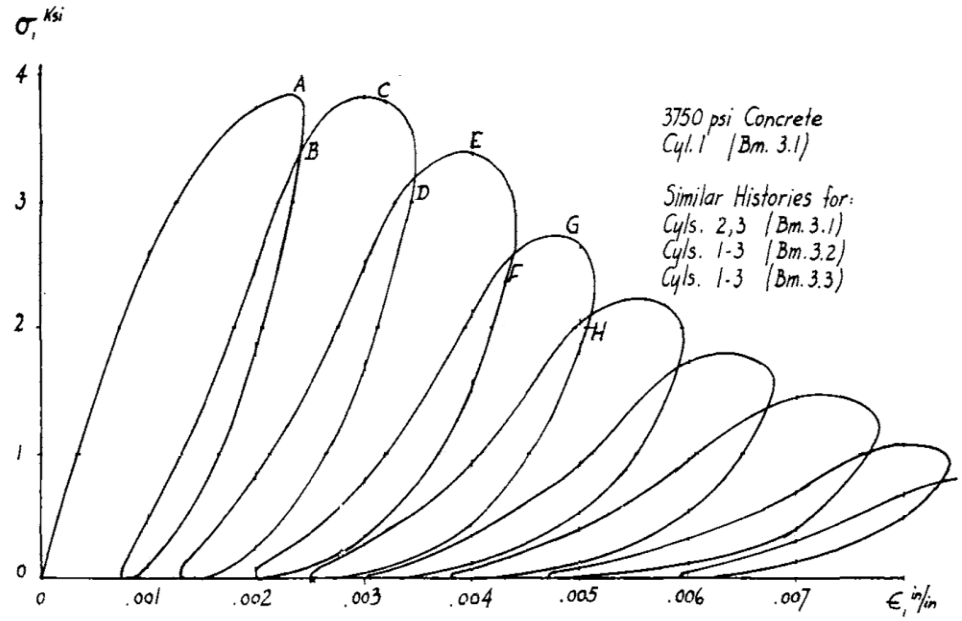

Fig 3.5 Concrete behavior under compression at low strain rate, (Sinha et al., 1964)

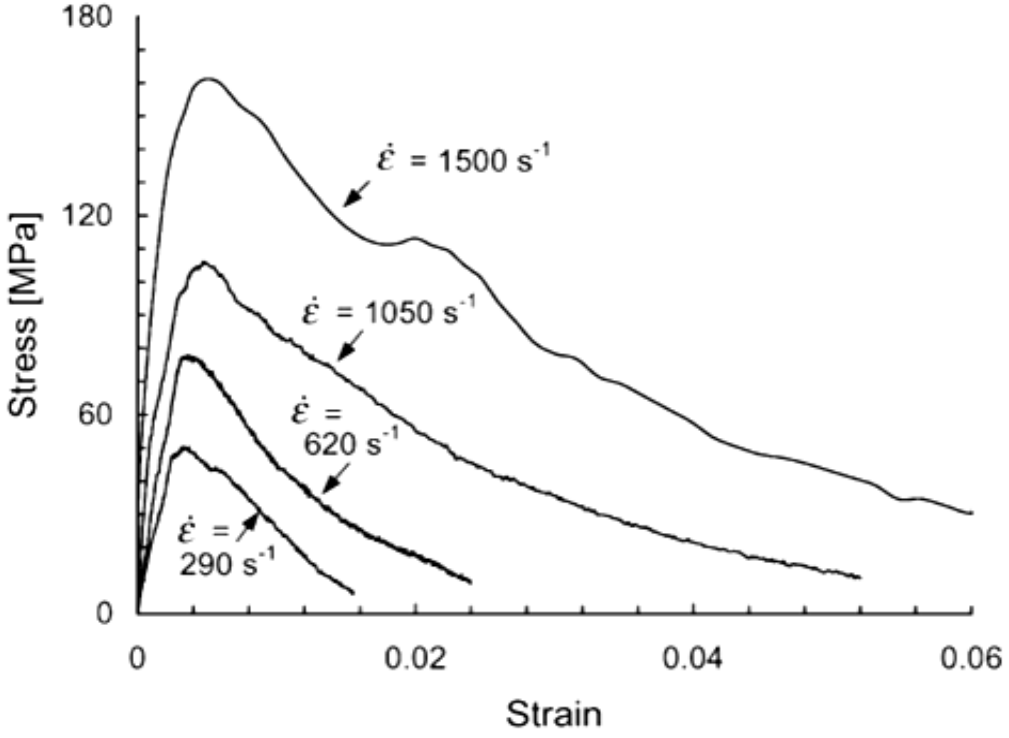

Fig 3.6 Concrete compression hardening curve at different strain rate (Grote et al., 2001)

3.2.4 Material Properties Under Tension

The behavior of concrete under tension was incorporated from the analytical study carried out by Lu and Xu, (2004) wherein the response of concrete was predicted at high strain rate. Fig. 3.7 describes the predicted stress-strain response of concrete under tensile loading at different strain rate. However, the variation of the dynamic to static strength ratio with strain rate under compressive and tensile loading has been shown in Fig. 3.8 and Fig. 3.9 respectively. It was found that the increase in the dynamic tensile strength of concrete is much higher than that of the dynamic compressive strength. At 100 s^{-1} strain rate, the dynamic compressive strength was found to be 1.5 times higher than that of the static compressive strength. However, the tensile strength was found to be 7 times higher than that of its static value. Therefore in order to calculate the fracture energy at high strain rate the dynamic tensile strength in the present study was increased 4 times and the displacement 2 times approximately. Consequently the fracture energy increased by 8 times as it is obtained by the multiplication of strength and displacement. On the other hand, the fracture energy will be overestimated if the dynamic strength is increased by 7 times. The material parameters used to predict the behavior of concrete are presented in Table 3.1. Moreover, the increase in the fracture energy of the concrete with increase in strain rate can also been observed in Fig 3.10. It is observed that the fracture energy increases gradually till the strain rate of $100s^{-1}$, however this change is significant as the strain rate increases from $100s^{-1}$.

Table 3.1 Material properties of concrete

Density, ρ (kg/m^3)	2400
Modulus of elasticity, E (N/m^2)	2.7386E+10
Poisson's ratio, ϑ	0.17
Dilation angle, ψ	30
Eccentricity	1.0
Initial equi-biaxial compressive yield stress to initial uniaxial compressive yield stress, f_{b0}/f_{c0}	1.16
Bulk Modulus, K	0.666
Fracture Energy, G_f (N/m)	720
Uniaxial Failure Stress (Tension), σ_{t0} (MPa)	10.8
Cracking displacement, U_{to} (m)	0.0001332
Tensile strength, $\sigma_{st,}$ MPa	3.86
Compressive Strength, MPa	30

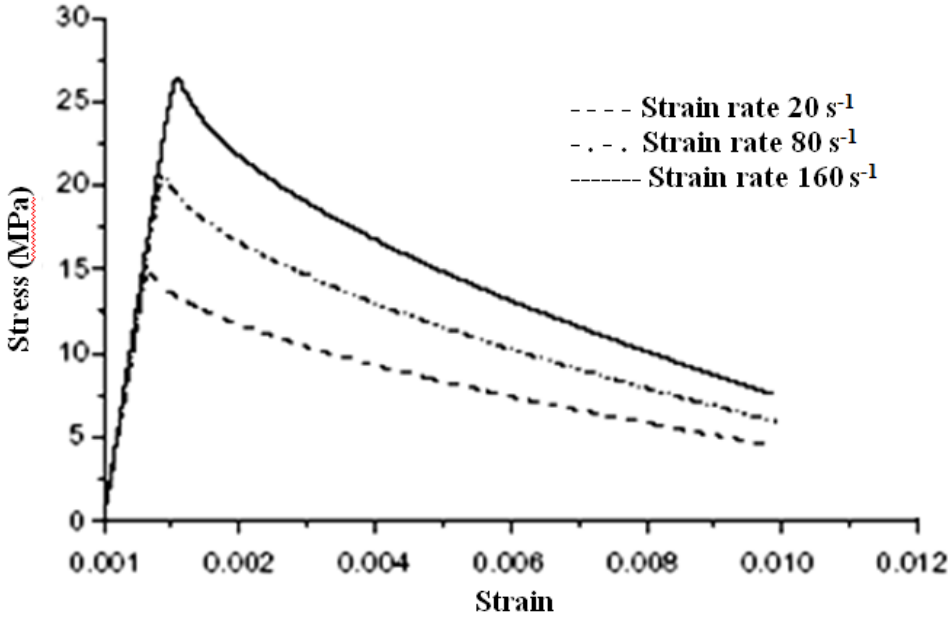

Fig 3.7 Predicted stress-strain curves for concrete under tension with different strain rates. (Lu and Xu, 2004)

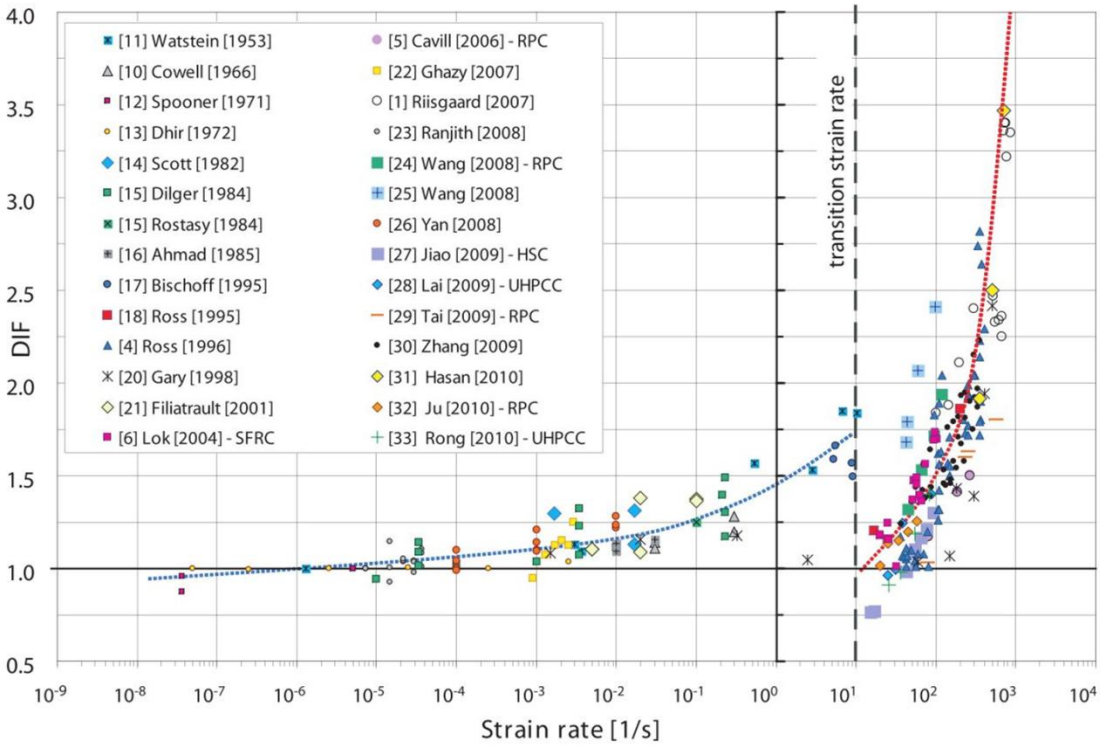

Fig 3.8 Effect of strain rate on compressive strength of concrete (Pajak, 2011)

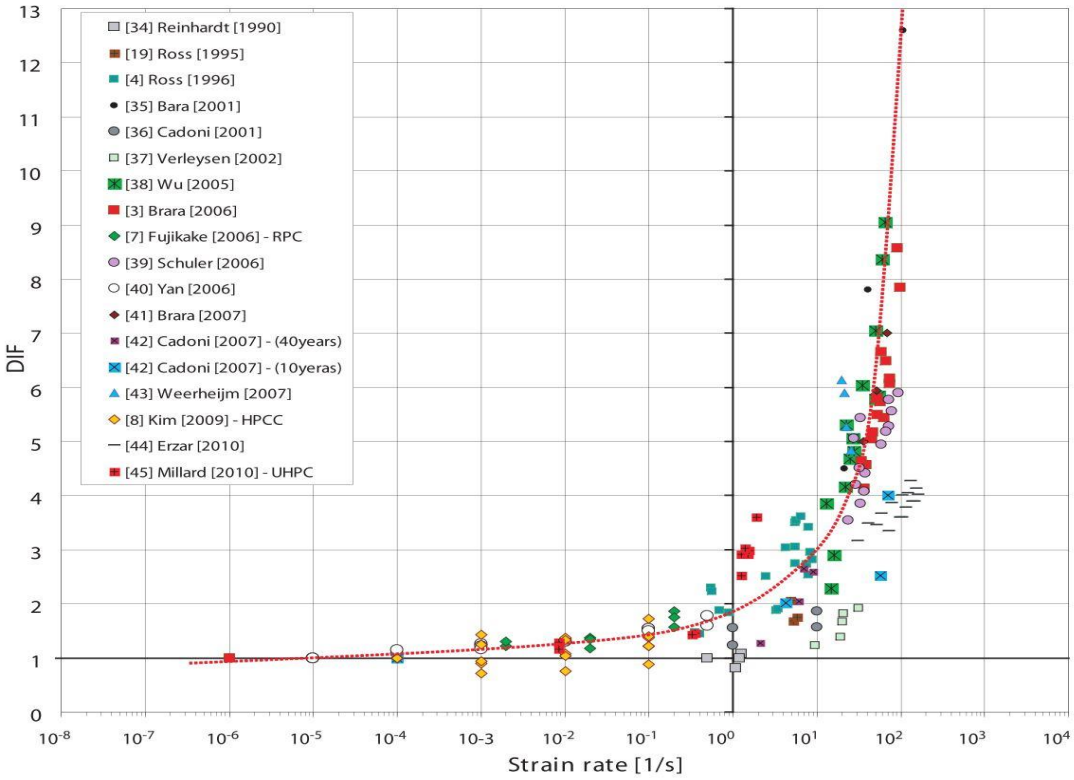

Fig 3.9 Normalized dynamic concrete tensile strength vs. strain rate (Pajak,2011)

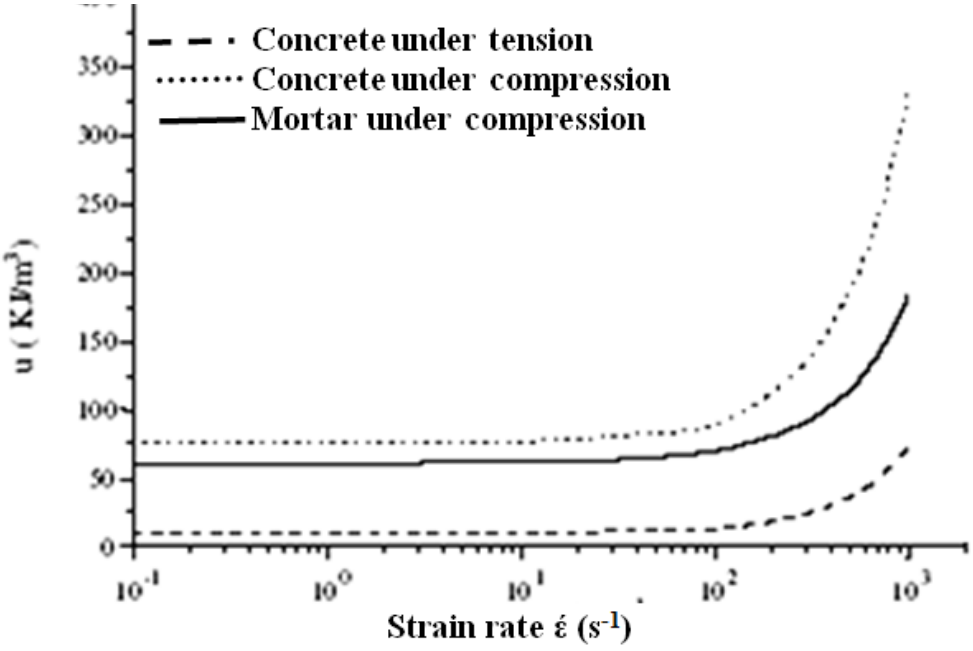

Fig 3.10 Variation of fracture energy with strain rate, (Lu and Xu, 2004)

3.3 CONSTITUTIVE MODELLING OF CONCRETE FOR THE EFFECT OF FIRE

The behavior of concrete under the elevated temperature is quite distinct from that of observed at ambient temperature. The fire influences both the mechanical and chemical properties of the concrete material. Hence, in order to model the concrete at elevated temperature proper stress-strain behavior as well as other properties should be identified. In the present study, however the material properties of the concrete have been adopted with reference of Eurocode 2 (2004).

3.3.1 Stress-Strain Behavior as per Eurocode 2

The stress-strain relationship for the concrete at elevated temperature has been obtained from the curve and formula give in Fig. 3.11. The proposed values of strength are based on steady state as well as transient state test and sometimes a combination of both. The model does not consider creep effect explicitly. This stress-strain relationship is based on two parameters (i) the compressive strength $\boldsymbol{f_{c,\theta}}$ and (ii) the strain $\boldsymbol{\varepsilon_{c1,\theta}}$ corresponding to $\boldsymbol{f_{c,\theta}}$.

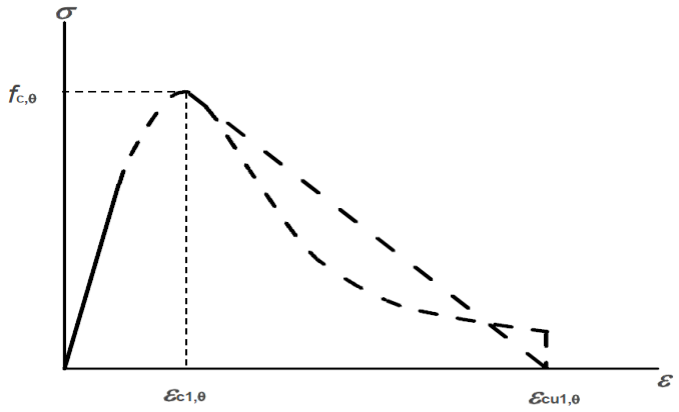

Range	Stress $\sigma(\theta)$
$\varepsilon \leq \varepsilon_{c1,\theta}$	$\dfrac{3\varepsilon f_{c,\theta}}{\varepsilon_{c1,\theta}\left(2+\left(\dfrac{\varepsilon}{\varepsilon_{c1,\theta}}\right)^3\right)}$
$\varepsilon_{c1(\theta)} < \varepsilon \leq \varepsilon_{cu\,1,\theta}$	For numerical purposes a descending branch should be adopted. Linear non-linear models are permitted

Fig 3.11 Constitutive model of concrete under compression at elevated temperature as recommended by Eurocode2.

Table 3.2 σ-ε relationship parameters for normal weight concrete

Concrete	Siliceous aggregate			Calcareous aggregate		
^{0}C	$f_{c,\theta} / f_{ck}$	$\varepsilon_{c1,\theta}$	$\varepsilon_{cu1,\theta}$	$f_{c,\theta} / f_{ck}$	$\varepsilon_{c1,\theta}$	$\varepsilon_{cu1,\theta}$
20	1.00	0.0025	0.0200	1.00	0.0025	0.0200
100	1.00	0.0040	0.0225	1.00	0.0040	0.0225
200	0.95	0.0055	0.0250	0.97	0.0055	0.0250
300	0.85	0.0070	0.0275	0.91	0.0070	0.0275
400	0.75	0.0100	0.0300	0.85	0.0100	0.0300
500	0.60	0.0150	0.0325	0.74	0.0150	0.0325
600	0.45	0.0250	0.0350	0.60	0.0250	0.0350
700	0.30	0.0250	0.0375	0.43	0.0250	0.0375
800	0.15	0.0250	0.0400	0.27	0.0250	0.0400
900	0.08	0.0250	0.0425	0.15	0.0250	0.0425
1000	0.04	0.0250	0.0450	0.06	0.0250	0.0450
1100	0.01	0.0250	0.0475	0.02	0.0250	0.0475
1200	0.00	-	-	0.00	-	-

However, the above described formulation is applicable for heating rates between 2 and 50 K/min. For concrete of normal strength with siliceous or calcareous aggregates values of each parameters shown in Fig. 3.11 were provided in Table. 3.2, linear interpolation may be used for intermediate values of temperature. Using the above equations, the stress-strain plot for a concrete compressive strength of 30 MPa has been plotted, Fig 3.12. Moreover on the basis of these curve the reduction in the modulus of elasticity with elevated temperature has also ben plotted as shown in Fig. 3.13.

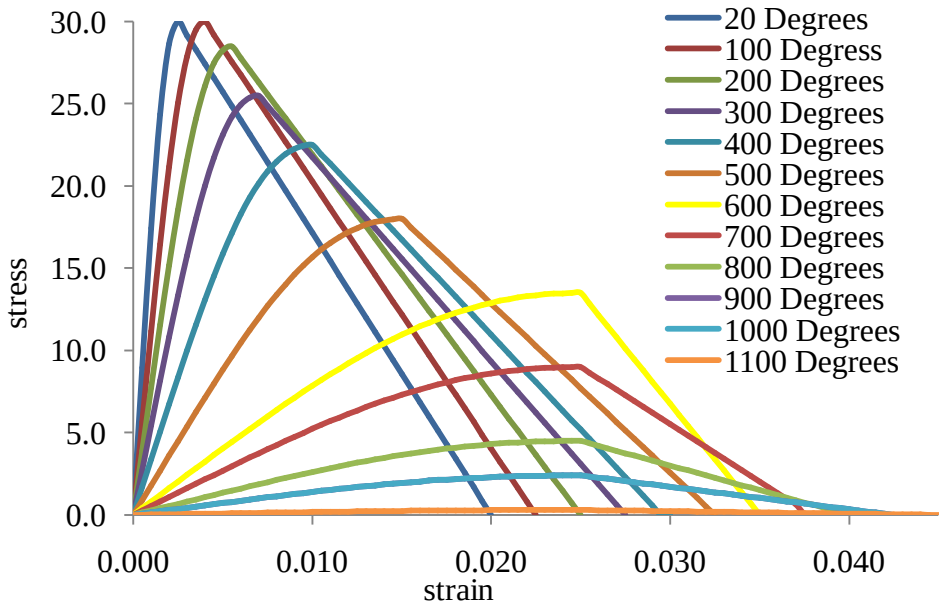

Fig. 3.12 Stress-strain plot according to Eurocode2

Further, for the tensile strength of concrete the code suggests conservative values. The reduction in the characteristic tensile strength of concrete may allowed by the coefficient $k_{c,t}(\theta)$, as define below.

$F_{ck,t}(\theta) = k_{c,t}(\theta)\, f_{ck,t}$,where $f_{ck,t}$ is characteristic tensile strength at ambient temperature.

$K_{c,t}(\theta) = 1{,}0$ for $20\ ^0C \leq \theta \leq 100\ ^0C$

$k_{c,t}(\theta) = 1{,}0 - 1{,}0\ (\theta - 100)/500$ for $100\ ^0C < \theta \leq 600\ ^0C$

Where, θ= temperature in ^0C

Fig. 3.14 shows the variation of coefficient $k_{c,t}(\theta)$ with temperature.

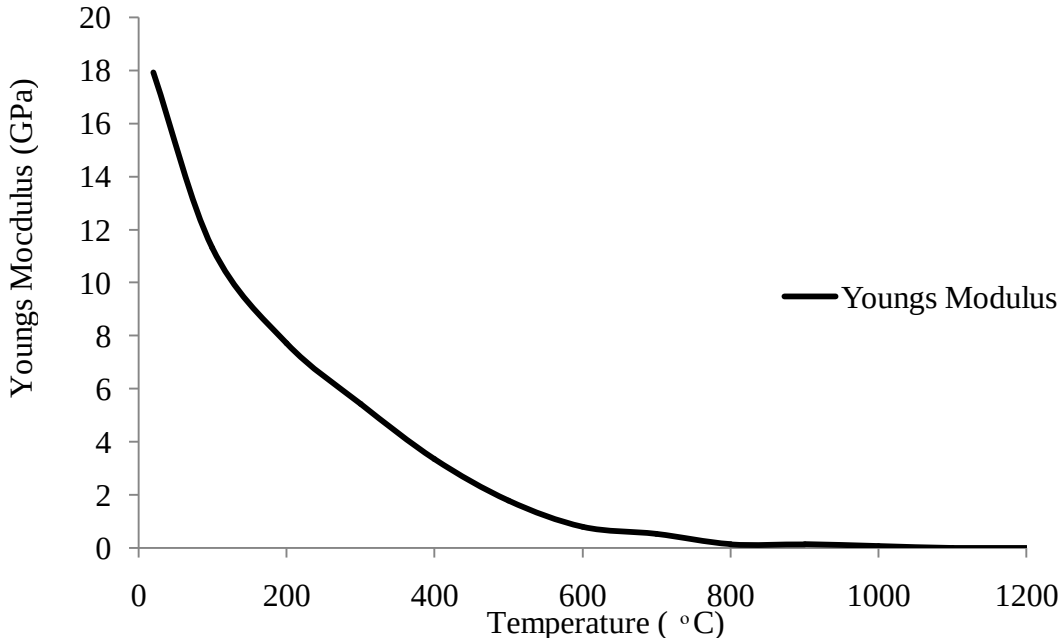

Fig 3.13 Variation of Youngs modulus of the concrete according to Eurocode 2

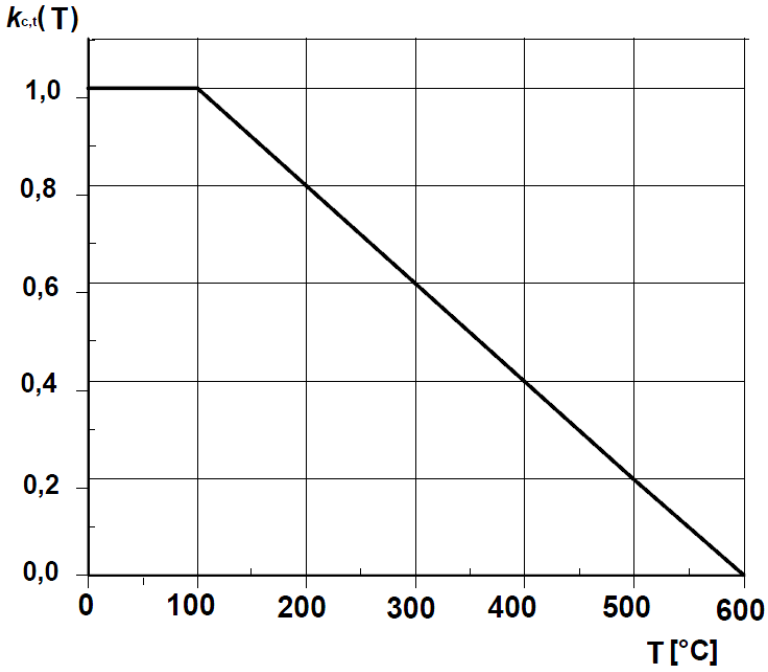

Fig. 3.14 Coefficient $k_{c,t}$ (θ) for decreasing tensile strength of concrete at elevated temperature as per Eurocode2

3.3.2 Thermal Expansion of Aggregate

The thermal strains for both the calcareous and siliceous type of aggregate are given in Eurocode 2 as a function of temperature. The equations are

Siliceous aggregates:

$$\varepsilon_c(\theta) = -1.8\times10^{-4} + 9\times10^{-6}\theta + 2.3\times10^{-11}\theta^3$$

$$\varepsilon_c(\theta) = 14\times10^{-3}$$

Calcareous aggregates:

$$\varepsilon_c(\theta) = -1.2\times10^{-4} + 6\times10^{-6}\theta + 1.4\times10^{-11}\theta^3$$

$$\varepsilon_c(\theta) = 12\times10^{-3}$$

Where θ is the concrete temperature (^{o}C)

The variation of expansion coefficient has been plotted in Fig 3.15 with the provision provide above as per Eorocode 2.

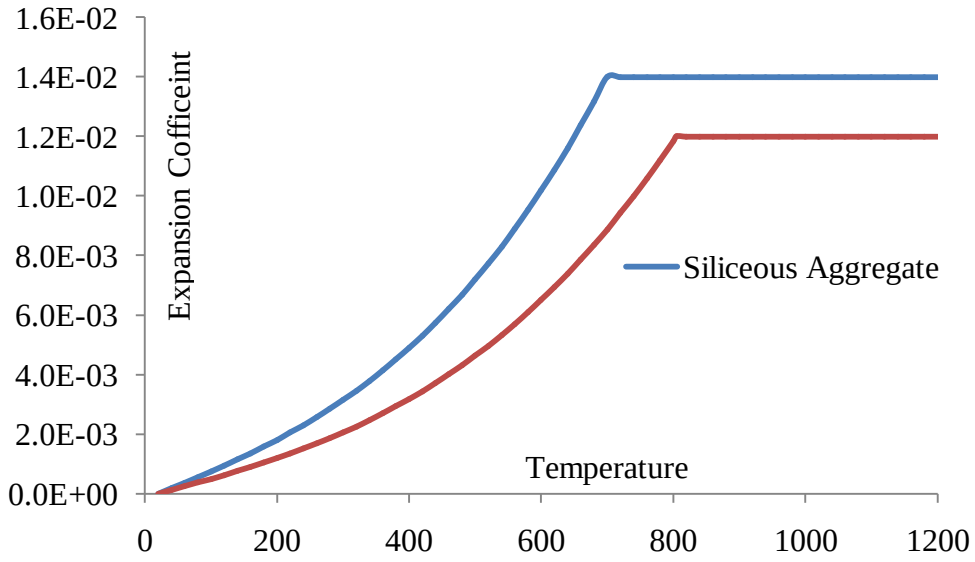

Fig 3.15 Variation of Expansion coefficient with the temperature according to Eurocode 2

3.3.3 Variation of Specific Heat with Temperature

The specific heat *c*p(θ) may be determined for dry concrete (*u* = 0%) from the following (Eurocode2):

Siliceous and calcareous aggregates:

For the moisture content of 1.5% and 3% c_{peak} is situated in between 100^0 C to 200^0C

$Cp(\theta)= 900$ (J/Kg K) for $20^oC \leq \theta \leq 100^oC$

$Cp(\theta)= 900 + (\theta-100)$ (J/Kg K) for $100^oC < \theta \leq 200^oC$

$Cp(\theta)=1000 + (\theta-200)/2$ (J/Kg K) for $200^oC < \theta \leq 400^oC$

$Cp(\theta)=1100$ (J/Kg K) for $400^oC < \theta \leq 1200^oC$

On the basis of these equation variation of specific heat with respect to temperature has been defined in Fig. 3.16.

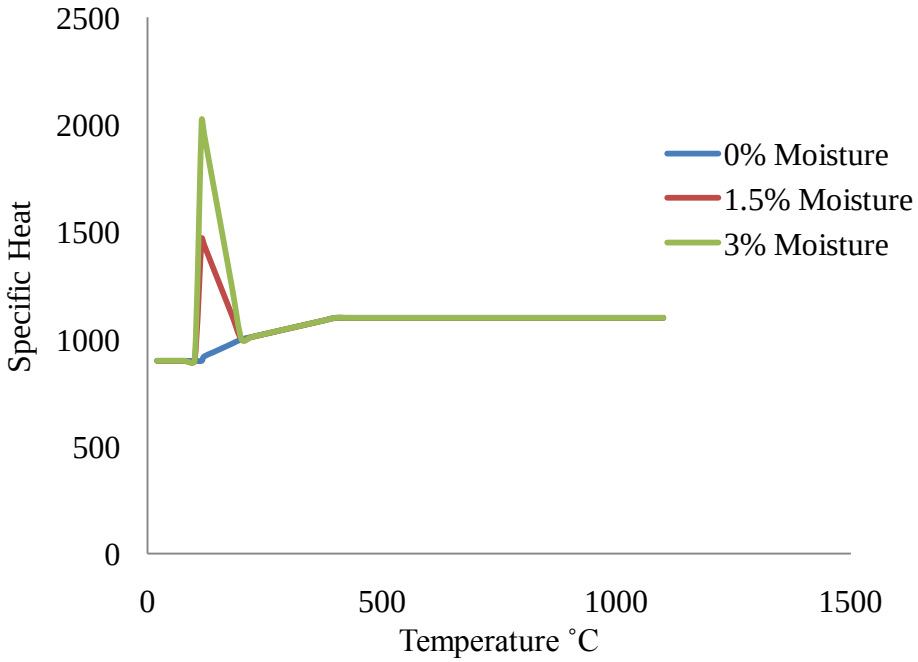

Fig 3.16 Variation of Specific Heat with the temperature according to Eurocode2

3.3.4 Thermal Conductivity

The thermal conductivity λc of concrete may be determined between lower and upper limit values, given in Eurocode2 based on the equation below.

The upper limit of thermal conductivity λc of normal weight concrete may be determined from:

$\lambda c=2-0.2451\ (\theta/100)+0.0107(\theta/100)^2$ W/m K for $20^oC \leq \theta \leq 1200^oC$

where θ is the concrete temperature.

The lower limit of thermal conductivity λc of normal weight concrete may be determined from:

$\lambda c = 1.36\text{-}0.136(\theta/100) + 0.0057\,(\theta/100)^2$ W/m K for $20^{o}C \leq \theta \leq 1200^{o}C$

where θ is the concrete temperature. With the help of these equation the relaion between Conductivity and rise in temperature were shown in Fig. 3.17

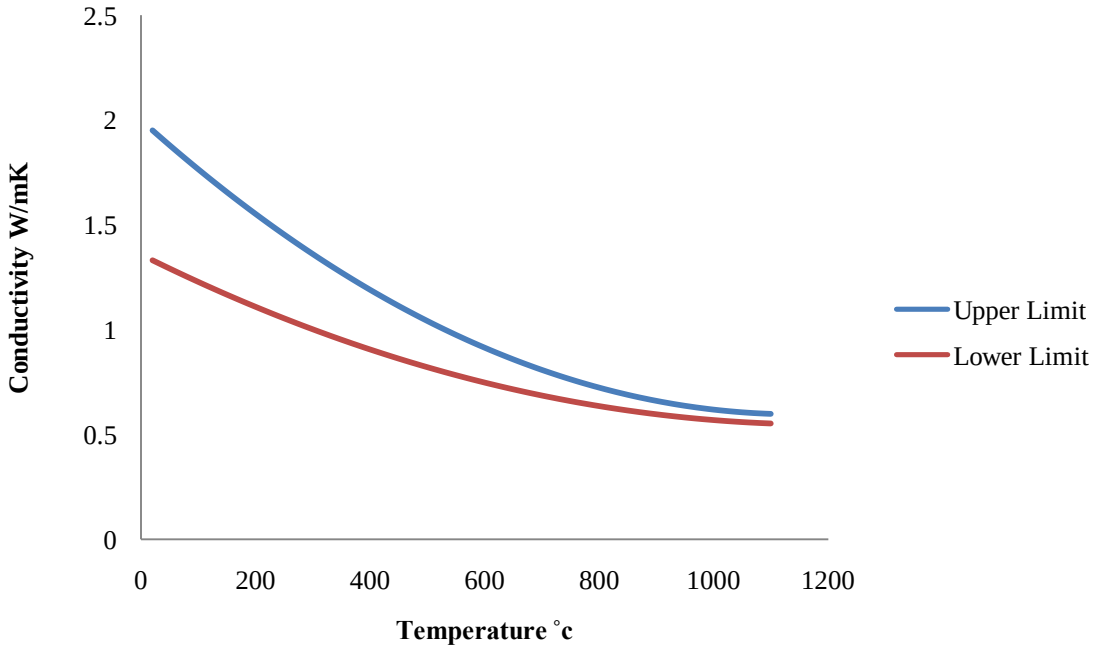

Fig 3.17 Variation of Specific Heat with the temperature according to Eurocode2

3.4 CONSTITUTIVE MODELLING OF REINFORCEMENT FOR IMPACT LOADING

The reinforcement in concrete structures is typically provided in the form of rebars. The geometric modeling and meshing of rebars already been discussed in the previous chapter.

The material behavior of the steel reinforcement was incorporated using the well known Johnson-Cook elasto-viscoplastic material model (1983, 1985) that is capable of predicting the flow and fracture behavior of ductile materials. It includes the effect of linear thermo-elasticity, yielding, plastic flow, isotropic strain hardening, strain rate hardening, softening due to adiabatic heating and damage. The equivalent von Mises stress $\overline{\sigma}$ of the Johnson-Cook model incorporates

the effect of strain hardening, strain rate and temperature through an uncoupled approach which enables the implementation of each of these phenomena independently, and expressed in the following manner;

$$\bar{\sigma}(\bar{\varepsilon}^{pl}, \dot{\bar{\varepsilon}}^{pl}, \hat{T}) = \left[A + B(\bar{\varepsilon}^{pl})^{n}\right]\left[1 + C\ln\left(\frac{\dot{\bar{\varepsilon}}^{pl}}{\dot{\varepsilon}_0}\right)\right]\left[1 - \hat{T}^{m}\right], \quad (3)$$

where A is quasi-static yield stress, B is a hardening constant, n is the hardening exponent, C is the strain-rate sensitivity parameter and m is the temperature sensitivity parameter. $\bar{\varepsilon}^{pl}$ is the equivalent plastic strain, $\dot{\bar{\varepsilon}}^{pl}$ is equivalent plastic strain rate, $\dot{\varepsilon}_0$ is a reference strain rate and $\hat{T}$ is non dimensional temperature defined as;

$$\hat{T} = (T - T_0)/(T_{melt} - T_0) \qquad T_0 \leq T \leq T_{melt} \quad (4)$$

where T is the current temperature, T_{melt} is the melting temperature and T_0 is the room temperature. The fracture model proposed by Johnson-Cook (1983, 1985) takes into account the effect of stress tri-axiality, strain rate and temperature independently on the equivalent fracture strain. The equivalent fracture strain $\bar{\varepsilon}^{pl}{}_f$ is expressed in the following form;

$$\bar{\varepsilon}^{pl}{}_f\left(\frac{\sigma_m}{\bar{\sigma}}, \dot{\bar{\varepsilon}}^{pl}, \hat{T}\right) = \left[D_1 + D_2\exp\left(D_3\frac{\sigma_m}{\bar{\sigma}}\right)\right]\left[1 + D_4\ln\left(\frac{\dot{\bar{\varepsilon}}^{pl}}{\dot{\varepsilon}_0}\right)\right]\left[1 + D_5\hat{T}\right], \quad (5)$$

Where D_1-D_5 are material parameters, $\frac{\sigma_m}{\bar{\sigma}}$ is the stress tri-axiality ratio and σ_m is the mean stress. The material parameters of reinforcing steel were considered identical to those of the Weldox 460 E steel obtained by Borvik et al. (2002), see Table 3.3.

Table 3.3: Material properties for Weldox 460 steel

Young's modulus; E (N/ mm^2)	$2x10^5$	T_{melt} (K)	1800
Poisson Ratio, ϑ	0.33	T_0 (K)	293
Density ,ρ (Kg/m^3)	7850	Specific heat Cp (J/ Kg K)	452
Yield stress, A (N/mm^2)	490	Inelastic heat fraction, α	0.9
B (N/ mm^2)	383	D1	0.0705
n	0.45	D2	1.732
Reference strain rate, $\dot{\varepsilon}$ (s^{-1})	$5x10^{-4}$	D3	-0.54
C	0.0114	D4	-0.01
m	0.94	D5	0.0

3.5 CONSTITUTIVE MODEL OF REINFORCEMENT FOR THE EFFECT OF FIRE

The Eurocode 2 (2004) provides the strength and deformation properties of reinforcing steel at elevated temperatures. Fig. 3.18 shows the mathematical model for σ-ε relationships of reinforcing steel at different temperatures. The stress-strain relationships are defined by three parameters; (i) the slope of the linear elastic range $E_{S,\Theta}$; (ii) the proportional limit $f_{sp,\Theta}$; (iii) the maximum stress level $f_{sy,\Theta}$. Eurocode2 gives values of these parameters for hot rolled and cold worked reinforcing steel at elevated temperatures and linear interpolation may be used for intermediate values of temperature.Eurocode2 also gives these parameters for two class of steel: class N and class X. In general it recommends class N. For our analysis, reinforcing steel was assumed to be from class N and hot rolled. The proportionality limit at ambient temperature was assumed to be 0.8 times the yield stress. Moreover, on the basis of these relationships, the variation of yield stress with elevated temperature has been plotted in Fig. 3.19.

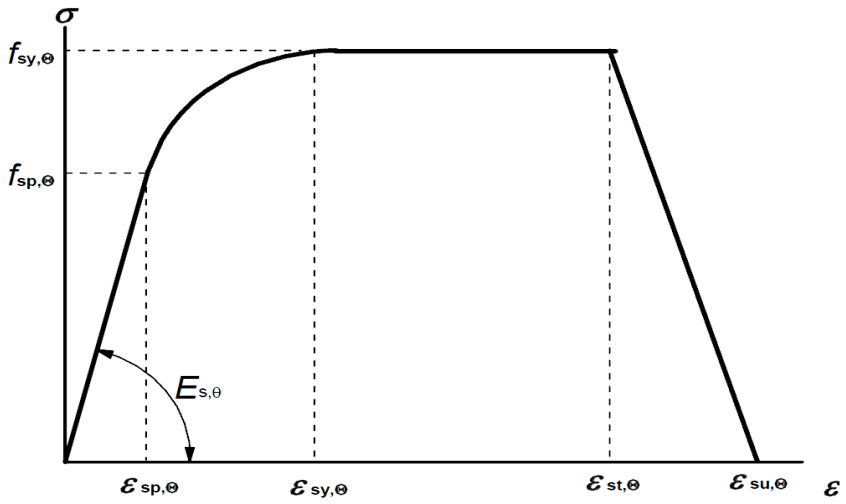

Range	Stress $\sigma(\theta)$	Tangent Modulus
$\varepsilon_{sp,\theta}$	$\varepsilon E_{s,\theta}$	$E_{s,\theta}$
$\varepsilon_{sp,\theta} \le \varepsilon \le \varepsilon_{sy,\theta}$	$f_{sp,\theta} - c + (b/a)\left[a^2 - \left(\varepsilon_{sy,\theta} - \varepsilon\right)^2\right]^{0.5}$	$\frac{b(\varepsilon_{sy,\theta} - \varepsilon)}{a\left[a^2 - \left(\varepsilon - \varepsilon_{sy,\theta}\right)^2\right]^{0.5}}$
$\varepsilon_{sy,\theta} \le \varepsilon \le \varepsilon_{st,\theta}$	$f_{sy,\theta}$	0
$\varepsilon_{st,\theta} \le \varepsilon \le \varepsilon_{su,\theta}$	$f_{sy,\theta}\left[1 - \left(\varepsilon - \varepsilon_{st,\theta}\right) / \left(\varepsilon_{su,\theta} - \varepsilon_{st,\theta}\right)\right]$	--
$\varepsilon = \varepsilon_{su,\theta}$	0.00	--
Parameter	$\varepsilon_{sp,\theta} = f_{sp,\theta}/E_{s,\theta}$ $\varepsilon_{sy,\theta} = 0.02$ $\varepsilon_{st,\theta} = 0.15$ $\varepsilon_{su,\theta} = 0.20$	
Functions	$a^2 = (\varepsilon_{sy,\theta} - \varepsilon_{sp,\theta})(\varepsilon_{sy,\theta} - \varepsilon_{sp,\theta} + c/E_{s,\theta})$ $b^2 = c\,(\varepsilon_{sy,\theta} - \varepsilon_{sp,\theta})E_{s,\theta} + c^2$ $c = \frac{(f_{sy,\theta} - f_{sp,\theta})^2}{(\varepsilon_{sy,\theta} - \varepsilon_{sp,\theta})E_{s,\theta} - 2(f_{sy,\theta} - f_{sp,\theta})}$	

Fig. 3.18 Mathematical model for stress-strain relationships of reinforcing steel at elevated temperatures

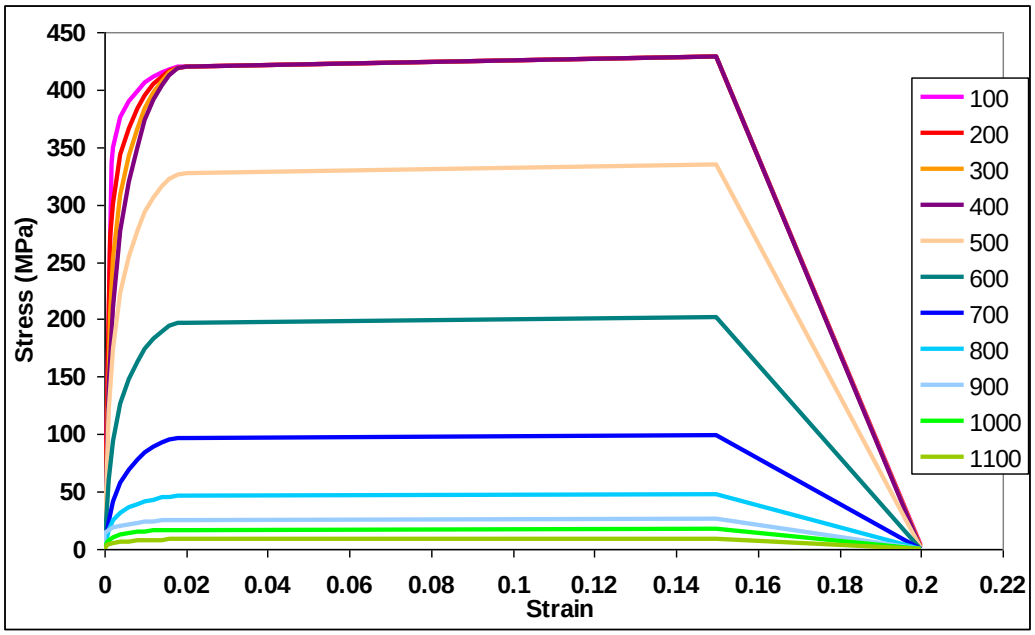

Fig. 3.19 Stress-strain curves of reinforcing steel at elevated temperatures

The expansion coefficient of steel was taken as 1.35 X 10^{-5} / ^{0}C and assumed to be constant over the entire temperature range.

3.6 MATERIAL MODELING FOR GEOMETRIC MODELS OF AIRCRAFT

To develop an exact dimensionally symmetric model of each and every aircraft is quite complicated task. The structure of modern large commercial aircrafts is very complex. The fuselage is constructed comprised of semi-monocoque configuration made up of thin sheets to bear the cabin pressure (tension) and shear loads. To carry the longitudinal tension and compression loads longitudinal stringers or longerons has been provided. Circumferential frames are provided to maintain the shape of fuselage and also to redistribute the loads to skin, (Starke Jr. and Staley, 1996). A detailed description about the different components of aircraft structure and the corresponding aluminium alloys is provided by Starke Jr. and Staley (1996).

The geometric modeling of two aircrafts developed in the present study has been discussed in the previous chapter. One aircraft being variant of Boeing 707 while another of 747 group. The above discussed, Johnson-Cook elasto visco-plastic model is a well-accepted and

numerically robust constitutive material model and highly utilized in modeling. This material model is particularly suited to model high strain rate deformation of metals. Hence this model has been employed in order to predict the behavior of geometric model of aircrafts. Major parts of Boeing 707-320 have been made up of Aluminum alloy Al 7178-T651. However, Al 7075-T651 has been reported as major contributor in body of Boeing 747-400, Fig. 3.20.

Aluminum alloys always have some important additional elements. A designating system has been developed which identifies the major constituents and defines the composition limits of different elements present in that particular alloy. The heat treatment and the properties of alloy were also described through a proper system. The majority of alloys used in aircraft industries fall in the 2XXX series when damage tolerance is the primary requirement and in 7XXX when strength is the primary requirement. Presently, 6XXX and 8XXX series alloys have also been introduced for manufacturing aircraft ,(Starke Jr. and Staley, 1996).The properties of Al 7178-T651 and Al 7075-T651 have been provided in Table 3.3 and Table 3.4 respectively.

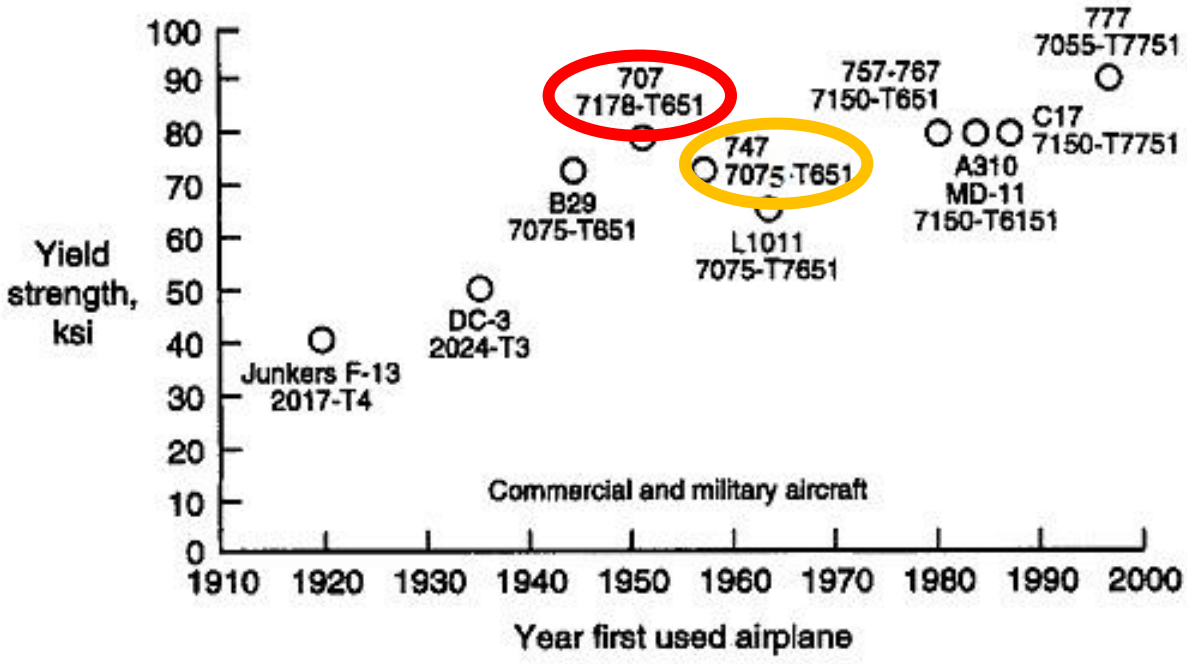

Fig. 3.20 The Yield strength of various aluminum aircraft alloys and the first year in which they were first used

Table 3.3: Material properties for Aluminum alloy Al 7178-T651(varmintal.net, 2012)

Young's modulus; E (N/ m^2)	7.17X 10^{10}
Poisson Ratio, ϑ	0.33
Density ,ρ (kg/m^3)	2823
Yield stress, A (N/m^2)	$4.7e^8$
B (N/ m^2)	$3.7e^8$
n	0.286
m	1
T_{melt} (K)	902

Table 3.4: Material properties for Aluminum alloy Al 7075-T651, (Borvik et al., 2010)

Young's modulus; E (N/ m^2)	7.10X 10^{10}
Poisson Ratio, ϑ	0.33
Density ,ρ (kg/m^3)	2795
Yield stress, A (N/m^2)	$4.3e^8$
B (N/ m^2)	$3.6e^8$
n	0.2821
m	1
T_{melt} (K)	908

3.7 CONCLUDING REMARKS

The present chapter elaborates all the material models adopted for concrete as well as reinforcing steel. Material parameters adopted in these constitutive models has been discussed. Material modelling for the geometric models of aircraft has been discussed separately. The concrete damaged plasticity model has been adopted for modeling the behavior of concrete under impact loading and fire. In case of impact loading of aircrafts parameters have been obtained from the available literature, while for fire analysis the provisions of Eurocode 2 has been adopted. However, for reinforcing steel as well the aircraft body the Johnson-cook elasto-visco plastic model has been preferred.

Chapter 4

RESPONSE OF CONTAINMENT AGAINST COMMERCIAL AND FIGHTER AIRCRAFT CRASH

4.1 GENERAL

The safety assessment of important structures like reactor containment vessel against deliberate or accidental crash of commercial and fighter aircraft has drawn significant attention throughout the world. The structural design of the upcoming reactor buildings has been amended by many countries keeping in view the threats of aircraft crash. The containment vessel is generally provided to mitigate the consequences of an unforeseen event in order to protect the plant, public and environment. Therefore, most of these structures, including the Boiling Water Reactor (BWR) as well as the Pressurized Heavy Water Reactor (PHWR) containments are constructed as double layered reinforced concrete shell structures. The purpose of the inner shell is to control the emission of radioactive radiation while the outer shell provides safety against possible external threat. In some countries however, a single reinforced concrete shell is constructed and strengthened by the steel liner at the inner face.

The numerical simulation of aircraft crash on nuclear containment structure is a complex phenomenon due to the nonlinear material behavior, large deformations and high rate of loading involved in the process. In spite of these complexities the problem has been significantly studied in last few decades keeping in view the disastrous after effects. However, the numerical modeling has been simplified by employing the reaction-time response approach suggested by Riera for the application of aircraft loading. Riera's approach has been widely accepted in the literature to simulate the aircraft crash on containment structure. The same approach has been employed in the present chapter to study the behavior of outer containment structure of BWR Mark III type nuclear power plant. The available reaction-time curves have been used to demonstrate the loading of aircrafts in order to identify the most vulnerable location on the containment structure. Further investigation has been carried out on this location to explore the most damaging aircraft. The results obtained have been discussed and compared. The mid height of the containment has been found to be the most vulnerable location. The Boeing 747-400 has been found have the most damaging potential. The strain rate has been found to play important role on the results of numerical simulation.

4.2 THE EFFECT OF STRAIN RATE

The strain rate is an important parameter to describe the behavior of material under impact loading. The effect of strain rate has been studied in order to seek its influence on the response of the containment as well as to calibrate the material model. The outer containment of the BWR-Mark III type of nuclear power plant has been subjected to the crash of Boeing 707-320 aircraft. The containment has been normally hit by the aircraft near the junction of dome and cylinder, Fig. 4.1. The geometric modeling and finite element discretization of containment structure has already been discussed in Chapter 2. It is important to mention here that at present the services of Boeing 707-320 aircraft have been restricted and it has been replaced by other advanced aircrafts. However, being one of the oldest aircraft of the Boeing family 707-320 it has been significantly studied in the open literature. Therefore, in the present study also the aircraft Boeing 707-320 has been considered to be the bench mark for validating the geometry, material properties and the response of the containment. The loading of the aircraft has been assigned through the reaction-time response curve shown in Fig. 4.2. The mesh was highly refined in the zone of impact of Ø 6 m, identified as the core region. The reaction force was converted in to pressure after dividing with the corresponding surface area and assigned to its respective location.

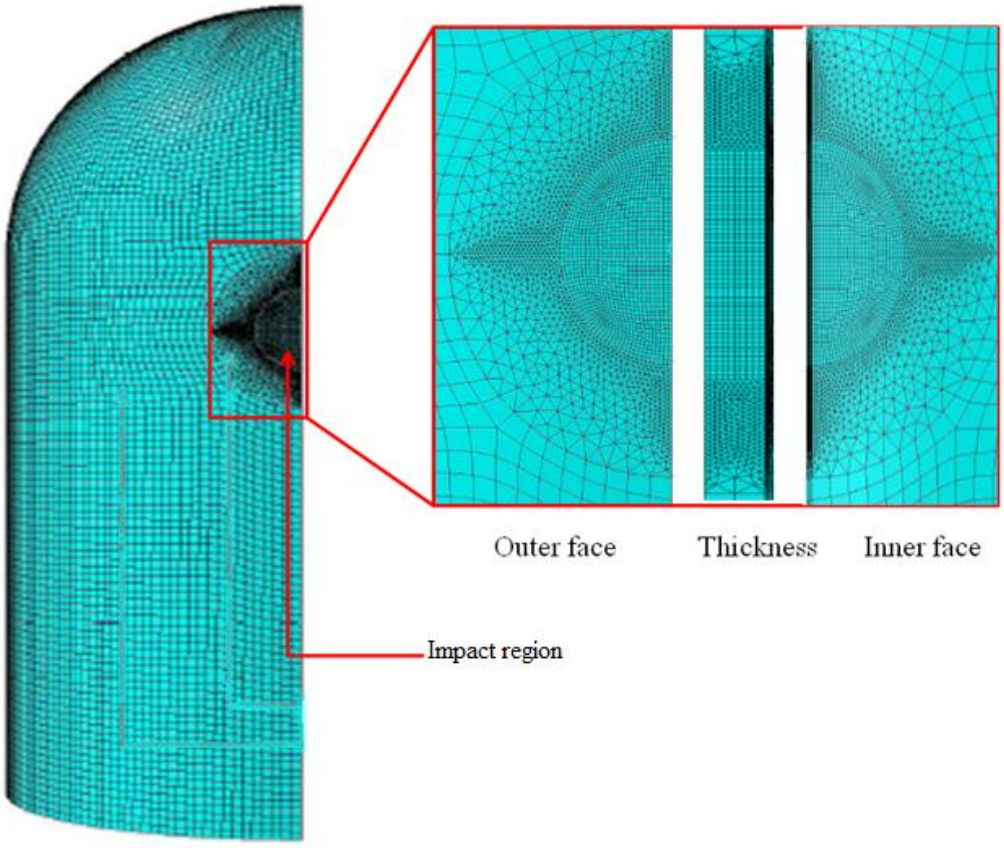

Fig. 4.1 Geometric drawing of containment BWR Mark III

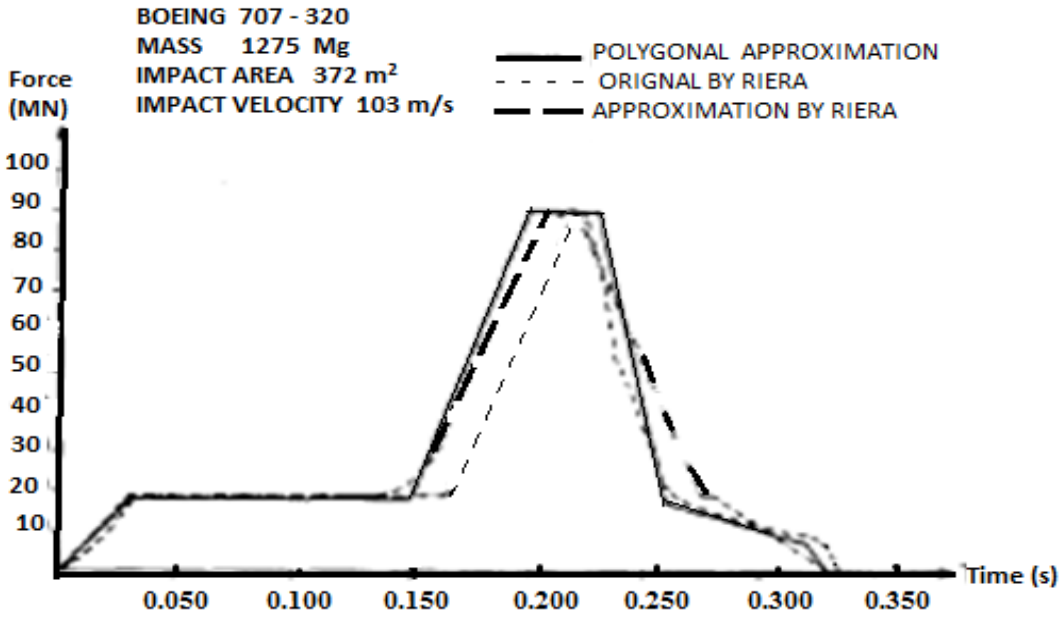

Fig. 4.2 Reaction time response of Boeing 707- 320 aircraft, Riera (1968)

In order to substantiate the effect of strain rate the individual stress-strain curves were incorporated to predict the behavior of material at a given strain rate. The stress-strain curves of concrete under compression were those corresponding to very low (without strain rate), at 290 s^{-1} and 620 s^{-1}as well as varying strain rate. The deformation of containment obtained from the above three material models was compared with the one wherein the combined effect of strain rate was considered. The yellow colored lines in Fig. 4.3 describe the longitudinal/maridonial and the circumferential axes at which the deformation curves were plotted. The deformation of the containment was found to be confined to the impact zone. Fig. 4.4 (a) and (b) describe the deformation along the longitudinal and circumferential axis of the containment respectively. Along both the axes, the deformation decreased consistently with an increase in the strain rate. The model without strain rate and 290 s^{-1} strain rate however, predicted very high deformations and the local failure of the containment at both impact locations. However, the deformation was found to be comparatively low for the sophisticated material model wherein the combined effect of strain rate was considered. Moreover, the results of this model were found in agreement with those of the 620 s^{-1} strain rate.

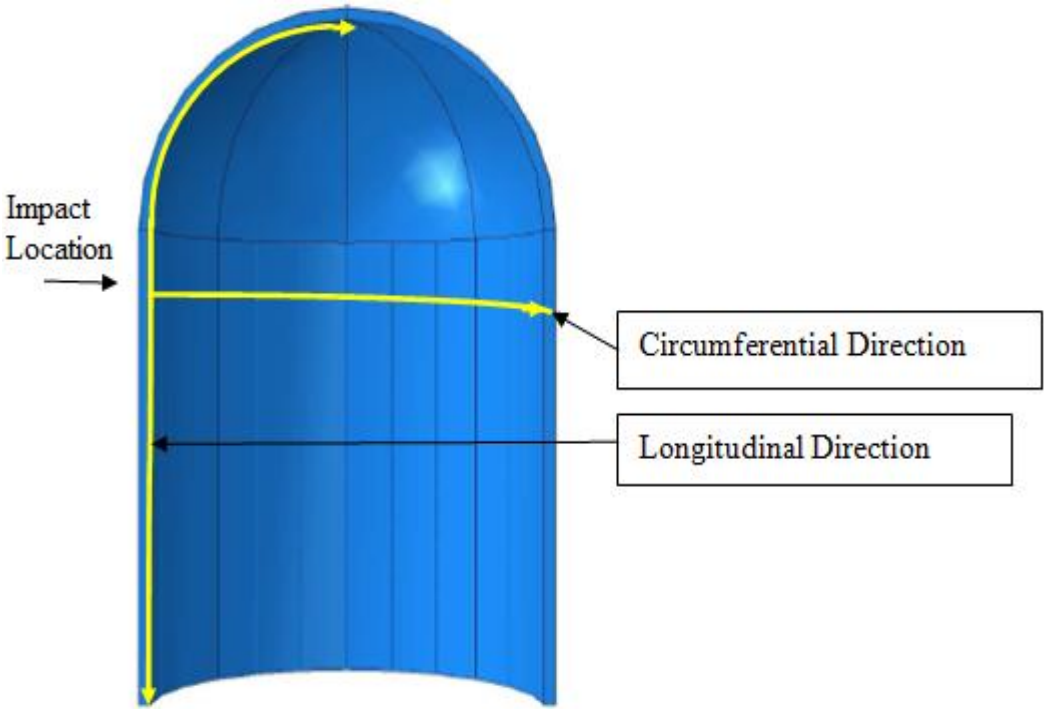

Fig. 4.3 Impact locations and the circumferential and longitudinal axes at which the deformation curves were plotted

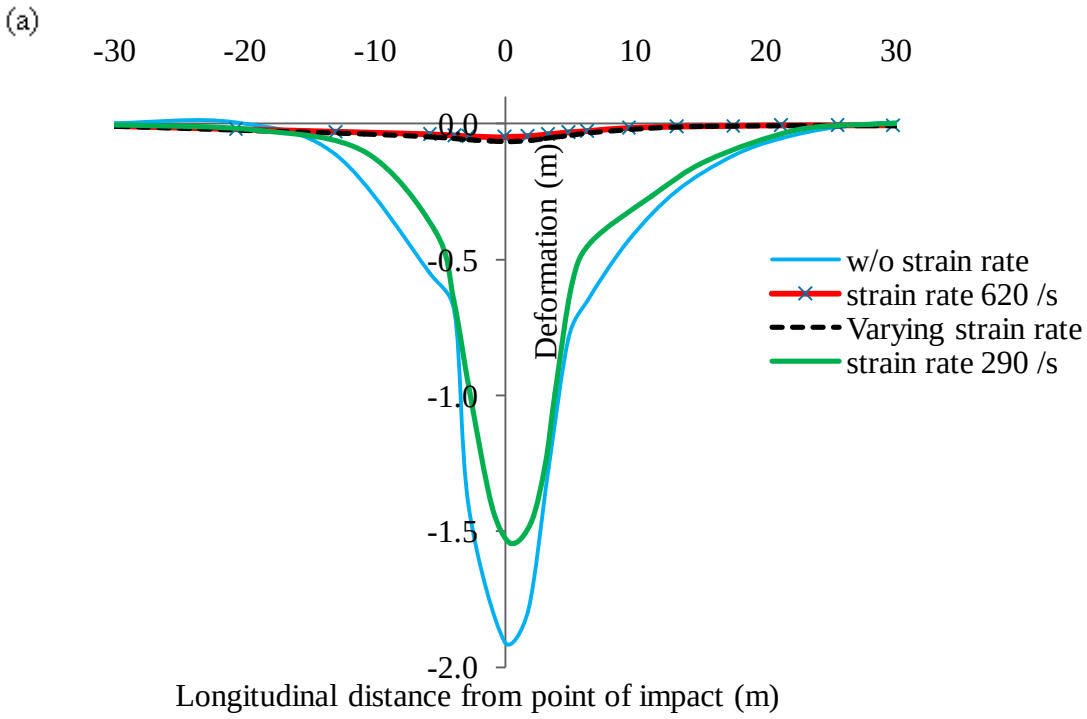

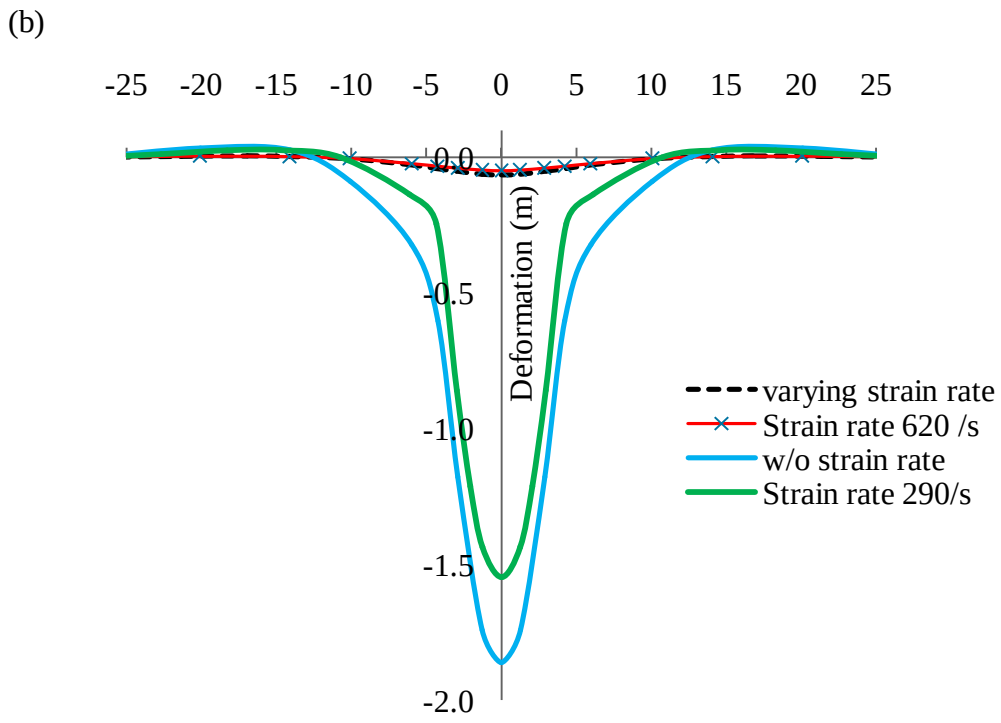

Fig. 4.4 Maximum deformation along (a) longitudinal and (b) circumferential axis at different strain rates

Fig. 4.5(a) and Fig. 4.6(a) highlight the elements chosen at the outer and inner face of the containment respectively in both materials to plot stresses and damage curves. The selected elements chosen to plot the results in outer and inner reinforcement sets have been displayed in Fig. 4.5(b) and Fig. 4.6(b) respectively. Fig. 4.7 (a) and (b) show the variation of compression and tension damage for concrete at varying strain rate at the outer and inner face of containment respectively. The three elements chosen each at the outer as well as inner face of containment were found to be completely damaged under compression and tension at low and 290 s^{-1} strain rates. Both the compression and tension damages reached their maximum value of 0.9 in each of these elements. However, for 620 s^{-1} strain rate the same elements predicted negligible damage both in tension as well as compression. Fig. 4.8 (a) and (b) predict the variation of stress in concrete in the direction of loading at the outer as well as inner face of containment respectively for different strain rates. In each of the three elements at the outer face the compressive stresses were found to be dominant. In the inner face elements however, very nominal tensile stresses were observed. A similar pattern of stresses has been found in the reinforcement, Fig. 4.9 (a) and (b). The front face reinforcement was found to be under compression while the inner face reinforcement under tension. The influence of strain rate on the variation of stresses in both concrete as well as reinforcement is also clearly visible. The stress variation is found to be consistent as well as in close agreement for the models with 620 s^{-1} and varying/combined strain rate. While the models with low and 290 s^{-1} strain rate predicted inconsistent variation of stresses in both materials.

(a)

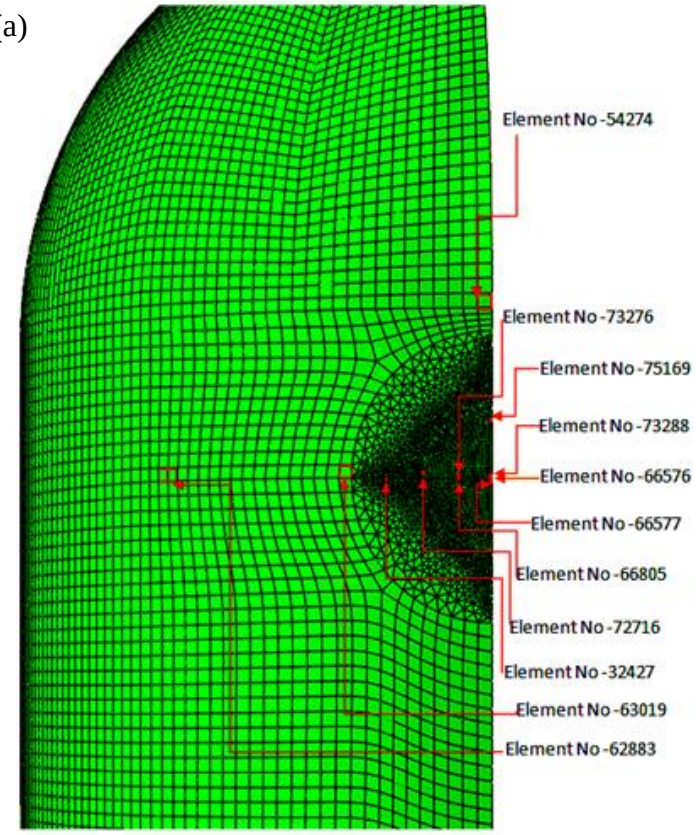

(b)

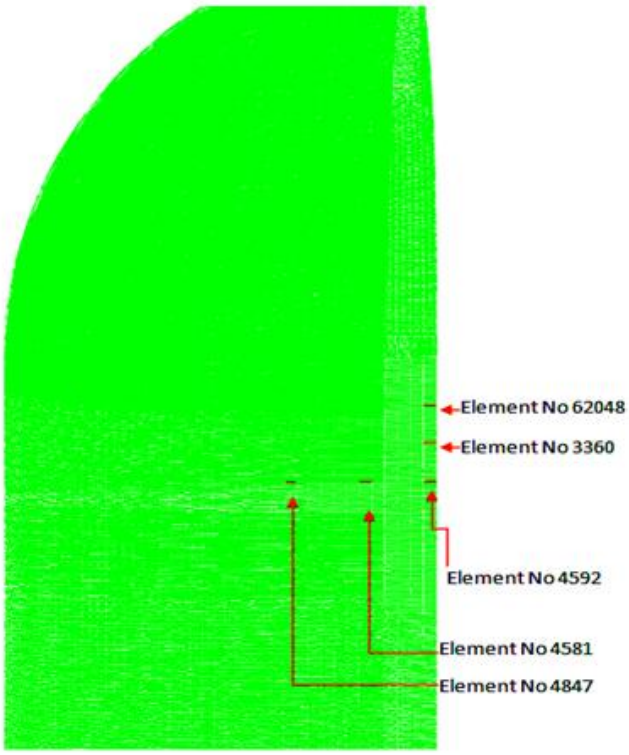

Fig. 4.5 Element selected at the outer face of containment to plot stresses and damage (a) Concrete and (b) Reinforcement

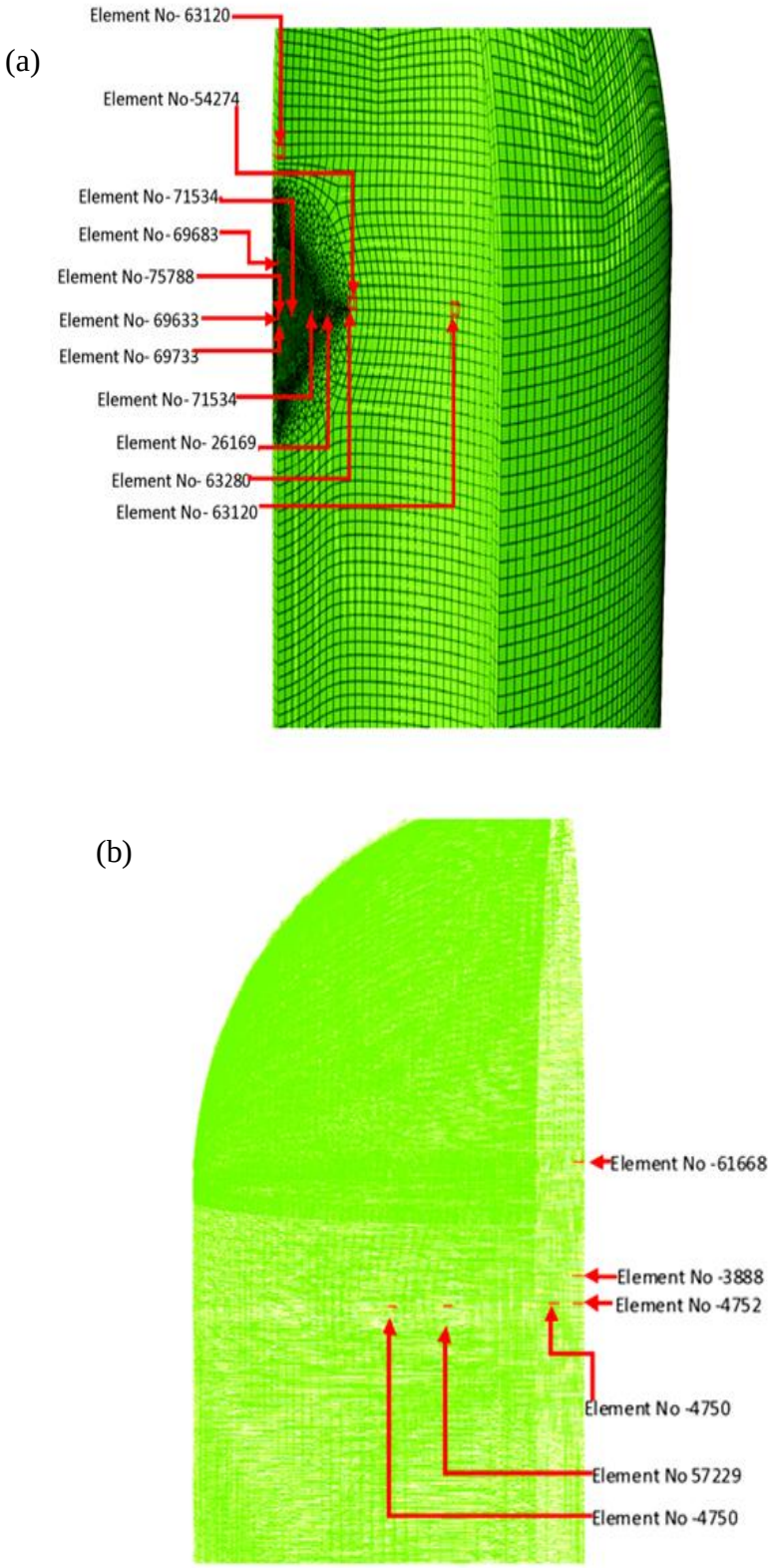

Fig. 4.6 Elements selected at the inner face of the containment to plot stresses and damage (a) Concrete and (b) Reinforcement

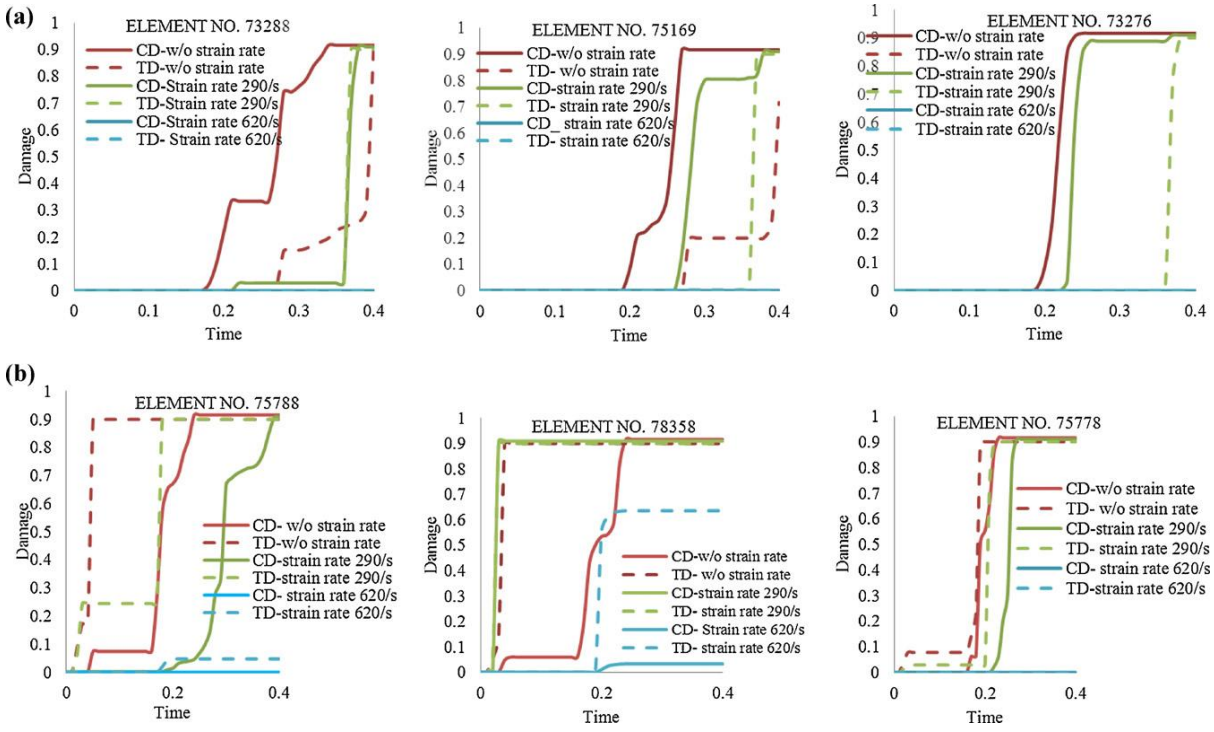

Fig. 4.7 Compression damage (CD) and tension damage (TD) in concrete for different strain rates: (a) at outer face of containment and (b) at inner face of containment

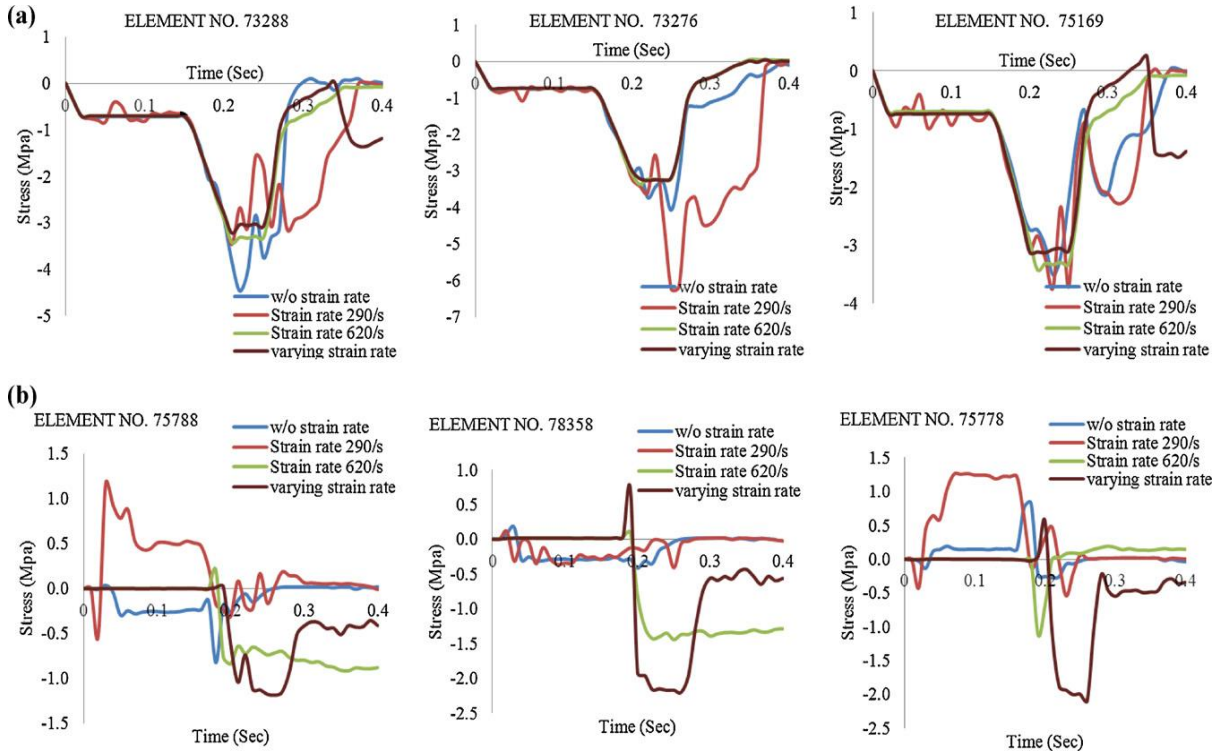

Fig. 4.8 Variation of normal stress (11) in concrete for different strain rates (a) at outer face of containment and (b) at inner face of containment

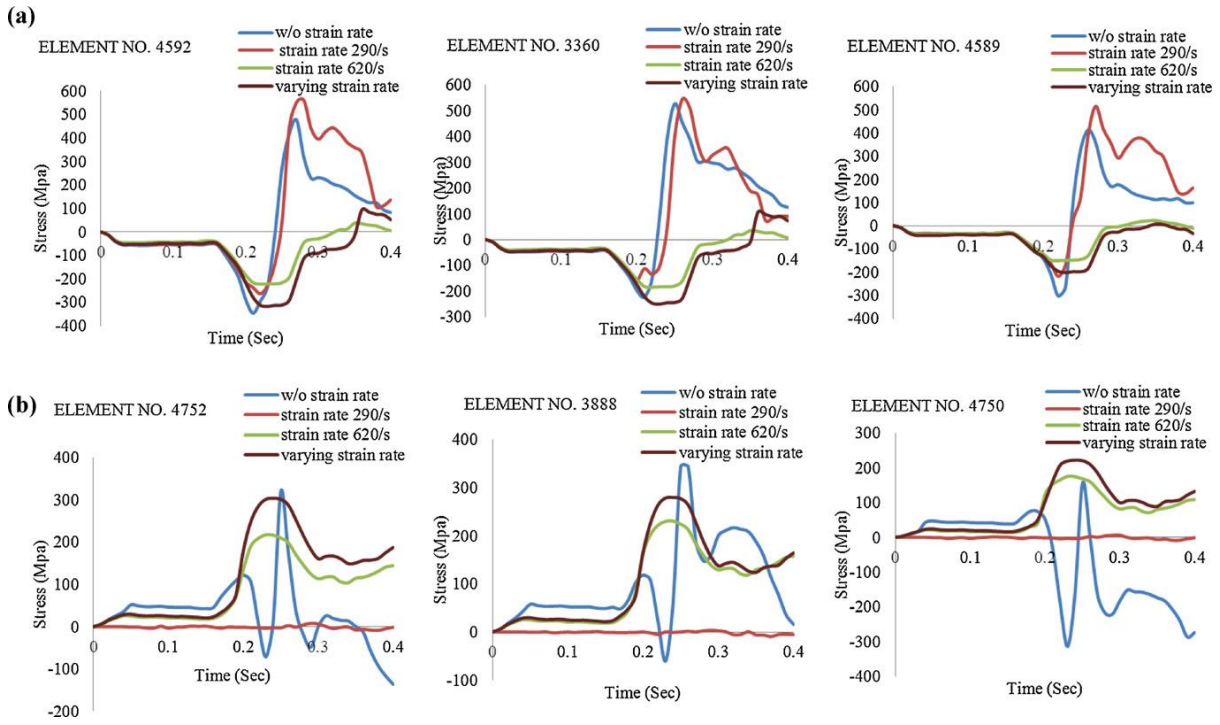

Fig. 4.9 Variation of stress (σ_{11}) in steel reinforcement for different strain rates (a) at outer face of containment and (b) at inner face of containment

The maximum deformation of the containment observed by Abbas et al. (1996) at the junction of dome and cylinder was 34.2 mm. Kukreja (2005) validated his material model with Abbas et al. (1996) and reported that the maximum deformation was 46 mm at the same location. In present study however, the maximum deformation with varying strain rate was found to be 66.9 mm at the same location. A close correlation between the predicted profiles of deformation as well as the peak deflection was found with that of the Abbas et al. (1996). The peak deflection occurred at 0.247 seconds as per the study carried out by Abbas et al., (1996) and at 0.25 seconds according to the present investigation. Moreover, Abbas et al. (1996) adopted 52, 20-noded isoparametric brick elements with a total number of 342 nodes to discretize the BWR containment. For a similar simulation, Kukreja (2005) considered a few hundred elements and in the present study a total number of elements in the containment was 514, 640. The small variation in the result, therefore, may be due to the effect of size and total number of element chosen for the analysis. Hence, in all further analysis the use of stress-strain relationship with varying strain data has been adopted. Logically, it can be also understood that strain rate may not be constant for different aircraft and strike location, therefore, option of varying strain rate is justified.

The maximum deformation contour has been plotted in Fig. 4.10. The peak deflection was found to be 67 mm at 0.25 seconds. The deformation was found to be highest at the impact location, it decreased as the distance from the impact location increased at longitudinal as well as circumferential axis. The positive sign shows the outward and the negative sign inward deformation. Fig. 4.11 describes the stresses (σ_{11}) developed in the containment in concrete as well as reinforcement. The stresses shown in concrete are in the direction of loading. The positive sign shows tension while the negative sign compression. The reinforcement has been modeled as truss element with three translational degrees of freedom therefore it will not undergo bending. However, as it has been descretized in to very small elements the displacement of the nodes causes the development of axial stresses. At the outer face of containment both concrete and reinforcement were found to be under compression at the location of impact. At a distance (on the circumferential axis) away from this location however, some tensile stresses were observed due to nominal bulging of the containment. The stress in concrete was found to be of the order of 3 to 4 MPa while in steel 326 MPa at the impact location. At the inner face, both the concrete and reinforcement were found to be under tension at the impact region. The maximum tension in concrete was found to be about 2 MPa while in steel 314 MPa.

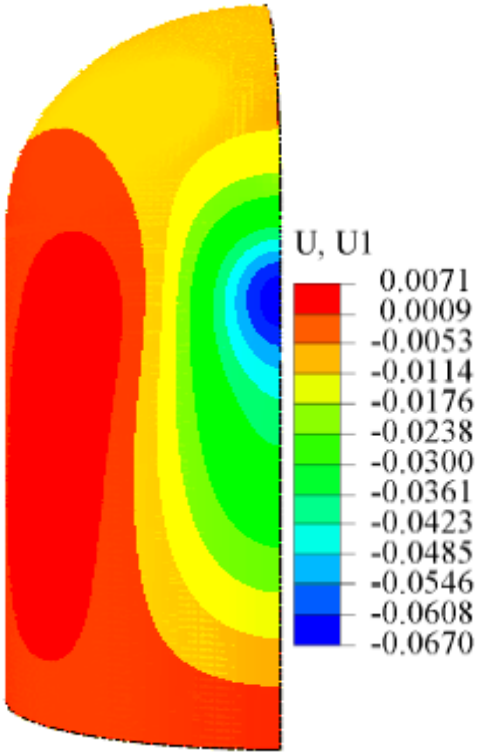

Fig. 4.10 Deformation contour against Boeing 707-320 aircraft at 0.25 sec.

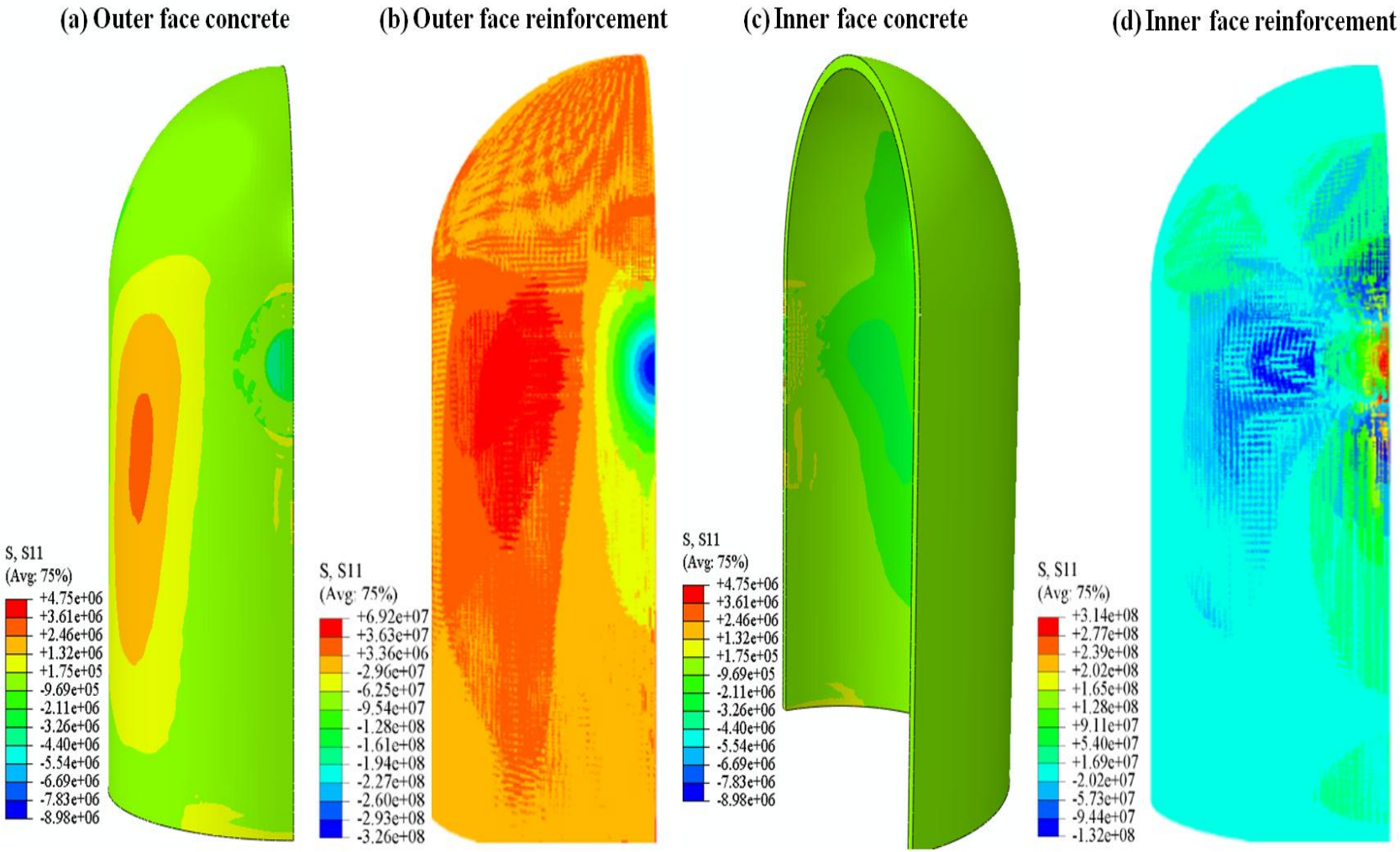

Fig. 4.11 Maximum stresses developed in the containment

Fig. 4.12 (a) shows the deformation of the containment measured along the longitudinal/meridonial axis at different time intervals. The negative sign shows the inward while the positive sign outward deformation of the containment. The deformation of the containment increased with an increase in the intensity of loading and reached its maximum value at ~0.26 seconds. The profile of deformation was found to be symmetric about the location of impact in the upward and downward directions. Subsequently the rebounding of the structure occurred as the load started decreasing. The rebounding of the structure however, was not found to be symmetric, please see the profile at time interval 0.29 seconds in Fig. 4.12 (a). The deformation along the circumferential axis at the different time intervals was shown in Fig. 4.12(b). The deformation was found to increase with an increase in the loading intensity. In this case however, some outward deformation was also noticed away from the impact region. The deformation was also found to be more localised as compared to that measured along the longitudinal axis.

Fig. 4.13 and 4.14 show the variation of all the stress components for six elements each at the outer and inner face of the containment respectively along the circumferential axis. Near the impact zone the normal stress components in y and z directions were found to be dominant while the other stresses were almost negligible, Fig. 4.13. It should be noticed that the impact force is acting in x-direction as a result of which the elements near the impact zone are deforming along this direction. However, the other two components are resisting the deformation and hence the stress intensity of these two components is higher. As the distance from the impact location increased, the shear stresses also became dominant. It should also be noticed that the stresses in all of these elements are high under compression. The tension in some elements could also be noticed during the rebounding of the structure. At the inner face, an opposite trend of stresses was observed. The elements near the impact zone were found to be under tension, which increased with an increase in the load and thereafter the rebounding of the structure changed the nature of stresses to compression, Fig. 4.14. Away from the impact zone however, the shear stresses were also found to be dominant.

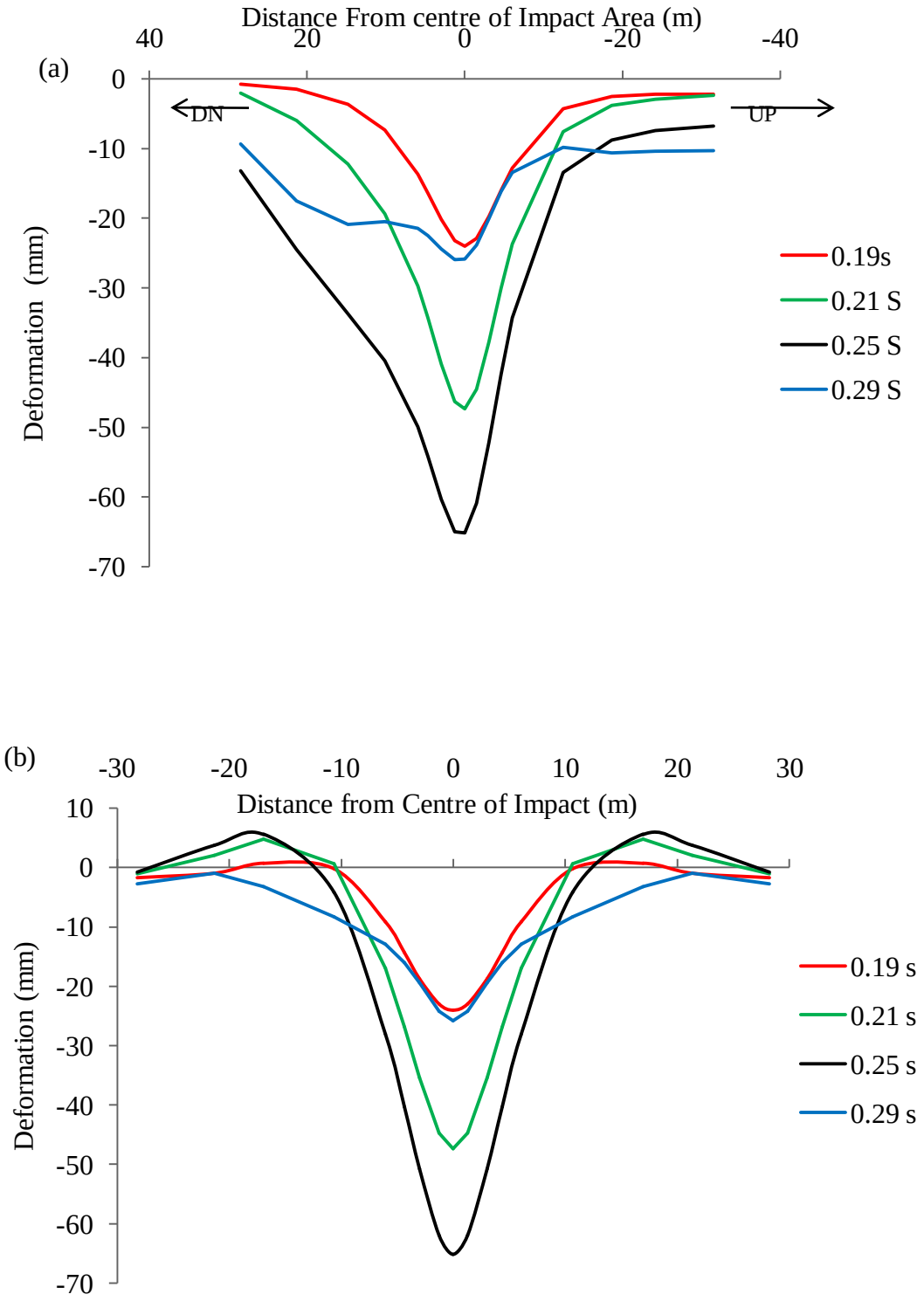

Fig. 4.12 Deformation of the containment along (a) longitudinal axis (b)circumferential axis

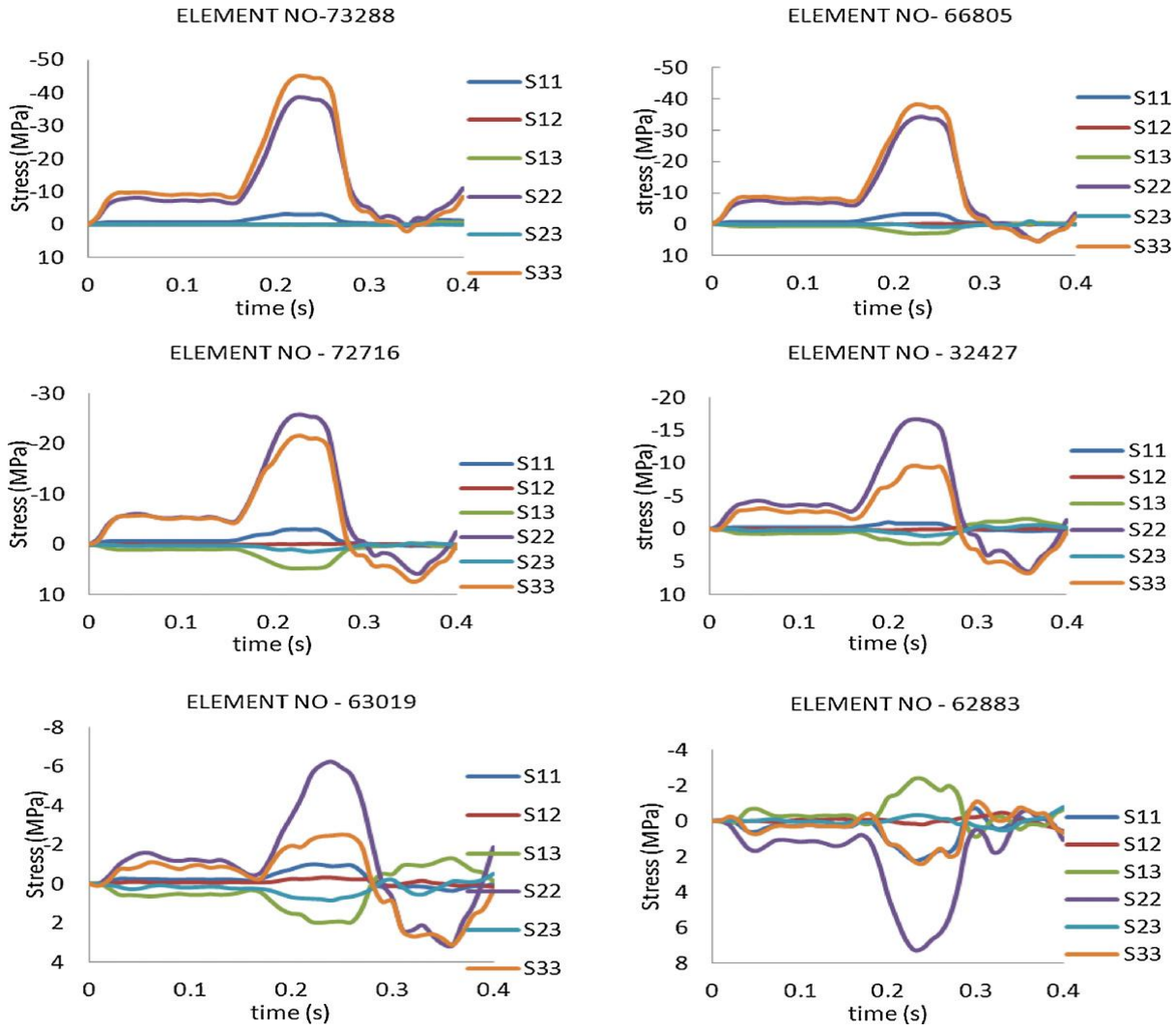

Fig. 4.13 Variation of stresses in concrete at the outer face of the containment

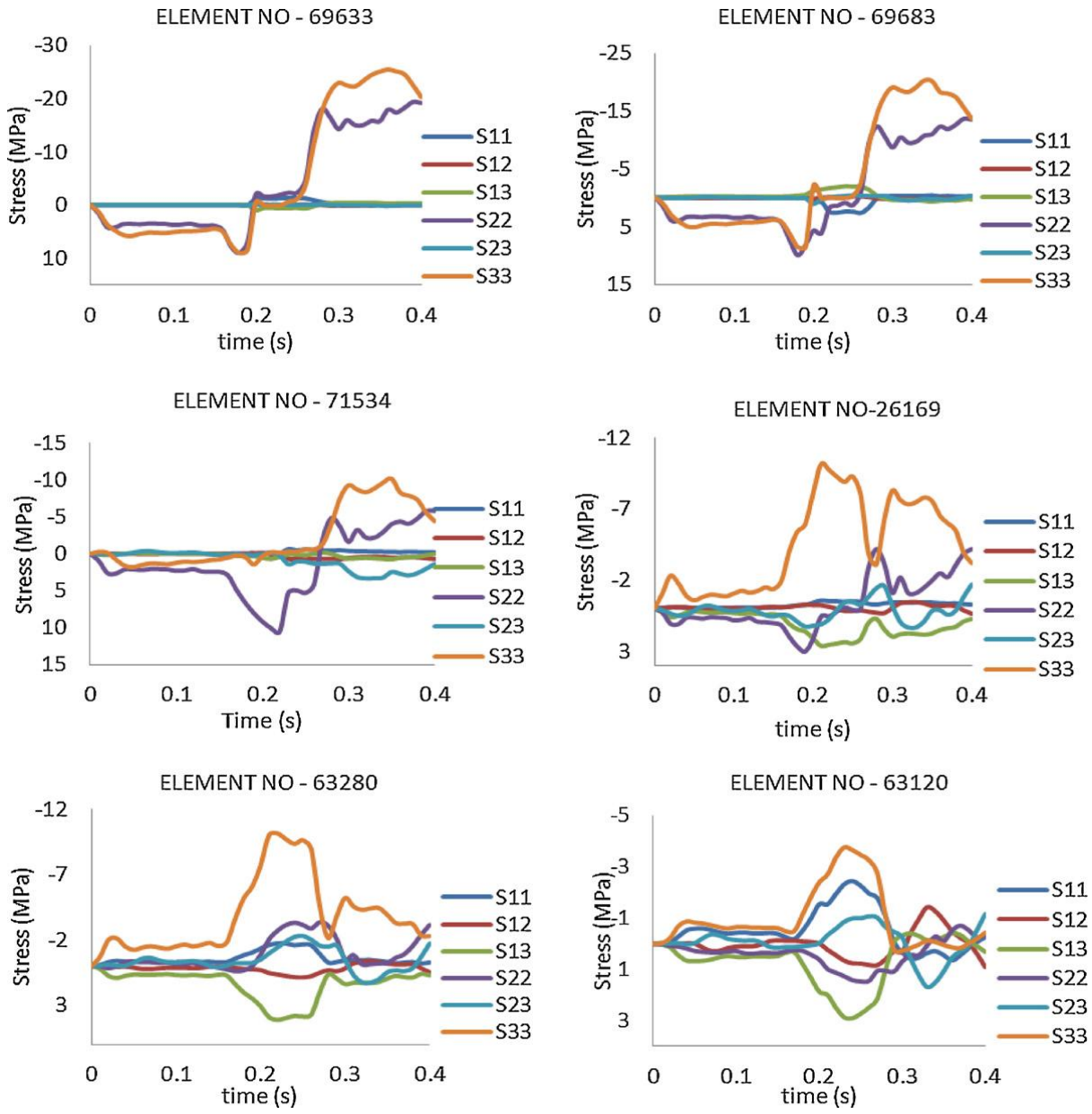

Fig. 4.14 Variation of stresses in concrete at the inner face of the containment

4.3 EFFECT OF IMPACT LOCATION

In order to evaluate the effect of strike location numerical simulations have been carried out wherein four different locations at the outer containment of BWR Mark III type nuclear containment have been studied under the crash of three different aircrafts. The “Location A” is chosen at containment wall 33.5 m above the base. The most studied location in the available

literature i.e. the junction of wall and dome of the containment has been identified as “Location B”. Moreover, at the curvature of the dome at the height of 56 m from the base the “Location C” has been considered. The “Location D” has been selected at the crown of the containment, Fig. 4.15. The “location A, C and D” have rarely been studied, particularly the “Location A” has not been studied in the open available literature.

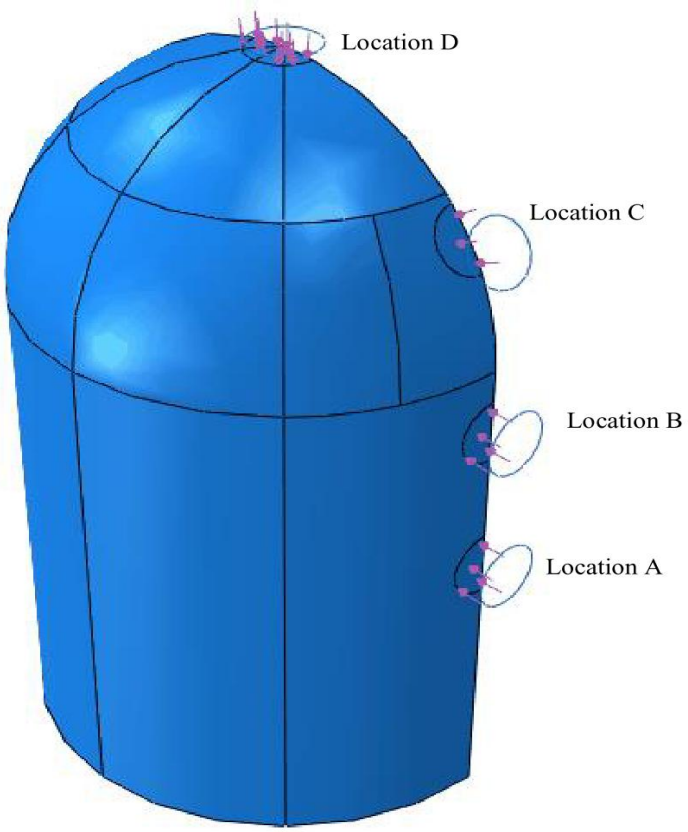

Fig. 4.15 Locations selected for impact of aircraft

The results have been obtained for three different aircrafts viz. Fighter jet Phantom F4, Boeing 707-320 and Airbus A 320. The angle of incidence has been considered normal to the containment surface. The reaction time response methodology has been adopted to define the aircraft loading on the containment, see Fig. 4.16. The loading of aircraft was assigned to the containment at a given constant area equivalent to the average of total cross-sectional area of fuselage and wings. The deformations and stresses in the concrete and reinforcement were determined at every location against each aircraft. The maximum deformation of the containment has been obtained and compared with those of the studies available in literature.

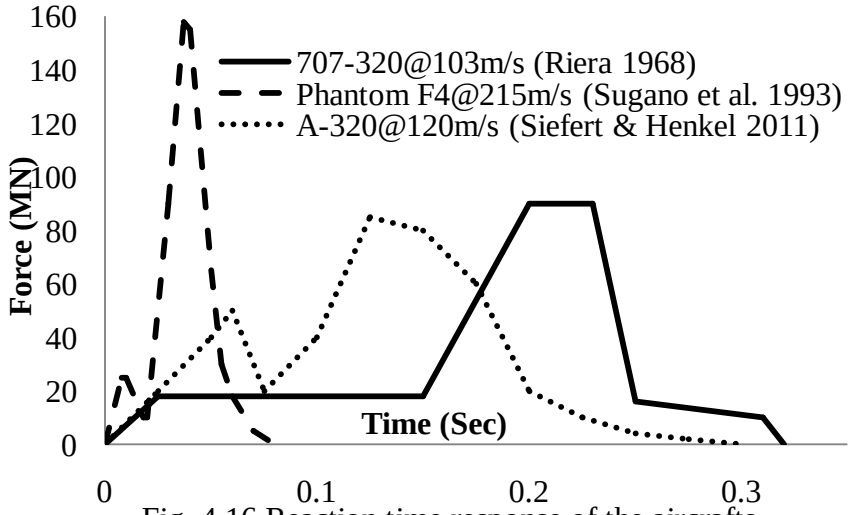

Fig. 4.16 Reaction time response of the aircrafts

The displacements contours in the concrete have been plotted at each location against the strike of Phantom F4, Boeing 707-320 and Airbus A320 aircrafts in Fig. 4.17, 4.18 and 4.19 respectively. At the top of each figure the inset view has been provided which describes the deformation at the rear face of the containment while the main figure shows the outer face. The maximum displacement contour in concrete due to crash of Phantom F4 has been plotted in Fig. 4.17. At "Location A" the maximum displacement in concrete is 99.42 mm, however, this value of displacement could be seen in a few elements on the rear face of containment. There is no study available in literature to compare the displacement results at "Location A". At "Location B" (junction of dome and cylinder), Abbas et al., (1996) reported maximum displacement of 44.2 mm in a BWR containment while Lo Frano and Forasassi (2011), 217 mm in an IRIS containment against Phantom F4. However, in the present study a maximum displacement of 79.68 mm has been noticed at this location against the same aircraft. Further, at "Location C and D" the available literature does not have any result for Phantom F4. In the present study, a maximum displacement of 42.5 mm and 33.35 mm has been noticed at these two locations respectively. It may therefore be concluded that the containment deformation is decreasing respectively from "Location A" to "Location D". At "Location D" the predicted maximum displacement is almost one third compared to that at "Location A". The "Location A" has experienced maximum deformation since it does not have any influence of boundary conditions and it is located in the cylindrical region of containment which is comparatively flexible. The deformation has decreased at "Location B" due to the transition of geometry of the containment in this region, from cylinder to dome. For "Location C and D" the membrane action is predominant hence the deformation is further reduced.

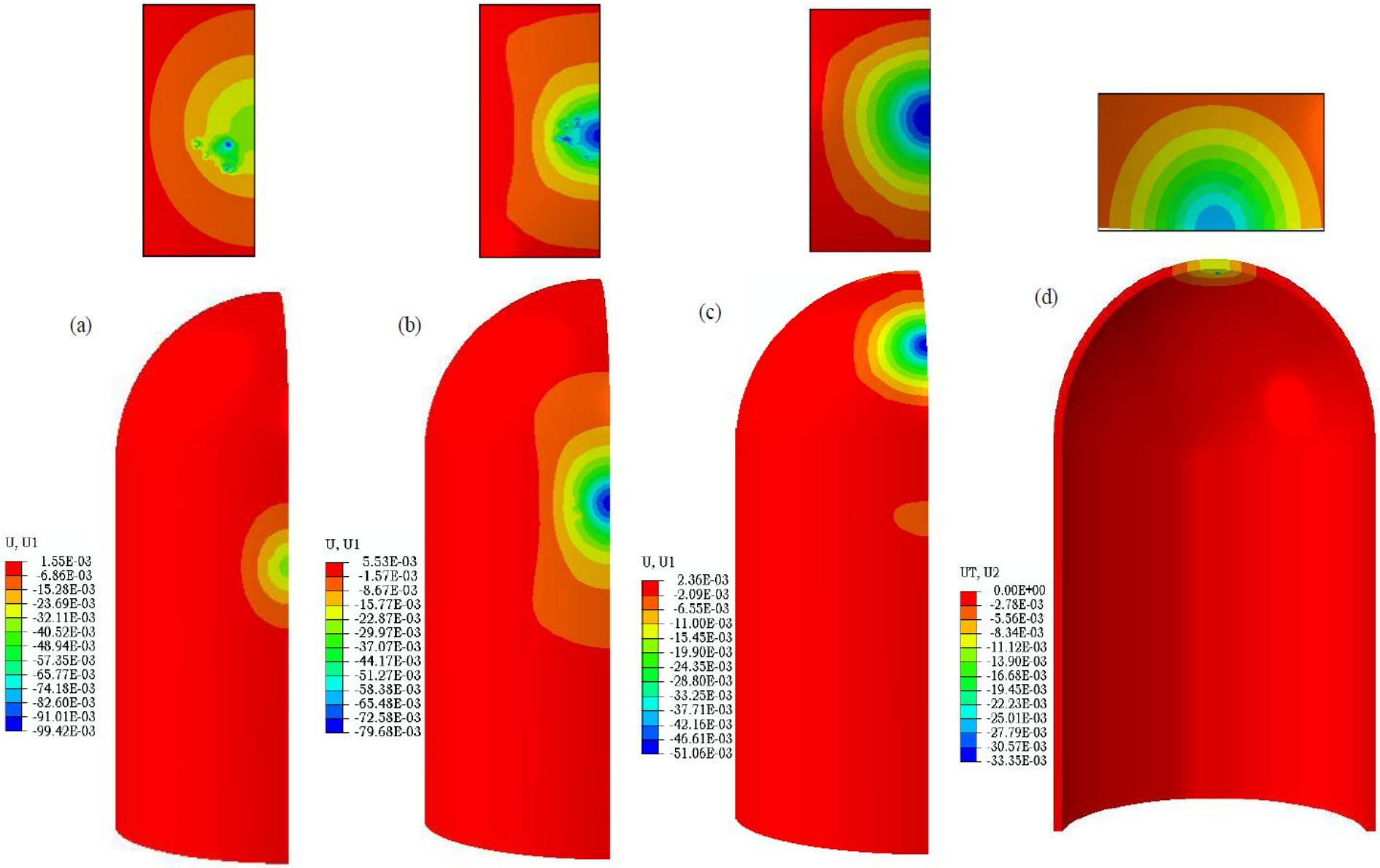

Fig.4.17 Maximum displacement (deformation) in concrete in the direction of loading for Phantom F4 at : (a) Location A (b) Location B (c) Location C (d) Location D

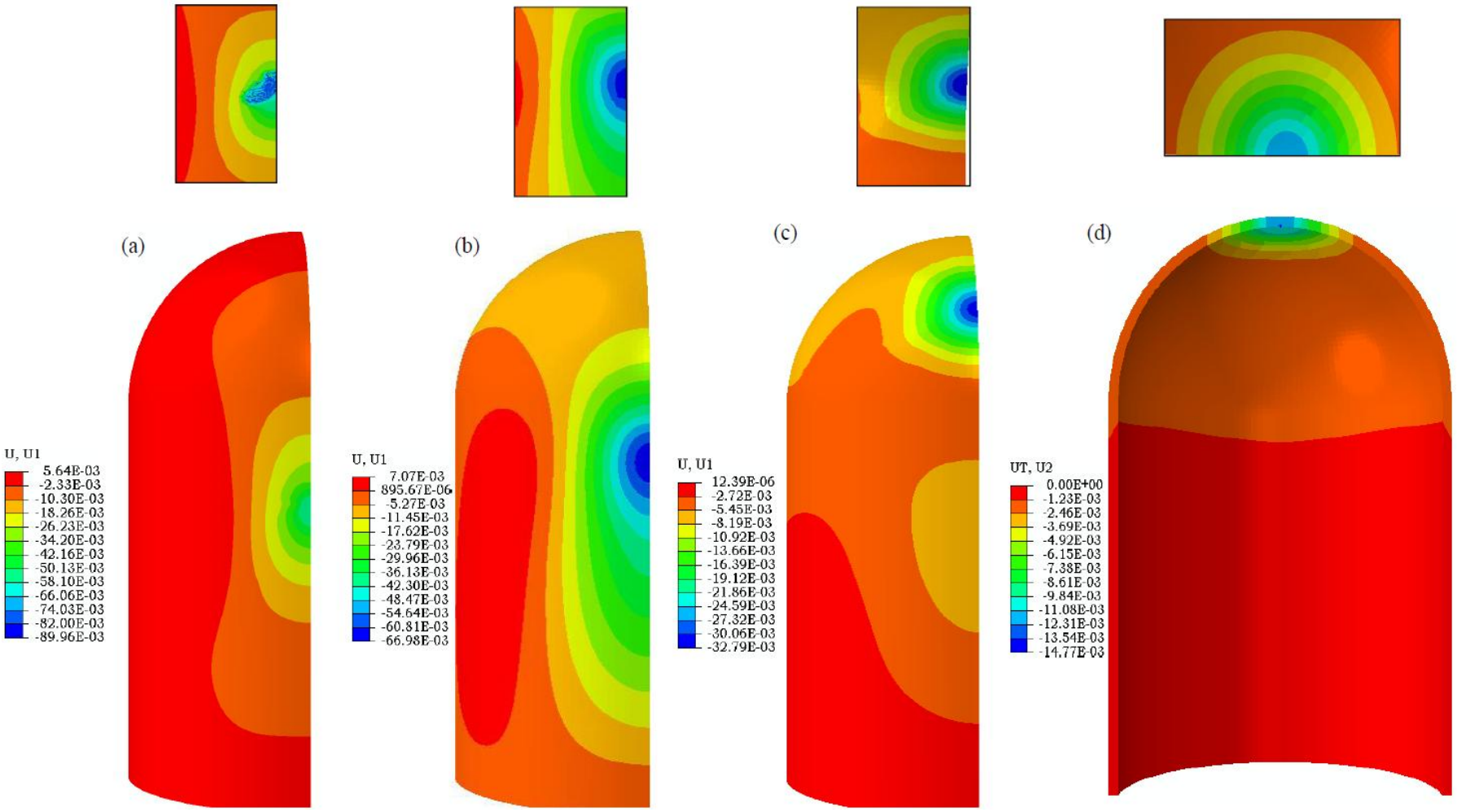

Fig.4.18 Maximum displacement (deformation) in concrete in the direction of loading for Boeing 707-320 at: (a) Location A (b) Location B (c) Location C (d) Location D

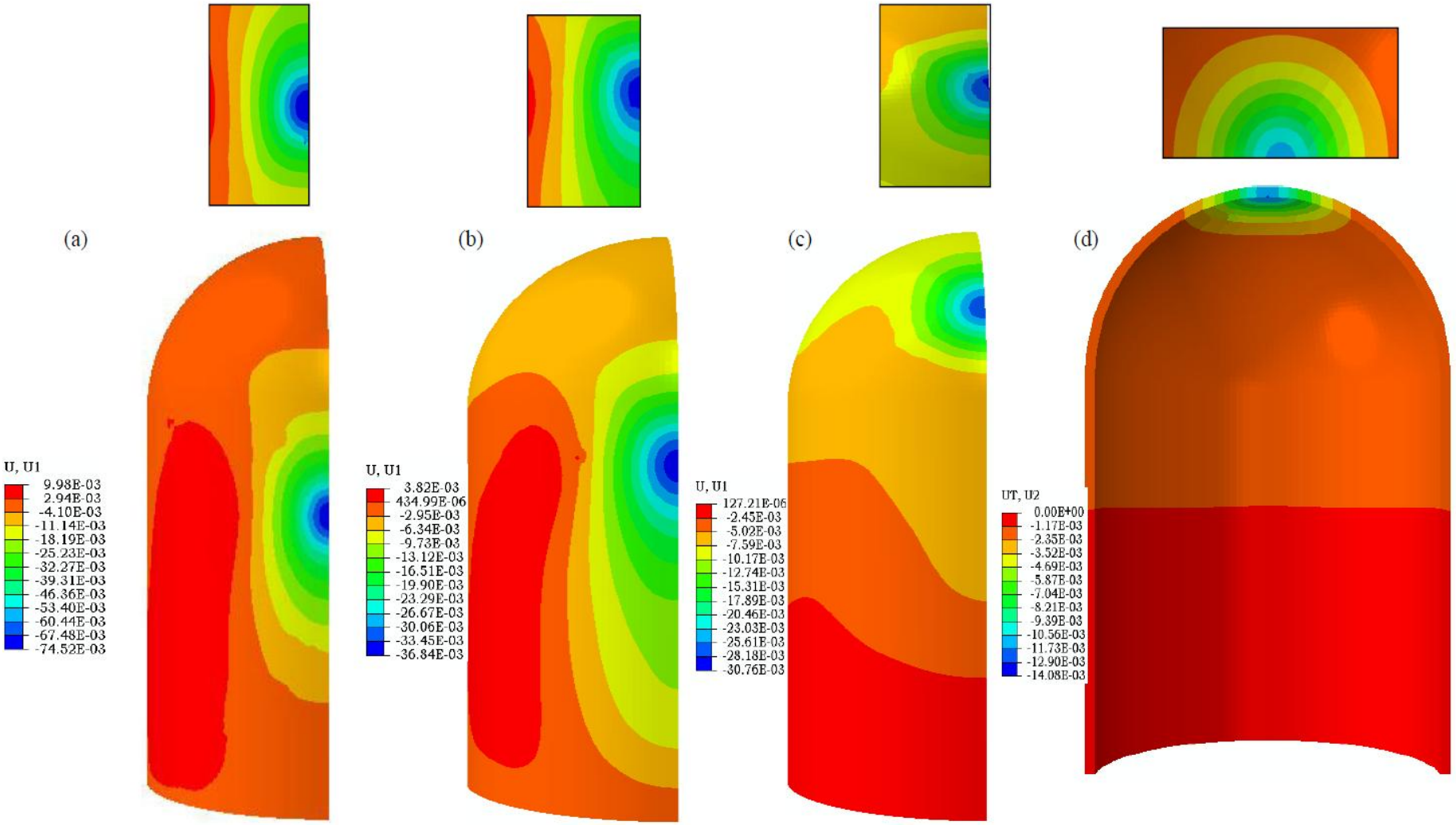

Fig. 4.19 Maximum displacement (deformation) in the concrete in the direction of loading Airbus A320 at: (a) Location A (b) Location B (c) Location C (d) Location D

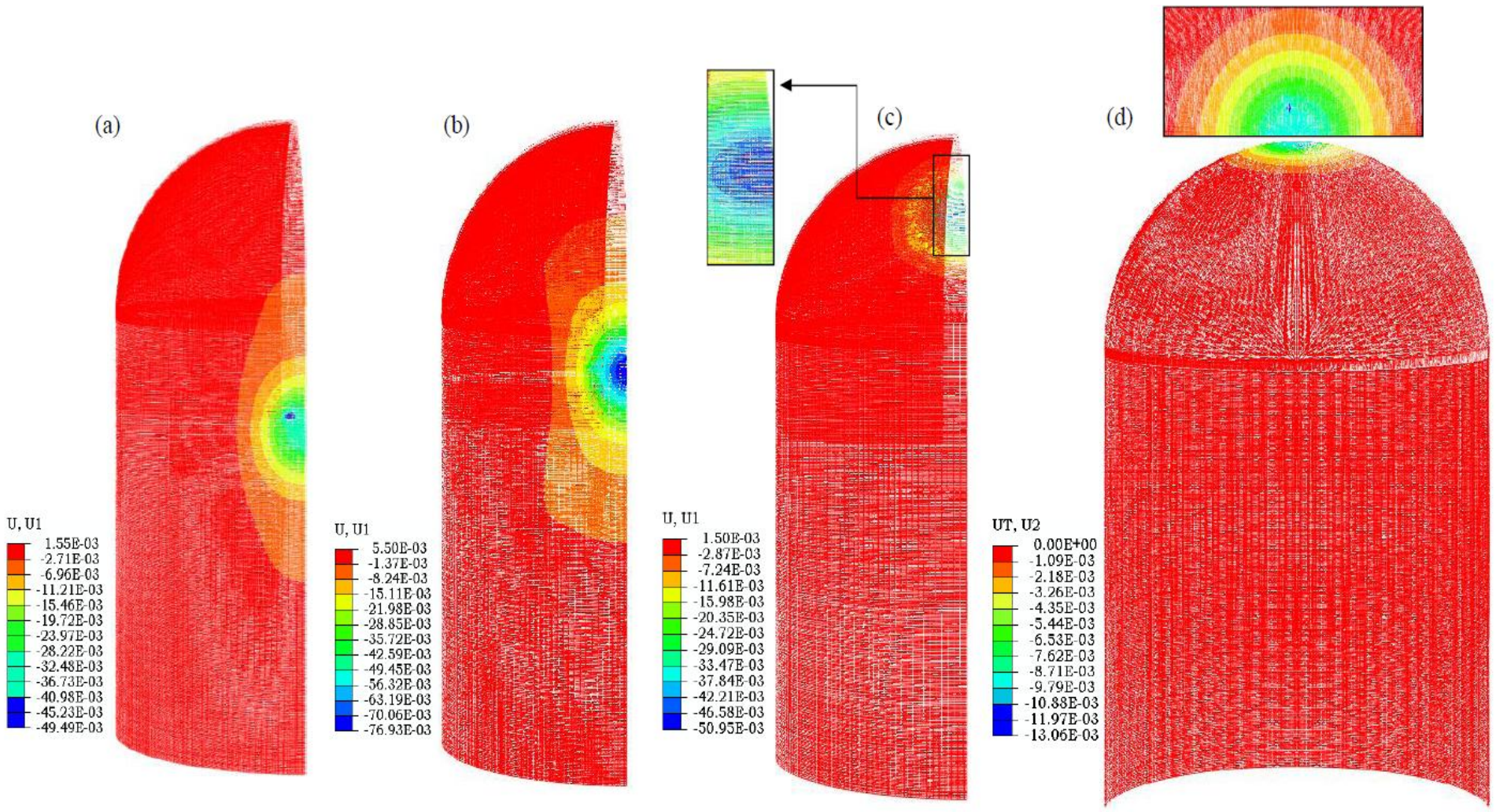

Fig. 4.20 Maximum displacement (deformation) in the inner reinforcement in the direction of loading Phantom F4 at: (a) Location A (b) Location B (c) Location C (d) Location D

The maximum value of the displacement due to the crash of Boeing 707-320 has been found to be lesser in comparison to Phantom F4 at each location of strike, Fig. 4.18. At "Location A" the maximum value of displacement in concrete is 89.96 mm; however, no result is available in literature to compare this observation. At "Location B" Abbas et al. (1996) observed a maximum displacement of 34.2 mm while Kukreja (2003), 46 mm, against Boeing 707-320. At the same location however, a maximum displacement of 66.98 mm has been found in the present study. At "Location C", maximum displacement in concrete due to crash of Boeing 707-320 is 32.79 mm. At "Location D" (crown of dome) the maximum displacement is close to 15 mm. However, there is no result available in literature for this location to be compared. It may therefore be concluded that the displacement occurred at "Location C", is twice as compared to that occurred at "location D" (Crown). Moreover, centre of overall height of containment building experienced the displacement approximately 6 times higher than that observed at the crown.

Against Airbus A320, the maximum value of displacement has been found to be 74.52 mm at "Location A" while 36.34 mm at "Location B", see Fig. 4.19. A maximum displacement of 50 mm has been reported by Siefert and Henkel (2011) in an assumed containment building (wall thickness 1.8 m) against same aircraft near the junction of dome and cylinder ("Location B" of this study). At "Location C", the maximum displacement has further reduced to 30.76 mm, while at crown, 14 mm. It can be pointed out from Figs. 4.17-4.19 that against same aircraft with same loading condition, crown of the containment is most robust point. Moreover, it can also be highlighted that midpoint of overall height is most vulnerable and weak region of containment.

As discussed in Chapter 2, there are two sets of reinforcement in the containment structure each in the circumferential and vertical/meridonal directions located near the front and rear face. The contour plot of nodal deformation in the inner reinforcement set has been plotted in Fig. 4.20 at each location against Phantom F4 aircraft. The inward nodal displacement i.e. in the direction of loading is indicated by the negative sign and the outward nodal displacement by the positive sign. It can be observed that displacements are significant in the impact zone only. The maximum displacement of 76.93 mm has been reported at "Location B" followed by 49.49 mm at "Location A", 42.38 mm at "Location C" and 13.06 mm at "Location D".

Fig. 4.21 shows the maximum displacements in the inner reinforcements against Boeing 707-320 aircraft. A maximum displacement of 89.80 mm has been observed just above the center of impact region at “Location A”. However, at “Locations B, C and D” it is 66.45 mm, 32.31 mm and 14.5 mm respectively. The maximum displacement in the inner reinforcement against Airbus A320 has been found to be 74.45 mm, 36.68 mm, 30.12 mm and 13.80 mm at “Location A, B, C and D” respectively, Fig. 4.22. The outward displacements are very low in intensity and could be noticed away from impact locations.

In the outer set of reinforcement, the displacements are not as high as compared to the inner set of reinforcement. For Phantom F4, the maximum displacement at outer reinforcement is 75.8 mm at Location B, Fig. 4.23b. However, at “location A”, the maximum displacement in the direction of loading is limited to 35 mm, Fig. 4.23a. At “Location C” the maximum displacement is 42.38 mm while at “Location D”, less than 10 mm, see Figs. 4.23(c) and (d) respectively.

Against Boeing 707-320 also the maximum displacement has been found to occur at “Location B”. However, the difference in the value of displacement between “Location A and B” is not as significant as against Phantom F4. The maximum displacement at “Location A” is 58.3 mm, while at “Location B”, 65.83 mm, see Fig. 4.24(a) and 4.24(b) respectively. At “Location C”, the maximum displacement is 32.03 mm and at “Location D”, 12.11 mm, see Fig. 4.24(c) and 4.24(d) respectively. Against Airbus A320, the maximum displacement in the outer reinforcement has been found to be 74.09 mm, 36.12 mm, 27.85 mm and 11.13 mm at “Location A, B, C and D” respectively, Figs. 4.25(a)-(d).

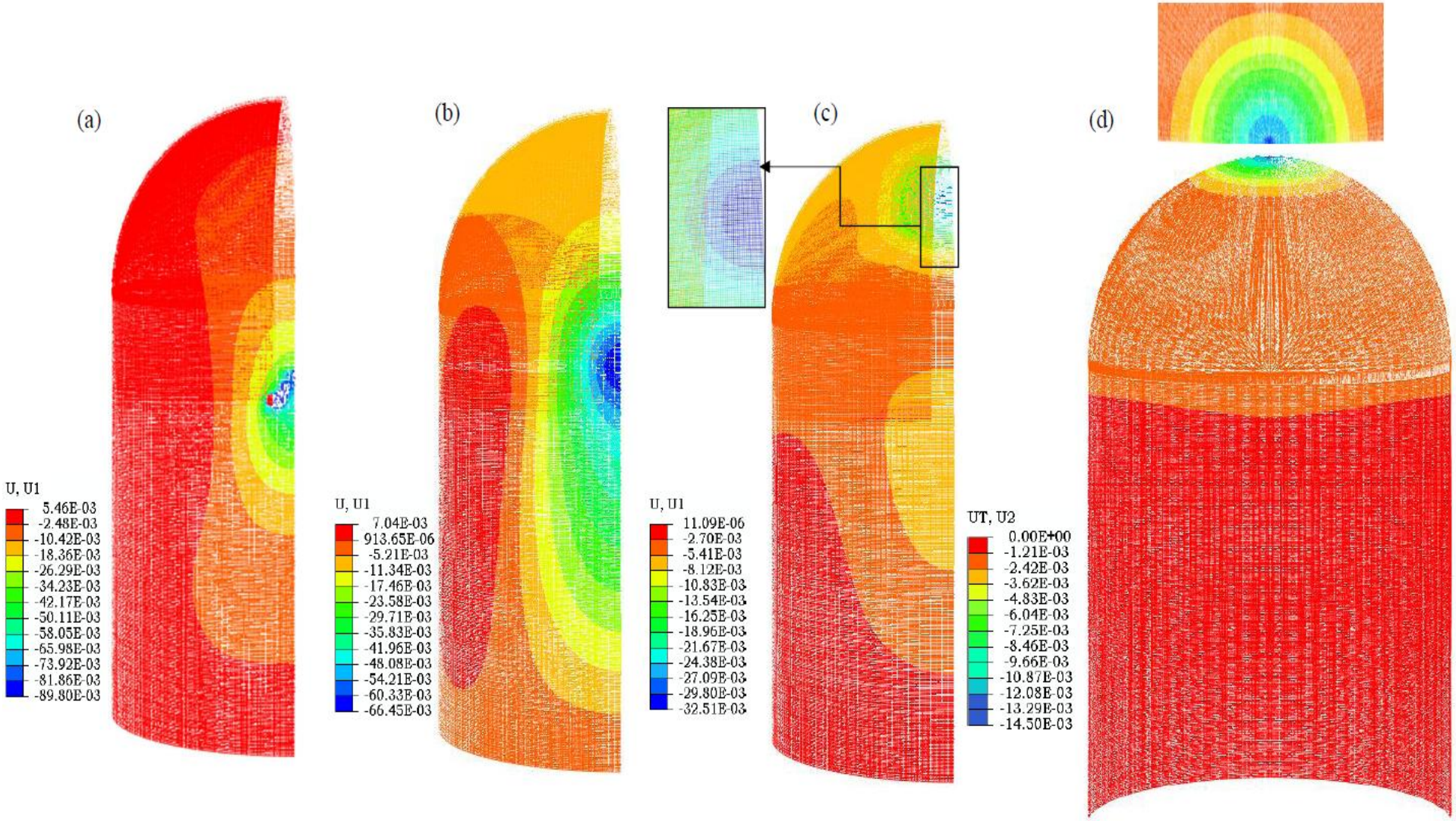

Fig. 4.21 Maximum displacement (deformation) in the inner reinforcement in the direction of loading for Boeing707-320 at: (a) Location A (b) Location B (c) Location C (d) Location D

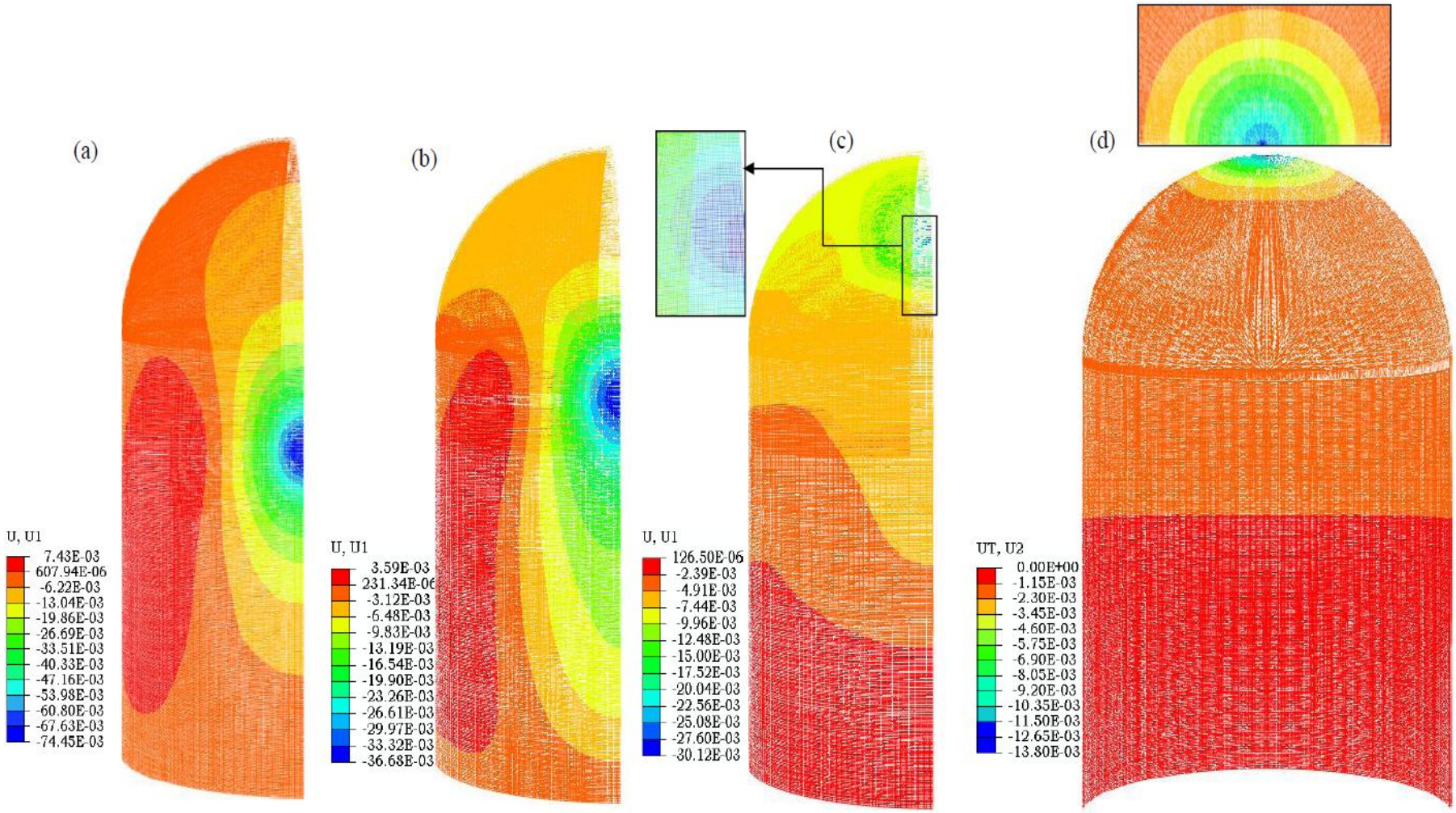

Fig. 4.22 Maximum displacement (deformation) in the inner reinforcement in the direction of loading Airbus A320 at: Location A (b) Location B (c) Location C (d) Location D

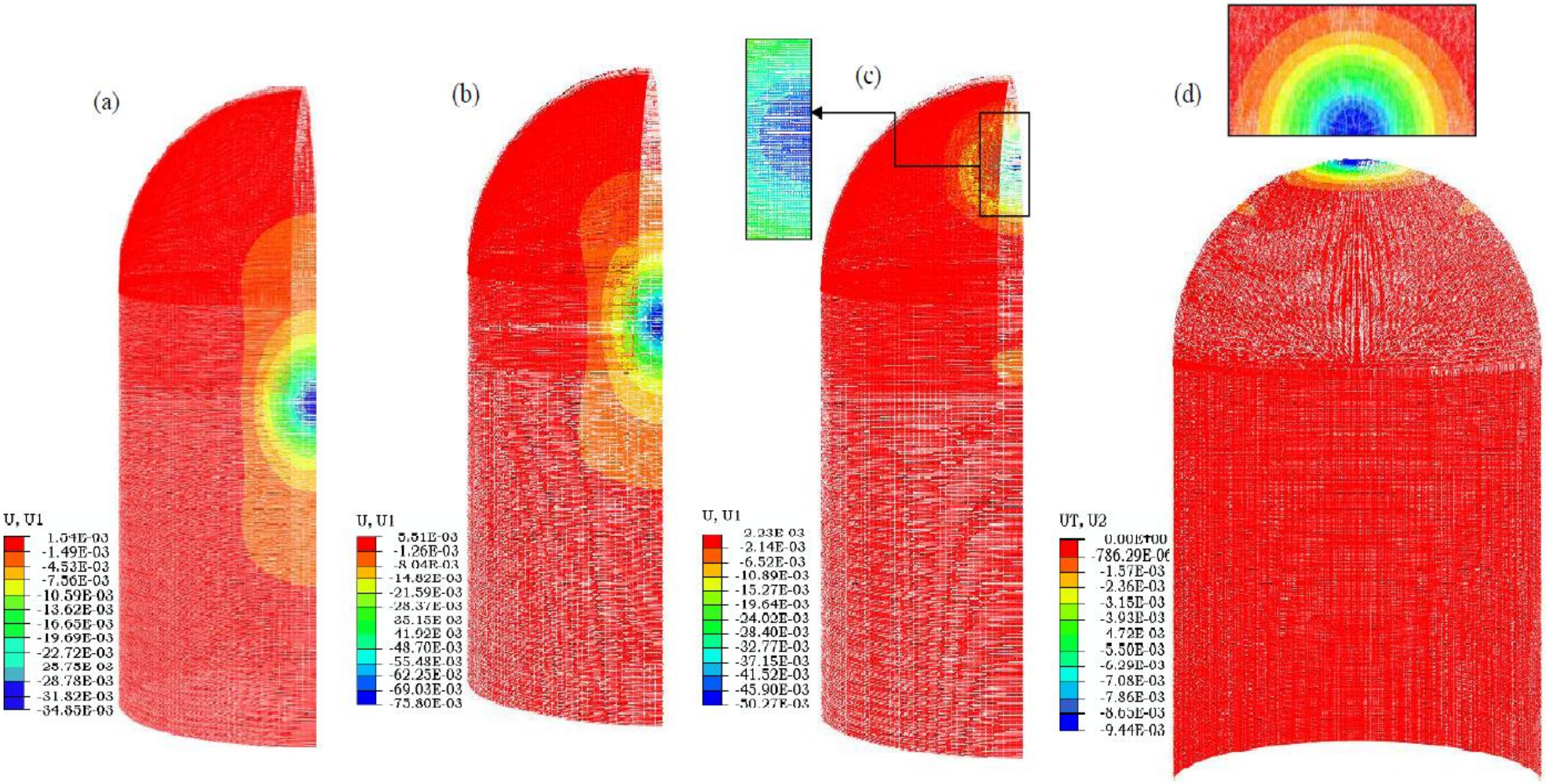

Fig.4. 23 Maximum displacement (deformation) in outer reinforcement in the direction of loading for Phantom F4 at: Location A (b) Location B (c) Location C (d) Location D

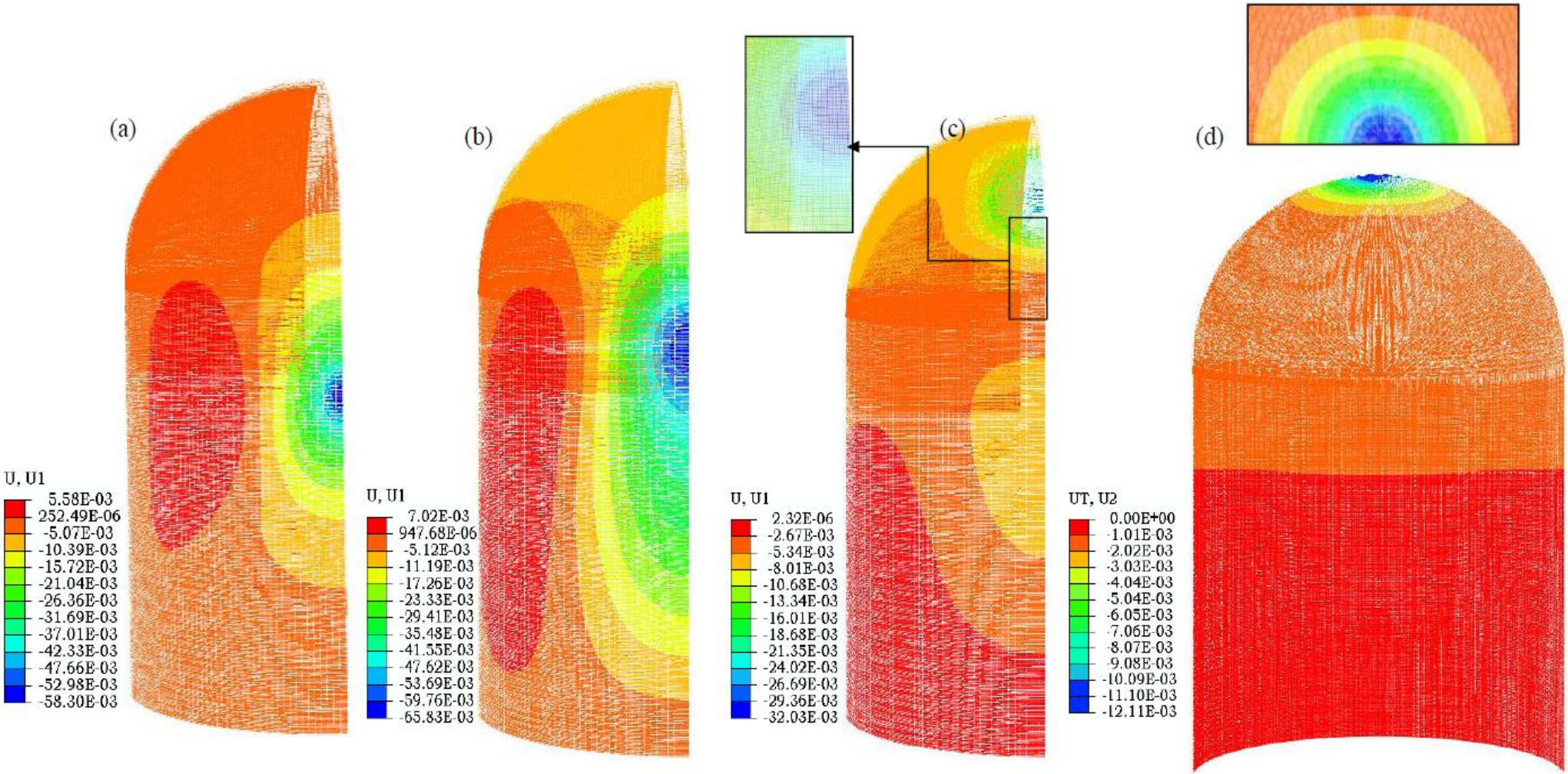

Fig. 4.24 Maximum displacement (deformation) in outer reinforcement in the direction of loading 707-320 at: Location A (b) Location B (c) Location C (d) Location D

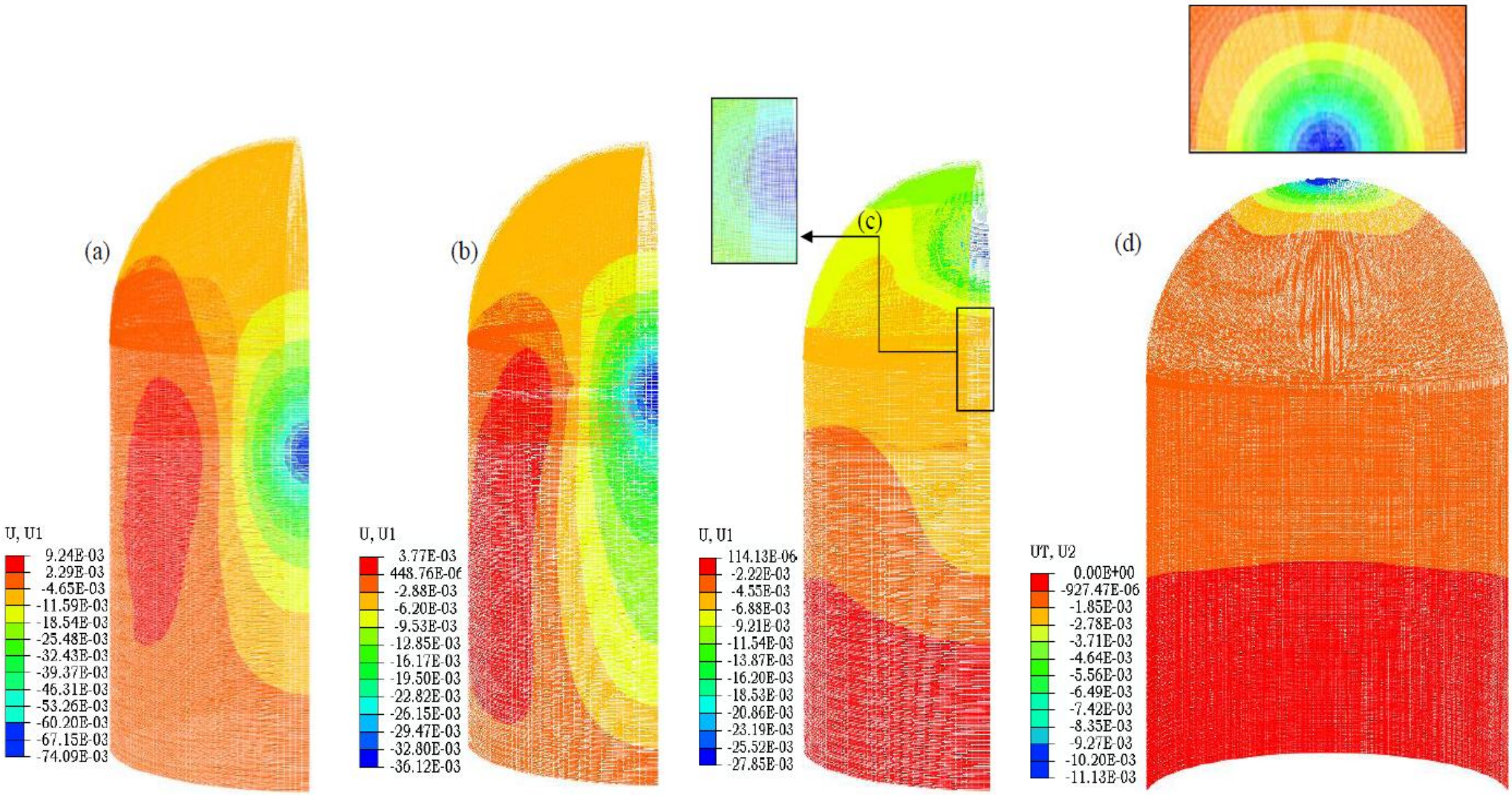

Fig. 4.25 Maximum displacement (deformation) in outer reinforcement in the direction of loading for A320 at: Location A (b) Location B (c) Location C (d) Location D

The variation of normal stresses (in the direction of loading) in concrete at different impact locations has also been studied under the peak pressure. The central node in the impact region from both faces (inner as well as outer) of containment has been selected and variation of stress with time has been plotted. The positive sign shows tension while the negative compression stress. At the front face of containment, the concrete has been found to be under compression, Fig. 4.26 (a), (b) and (c).Impact duration of Phantom F4, is quite small (0.08 sec only), hence concrete has high compression stress, confined to impact region. The stress concentration is higher at "Location C and D" since these two locations have undergone lowest displacement. It could also be noticed that the trend of maximum stress is exactly opposite to that of the maximum displacement against each aircraft. The "Location A" has experienced lowest stress followed by "Location B, C and D" respectively. At the rear face, concrete initially experienced nominal tension followed by compression, Fig. 4.27. However, the magnitude of compression stress is very low at the inner face compared to that at the front face of the containment.

The axial-stress variation at the central node of inner reinforcement has been plotted in Fig. 4.28. In case of Phantom F4, the inner reinforcement initially experienced some tension and latter compressive stress developed, Fig 4.28(a) .For Boeing 707-320 and Airbus A320 the inner reinforcement is mainly in tension except at Location A, where compression is also noticed at a later stage, see Fig 4.28(b) and (c). In the outer set of reinforcement an exactly reverse behavior has been noticed for Phantom F4, initial compression and then tension, Fig 4.29(a). For Boeing 707-320 and Airbus A320, the outer face reinforcement is dominantly under compression, except at location A, where tension has also been noticed at a later stage, see Figs. 4.29(b) and 4.29(c).

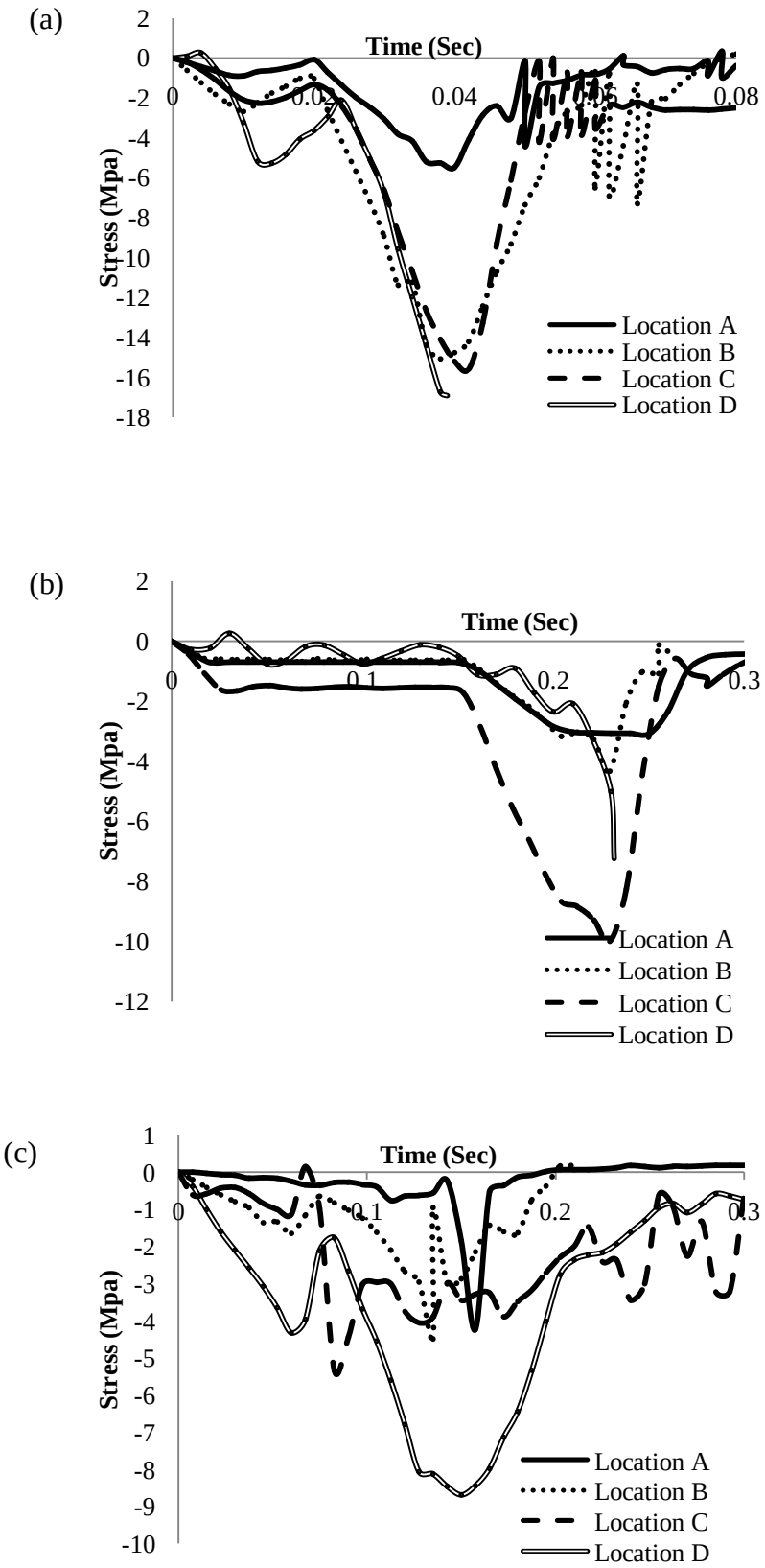

Fig. 4.26 Normal stress in the central node of concrete in impact region at front face: (a) Phantom F4 (b) Boeing 707-320 (c) Airbus A320

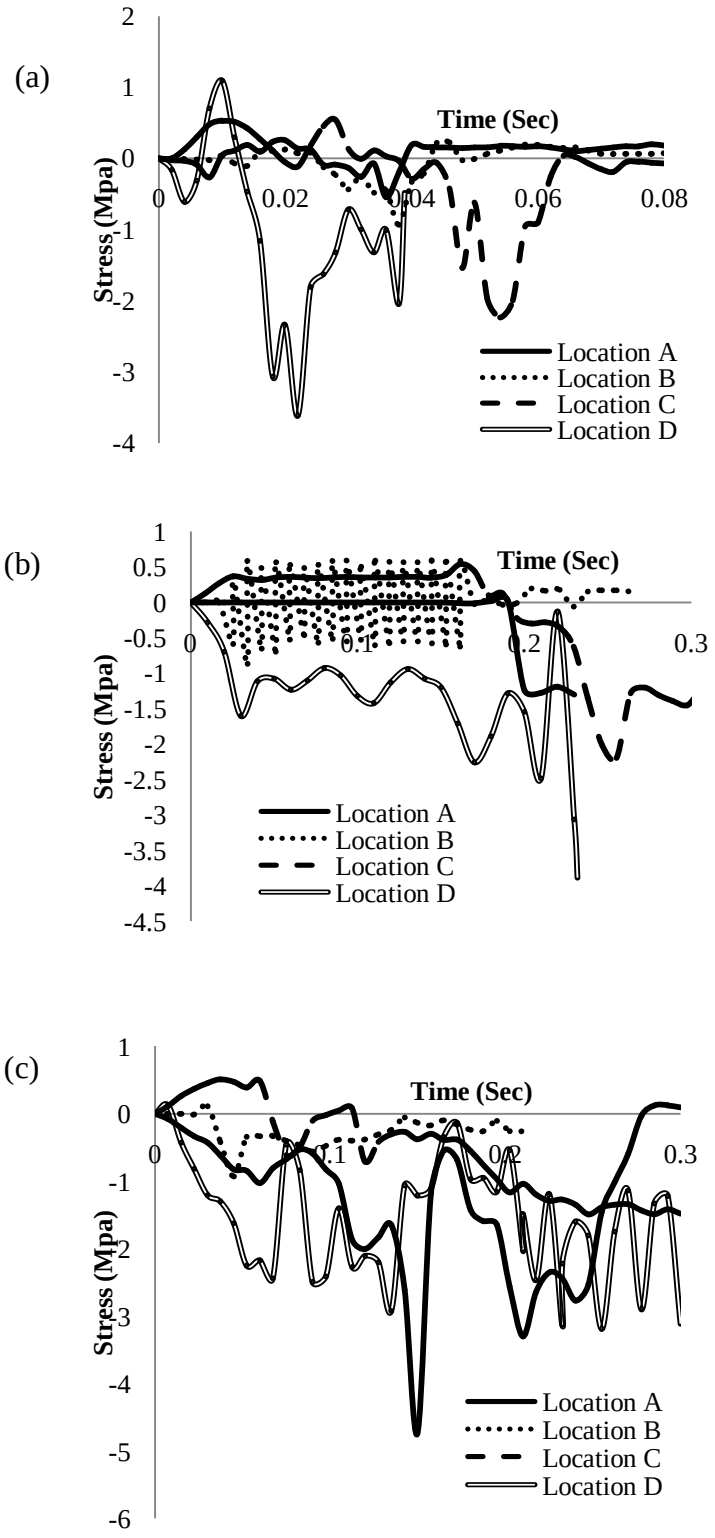

Fig. 4.27 Normal stress in the central node of concrete in impact region at rear face: (a) Phantom F4 (b) Boeing 707-320 (c) Airbus A320

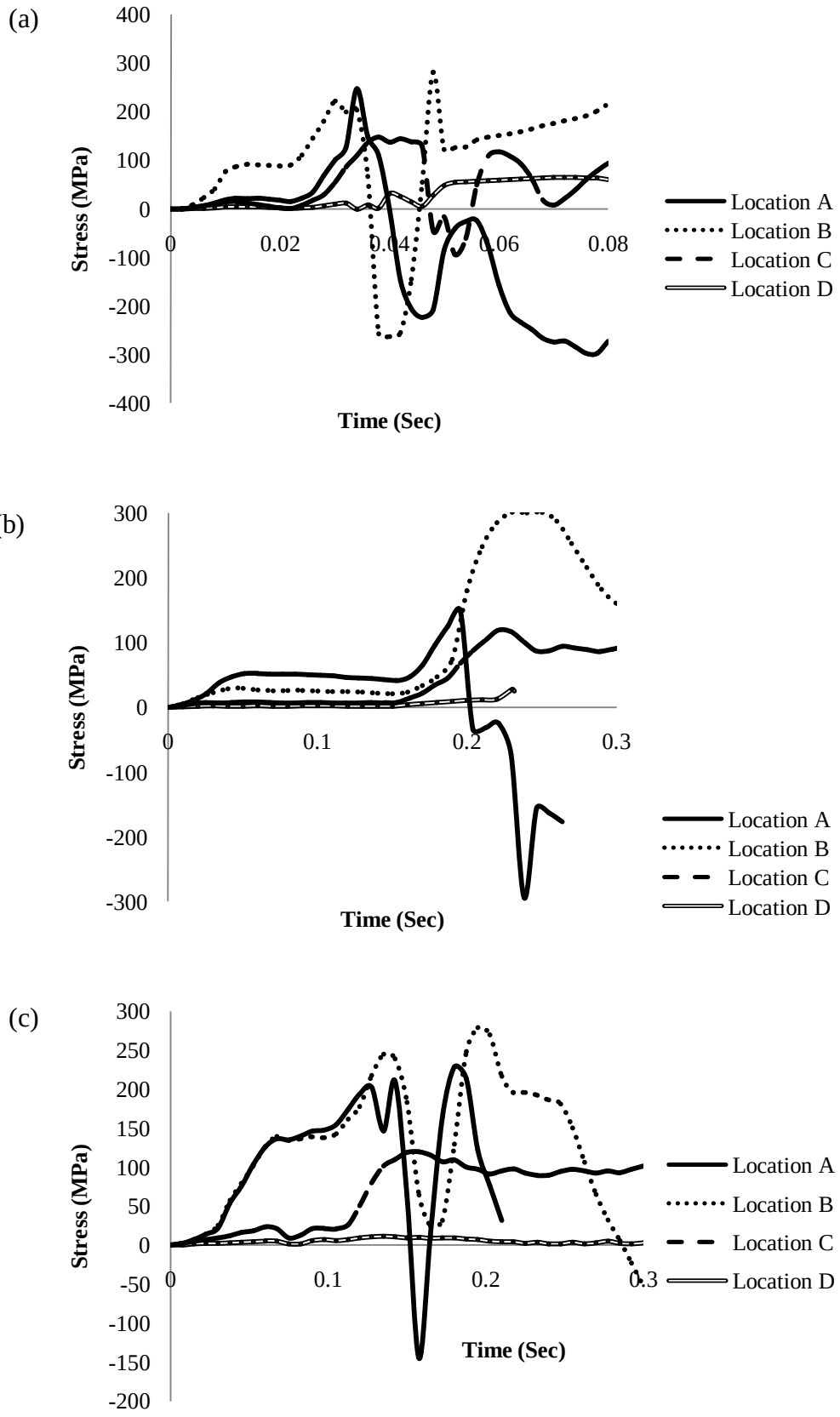

Fig. 4.28 Normal stress in the central node of impact region in inner reinforcement: (a) Phantom F4 (b) Boeing 707-320 (c) Airbus A320

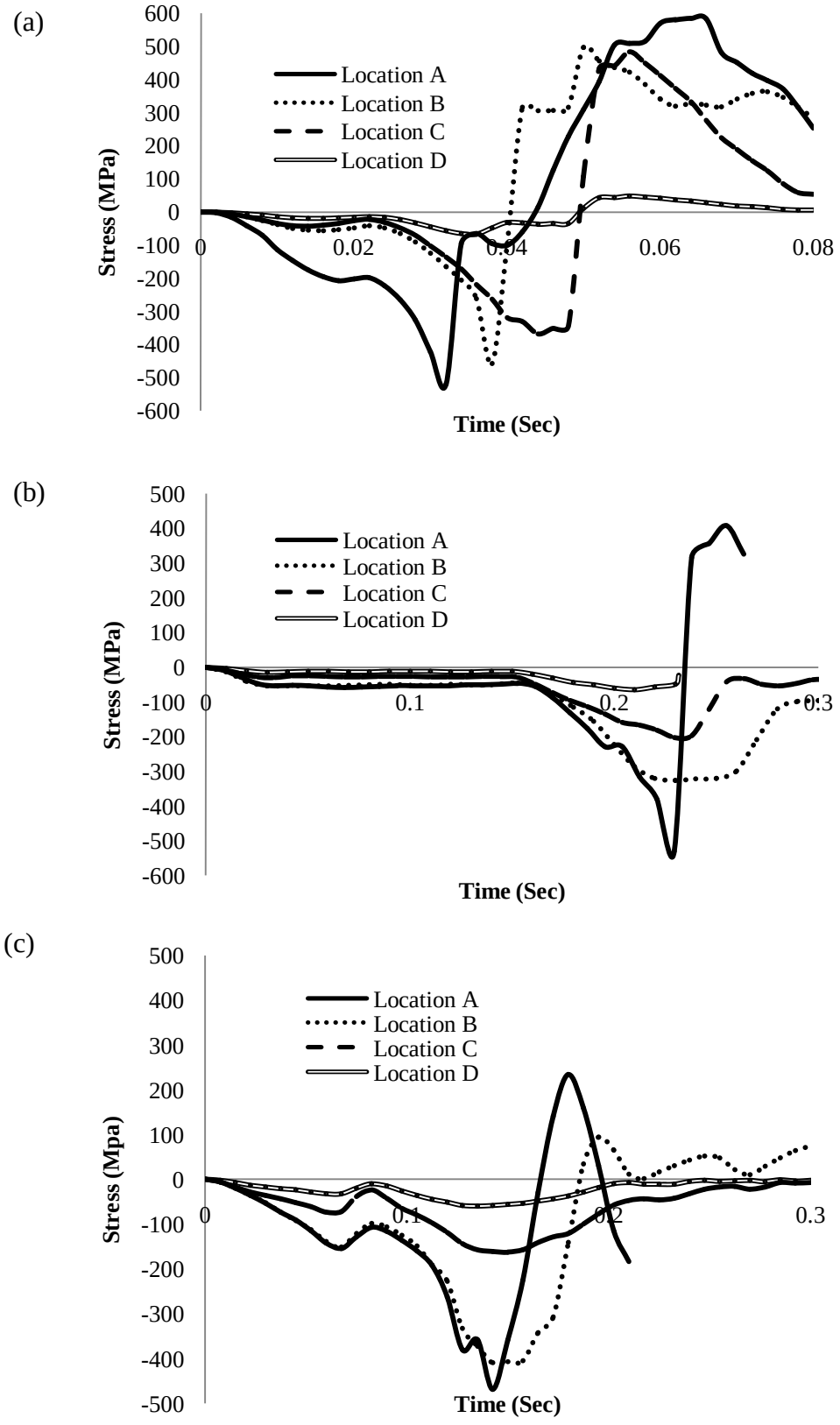

Fig. 4.29 Normal stress in the central node of impact region in outer reinforcement: (a) Phantom F4 (b) Boeing 707-320 (c) Airbus A320

One of the most important characteristics of concrete is its low tensile strength, particularly at low-confining pressures, which results in tensile cracking at a very low stress compared with compressive stresses. The tensile cracking reduces the stiffness of concrete structural components. Therefore, the use of continuum damage mechanics is necessary to accurately model the degradation in the mechanical properties of concrete. However, the concrete material also undergoes some irreversible (plastic) deformations during unloading such that the continuum damage theories cannot be used alone, particularly at high confining pressures. Therefore, the nonlinear material behavior of concrete can be attributed to two distinct material mechanical processes; damage (micro-cracks, micro-cavities, nucleation and coalescence, grain boundary cracks, and cleavage in regions of high stress concentration) and plasticity.

The damage experienced by the concrete of the containment under tension is highlighted in Figs. 4.30-4.32 for different aircrafts. The damage of the material under tension and compression has been assumed to occur when the corresponding damage parameter d_t and d_c respectively reached a value of 0.9. The damage parameter varies from 0 to 0.9 corresponding to undamaged and completely damaged material respectively. At each location the area under the application of impact load has been found to be dominantly under compression hence no sign of tension failure could be seen in these regions at the front face. However, the tension failure of concrete has been found to occur at rear face the impact region. It may therefore be concluded that the containment has experienced punching failure due to the concentrated loading. In case of crash of Boeing 707-320 and Airbus A320 at “location A and B”, some tension damage has also been noticed at the base of containment; see Figs. 4.31(a)-(b), 4.32(a)-(b). It should be noted that the spalling of concrete from the outer containment may damage the inner containment in case if the containment is a double layered structure. The number of completely damaged elements is very less at impact location D (crown). Hence, the results with removed elements have not been provided for this case.

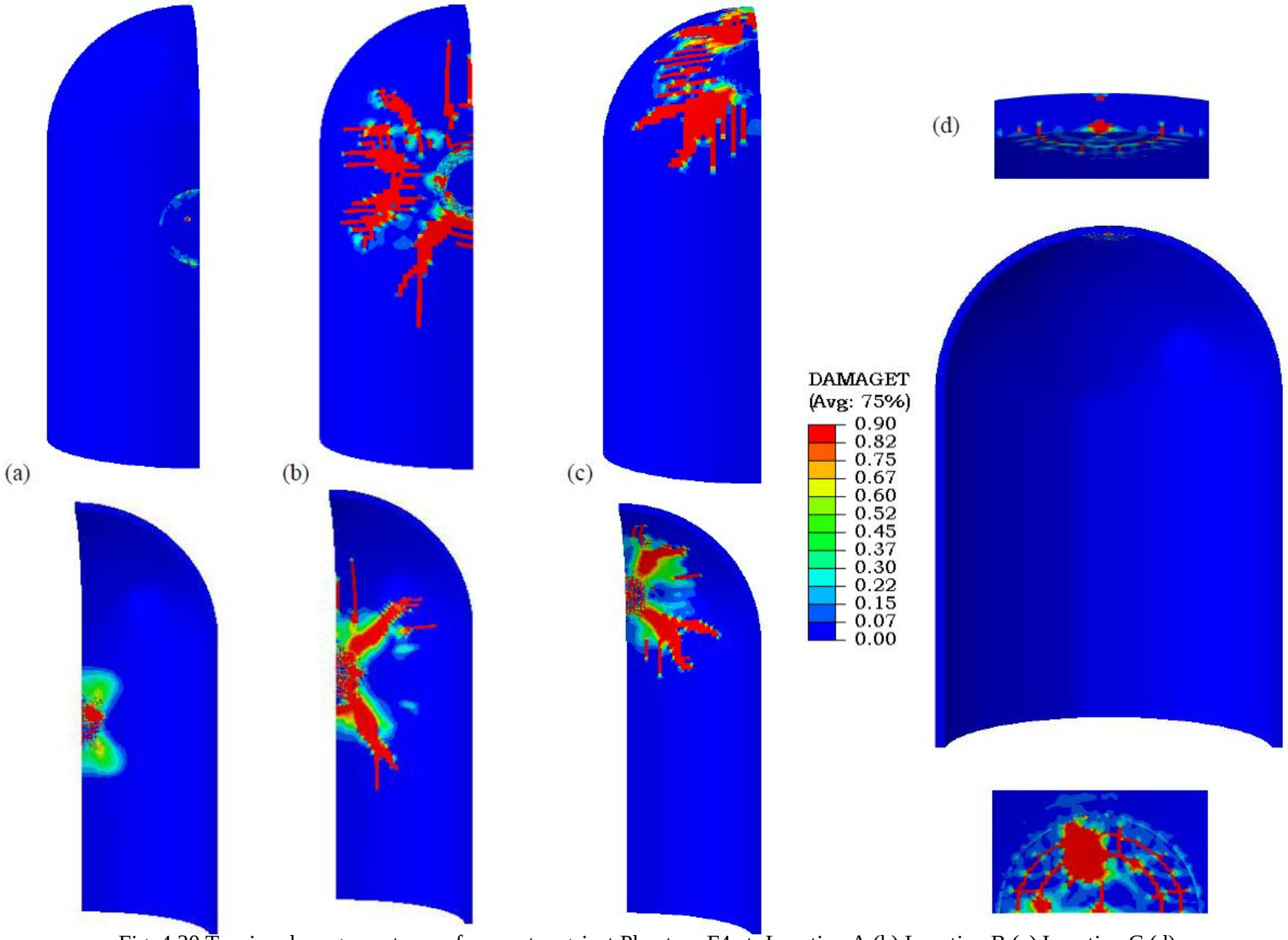

Fig. 4.30 Tension damage contours of concrete against Phantom F4 at: Location A (b) Location B (c) Location C (d) Location D

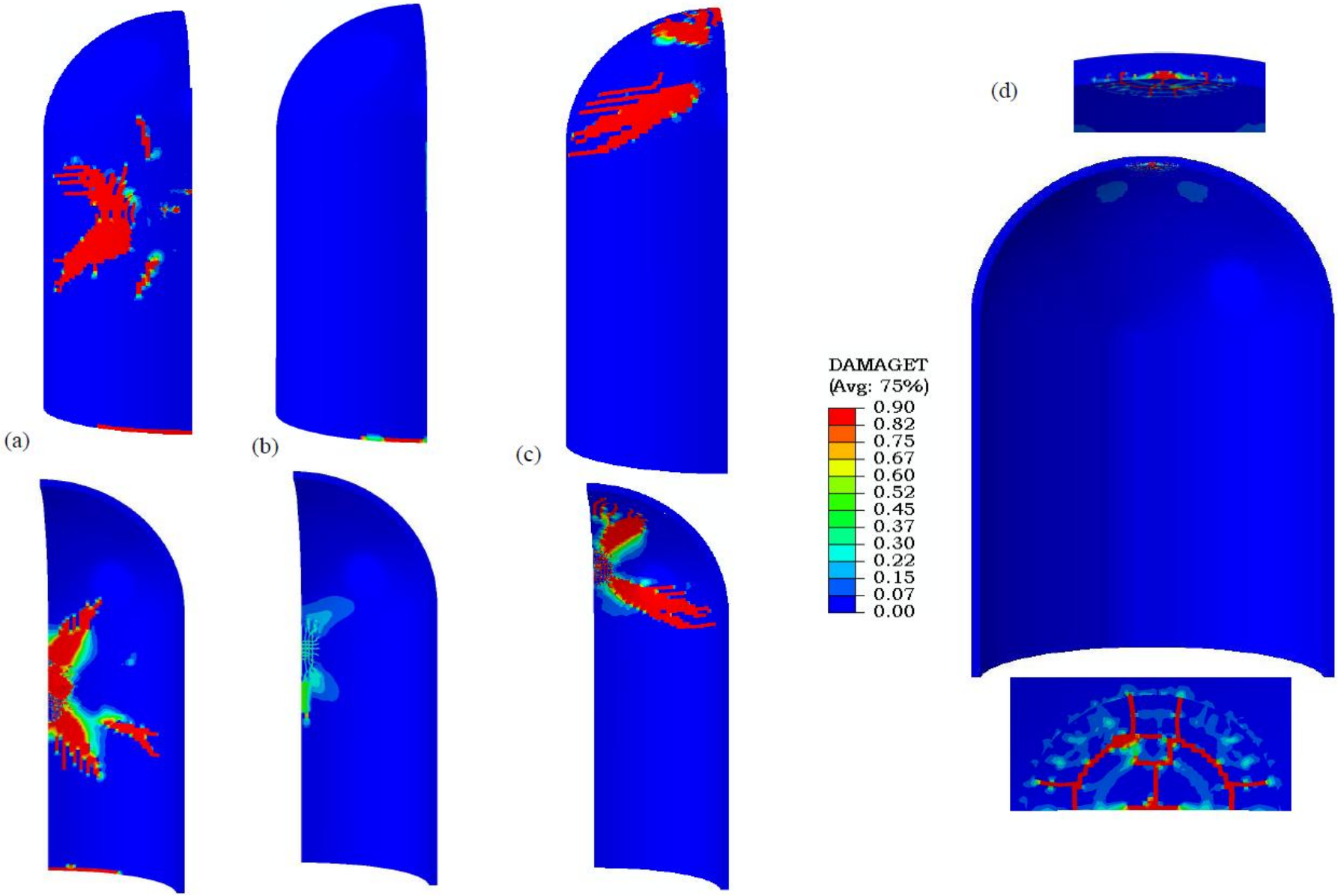

Fig. 4.31 Tension damage contours of concrete against Boeing 707-320 at: Location A (b) Location B (c) Location C (d) Location D

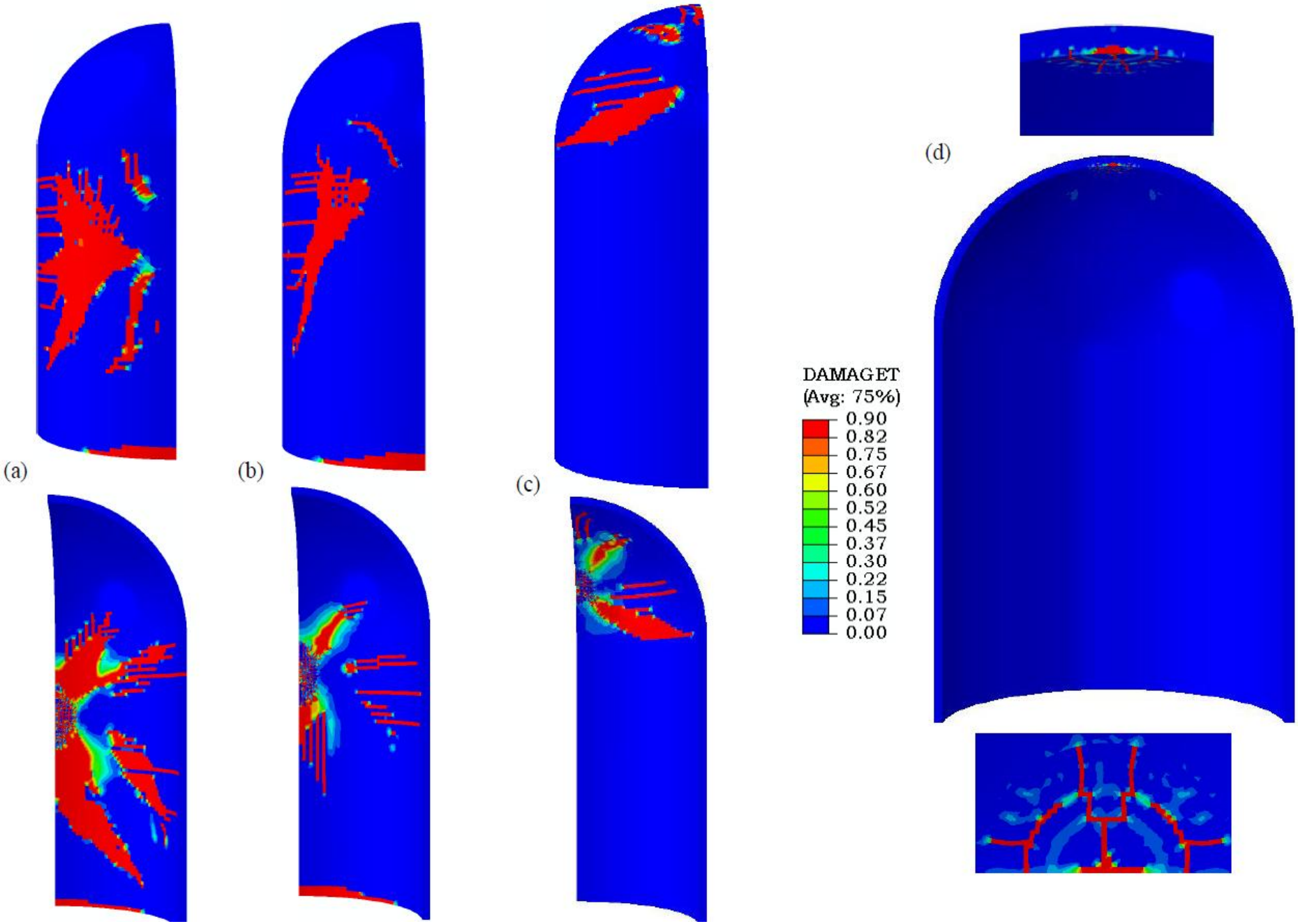

Fig. 4.32 Tension damage contours of concrete against Airbus A320 at: Location A (b) Location B (c) Location C (d) Location D

4.4INFLUENCE OF DIFFERENT AIRCRAFTS ON THE CONTAINMENT RESPONSE

The numerical simulations were carried out wherein five different aircrafts including the latest commercial as well as fighter jets were considered to hit the outer containment of the BWR Mark III type nuclear power plant. The containment with dome has been meshed in two distinct manner based on the size of the impacting aircraft, as discussed in Chapter 2. The same figure has been shown here in order to highlight the elements chosen for plotting the results and their corresponding location on the structure, see Fig. 4.33. The aircrafts employed were Boeing 747-400, Boeing 767-400, Airbus A-320, Boeing 707-320 and Phantom F4.The characteristics of these aircrafts have been explained in Table 4.1. The corresponding reaction time-response curves are plotted in Fig. 4.34.

The most vulnerable location i.e. the mid height of the containment (33.5 m from the base) was chosen for the impact and the angle of incidence was considered normal to surface. The local as well as global deformation of the structure was measured and the stresses in the concrete and reinforcement were obtained against each aircraft. The results of the present investigation have been compared with those of the previous studies with respect to the maximum local deformation in the direction of loading. It should be noted that the maximum deformation of the containment was the major finding of the previous studies.

Table 4.1 Details of Aircrafts and their Reaction Time curve

	Boeing 707-320	**Phantom F4**	**Boeing 747-400**	**Airbus A320**	**Boeing 767-400**
Length of Aircraft	46.6	17.74	70.7	37.57	48.5
Wingspan (m)	44.42	11.77	64.4	34.10	47.5
Dia of Fuselage (m)	3	2.42	6	3.95	5.03
Velocity of Impact	103	215	120	120	150
Peak Impact Force (MN)	90	158	435	85	250
Total Time of Impact (Sec)	0.032	0.08	0.55	0.3	0.40
Weight (Kg)	152400	14200	385554	73500	204120
Fuel (kg)	61000	4800	164064	30190	90770

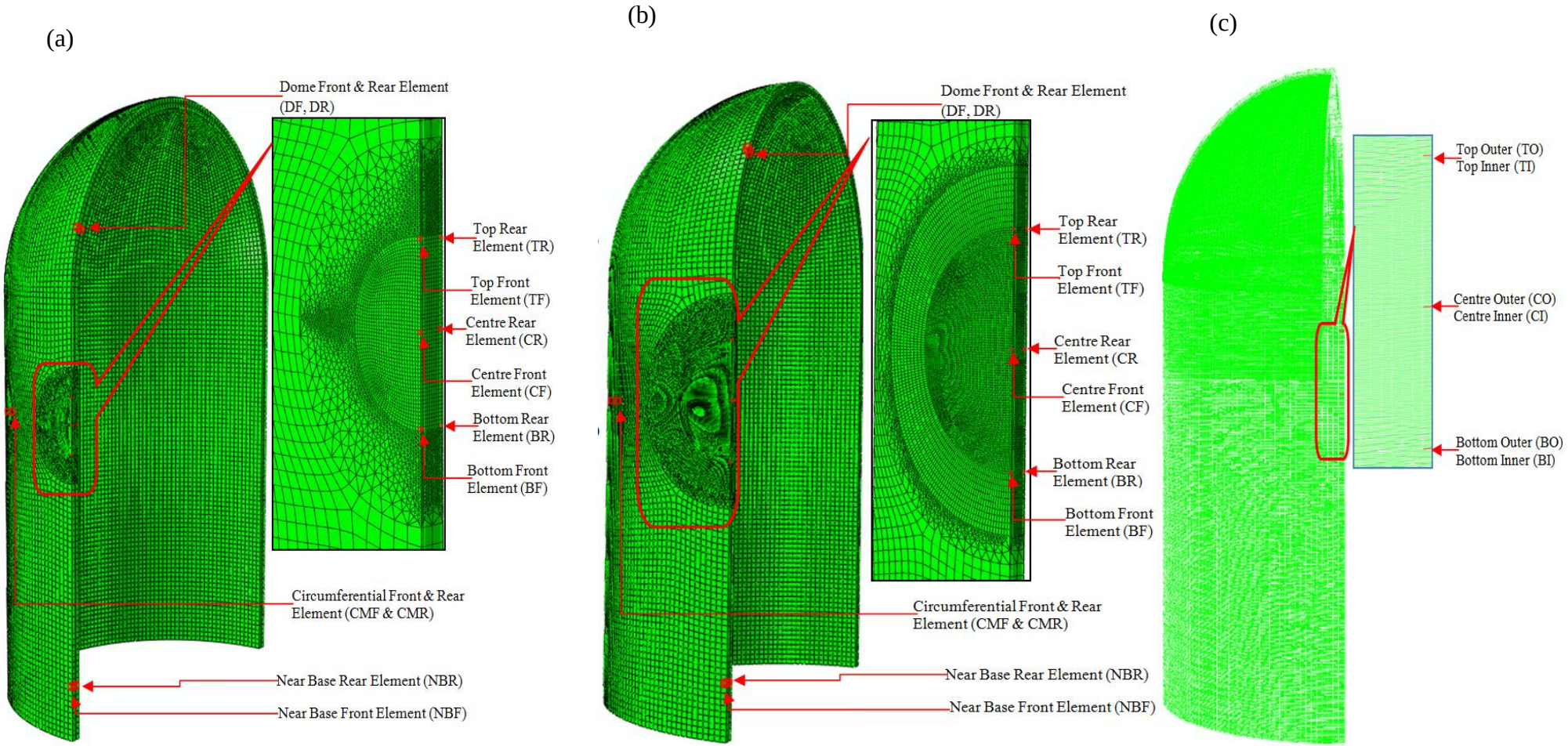

Fig. 4.33 Discretization of the containment subjected to impact by (a) Phantom F4, Boeing 707-320 and Airbus A320; (b) Boeing 747-400 and Boeing 767-400; (c) Discretization of the reinforcement

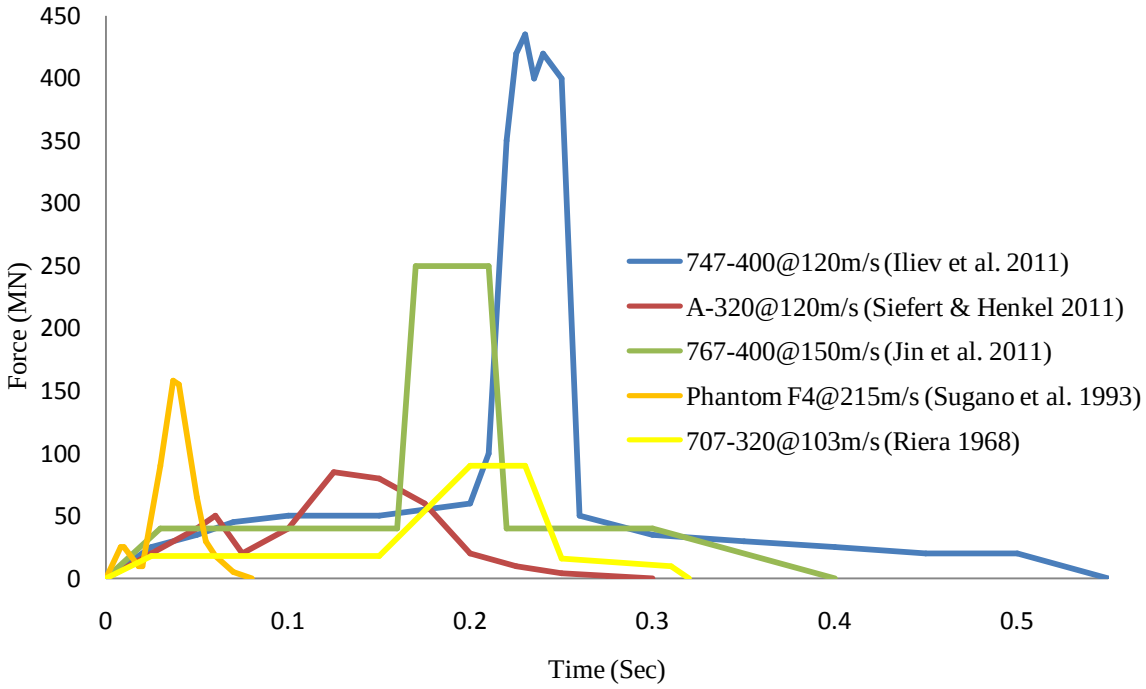

Fig. 4.34 Reaction time response of the aircrafts

Arros and Doumbalski (2007) studied the response of a fictitious containment subjected to Boeing 747-400 aircraft and found a maximum deformation/displacement, 1067 mm. Lo Frano and Forasassi (2011) obtained the response of IRIS containment against the same aircraft and reported a maximum deformation of 927 mm. In the present study the maximum deformation of BWR Mark III type containment was found to be 998.9 mm against the same aircraft, see Fig. 4.35 (a). The deformation shown in Fig. 4.35 is at the inner face of the containment in the direction of loading. The positive sign shows the outward while the negative sign inward deformation. The deformation has been found to be maximum at the location of impact. It should also be noted that the thickness of wall of the IRIS containment studied by Lo Frano and Forasassi (2011) as well as the BWR containment employed in the present study was 1.2 m. Arros and Doumbalski (2007) however, did not mention the wall thickness of the containment studied by them.

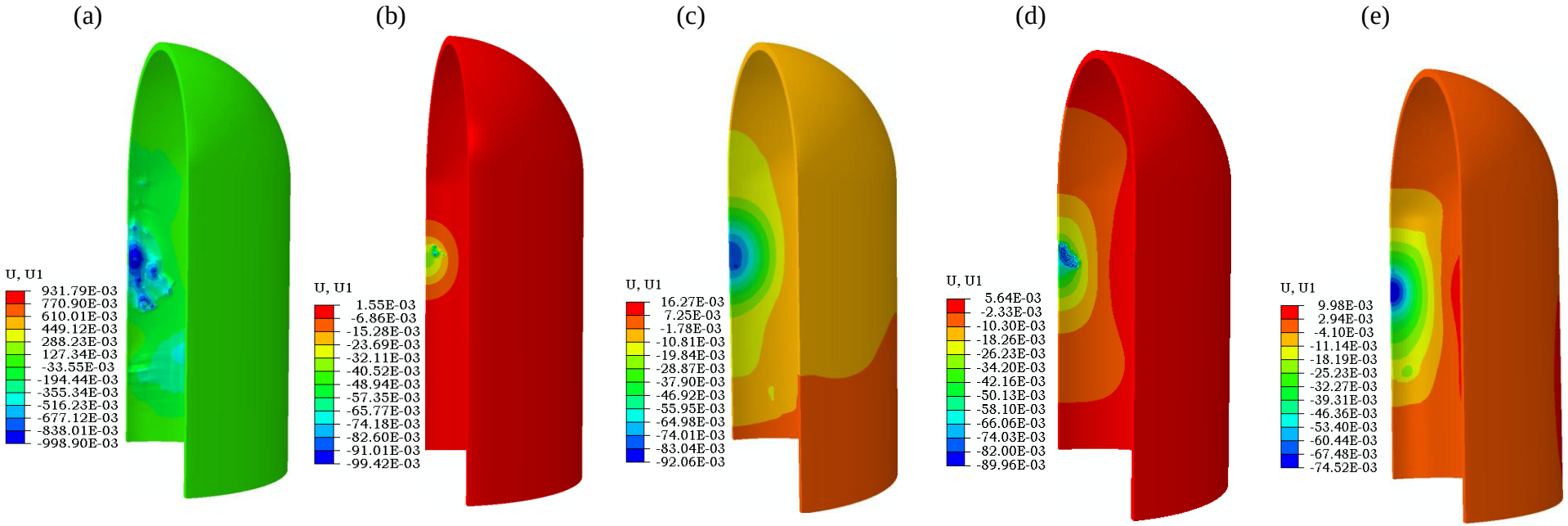

Fig. 4.35 Maximum displacement (deformation) in concrete in the direction of loading: (a) 747-400 (b) Phantom F4 (c) 767-400 (d) 707-320 (e) A320

Lo Frano and Forasassi (2011) also studied the response of the IRIS containment against Phantom F4 fighter jet and reported a maximum deformation 217 mm. Abbas (1992) studied the response of BWR Mark III type containment against Phantom F4 fighter jet and found a maximum deformation 44.2 mm. In the present study a maximum local deformation of 99.42 mm has been noticed in the BWR Mark III type containment against Phantom F4 fighter jet, see Fig. 4.35 (b).

For the Boeing 767-400 aircraft crash however, no previous investigation has been found in the available literature. In the present study however, a maximum deformation of 92.06 mm at the inner face of the containment has been observed against this aircraft, Fig. 4.35 (c). For Boeing 707-320 aircraft the maximum deformation was found to be 34.2 mm by Abbas et al. (1996), 46 mm by Kukreja (2005) and 89.96 mm in present study {Fig. 4.35(d)} against BWR Mark III type containment. Siefert and Henkel (2011) reported a maximum deformation of 50 mm in an assumed containment building with wall thickness 1.8 m subjected to Airbus A-320 crash. Fig. 4.35 (e) on the other hand shows a maximum deformation 74.52 mm against the same aircraft as a result of present investigation.

The nodal deformation of the inner face reinforcement has been plotted in Fig. 4.36 against each aircraft. The truss element with three translational degrees of freedoms at each end node predicted inward nodal deformation (in the direction of loading) by the negative sign and outward nodal deformation by the positive sign. As seen, the inward deformation has been found maximum at the impact region. The maximum nodal deformation has been found to be 1.2 m against Boeing 747-400 aircraft followed by 89.8 mm, 85 mm, 74.4 mm and 49.5 mm against Boeing 707-320, Boeing 767-400, A320 and Phantom F4 respectively. It should be noted that the Boeing 747-400 carries highest mass (385500 kg) followed by Boeing 767-400 (204120 kg), Boeing 707-320 (152400 kg), Airbus A320 (73500 kg) and Phantom F4 (14200 kg) respectively. At some point away from the impact region some outward deformation was also noticed. The deformation of the outer face reinforcement has been found to be significantly lesser compared to that of the inner face reinforcement, Fig. 4.37. The maximum deformation was found in the impact region in the direction of loading and the maximum intensity against Boeing 747-400 and minimum against Phantom F4.

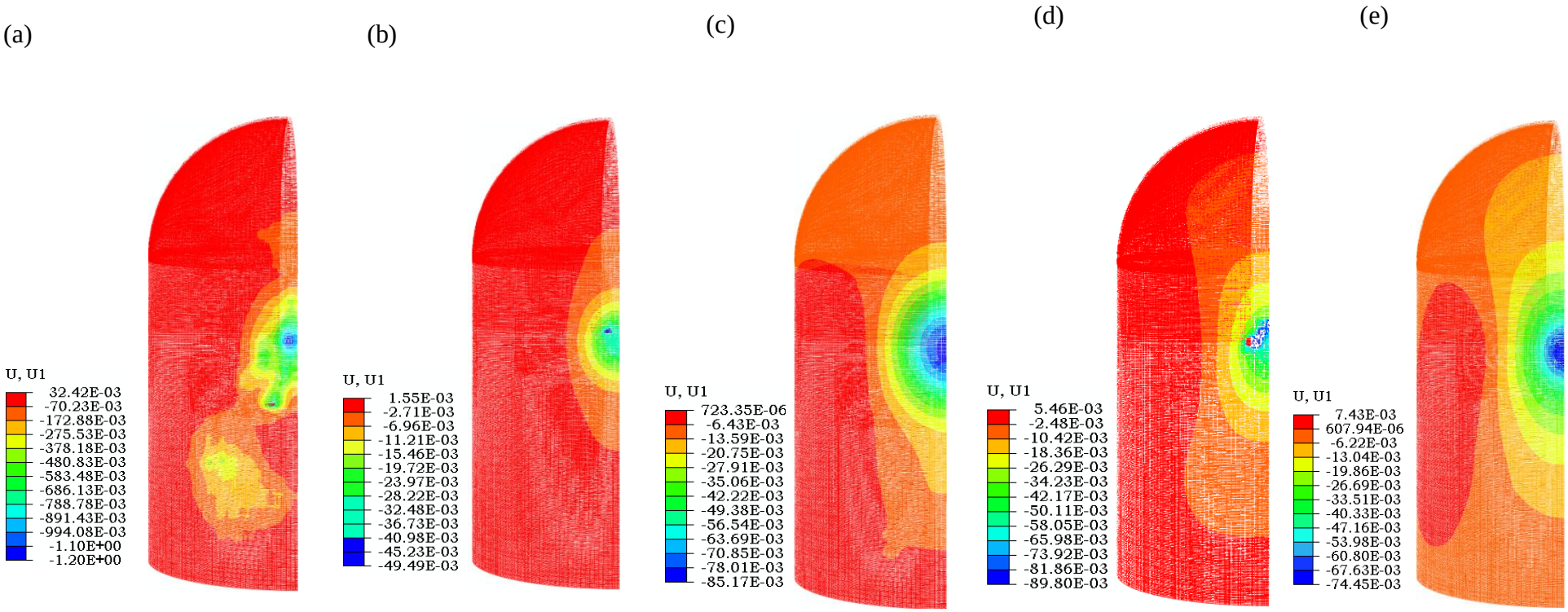

Fig. 4.36 Maximum displacement (deformation) in the inner reinforcement in the direction of loading: (a) 747-400 (b) Phantom F4 (c) 767-400 (d) 707-320 (e) A320

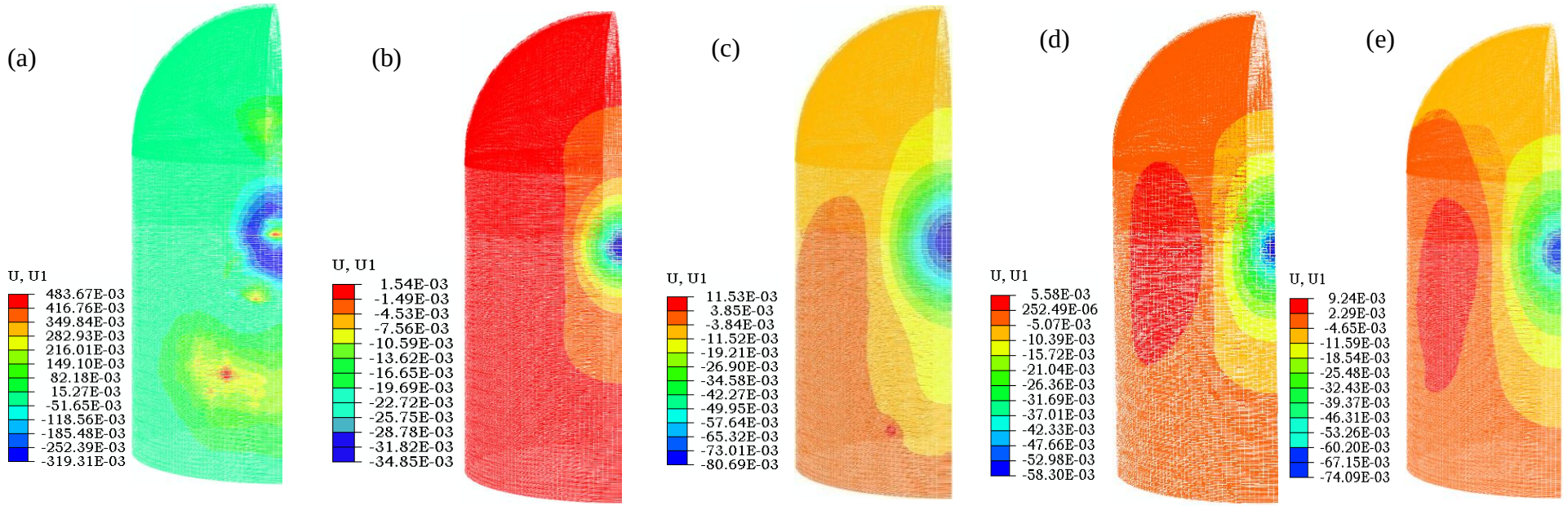

Fig. 4.37 Maximum displacement (deformation) in outer reinforcement in the direction of loading: (a) 747-400 (b) Phantom F4 (c) 767-400 (d) 707-320 (e) A320

The normal stresses in concrete in the direction of loading shown in Fig. 4.38 are plotted at the peak pressure. The concrete under the local impact region has been found to be under compression while away from this region (in longitudinal as well as circumferential directions) nominal tensile stresses were also noticed. This is due to the fact that the containment due its high stiffness when compressed by significant localized force developed outward bulging in the surrounding area. This behavior though observed against all the aircrafts, has been found more prominent against Boeing 747-400. The crushing of concrete in the impact region has also been found to be more significant against this aircraft. The axial stresses developed in the outer layer of the reinforcement shown in Fig. 4.39 have been found to be very high as compared to that of the concrete. In general the compressive stresses were found to be higher than the tensile stresses in the outer layer of reinforcement due to the predominant compression at the outer face of containment. However, for Boeing 747-400 aircraft the tensile stresses were seen to be dominant. In addition, significant plastic deformations of the reinforcement were also noticed in the impact region for this aircraft, Fig. 4.39(a). For other aircrafts however, the magnitude of stresses developed in the reinforcement was found lesser than the yield strength, Figs. 4.39(b)-(e). As expected, the inner layer of reinforcement experienced predominant tension against all the aircrafts, see Fig. 4.40. The magnitude of stresses was again found to be highest against Boeing 747-400 aircraft and the reinforcement underwent large plastic deformations, Fig. 4.40(a). Some bending of the inner reinforcement was also noticed for Boeing 707-320 aircraft, Fig. 4.40(d). However, the bending observed in this case may not be categorized as the plastic deformation since the magnitude of stress in the reinforcement was lesser than the yield strength. In general, from these observations it may be concluded that the overall behavior of the containment is fairly accurately predicted through the numerical simulations.

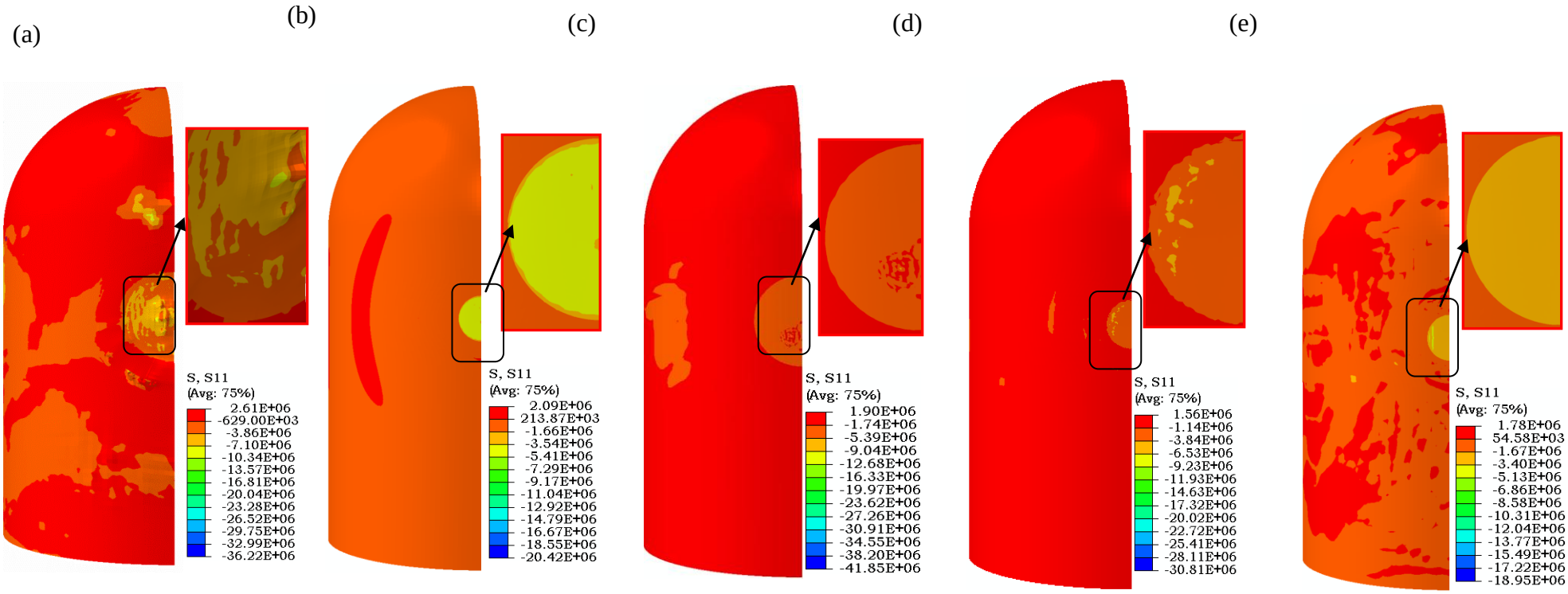

Fig. 4.38 Maximum normal stress in concrete in the direction of loading: (a) 747-400 (b) Phantom F4 (c) 767-400 (d) 707-320 (e) A320

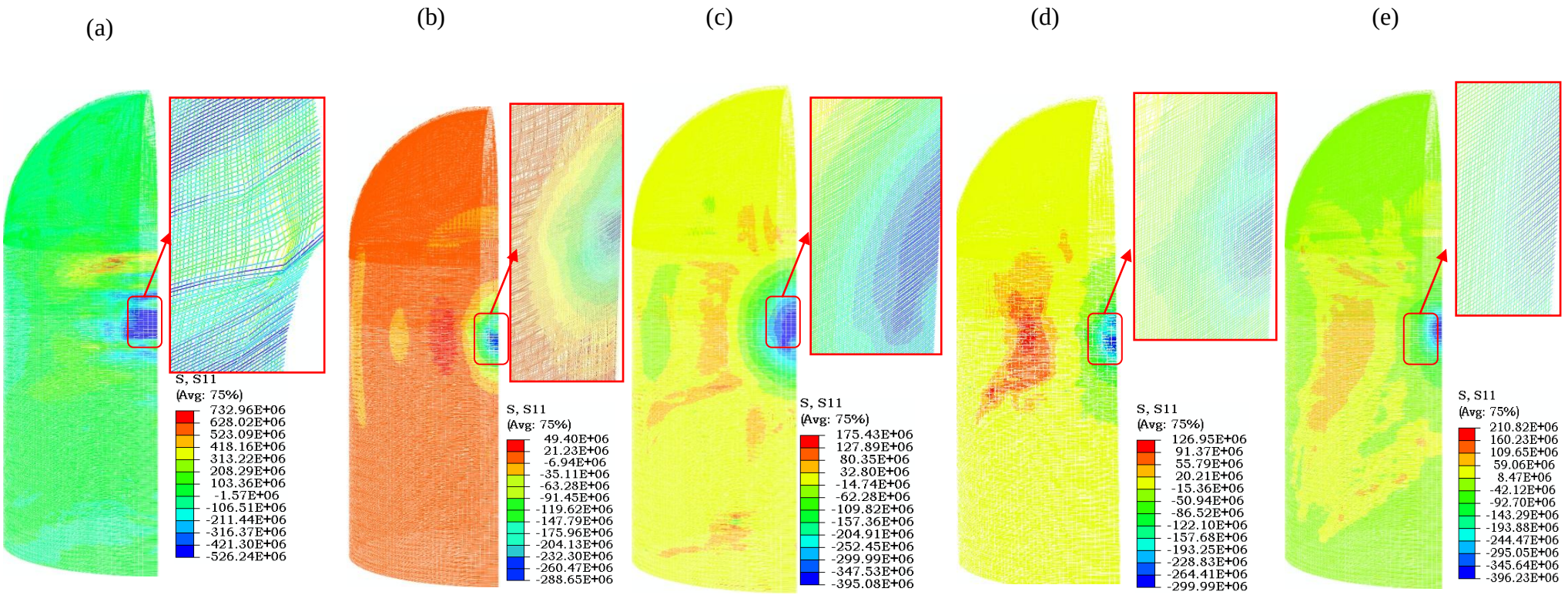

Fig. 4.39 Maximum axial stress in the outer reinforcement: (a) 747-400 (b) Phantom F4 (c) 767-400 (d) 707-320 (e) A320

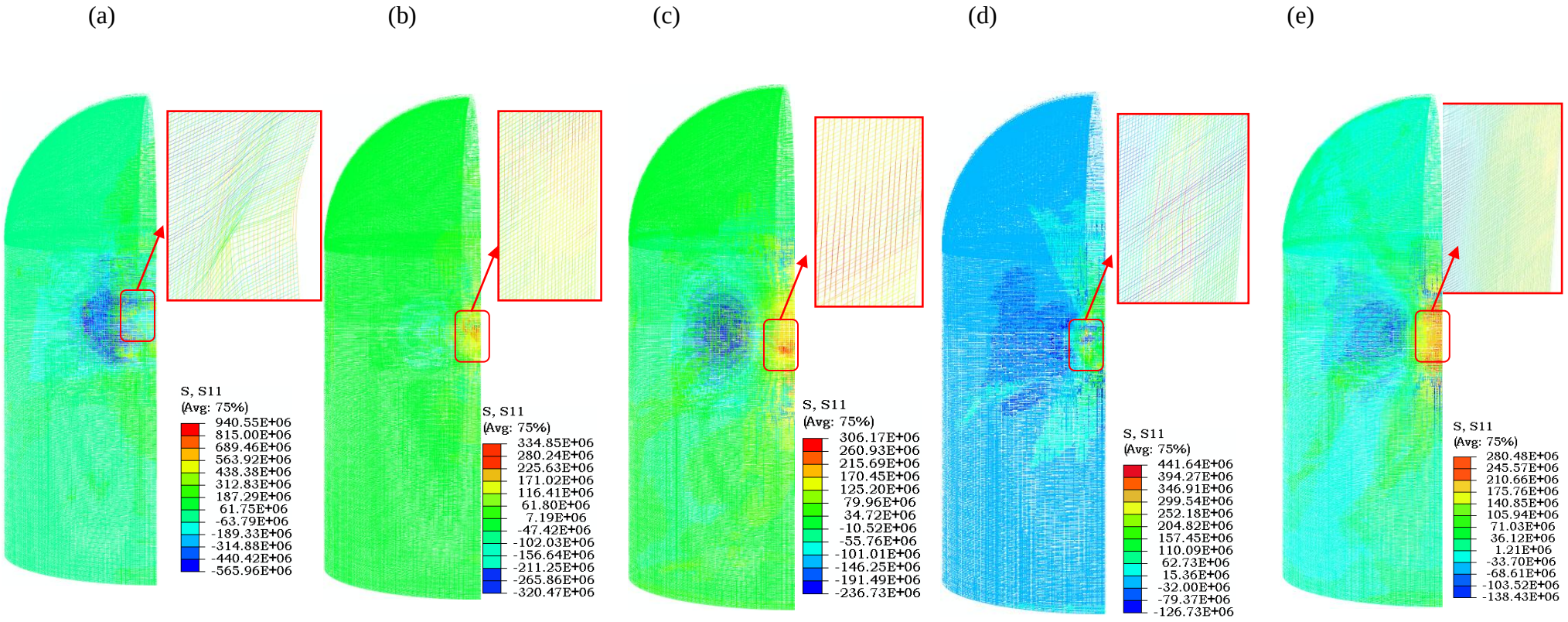

Fig. 4.40 Maximum axial stress in the inner reinforcement: (a) 747-400 (b) Phantom F4 (c) 767-400 (d) 707-320 (e) A320

The variation of normal stresses has also been plotted with respect to time for a few selected elements of concrete and the reinforcement highlighted in Fig. 4.33(a), (b) and (c) respectively. The location of these elements has been carefully chosen in order to obtain the response throughout the body of the containment. Three elements of concrete each at the front and rear face of the containment were selected in the circular region under the application of load and three elements away from the impact zone (one at the central circumferential axis and two at central longitudinal axis). Figs. 4.41 and 4.42 show the variation of stress for concrete elements and Fig. 4.43 for the reinforcement. The stress variation has been plotted till the execution of the peak load for all the aircrafts, see Fig. 4.34. The front face element (TF) at the top of the impact region [Fig. 4.41(a)] shows compression with maximum intensity 5 MPa against Phantom F4. It should be noted that the impact velocity of Phantom F4 was highest among all the aircrafts, 250 m/s, while the peak load was attained in lowest time period, 0.036 seconds., see Fig. 4.35(b). However, the damage caused by this aircraft to the containment material has been found to be negligible, see Fig. 4.44.

At the corresponding inner face element (TR) however, nominal tension followed by nominal compression was found, Fig. 4.41(b). At the same location, the stress in the reinforcement has been found to be comparatively high at the front as well as rear face of the containment, Fig. 4.43(a) and (b). At the front face reinforcing element (TO) initial compression has been observed followed by tension, Fig. 4.44(a). At the rear face (TI) however, only tensile stresses were seen with maximum intensity 200 MPa for Boeing 747-400 aircraft, Fig. 4.43(b). At the midpoint of the impact region also the stresses have been found to be low in concrete, Fig. 4.42(c) and (d), but very high in the reinforcement, Fig. 4.43(c) and (d). In the front face reinforcing element (CO) initial compression has been observed followed by tension. The intensity of compression was close to 600 MPa for all the aircrafts except for Boeing 747-400and Boeing 707-320, while tension was found to be 600 MPa for Boeing 747-400 and Phantom F4, [Fig. 4.43(c)]. At the inner face reinforcing element (CI), dominant tension has been observed which is close to 600 MPa against Boeing 747-400 and Phantom F4 at the peak load, [Fig. 4.43(d)]. The elements of concrete at the lower impact region BF and BR predicted compression [Fig. 4.41(e)] as well as a combination of tension and compression [Fig. 4.41(f)] respectively with low intensity. The corresponding reinforcing element at front face (BO) predicted initial compression with a maximum 408 MPa for Phantom F4 and subsequent tension with a maximum 525MPa for Boeing 747-400, Fig. 4.43(e). The inner face reinforcing element (BI) predicted dominant

tension varying between 150-200 MPa for all the aircrafts, Fig. 4.43(f). It may be concluded here that the front face concrete element under the impact region predicted only compression while the inner face concrete elements predicted a combination of the tensile and compressive stresses.

An opposite and identical behavior was observed in the reinforcement elements; at outer face a combination of tension and compression and at inner face dominant tension. The elements of concrete away from the impact region predicted comparatively low stresses than those within the impact region. Among these elements however, the stresses were found to be highest at the central circumferential axis at the front as well as rear face of the containment, Fig. 4.42. The front face element (CMF) predicted initial tension with a maximum close to 1 MPa for all the aircrafts [Fig. 4.42(a)] followed by compression of maximum 2.5 MPa for Boeing 747-400, 767-400 and A320 aircrafts. The inner face element (CMR) was found under consistent compression against all the aircrafts, [Fig. 4.42(b)]. This is an opposite behavior to those of the concrete elements studied under impact region wherein the outer face elements were found under consistent compression while the inner face elements, under a combination of tension and compression. At the base of the containment the stresses were found negligible except a little compression noticed against Boeing 767 aircraft at the front (NBF) as well as rear face (NBR), Fig. 4.42(c) and (d) respectively. At the dome also, stresses in general were found negligible but nominal compression was seen for Boeing 747 aircraft at the front (DF) as well as rear face (DR), Figs 4.42(e) and (f) respectively.

The damage of the material under tension or compression has been assumed to occur when the corresponding damage parameter, d_t or d_c respectively, has reached a value of 0.9. The value of the damage parameter varies between 0 - 0.9 for undamaged and complete damaged material respectively. The damage experienced by the concrete under tension is highlighted in Fig. 4.44 against each aircraft. It can be seen that the Boeing 747-400 caused most significant damage to the containment leaving a major portion of the concrete ineffective, Fig. 4.44(a1) and (a2). It may be concluded that the containment could not sustain the impact of Boeing 747-400 aircraft and underwent a complete failure. The failure of concrete was also found significant against Boeing 767-400 aircraft. There is no damage of concrete in the impact region whereas around the impact region the concrete is completely damaged indicating punching failure, Figs 4.44(c1) and (c2). Some local damage of concrete was also noticed against Airbus A320 and Boeing 707-320 aircraft, however, it was not so significant. Phantom F4 on the other hand, did not cause any damage to the containment.

However, the stresses in concrete and reinforcement against this aircraft were found to be very high as is discussed above.

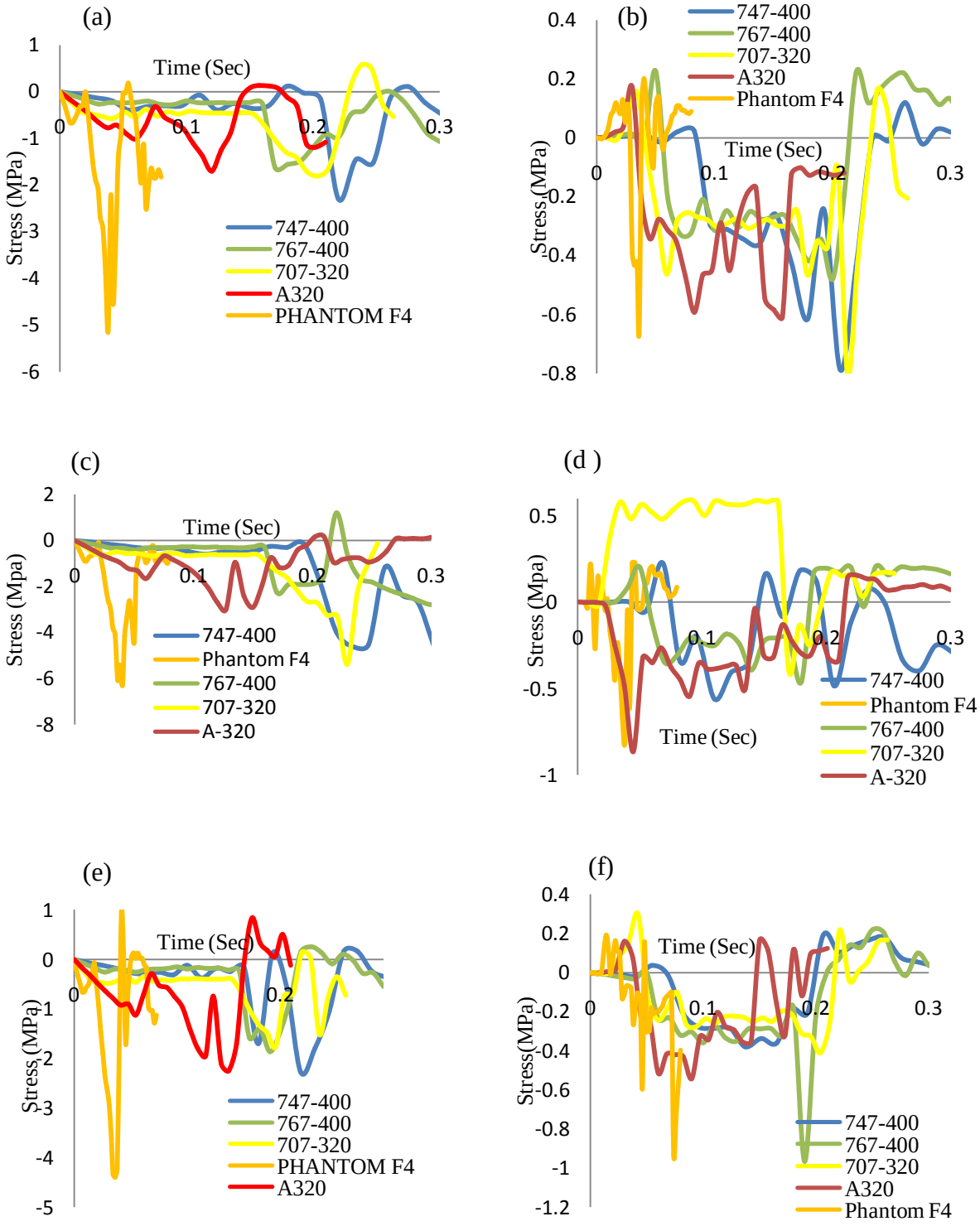

Fig. 4.41 Variation of normal stress (σ_{11}) in concrete for different aircrafts: (a) TF (b) TR (c) CF (d) CR (e) BF (f) BR

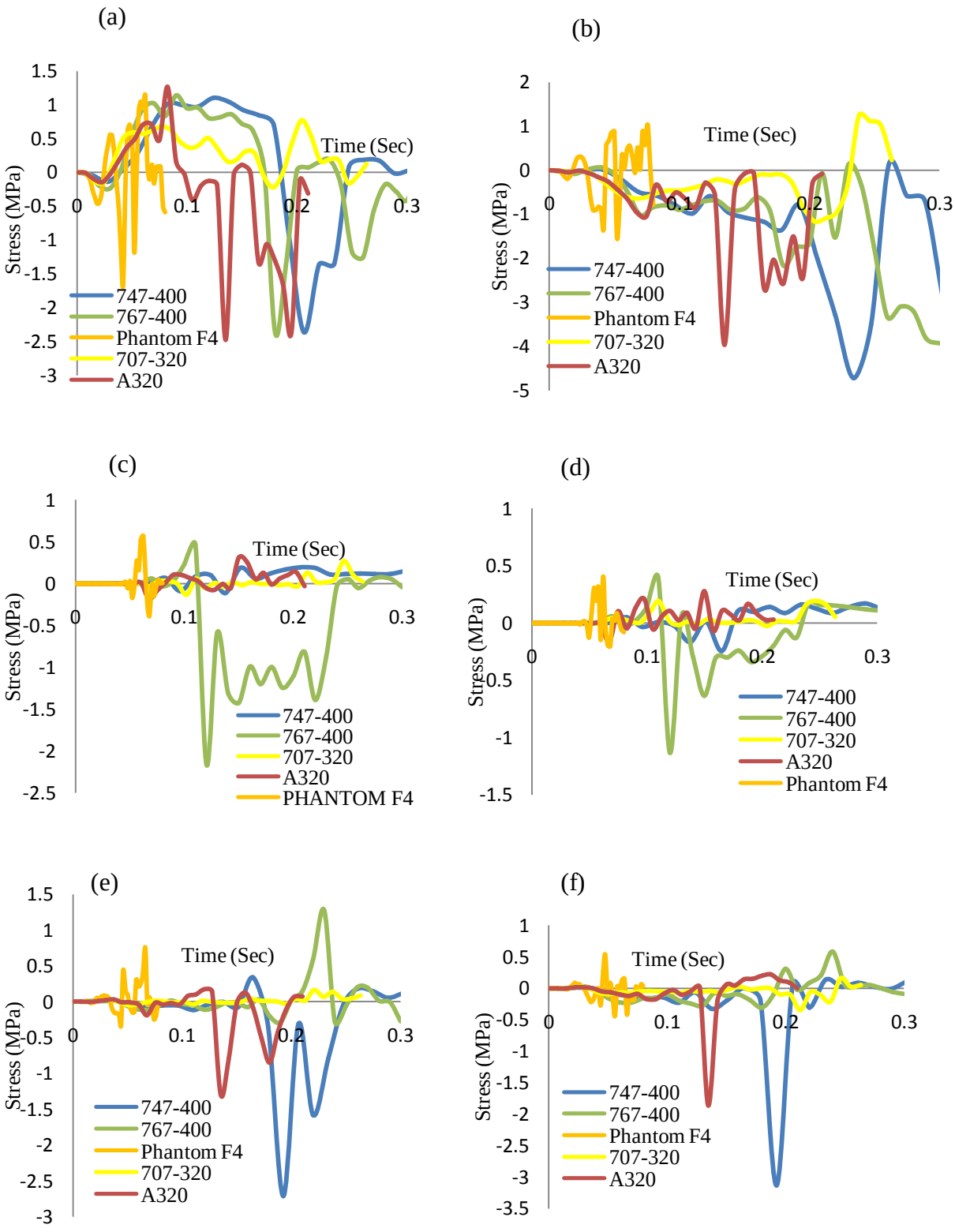

Fig. 4.42 Variation of normal stress (σ_{11}) in concrete for different aircrafts: (a) CMF (b) CMR (c) NBF (d) NBR (e) DF (f) DR

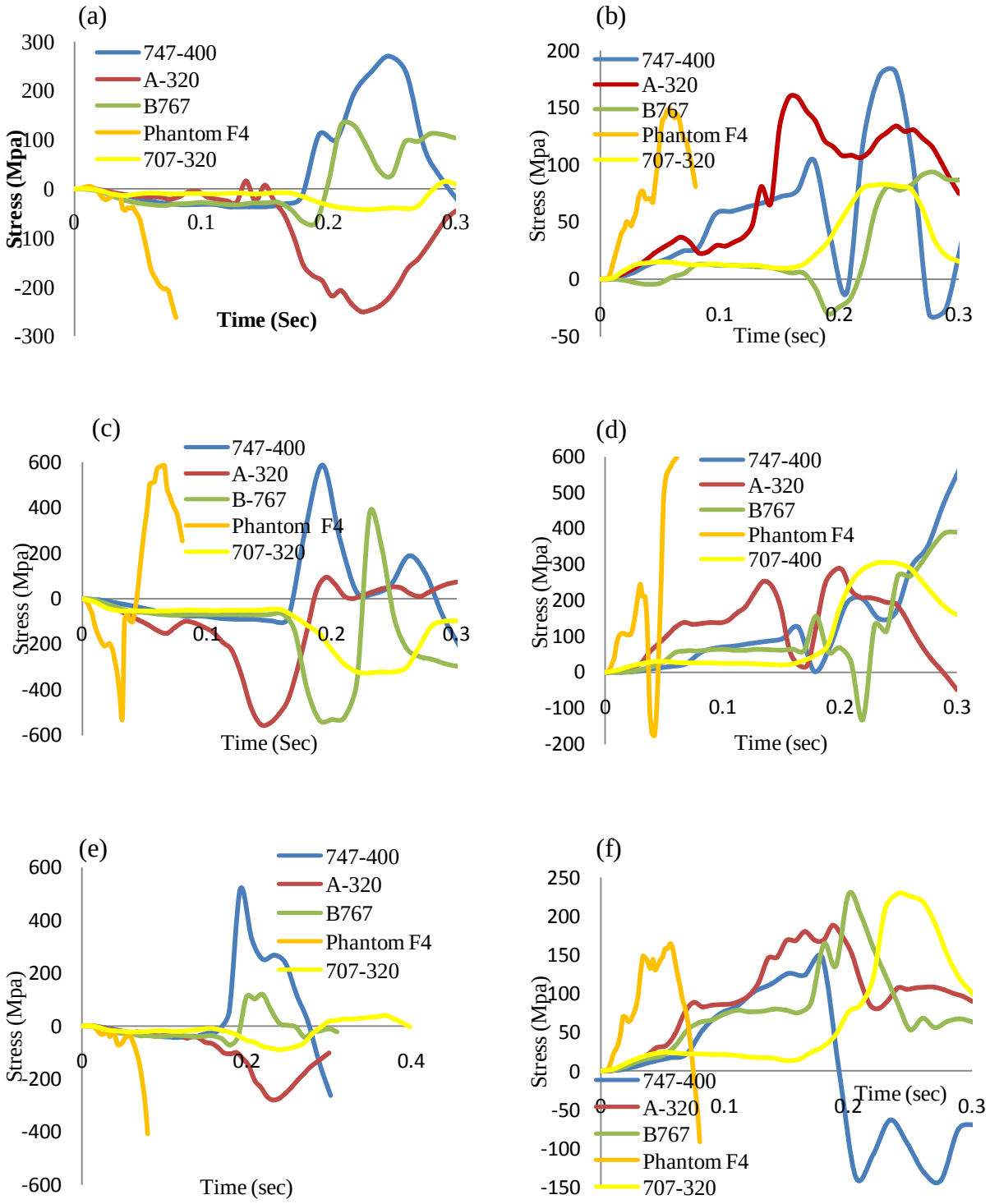

Fig. 4.43 Variation of axial stress (σ_{11}) in reinforcement for different aircrafts: (a) TO (b) TI (c) CO (d) CI (e) BO (f) BI

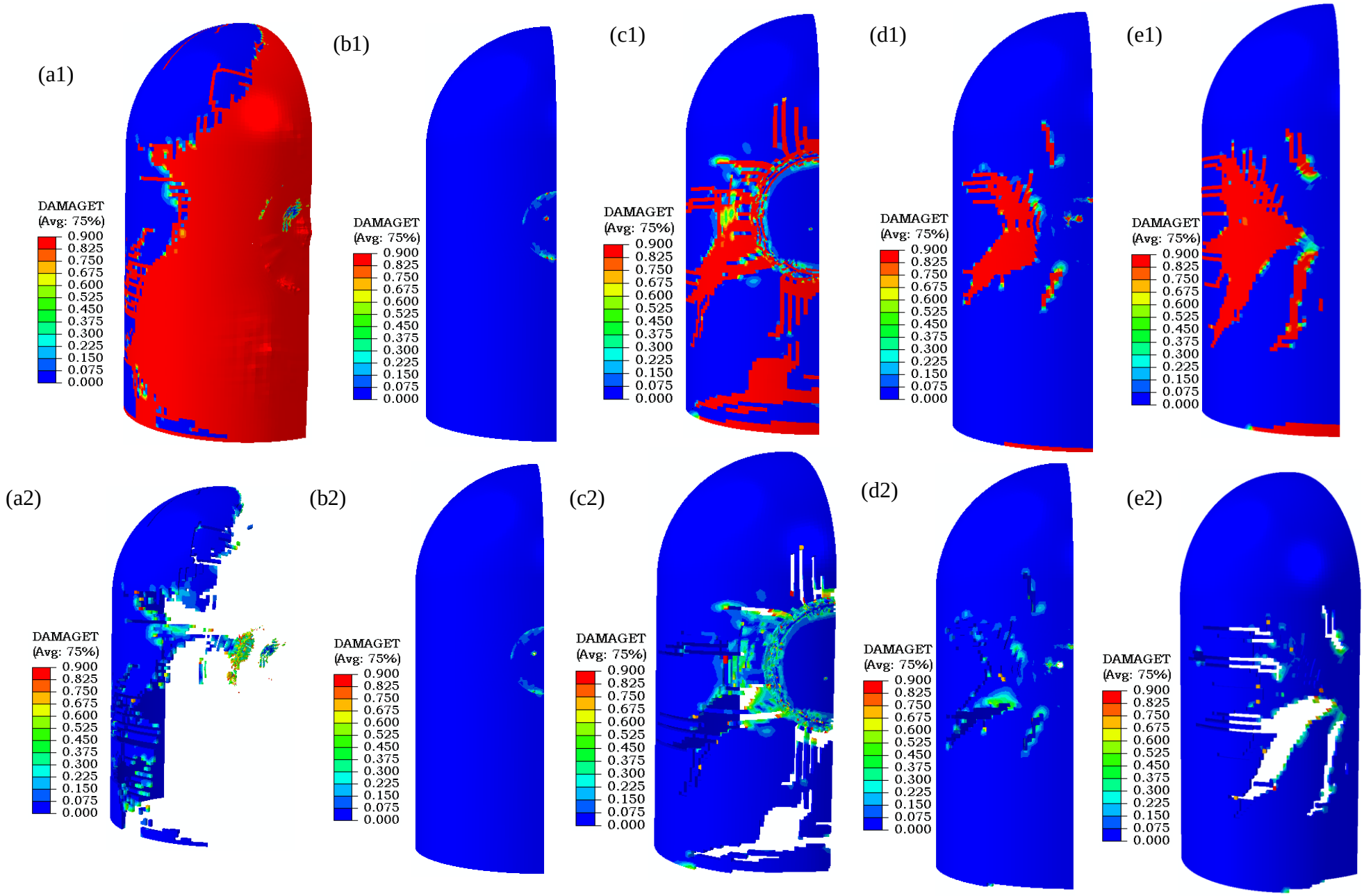

Fig. 4.44 Tension damage contour of concrete: (a) 747-400 (b) Phantom F4 (c) 767-400 (d) 707-320 (e) A320

It is important to mention here that the results for different aircrafts discussed up to this point are exclusively based on the material behavior of concrete subjected to varying strain rate (290 s^{-1}, 620 s^{-1}, 1050 s^{-1} and 1500 s^{-1}) as mentioned in Chapter 3. However, in order to further study the influence of strain rate, the analysis of containment for each aircraft has also been carried out employing the stress-strain relation of concrete at a constant strain rate 620 s^{-1}. The results thus obtained are shown in Fig. 4.45 in the form of tension damage of concrete experienced by the containment. As such, the predicted damage at 620 s^{-1} strain rate has been found in agreement with that of the results of varying strain rate (Fig. 4.44) for Phantom F4, Boeing 707-320 and A 320 aircrafts. However, for Boeing 747-400 aircraft the damage predicted at the constant strain rate has been found to be spread over a smaller area [Figs. 4.45(a1, a2)] as compared to what has been predicted by the varying strain rate, Fig. 4.44(a1, a2). On the other hand, a larger area of containment was found to be damaged for Boeing 767-400 aircraft at the constant strain rate, Figs. 4.45(c1, c2), when compared to that of the combined strain rate, Fig. 4.46(c1, c2).

The variations of tension damage with respect to time has also been plotted for the elements of concrete highlighted in Figs. 4.35(a) and (b) for varying strain rate and 620 s-1 strain rate, see Fig. 4.46 and 4.47 respectively. In general the damage predicted by the combined strain rate has been found to be slightly higher. For Boeing 747-400 and 767-400 aircraft however, all the selected elements were found to be completely damaged for the constant as well as varying strain rate. For the front face element in the central impact region (CF) however, the damage was found to be zero at constant strain rate, Fig. 4.47(g). The same can also be confirmed from contour plots shown in Figs. 4.45(a1 and a2). The element at the same location but inner face (CR) however, experienced complete damage for all the aircrafts at varying strain rate as well as constant rate, see Figs. 4.46(h) and 4.48(h) respectively.The compression damage plotted at constant strain rate for elements, DF, CF, CMF and NBF has been found to be low and could not reach the damage threshold for any aircraft, Fig. 4.48. At the inner face of the containment the compression damage was found negligible. In general it is seen that the compression damage is not critical at any location in the containment corresponding to any aircraft. It should be noted that the compression damage has been obtained only for 620 s^{-1}strain rate.

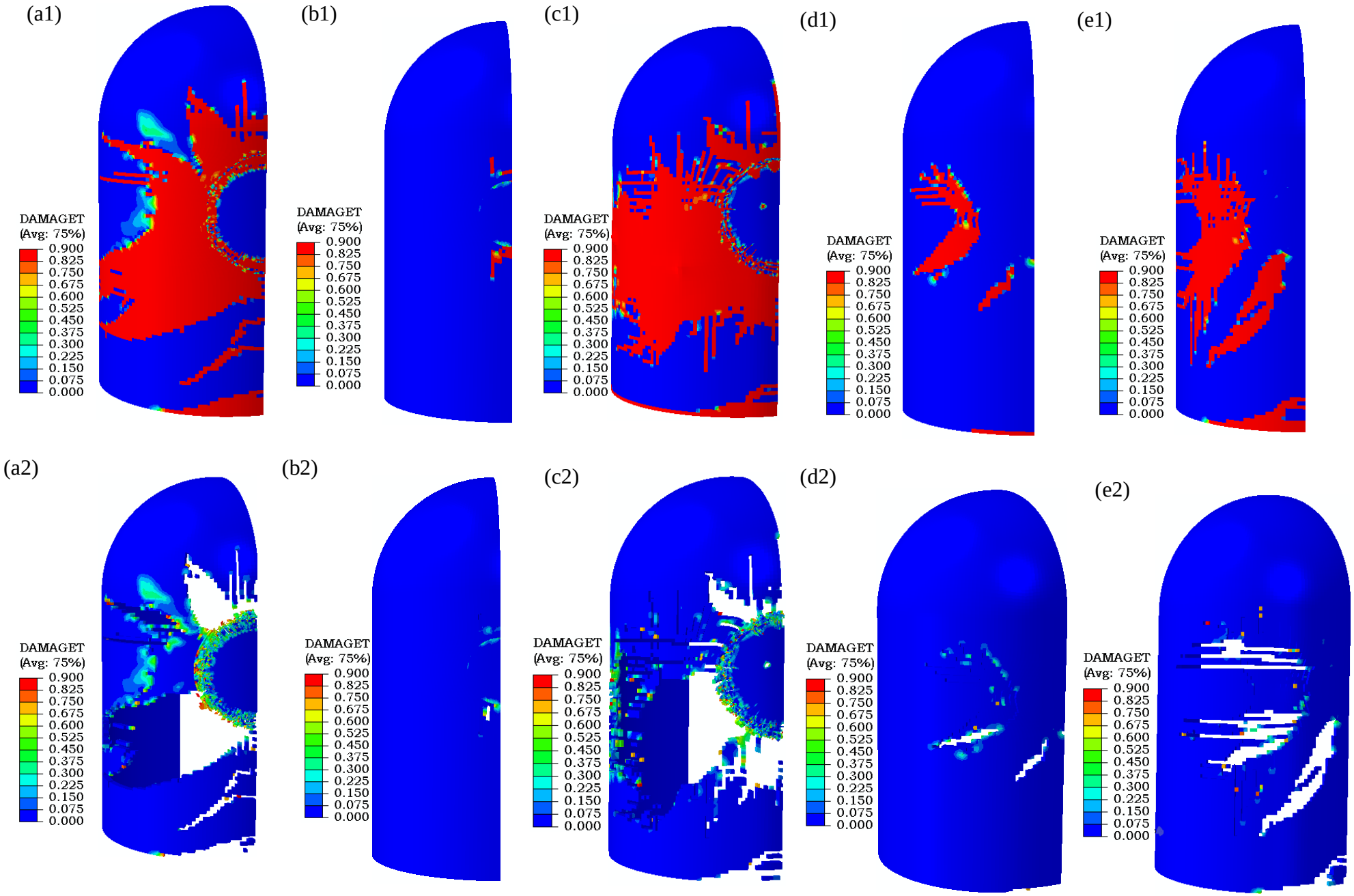

Fig.4. 45 Tension damage contour of concrete at 620 s^{-1} strain rate (a) 747-400 (b) Phantom F4 (c) 767-400 (d) 707-320 (e) A320

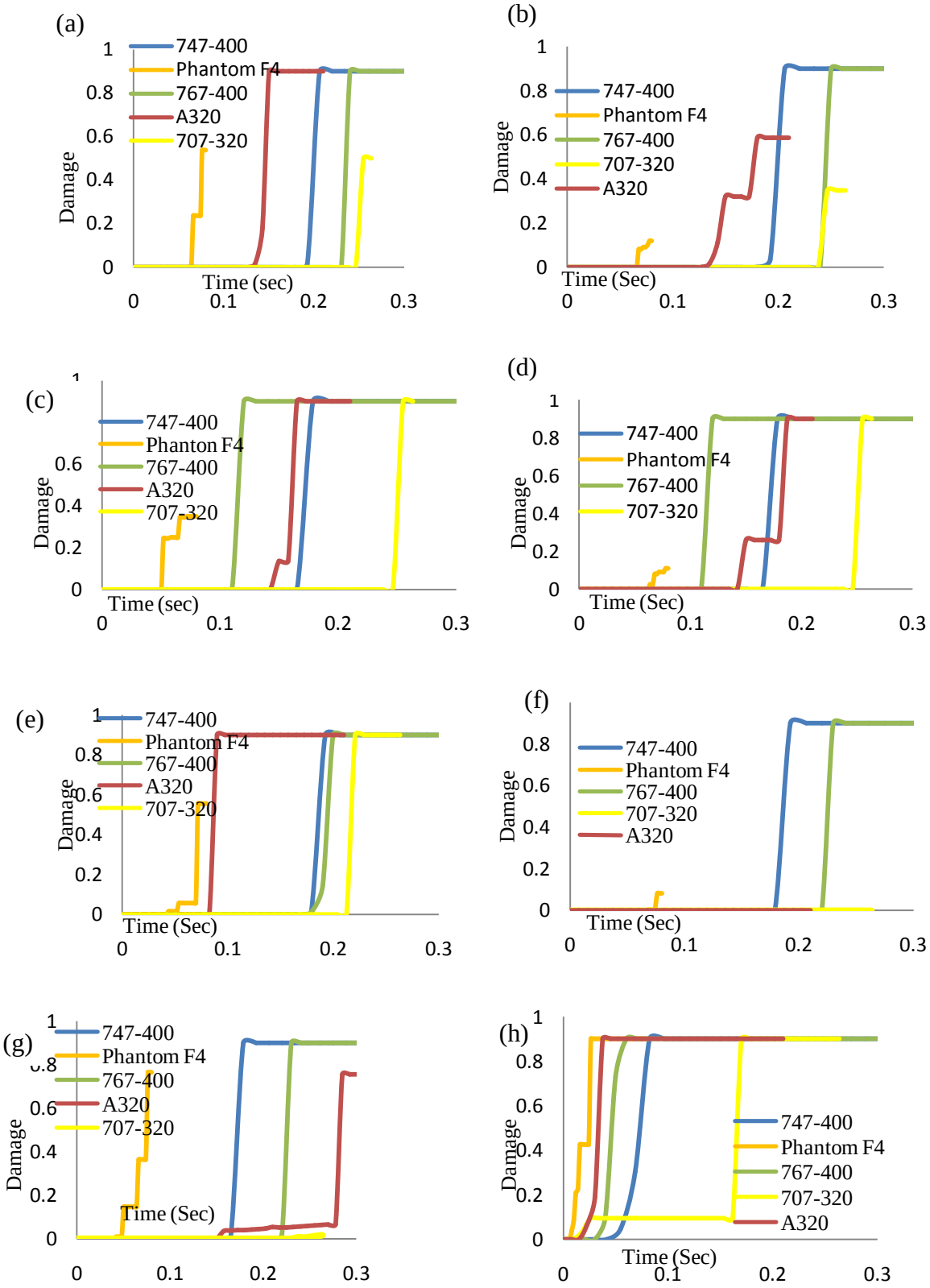

Fig. 4.46 Tension damage in concrete at varying strain rate: (a) DF (b) DR (c) NBF (d) NBR (e) CMF (f) CMR (g) CF h) CR

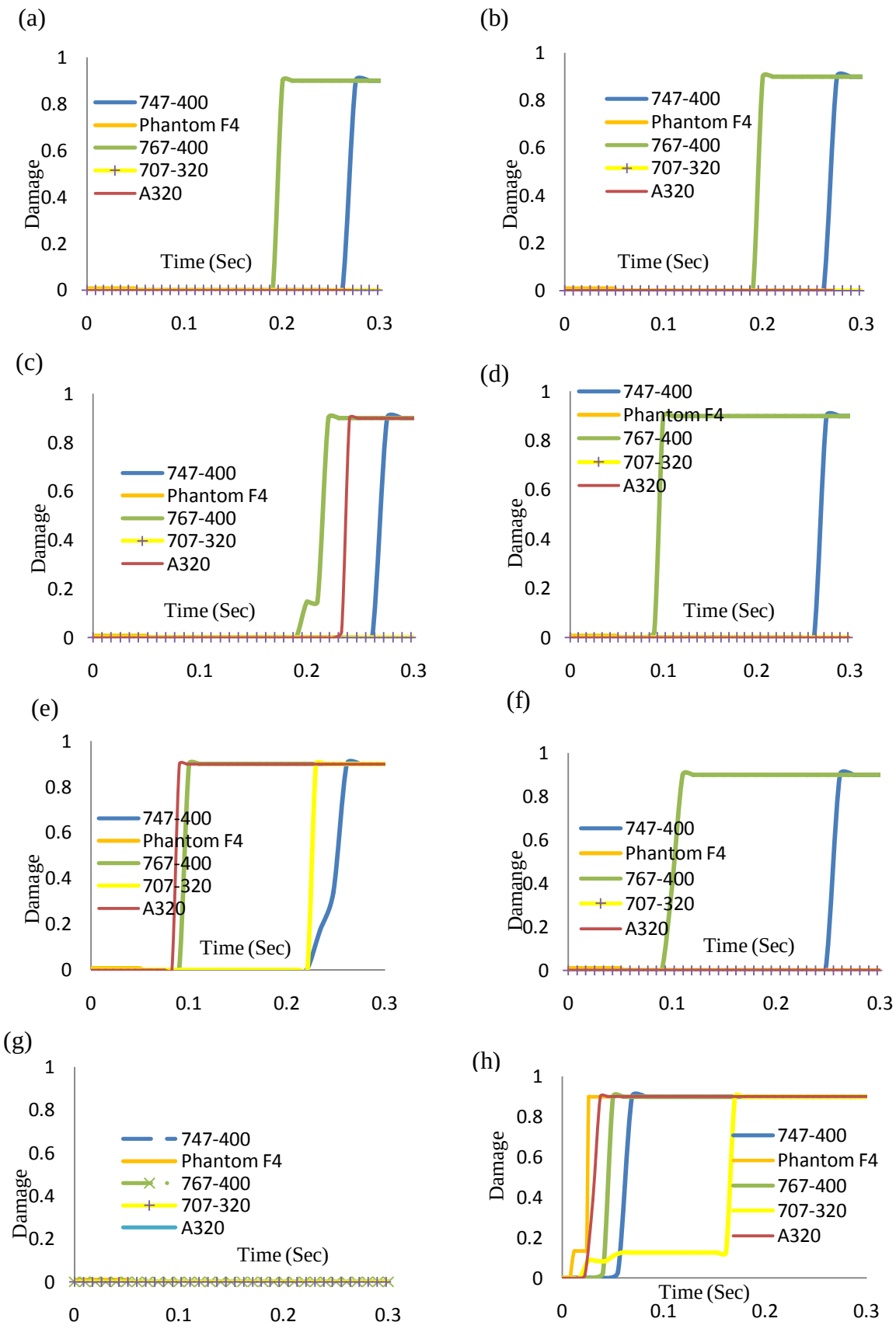

Fig. 4.47 Tension damage in concrete at 620 s^{-1} strain rate: (a) DF (b) DR (c) NBF (d) NBR (e) CMF (f) CMR (g) CF (h) CR

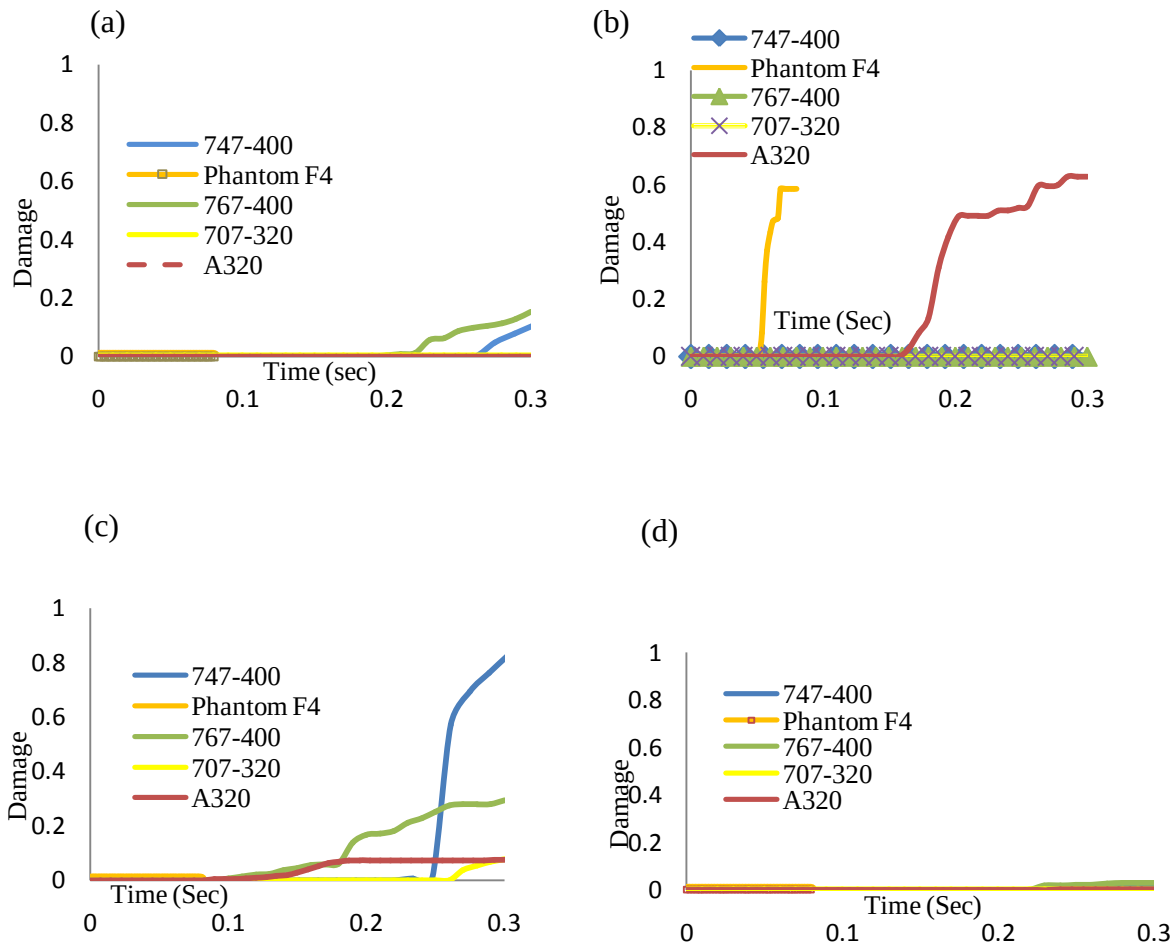

Fig. 4.48 Compression damage in concrete at 620 s^{-1} strain rate: (a) DF (b) CF (c) CMF (d) NBF

The global deformation at the front and rear face of the containment wall has been plotted along the central longitudinal axis 15 m above and below the centre of impact for varying strain rate, Fig. 4.49. The maximum deformation was found against Boeing 747-400 aircraft at the front and rear face. At the front face, the concrete in the central impact region (ø5.5 m) was significantly distorted against Boeing 747-400 aircraft, therefore the full deformation curve could not be generated, Fig. 4.49(a). Moreover, nominal outward deformation was also noticed 10 m beyond the centre of impact both in the upward and downward directions. At the rear face, the maximum deformation against Boeing 747-400 aircraft was found close to 1 m at the center of impact region, Fig. 4.49(b). For other aircrafts however, no sign of outward deformation was noticed and the magnitude of global deformation was found comparatively low (up to 0.1 m) and almost equivalent at front and rear face. A comparison of the global deformation of the rear face of containment has also been carried out for varying and constant strain rate, Fig. 4.50. In general the constant strain

rate predicted lesser deformation but close to that of the varying strain rate, except for Boeing 747-400, for which a significant effect of the strain rate was noticed. The maximum global deformation was found almost 1.0 m and 0.2 m for varying and constant strain rate respectively for Boeing 747-400 aircraft. The reason behind such behavior may be the predominant distortion and damage of concrete predicted at varying strain rate particularly in the central impact region, see Figs. 4.44(a1) and (a2). On the other hand, at constant strain rate the containment did not experience any damage in the central impact region, Figs. 4.45(a1) and (a2). Around the impact region however, significant damage was noticed in this case.

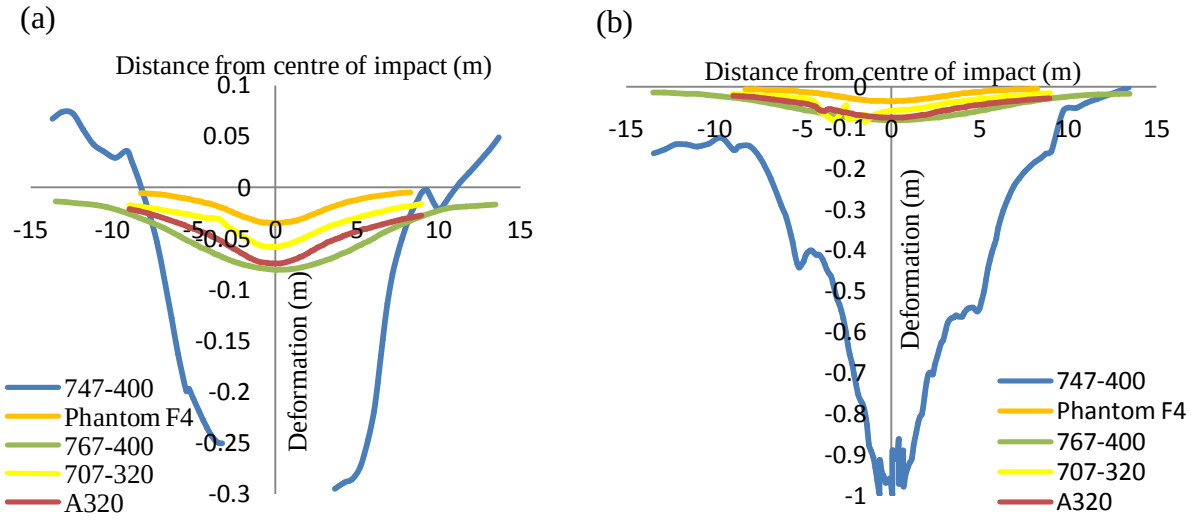

Fig. 4.49 Global deformation of the containment along the central longitudinal axis at varying strain rate (a) front surface (b) rear surface

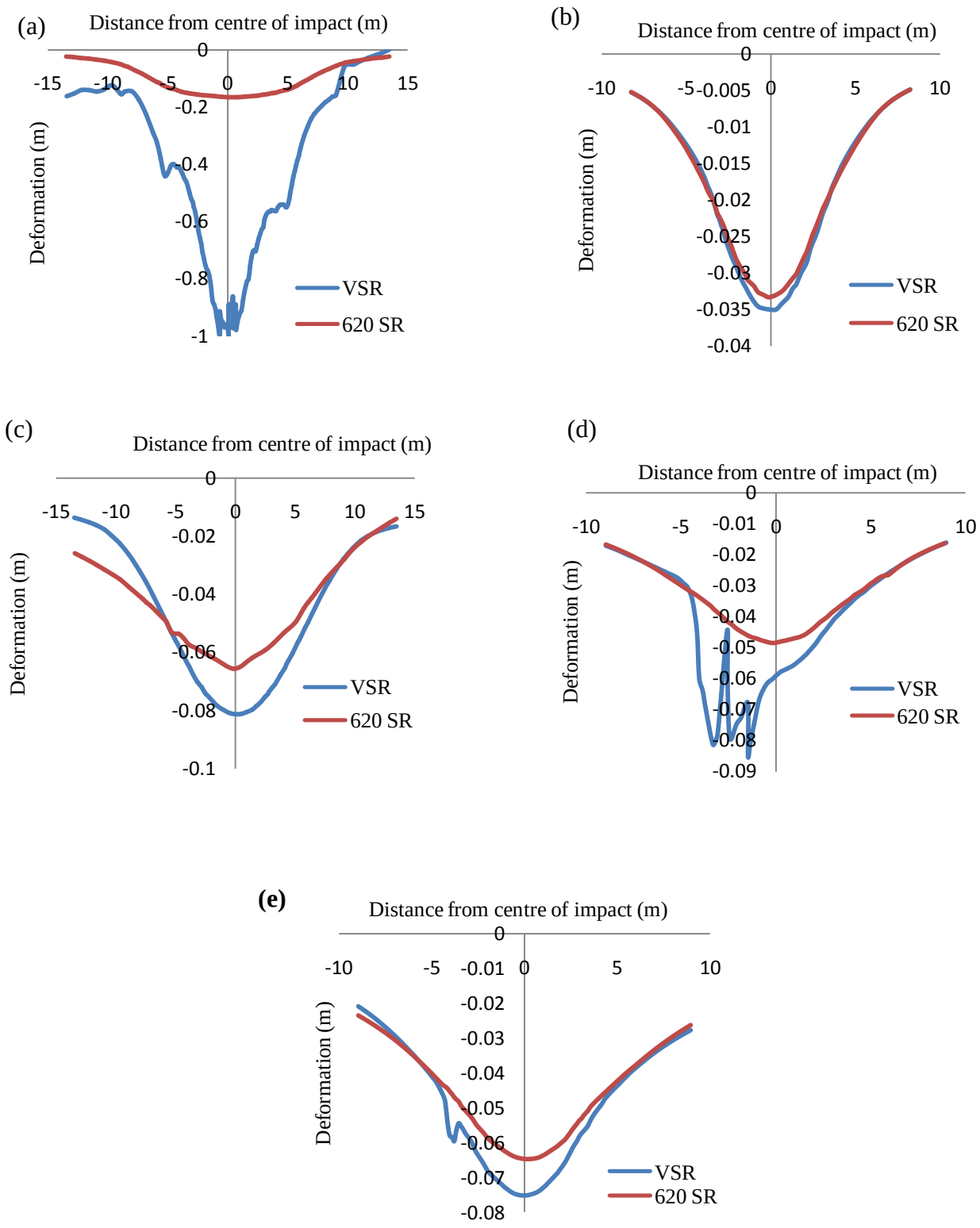

Fig. 4.50 Comparison of global deformation for varying and 620 s^{-1} strain rate at rear face of containment along central longitudinal axis: (a) 747-400 (b) Phantom F4 (c) 767-400 (d) 707-320 (e) A320

4.5 CONCLUDING REMARKS

In order to verify the material parameters opted in present study and to seek the effect of strain rate, three dimensional numerical simulations were carried out using ABAQUS/Explicit finite element code to predict the response of BWR Mark III type nuclear containment against crash of Boeing 707-320 aircraft. The strain rate was found to be an important parameter to effect the deformation in containment. The results of the simulation at varying strain rate have been found in close agreement with that of the simulation performed at 620 s^{-1} strain rate. Moreover, these results have been found to be a good correlation with data available in open available literature. Hence, in the remaining part of the study varying strain rate data has been adopted.

In order to seek the effect of strike location the structural safety of BWR Mark III type nuclear containment has been studied against the direct hit of Phantom F4, Boeing 707-320 and Airbus A320 aircrafts. Four different crash locations have been identified on the containment surface;

Location-A; Mid height of containment, Location-B; Near the junction of cylinder and dome
Location-C; At the curvature of dome, Location-D; At the crown of dome

Against each aircraft the displacement has been found to be maximum at Location A, followed by Location B, C and D respectively. On the other hand, the normal stress (in the direction of loading) has been found to be maximum at location D followed by location C, B and A, see Fig. 3. The reinforcement located near the inside face of the containment has experienced low stresses in comparison to the reinforcement located near the front face.

The response of the outer containment of BWR Mark-III type nuclear power plant has been studied against commercial and fighter aircraft crash to find out of effect of size and incidence velocities of aircrafts. The location of impact was considered at the mid height of the containment and the angle of incidence normal to the surface. The local deformation obtained in the present study was found in agreement with the available results in literature. The Boeing 747-400 and Boeing 767-400 aircrafts caused most significant damage to the concrete leading to the global failure of containment. The scabbing of concrete around the impact region was also noticed against Airbus A320 and Boeing 707-320 aircrafts resulting in local failure of the containment. Phantom F4 on the other hand, did not cause any damage to the concrete. The damage of concrete was found to be critical under tension.

Chapter 5

EVALUATION OF REACTION-TIME RESPONSE CURVE AND AREA OF IMPACT

5.1 GENERAL

The reaction-time response curve (RT) of aircrafts is widely used as the loading function to evaluate the response of any structure. As per the current design practice, the reaction versus time curve of an aircraft obtained against the flat non-deformable target is used as the loading function to seek the response of containment. In the present chapter the effect of target curvature and deformability has been taken in to account in order to evaluate the reaction-time response of the aircraft. Two different aircrafts chosen for the present study are Boeing 707-320 and Boeing 747-400. The Boeing 707-320 has been chosen to enable the validation of the results of present study with those available in the literature. The Boeing 747-400 has been studied due to the fact that it is the largest available aircraft and hence possesses highest damaging potential. Further, it is also being used for long distance flights and hence contains large amount of fuel. The geometric and finite element modeling of both of these aircrafts have been discussed in Chapter 2. It has been observed that the increase in target curvature is responsible for the time delay in the peak impact force and reduction in its magnitude. The reaction time curve obtained against deformable target has been found to be lesser than rigid target of same diameter. The response of containment building has been studied against the geometric model of aircraft as well as the reaction-time curves. The response of containment against the geometric model of aircraft has been found to be very close to that obtained against the reaction time curve used with area trifurcation scheme.

5.2 EVALUATION OF REACTION-TIME CURVE

The calculation of the reaction-time curve for reproducing the force exerted by aircraft on a structure involves very high degree of complexity. Particularly in the past, with limited computational resources the exploration of this problem would have pushed the researchers to their threshold. Their tremendous efforts however, enabled the determination of reaction-time curve and facilitated the investigation of aircraft crash on the containment structure, which in turn is a highly complex phenomenon. However, the evaluation reaction-time curve was based on some basic assumptions with respect to the aircraft as well as the target structure. The two important assumptions pertaining to the target structure are;

i) The target is assumed to be flat

ii) The target is assumed to be analytically rigid

The present study is focused to reevaluate the limitations of these two assumptions and their significance on the response of the containment structure.

5.2.1 Validation of Geometric Model

The development of geometric model of aircraft and its finite element characterization has been discussed in detail in Chapter 2. The constitutive modeling of the aircraft as well as the target structure has also been discussed in Chapter 3.

In order to validate the geometric as well as constitutive model of Boeing 707-320 and Boeing 747-400 aircrafts the reaction-time response curves have been obtained against the flat rigid target. A rectangular analytically rigid flat plate of side length 80 m has been developed for this purpose using ABAQUS/CAE, see Fig. 5.1.

The ABAQUS finite element code however, does not recognize a discrete or analytical rigid part for the analysis of any problem. Therefore it recommends that all the rigid surfaces must be assigned a reference point to enable the characterization of their boundary conditions and inertia. The constraints applied to the reference point are applied to the entire rigid body. The location of the rigid body reference point affects the prescribed constraints and also the interpretation of the force and moment reactions. If the model includes a dynamic analysis involving rotations, the rotary inertia of the rigid body must be made consistent with the location of its rigid body reference point.

In the present investigation all degrees of freedom have been constrained at the reference point to make the target perfectly rigid. In addition, the significance of the position of reference point has also been studied by hitting a small prismatic bar (20m x 10m x 10m), see Fig. 5.2. The prismatic bar has been hit at the center of the rigid plate while the reference point has been allocated two different positions i.e., center of the plate and mid of the top edge of the plate. It has been noticed that for the identical meshing of the prismatic bar the reaction-time curves obtained at two different locations were also identical.

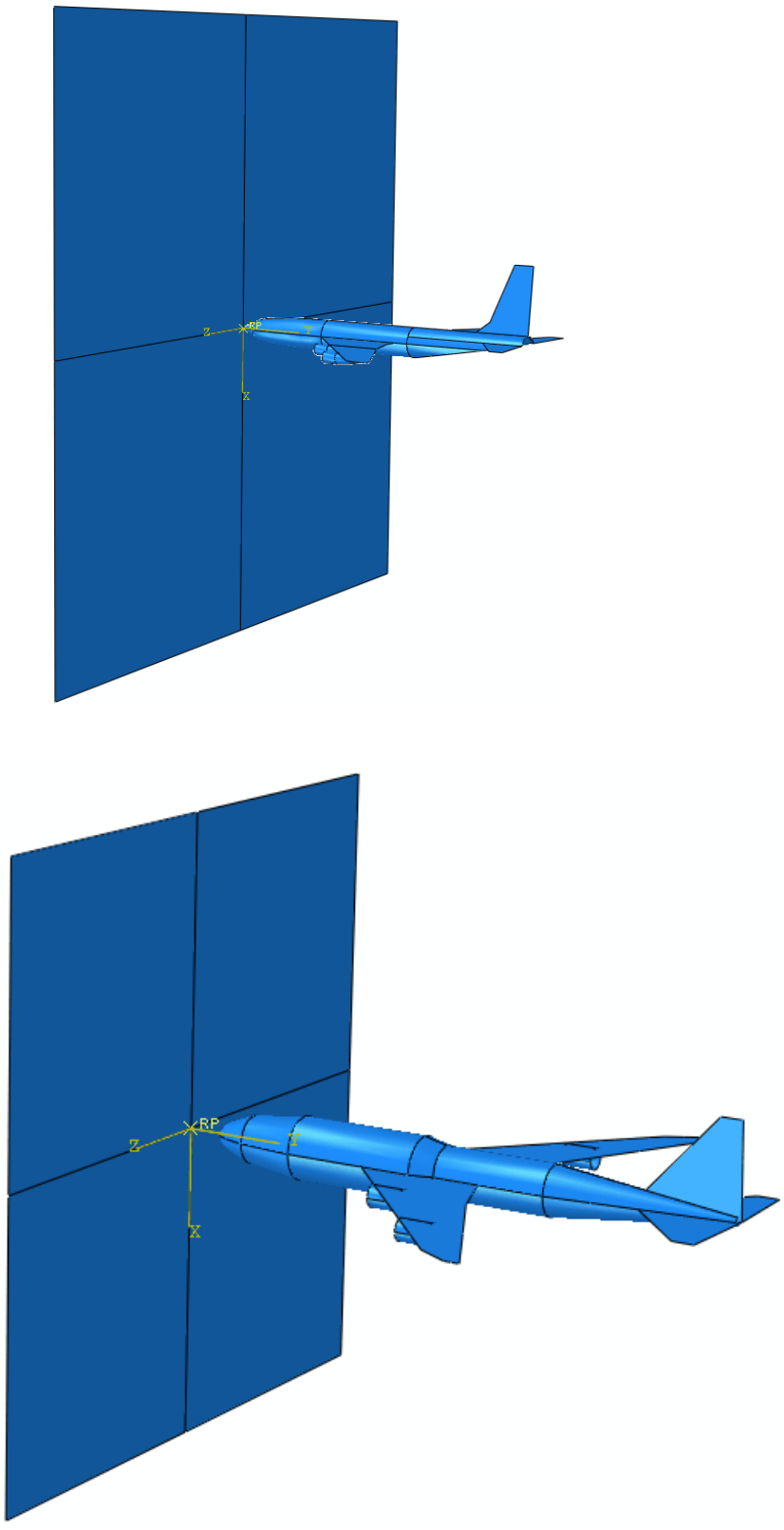

Fig. 5.1 Non deformable Flat Target (D_{Inf}) employed to obtain the reaction-time response of aircraft (a) Boeing 707-320 (b) Boeing 747-400

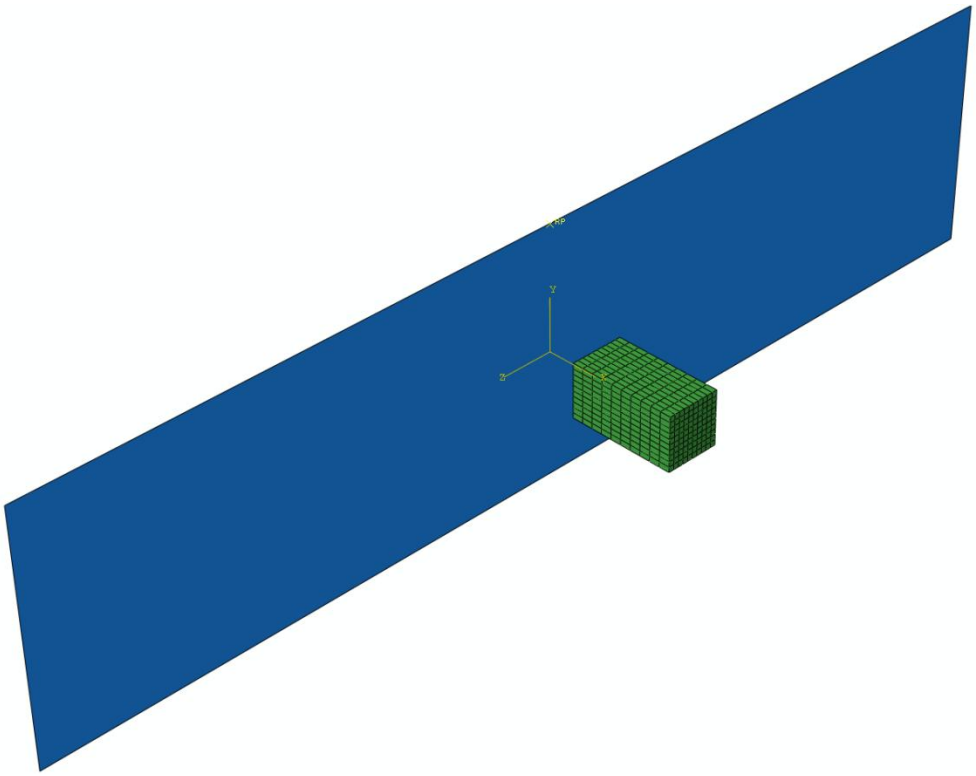

Fig. 5.2 Prismatic bar employed to obtain the reaction-time response against non-deformable flat (D_{Inf}) target targets

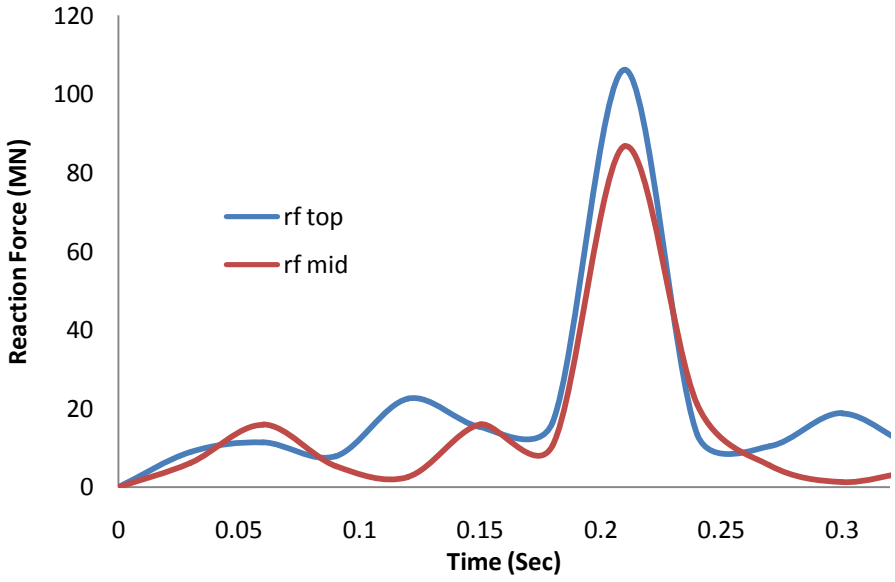

Fig. 5.3Effect of location of the reference point on the reaction-time response of Boeing 707-320 aircraft

Subsequently, simulations have been performed on the rigid plate considering the Boeing 707-320 as the projectile. In this case however, some change in the reaction-time curve has been noticed at two different positions of reference points, see Fig. 5.3. When the reference point is located at the top edge of the plate the resultant peak of the reaction force has been found to be 20 MN higher. This difference was resorted to the complicated structure of aircraft and more importantly its asymmetric geometry about the horizontal plane. In another simulation the Boeing 707-320 aircraft has been crashed at the center of a curved target, Fig. 5.4 (a). However, the reference point in this case has been kept at the center of the top edge as well as 5° and 15° away from the center of the top edge. A decrease in average impact force has been noticed as the reference point moved away from the center, Fig. 5.4 (b). Therefore, keeping in view the accuracy as well as consistency of the results the reference point for further simulations was considered at the center of the impact location. The output data points chosen for a simulation have also been found to affect the numerical results. The results of a simulation are actually represented as the average of the number of output. If the number of output is larger (i.e., smaller is the output interval) the numerical results will be more accurate and vice versa. However, the number of output data point cannot be increased beyond a certain limit since it significantly increases the computational time of the analysis. In the present study, the number of output data points has been varied as 20, 100 and 8000 for obtaining the reaction-time response of Boeing 707-320 aircraft. The results obtained are plotted in Fig. 5.5. The importance of the number of output data points is clearly visible through these results. When the output data points were increased from 20 to 100 a significant increase in the peak force was observed between 0.2 and 0.25 seconds, when the wings are hitting the target. It was therefore decided to increase the number of data points to 8000 in order to obtain the accurate results, however, further increase in the output data points was not possible due to the limitation of the available computational facility. The output was thus recorded at a constant increment of 0.4 μs (0.00004 sec.) while the total time of the phenomenon was 0.32 seconds, Fig. 5.5.

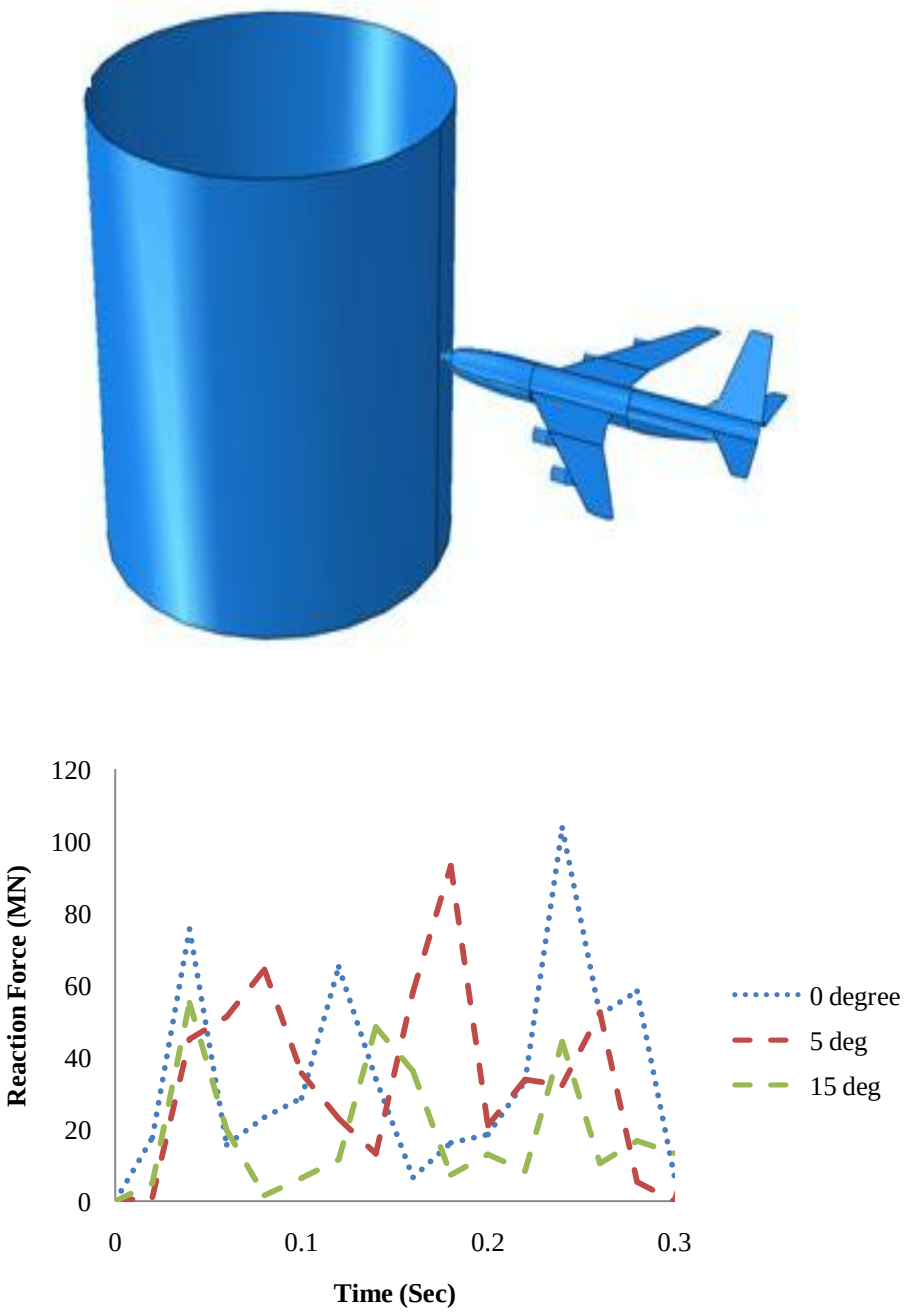

Fig. 5.4 Effect of the location of reference point on the reaction-time response of Boeing 707-320 aircraft

The reaction-time curve of Boeing 707-320 thus obtained against non-deformable (rigid) flat target has been compared with the reaction-time curve calculated through the analytical expression proposed by Riera (1968), see Eqn. 1.1 in chapter 1. A close correlation between the two has been found, see Fig. 5.6. The analytical expression proposed by Riera (1968) requires mass density, crushing strength and incidence velocity of the aircraft as input parameters. The reaction-time curve of Boeing 747-400 aircraft has also been obtained

through numerical simulations corresponding to 8000 output data points, Fig. 5.7. However, in this case the total time of the phenomenon was 0.55 sec. hence the data was recorded at a constant increment of 68 µs. The reaction-time curve thus obtained from the numerical simulation has been found to have close agreement with that obtained through the analytical expression proposed by Riera (Eqn. 1.1). It may be concluded here that the geometric models of Boeing 707-320 and Boeing 747-400 are reasonably accurate and hence can be employed for the further investigation of the problem. It should also be noted that the above reaction-time curves of Boeing 707-320 and Boeing 747-400 aircrafts have been obtained at 103m/s and 120 m/s incidence velocity. The incidence velocities have been considered equivalent to those witnessed during the aircraft crash reported in the past (Riera, 1968, Iliev et al., 2011).

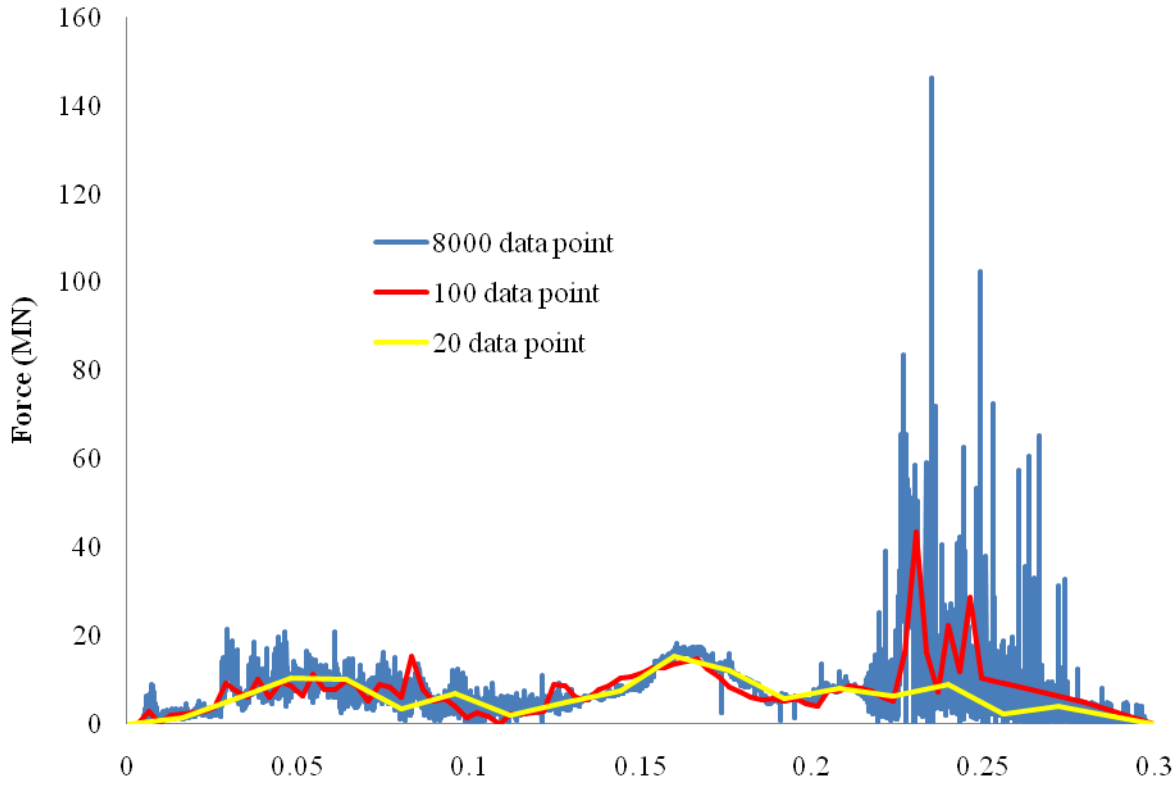

Fig. 5.5 Reaction-time response curves of Boeing 707-320 aircraft against non-deformable flat target by varying the number of output data points

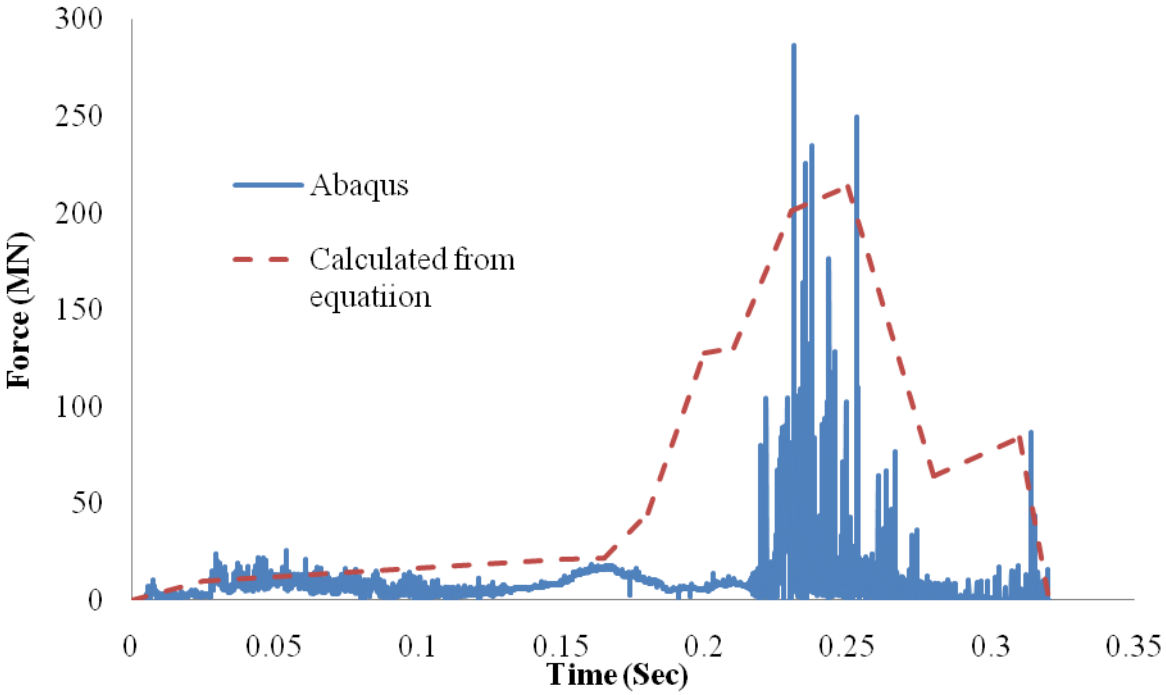

Fig. 5.6 Reaction-time response curve of Boeing 707-320 against non-deformable flat target

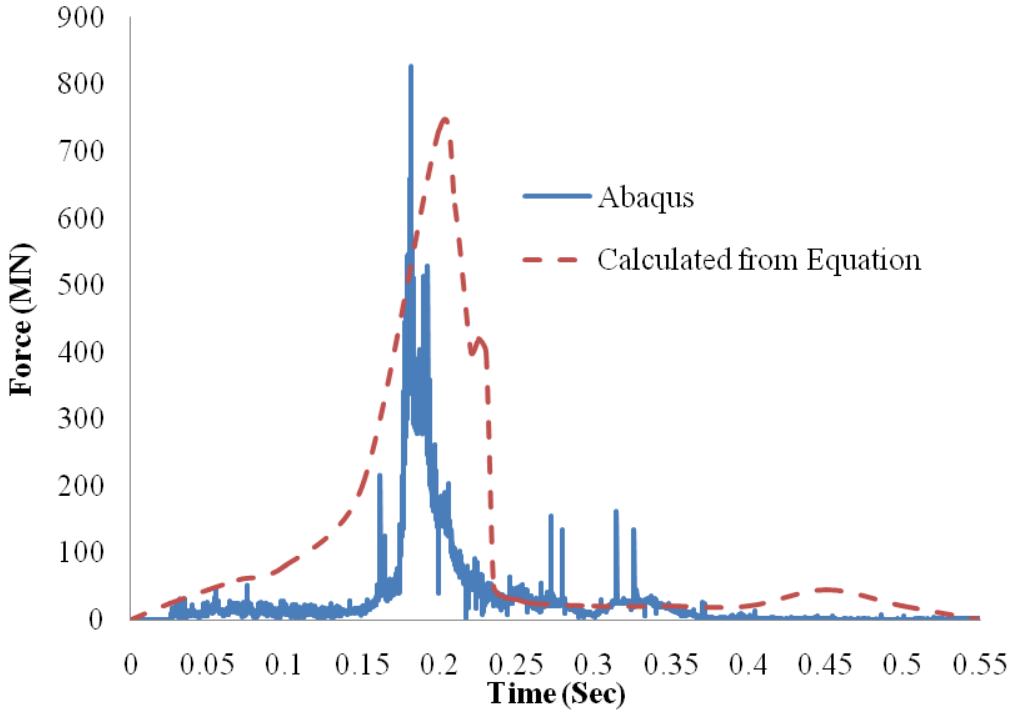

Fig. 5.7 Reaction-time response curves of Boeing 747-400 against non-deformable flat target

5.2.2 Effect of Target Curvature

To study the effect of target curvature, the geometric models of both aircrafts have been crashed against non-deformable curved targets with two different diameters i.e., ø42 m (D42) and ø100 mm (D100), as shown in Fig. 5.8. It should be noted that the diameter of the BWR containment considered in the present study is also 42 m. The incidence velocities of Boeing 707-320 and Boeing 747-400 aircraft have been considered identical to those employed against the non-deformable rigid targets. It has been noticed that with increase in target curvature there has been a decrement in the peak impact force. In addition, a time delay has also noted in the arrival of peak impact force.

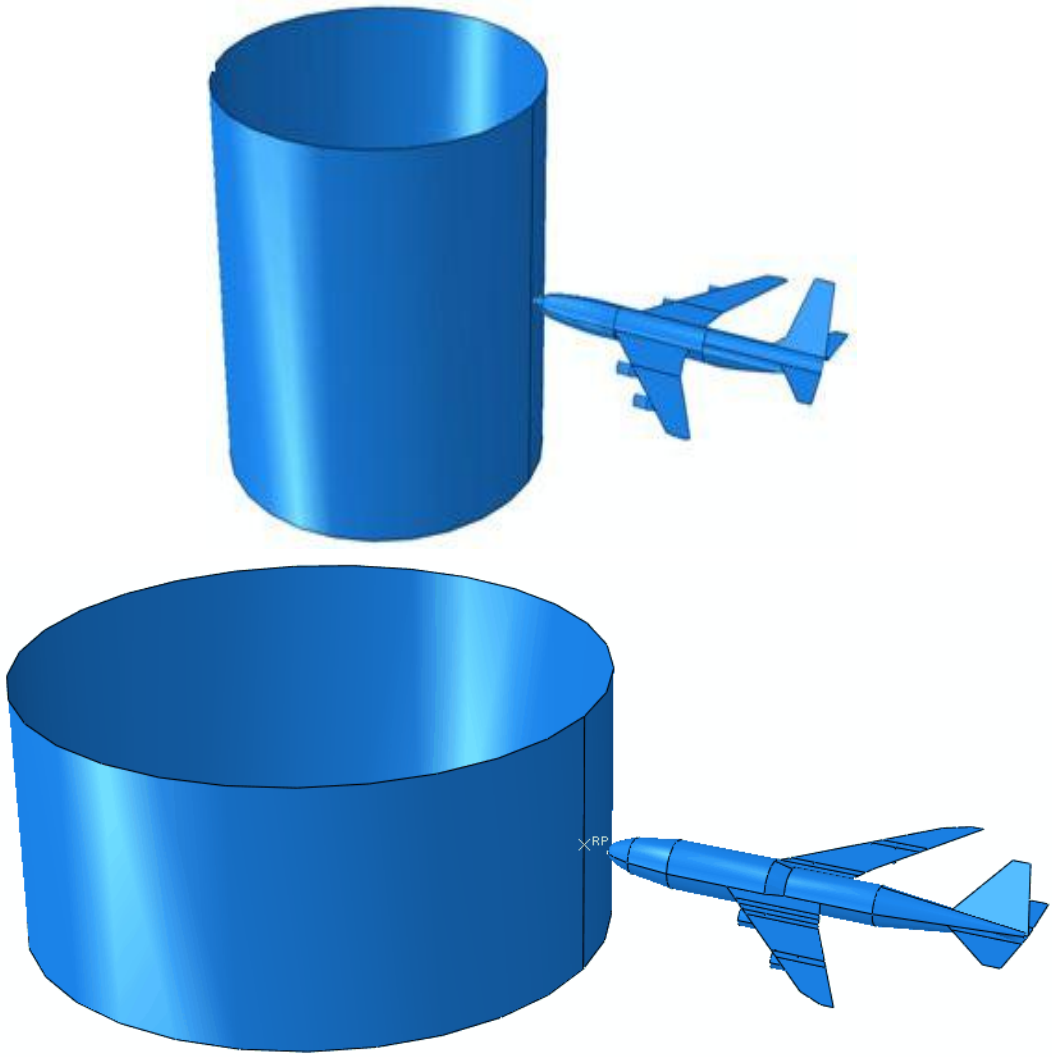

Fig. 5.8 Non-deformable targets of varying curvature (a) 42m (D42) and (b) 100 m (D100) employed for obtaining the reaction-time response of aircrafts

For Boeing 707-320 aircraft the maximum impact force has been found to be 160 MN at 0.295 sec. against D42 target and 200 MN at 0.259 sec. against D100 target, Fig. 5.9.

However, against the non-deformable flat target (D_{inf}) the maximum impact force has been found to be 286 MN at 0.231 sec. For Boeing 747-400 aircraft also a similar response has been noticed. The maximum impact force in this case has been found to be 469 MN at 0.21 sec. against D42, 510 MN at 0.197 sec. against D100 and 823 MN at 0.181 sec. against D_{inf}, Fig. 5.10. Therefore, as the curvature of the target is decreased the peak impact force has been found to increase while the time of its arrival has decreased. This is due to the fact that in case of flat target the main component of reaction is in the normal direction to the target surface opposite to the applied force, while the other two directional components are negligible. However, when the curvature was introduced in the target geometry, these two components of reaction have also developed which became prominent with an increase in curvature. Hence the reaction force in the direction opposite to the applied force decreased. For Boeing 707-320 aircraft the peak impact force has been found to decrease by 30% and 44% respectively for the D100 and D42 target as compared to D_{inf}. For Boeing 747-400 aircraft the decrement was 38% and 43% respectively for D100 and D42 targets as compared to D_{inf}. Hence, it may be concluded that effect of target curvature cannot be neglected while obtaining the reaction time curve for the aircraft. It may also be concluded that the acceptance of the reaction curve obtained against flat target (D_{inf}) as the design load will result in the overestimation of the resultant design parameters.

In order to verify the above results, a simple hollow tube of aluminum alloy AL-7178-T651 was impacted against the above three targets of varying curvature, Fig. 5.11. The length, diameter and thickness of the tube was 40 m and 10 m respectively. A similar trend has been noticed in the reaction-time curves, Fig, 5.12. Hence, it can be concluded that the decrement in the peak impact force is a phenomenon purely related to the target curvature and not due to the complex geometry of the aircrafts.

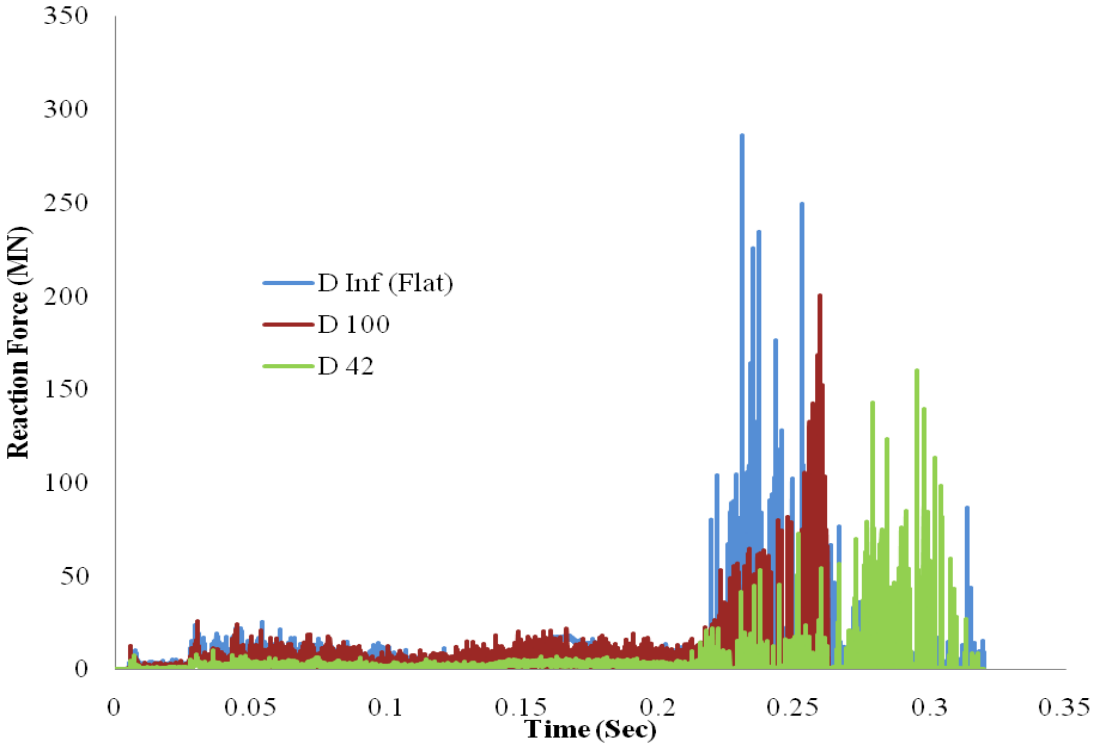

Fig. 5.9 Reaction-time response curves of Boeing 707-320 aircraft against non-deformable targets of varying curvature

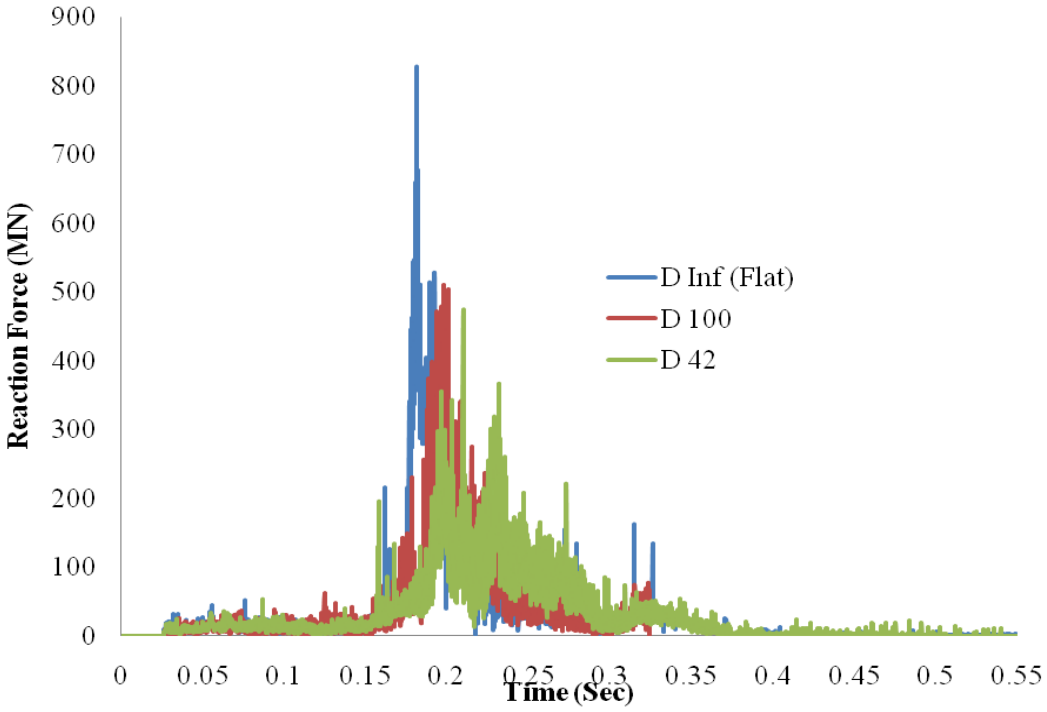

Fig. 5.10 Reaction time response curves of Boeing 747-400 aircraft against non-deformable targets of varying curvature

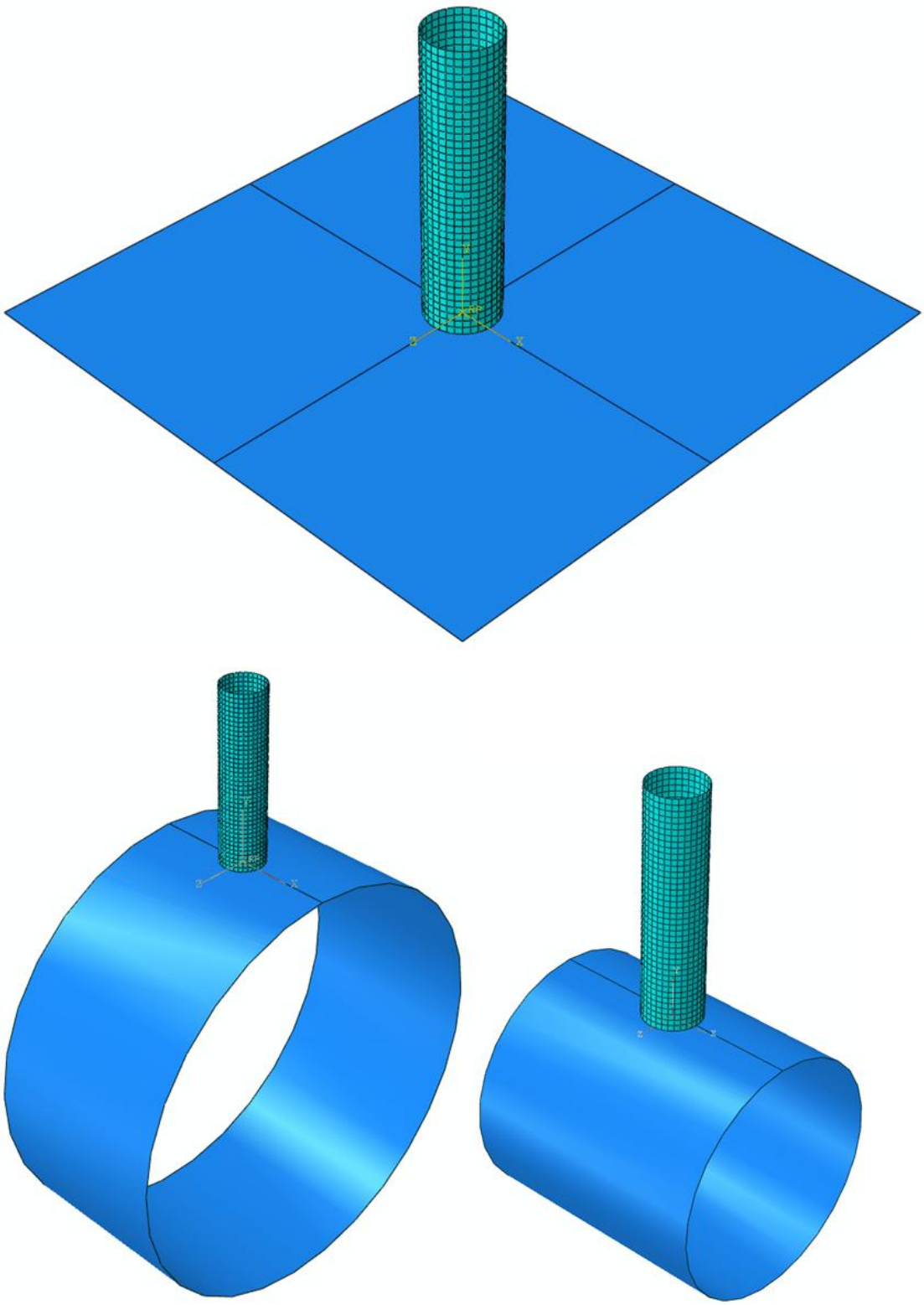

Fig. 5.11 Aluminum tube employed to obtain the reaction-time response against non-deformable flat target

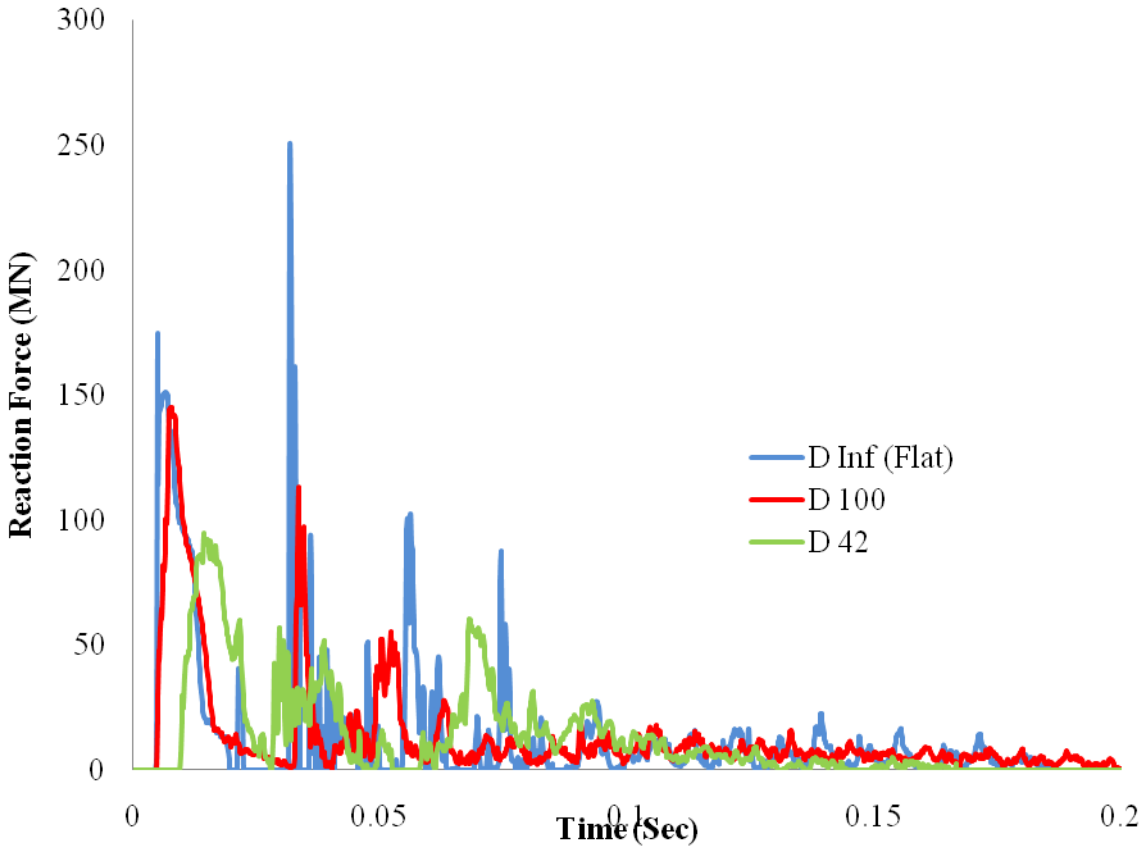

Fig. 5.12 Reaction time response curves of aluminium tube against non-deformable targets of varying curvature

5.2.3 Effect of Target Deformability

In order to evaluate the influence of target flexibility, both aircrafts have been crashed on the outer containment of a BWR NPP. However, some modifications have been applied here on the containment geometry as compared to what has been considered in the previous chapter. Instead of half, full containment has been modeled for striking the geometric models of the aircraft. Moreover, in order to optimize the total number of elements, the rooftop of the containment has been considered flat instead of semi-spherical dome, Fig. 5.13. Therefore, the total height of the containment is reduced to 46 m but the external diameter remained unchanged i.e., 42 m. To avoid the effects of boundary conditions the strike location has been chosen at the mid height of the containment i.e., at 23 m from the base.

The reaction-time curve thus obtained has been compared with that obtained against the non-deformable curved target of equivalent diameter (D42). A significant downfall in the peak impact force has been noticed in case of the deformable target; see Figs. 5.14 and 5.15 respectively for the Boeing 707-320 and Boeing 747-400 aircraft. The peak impact force against deformable target has been found to decrease by 40% for Boeing 707-320 and 40.5%

for Boeing 747-400 aircraft. The reduction in reaction force against the containment structure is due to the fact that some energy has been dissipated in the deformation of the structure. Thus the net reaction obtained is lesser than that obtained against non-deformable target of same diameter. Hence, it may be concluded that the reaction time response curve is a function of the stiffness of the target.

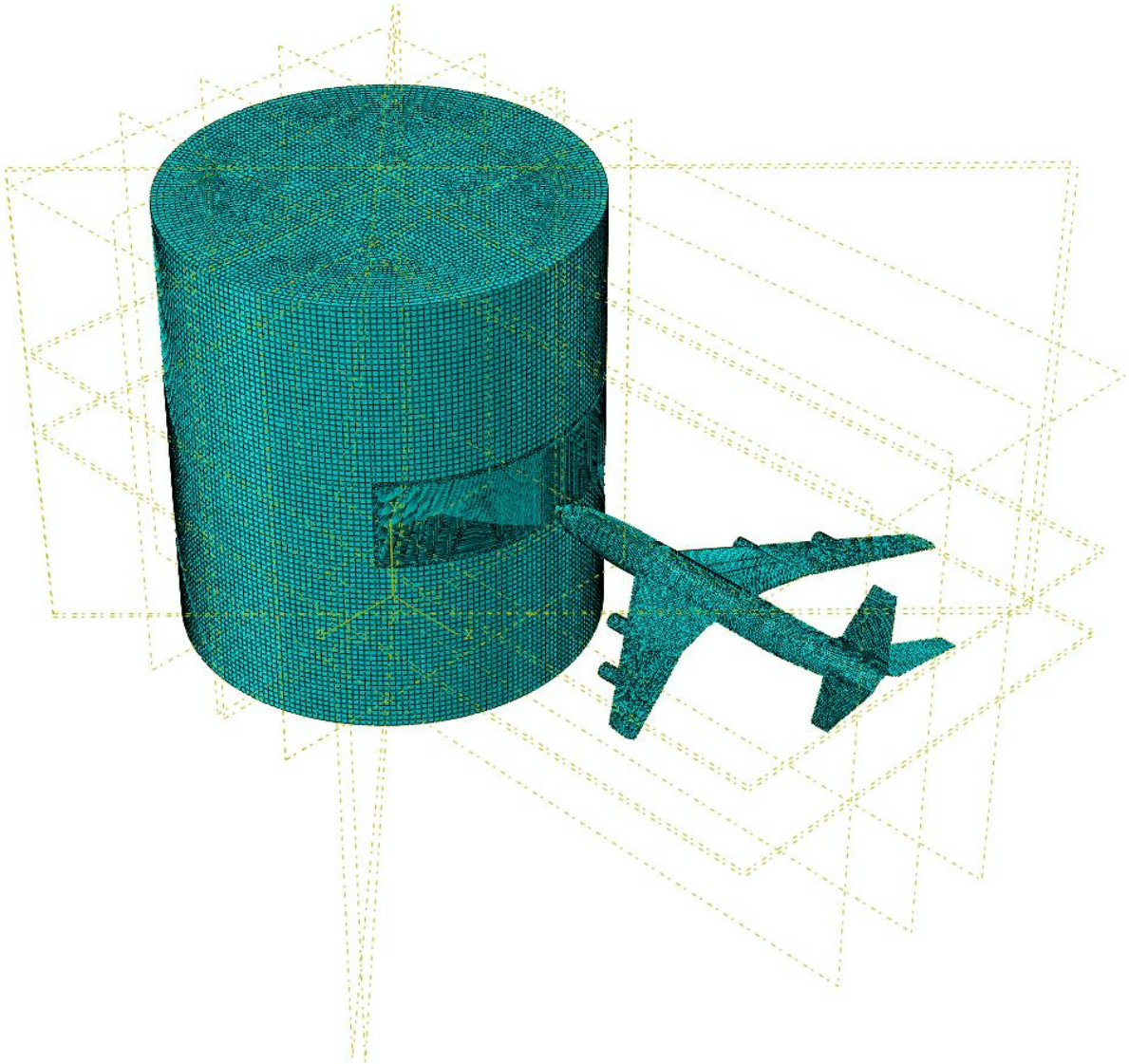

Fig. 5.13 BWR nuclear containment hit by the Boeing 707-320 aircraft

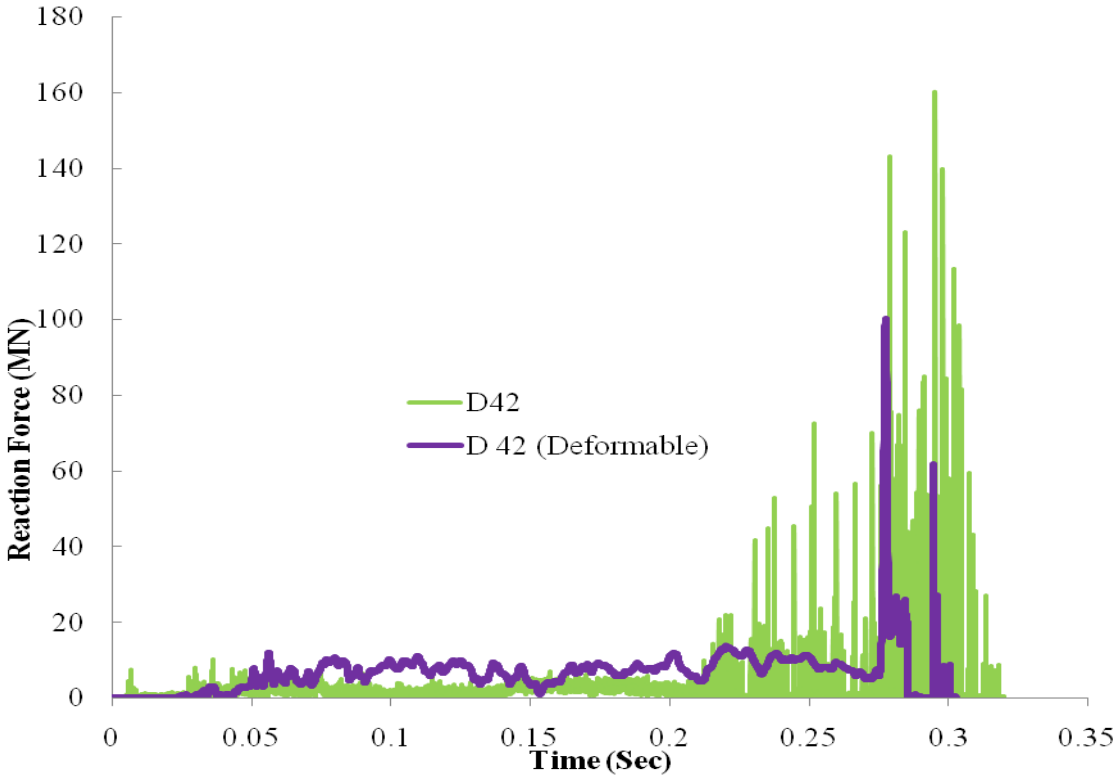

Fig. 5.14 Reaction time response curves of Boeing 707-320 aircraft against non-deformable (D42) and deformable target (BWR containment) of identical curvature

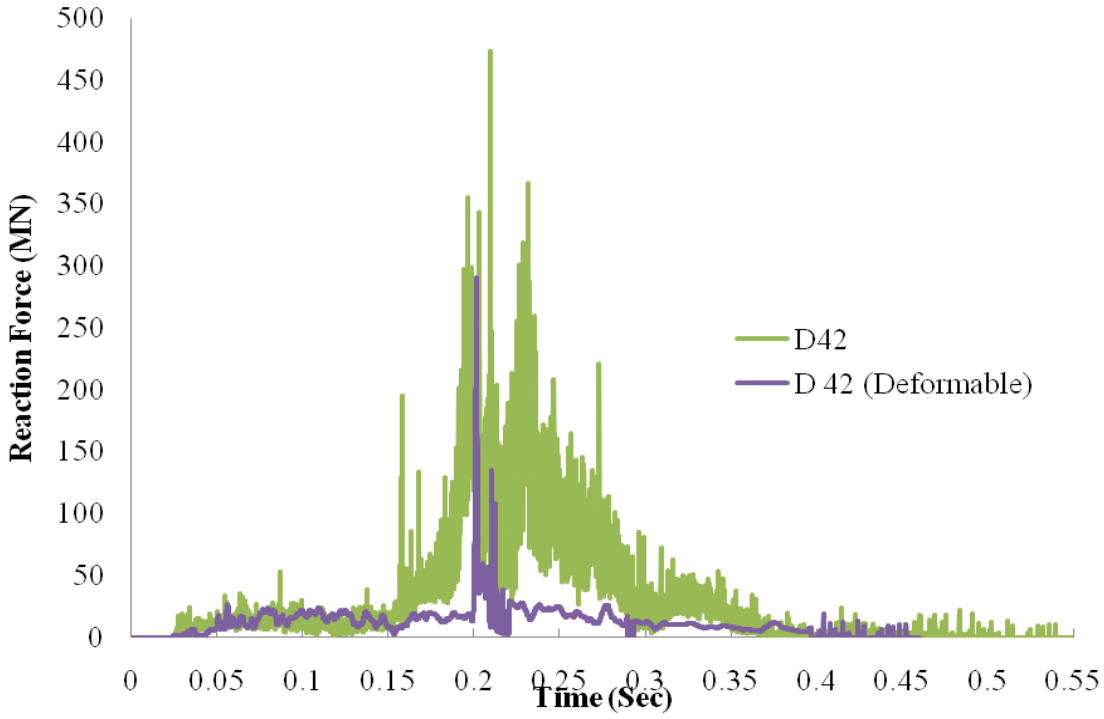

Fig. 5.15 Reaction time response curves of Boeing 747-400 aircraft against non-deformable (D42) and deformable target (BWR containment) of identical curvature

5.3 CALCULATION OF EFFECTIVE IMPACT AREA

In order to evaluate the containment response through the reaction-time approach, the extent of area chosen for the application of the load will be highly important. A smaller area will increase the intensity of the pressure and hence the response will be localized and overestimated, while a larger area will reduce the deformations and hence underestimate the response. The impact area of an aircraft is never constant. It is a function of time as well as incidence velocity of the aircraft. The majority of the studies available in literature employed the average of the contact area of aircraft as the impact area. In chapter 4 also the area of impact has been assumed to be the average contact area and hence considered constant throughout the impact phenomenon.

The imprecision related to area of impact has already been discussed under the article 1.2.4 of chapter 1. To resolve the uncertainty of impact area, a fresh calculation has been performed in the present study. The numerical as well as analytical approaches have been employed to evaluate the actual impact area as a function of time and incidence velocity. The crushed profile of Boeing 707-320 aircraft against non-deformable flat target has been studied at different time interval, see Fig. 5.16. This enabled the evaluation of impact area with respect to time through the numerical simulation. In addition, the impact area has also been calculated analytically. The detailed dimensional drawings of Boeing 707-320 provide the description of actual cross-sectional area at any point along the length of aircraft (Boeing, 2013). Moreover, Abbas (1992) plotted the variation of impact load for Boeing 707-320 with respect to distance from the nose of aircraft. With the help of these data an effective cross-sectional area verses time graph of Boeing 707-320 has been plotted for an incidence velocity 103 m/s, Fig. 5.17. However, it has been reported by Yang and Godfrey (1970) that the contact area between the aircraft and target increases by 10 to 15% as compared to the actual cross-sectional area of aircraft. Therefore the cross-sectional area calculated above was increased by 15% to obtain the contact area for Boeing 707-320 aircraft.

The contact area versus-time curve thus obtained has been found to have close correlation with that of the curve proposed by Riera (1968), Fig. 5.17. In all these curves, initial sharp rise is due to the crushing of nose of the aircraft which is comparatively stiffer. There is again a steep rise in the contact area as soon as the wings come in contact. The tail of the aircraft generally not come in the contact particularly during the normal impact due to the fact that the crushed body of the aircraft restricts the contact of the tail with that of the containment.

Hence, the contact area becomes constant once the complete wings come in the contact. The average area calculated from Riera (1968) curve is 28.25 m^2 while that obtained from the present investigation is 28.4 m^2 and 28.85 m^2 through analytical and numerical approach respectively, Fig. 5.17. It has also been noticed from Fig. 5.17 that the maximum contact area from all the studies is approximately equivalent to 40 m^2.

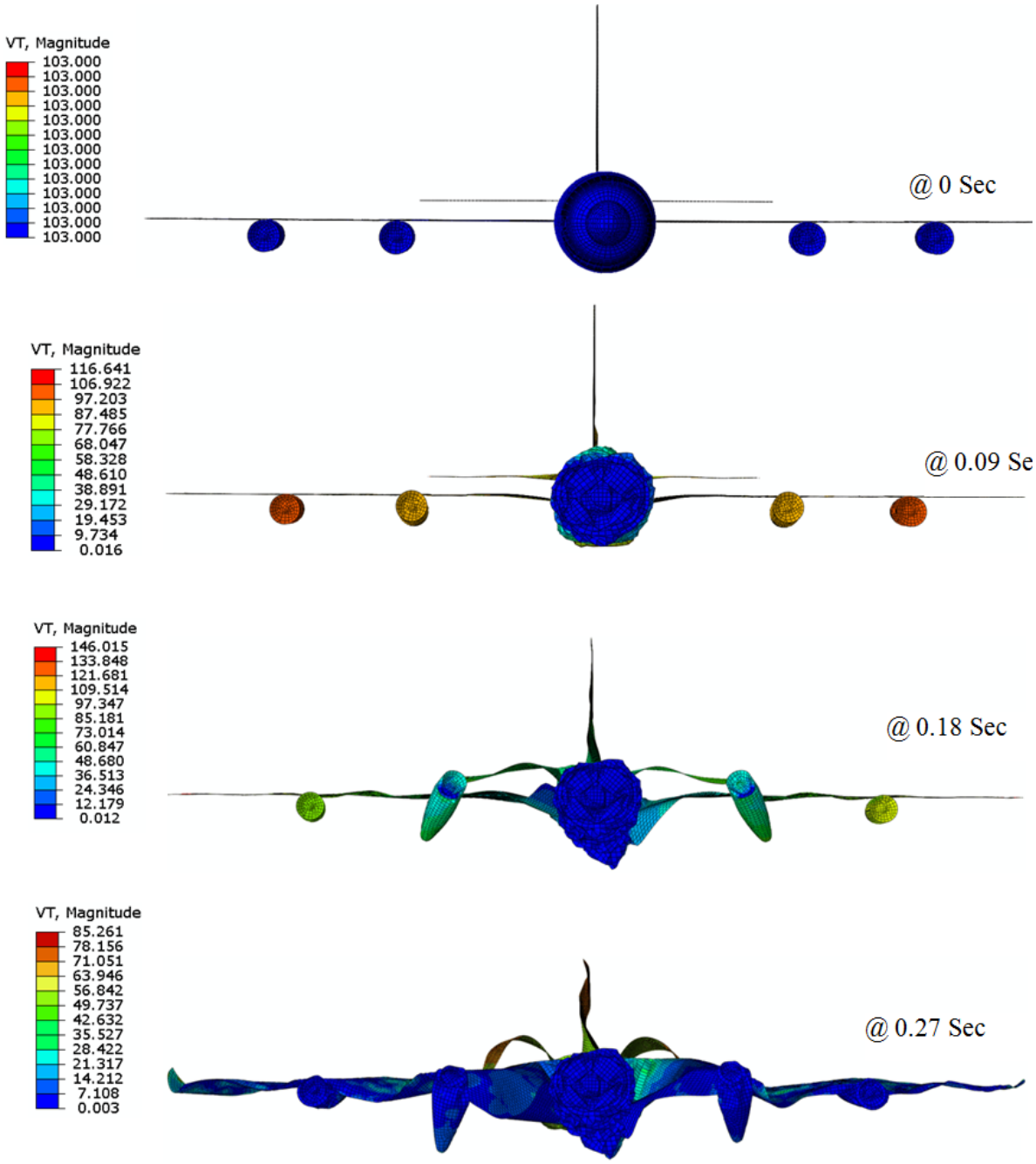

Fig. 5.16 Crushing behaviour of Boeing 707-320 aircraft against non-deformable flat target

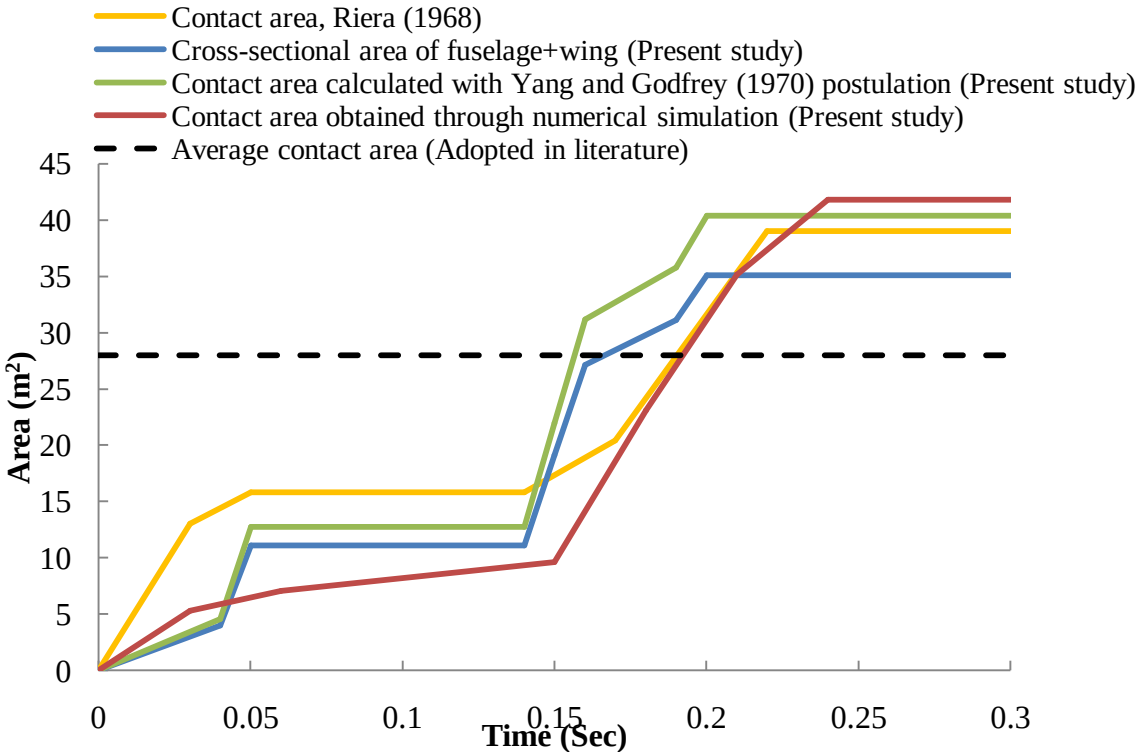

Fig. 5.17 Area of contact for Boeing 707-320 aircraft obtained through different methods

The contact area variation for Boeing 747-400 has been plotted in Fig. 5.18. A similar trend has been obtained in the nature of contact area curves due to the fact that this aircraft is an enlarged upgraded model of Boeing 707 series. The maximum contact area of Boeing 747-400 aircraft has been obtained to be 118 m^2 and 122 m^2 from the analytical and numerical approach respectively. It should be noticed that the cross-section calculated in this case has also been increased by 15% in order to obtain the contact area. It should also be noticed that Iliev et al. (2011) assumed a contact area of 116.26 m^2 for Boeing 747-400.

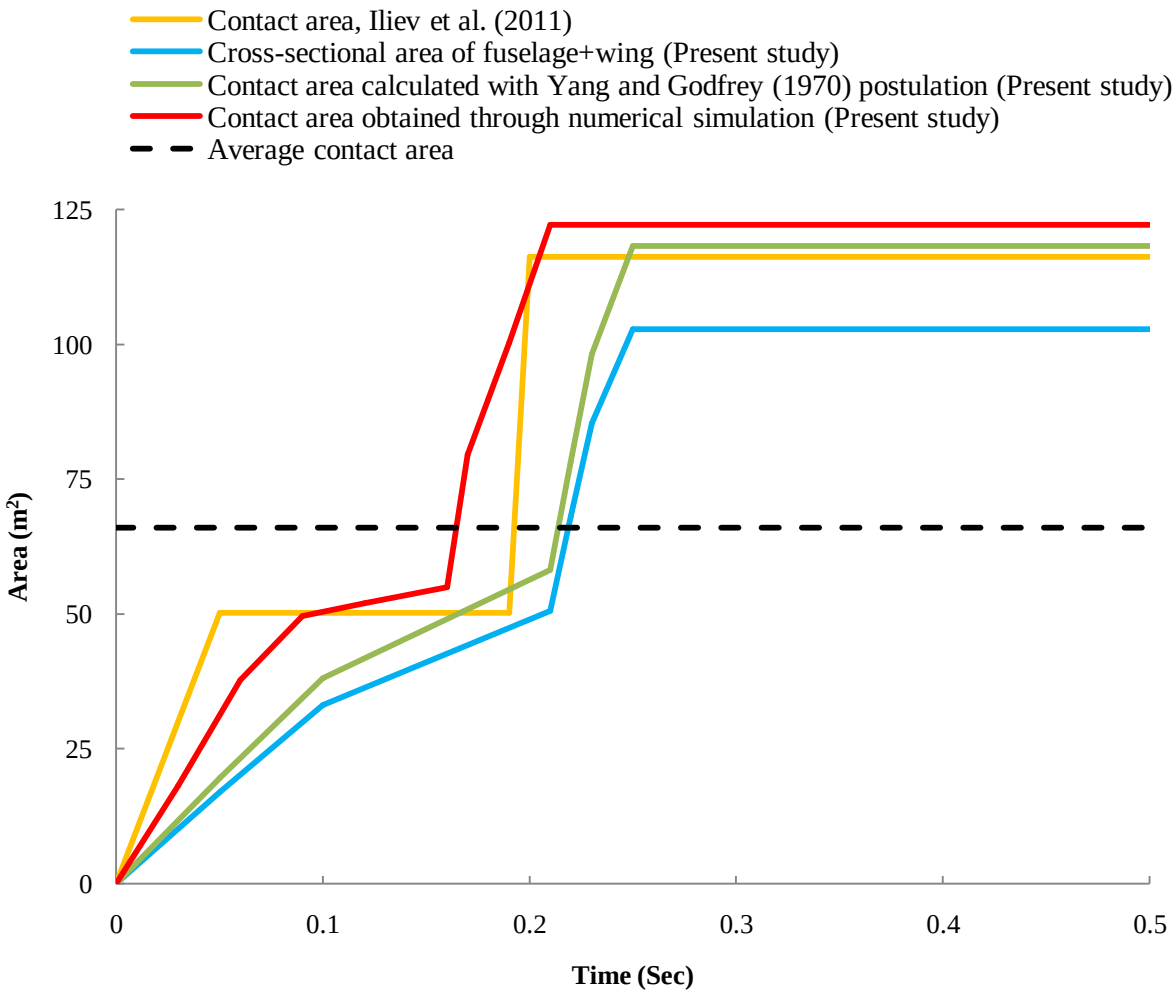

Fig. 5.18 Area of contact for Boeing 747-400 aircraft obtained through different methods

5.4 RESPONSE OF CONTAINMENT

A comparative study of the response of containment has been performed adopting different loading approaches. The aircraft crash on the BWR Mark III containment has been simulated through the geometric model as well as reaction-time curve. It is important to mention that the reaction-time curve employed to seek the response of containment is the one that has been obtained against the deformable curved target (BWR containment) instead of that obtained against rigid flat or rigid curved target, see Fig. 5.14 and 5.15. It should also be noted that the resultant reaction-time curve had fluctuations in its profile due to which an average profile had been has been assumed before its application.

However, the reaction-time curve has been applied on the containment using two different approaches. In the first approach, the area of application has been considered to be the average of the total contact area indicated in Fig. 5.17 and 5.18 respectively for Boeing 707-320 and Boeing 747-400 aircraft. The respective reaction-time curve has been applied as a function of time over the average area assumed to be of circular shape.

However, the contact area shown in Fig. 5.17 and 5.18 is actually varying with respect to time. Hence, in order to seek the influence of its variation, in the second approach, the total contact area has been trifurcated in the following manner;

(i) A1: Fuselage

(ii) A2: First set of engine and corresponding portion of wings

(iii) A3: Second set of engine and corresponding portion of wings.

The shape of A1, A2 and A3 has been assumed in accordance with respective component of aircraft for which it has been designated, see Fig. 5.19(a). The reaction force of each component of aircraft has been applied on the corresponding area with respect to time.

The total sum of A1, A2 and A3 has been found to be approximately 40 m^2 and 120 m^2 for Boeing 707-320 and Boeing 747-400 aircraft respectively which in turn is equivalent to the maximum contact area shown in Fig. 5.17 and 5.18 respectively.

The corresponding reaction-time curve applicable for A1, A2 and A3 has been systematically segregated, see Fig. 5.19(b). The reaction force corresponding to the aircraft fuselage has been applied on A1 with respect to time. In order to obtain the reaction force offered by wings and engines, the reaction force of fuselage was subtracted from the total reaction force. The resultant was divided in two equal parts for obtaining the reaction offered by the first and second set of engines (and portions of wings in contact with engines). The reaction force thus obtained was applied on the corresponding area (A2 and A3) with respect to time. The reaction force corresponding to a given area became operational at its respective time.

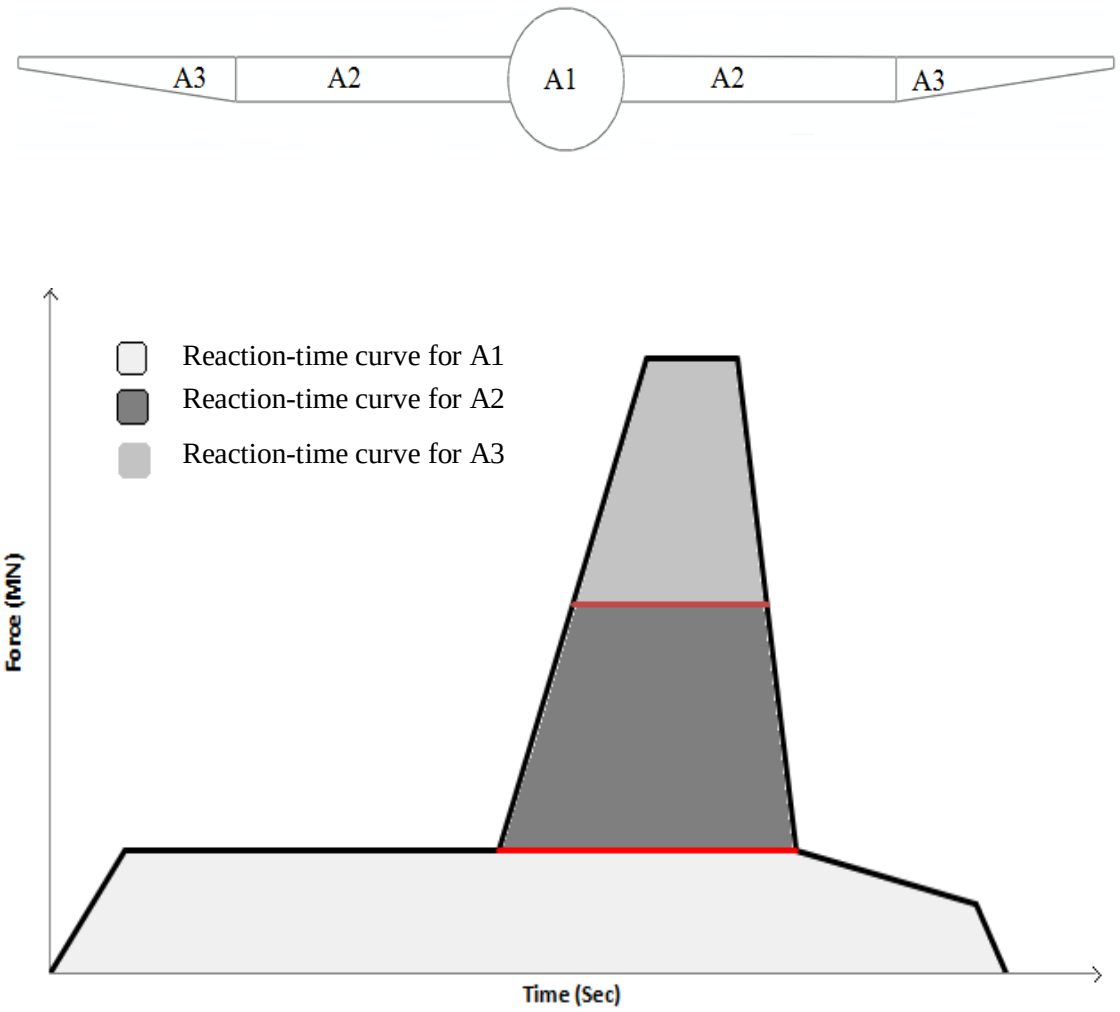

Fig. 5.19 (a) Proposed area trifurcation scheme (b) corresponding division of load

Hence, the load and the contact area both have been considered a variable of time in this approach. The present analysis though, uses the reaction-time response approach for evaluating the behavior of containment. However, it represents the actual phenomena more accurately than the average area approach discussed above. Hence, the response of the containment in the present study has been studied through three independent approaches;

(i) Average area approach for the application of reaction-time curve

(ii) Area trifurcation approach for the application of reaction-time curve

(iii) The geometric model of aircraft impacted on the containment

It should be noted that through each of the above approach the aircraft has been considered to hit the containment at its mid height, 23 m from the base. The results obtained have been compared and discussed. The deformation in the containment, at the center of the

impact location has been plotted in Fig. 5.20. The negative sign shows inward deformation while the positive sign outward deformation. Against Boeing 707-320 aircraft, a maximum displacement/deformation in the direction of loading has been found to be 65.6 mm, 22.7 mm and 23.08 mm through average area approach, area trifurcation approach and through the geometrical model of aircraft respectively, Fig. 5.20(a). Similarly, for Boeing 747-400 aircraft the maximum displacement/deformation of containment in the direction of loading has been found to be 94 mm, 39.09 mm and 36.89 mm with average area approach, area trifurcation approach and through the geometric model of aircraft respectively, Fig. 5.20(b). In general the deformation against Boeing 747-400 aircraft has been found to be higher compared to Boeing 707-320 aircraft. Further, the deformation predicted by the average area method has been found to be very high compared to area trifurcation approach and geometric model of aircraft. The area trifurcation approach and the geometrical model of aircraft resulted in almost same displacement profile as well as the resultant magnitude. It has been noticed that the displacement in the impact region increases with an increase in the loading. However, as the load is reduced the elastic recovery of the target has been found to occur due to which the final displacement is significantly reduced. The elastic recovery has been found to be very significant corresponding to the average area approach. For area trifurcation approach also the elastic recovery was noticeable. Against the impact of geometric model of aircraft however, elastic recovery was found to be insignificant.

The deformation of a node, 10 m above the center of impact has also been plotted in Fig. 5.21. The relative decrease in the value of maximum deformation can be seen at this location compared to what has been observed at the impact location. The resultant deformation through area trifurcation approach and the geometric model were again found to be in agreement. However, the average area approach has resulted very high deformations.

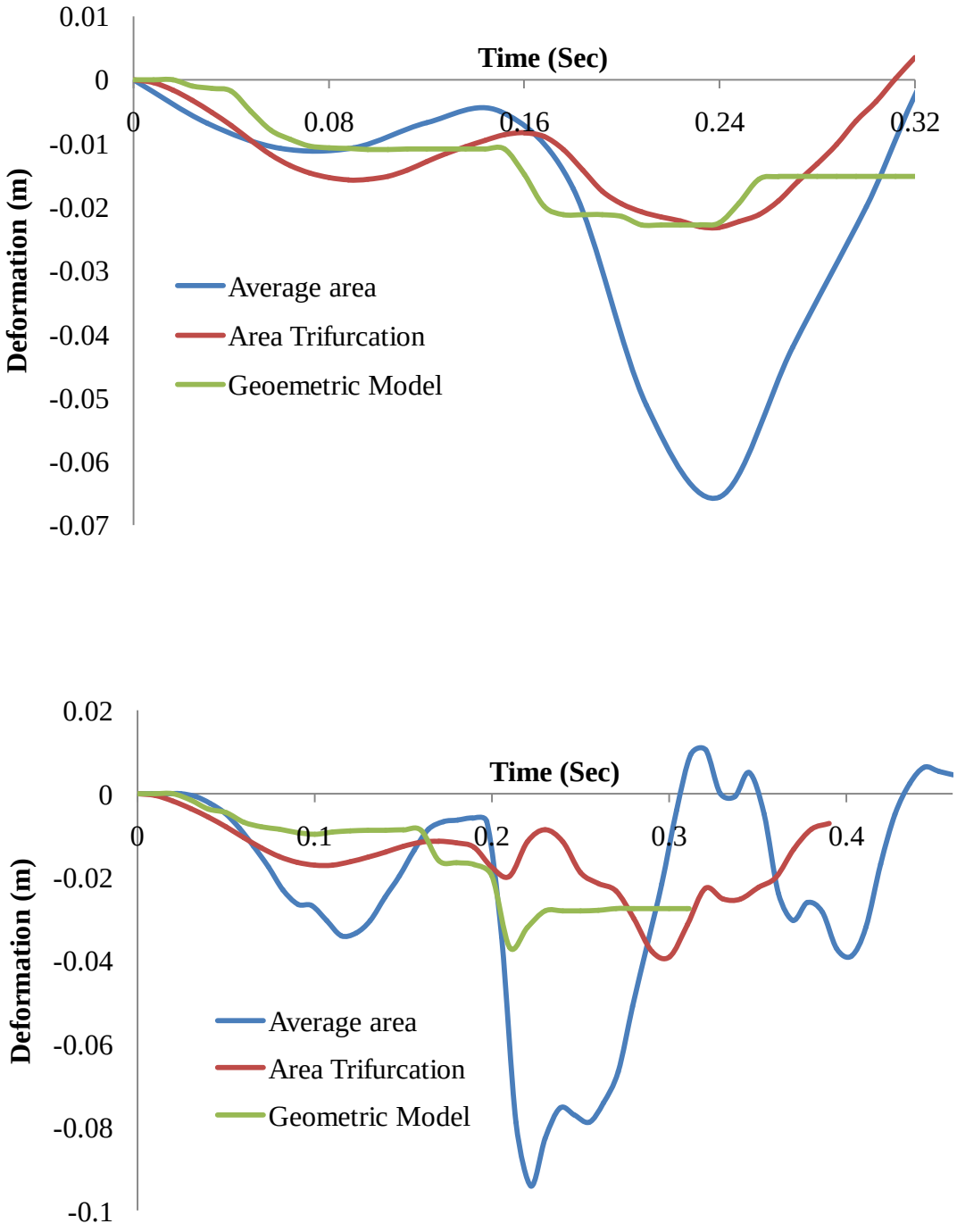

Fig. 5.20 Deformation in containment at the point of impact against aircraft (a) Boeing 707-320 (b) Boeing 747-400

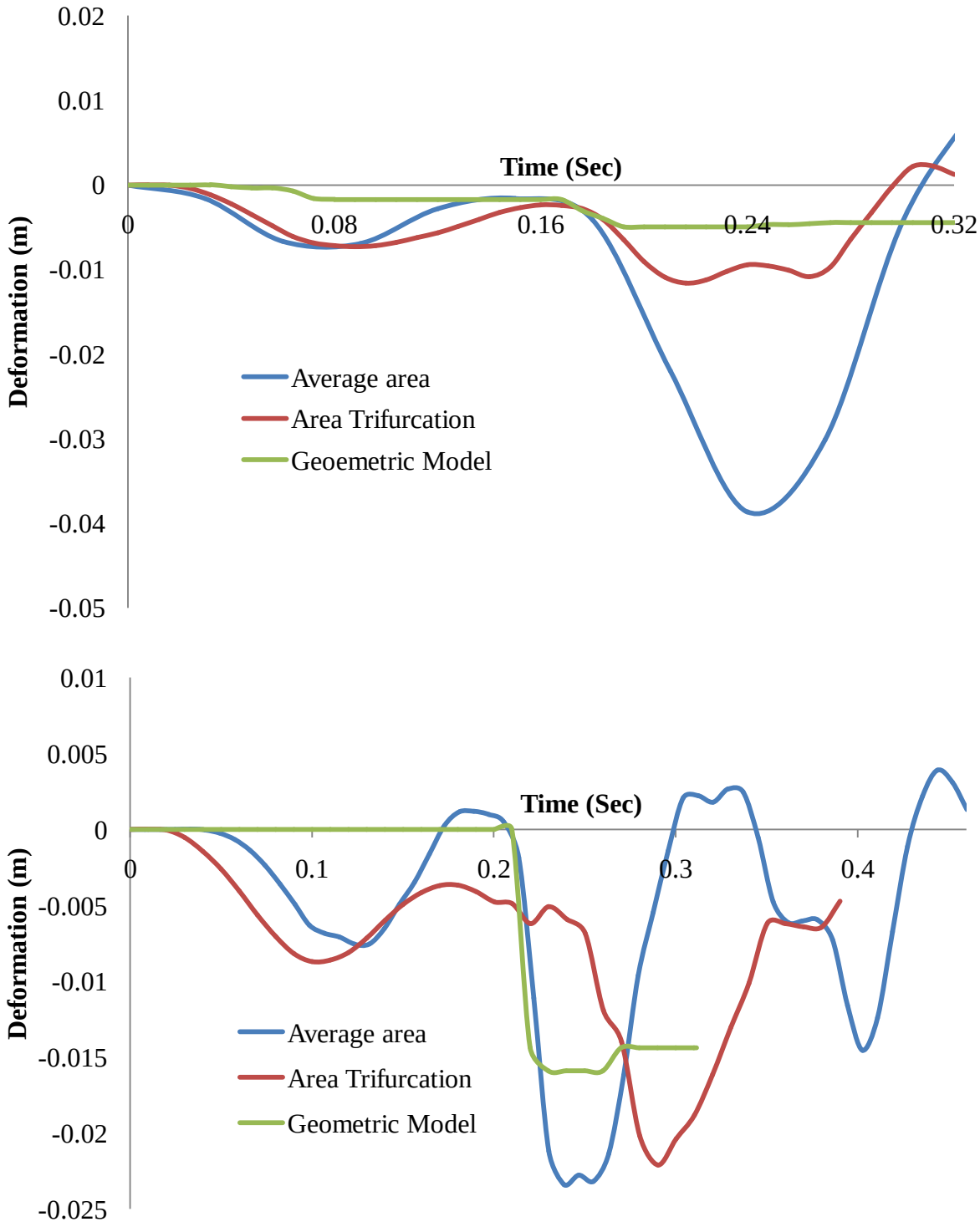

Fig. 5.21 Deformation in containment at 10 m above the point of impact against aircraft (a) Boeing 707-320 (b) Boeing 747-400

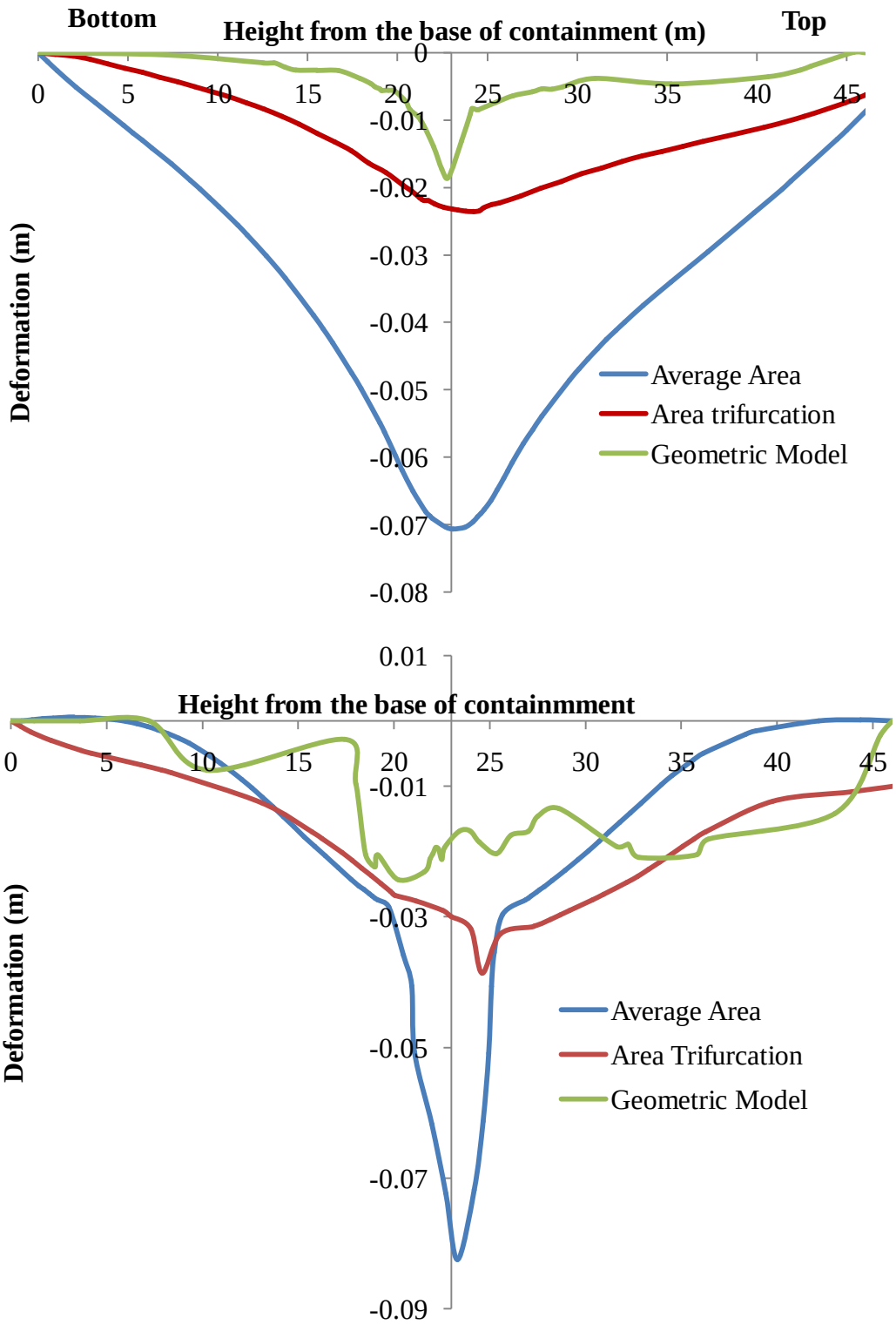

Fig. 5.22 Deformation in containment along the longitudinal axis against ; (a) Boeing 707-320 aircraft (b) Boeing 747-400 aircraft

An axis passing along the front surface of containment normal to the axis of loading is selected to observe the pattern of deformation through the height of containment. The nodal

deformation along this axis has been plotted when the containment has undergone maximum deformation, Fig. 5.22. A significantly high deformation has been noticed corresponding to average area approach. For the other two approaches however, the deformation is comparatively low as well as in agreement to each other. Boeing 747-400 aircraft predicted large deformation along the longitudinal axis also. Further, the deformation against Boeing 747-400 predicted by the average area approach was more localized and steep towards the impact zone, Fig. 5.22(b). Due to the intensive localization, the deformation predicted by average area approach diminished at some point away from the impact zone compared to other two approaches, Fig. 5.22(b).

The stress distribution in the containment along the vertical axis normal to the direction of loading has been plotted in Fig. 5.23. These stresses have been plotted at the front face at the time when the containment has undergone maximum deformation. The negative sign shows the compression and the positive tension. The normal stress opposite to the direction of loading has been plotted. The other two normal stress components will be insignificant. The region near the impact zone has been found to be under compression for Boeing 707-320 aircraft. Nominal tensile stresses have also been noticed at the periphery of the impact zone corresponding to average area and trifurcation approach. However, corresponding to geometric model, no tension was noticed. The maximum compressive stress has been found to be 2.83 MPa, 2.87 MPa and 1 MPa against average area approach, area trifurcation approach and geometric model. The compressive stresses produced by the Boeing 747-400 aircraft are lesser in magnitude due to the fact that the resultant deformations caused by this aircraft are higher. However, the tensile stresses developed away from the impact zone were higher against Boeing 747-400. The maximum tensile stress of 2.52 MPa has been noticed corresponding to average area approach.

The deformation contours in the outer set of the reinforcement are shown in Fig. 5.24 against Boeing 707-320 aircraft. The negative sign shows in the direction of loading while positive shows outward bulging. The deformations are highly localized near the impact zone. The maximum deformation has been found to be 71.38 mm, 23.60 mm and 8.17 mm corresponding to average area approach, area trifurcation approach and geometric model respectively. At the inner face reinforcement, the deformations have been found to be higher, Fig. 5.25. The maximum deformation has been found to be 74.19 mm, 23.16 mm and 10.82 mm against average area approach, area trifurcation approach and geometric model of aircraft.

Fig. 5.26 shows the contour of axial stresses in the outer reinforcement due to crash of Boeing 707-320 aircraft. These stresses have been plotted at the time when the containment has undergone maximum deformation. The positive sign shows tension, while the negative,

compression in the reinforcement. The maximum stress has been found to be 235 Mpa, 76 MPa and 20 MPa against average area approach, area trifurcation approach and geometric model respectively. For the inner set of reinforcement, the magnitude of stress was lesser compared to the outer reinforcement. The maximum stress was 108.62 MPa, 34.7 MPa and 12.5 Mpa against average area method, area trifurcation method and geometric model respectively, Fig. 5.27.

The deformation contour of the outer reinforcement has been plotted in Fig. 5.28 against Boeing 747-400 aircraft. These deformations have also been plotted at the time when the containment has experienced maximum deformation. The maximum deformation has been found to be 62.97 mm, 32.65 mm and 29.50 mm for average area approach, area trifurcation approach and geometric model respectively. The deformations of the inner reinforcement have been found to be higher for Boeing 747-400 aircraft also, Fig. 5.29. The maximum inward deformation is 70.47 mm, 32.88 mm and 38.32 mm for average area, area trifurcation and geometric model scheme respectively.

For Boeing 747-400 aircraft the axial stress variation in the outer set of reinforcement is shown in Fig. 5.30. The maximum stress has been found to be 142 MPa, 100 MPa and 104 MPa for average area approach, area trifurcation approach and the geometric model respectively. In the inner set of reinforcement stresses are quite low as compared the outer set of reinforcement, Fig. 5.31.

It may be concluded from the above results that stresses developed in the concrete as well reinforcement are within the permissible limit. The average area approach predicted very high deformations in the containment. However, the deformations predicted by the area trifurcation approach and the geometric model of the aircraft are comparatively low and in close agreement. The trifurcation approach is therefore more accurate and realistic and hence can be employed to evaluate the response of the containment.

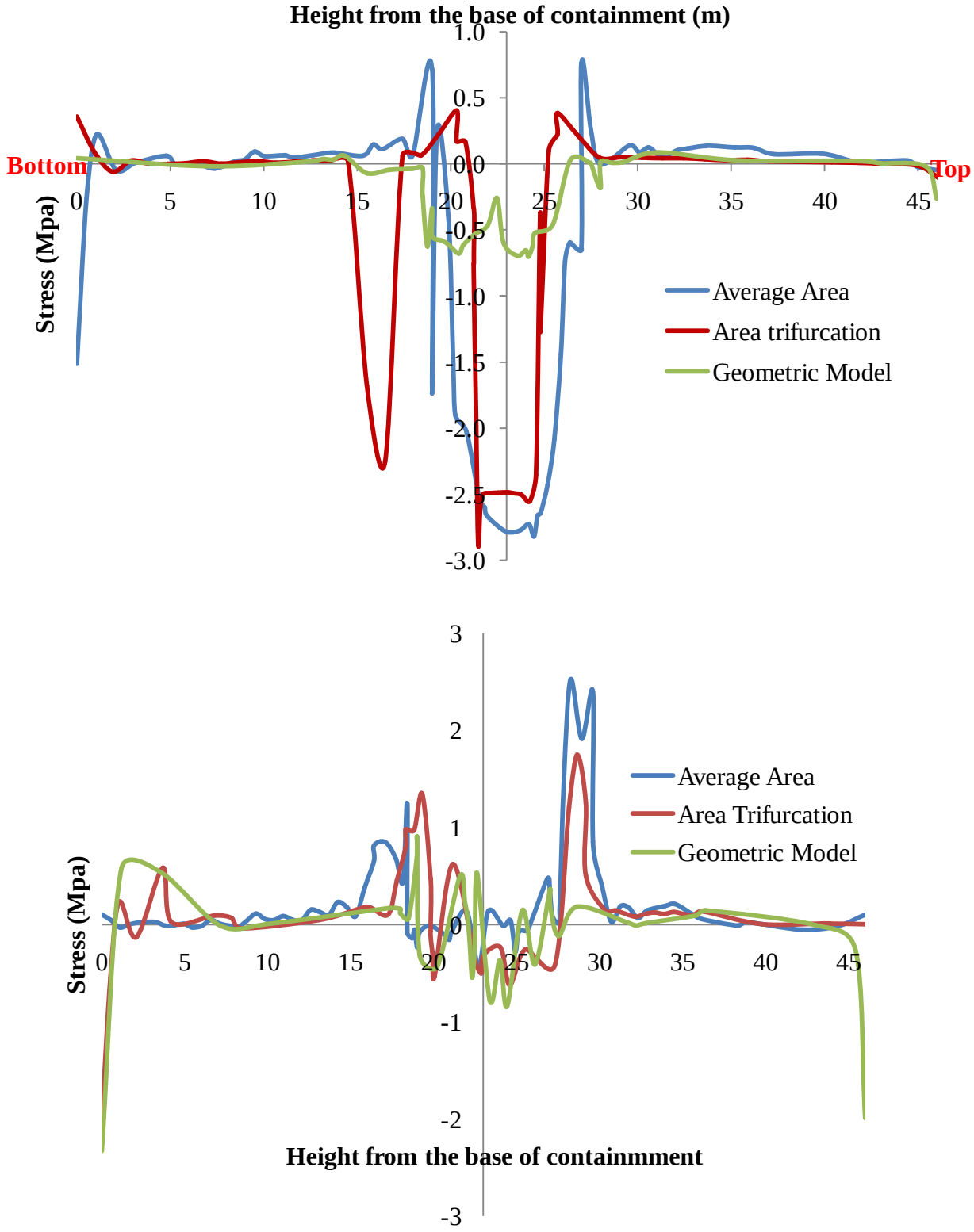

Fig. 5.23 Stress variation in containment along the longitudinal axis against;
(a) Boeing 707-320 aircraft (b) aircraft Boeing 747-400

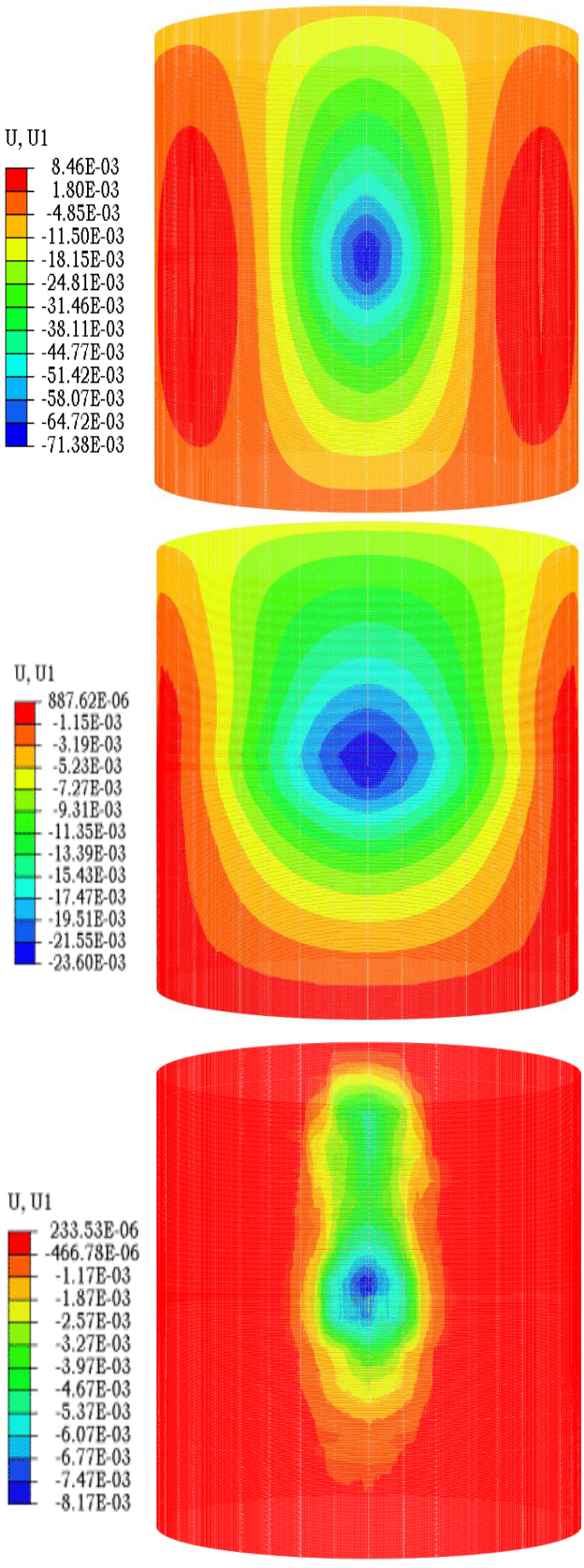

Fig. 5.24 Deformation contour of outer reinforcement against Boeing 707-320 aircraft (a) Average area (b) Area trifurcation (c) Geometric model

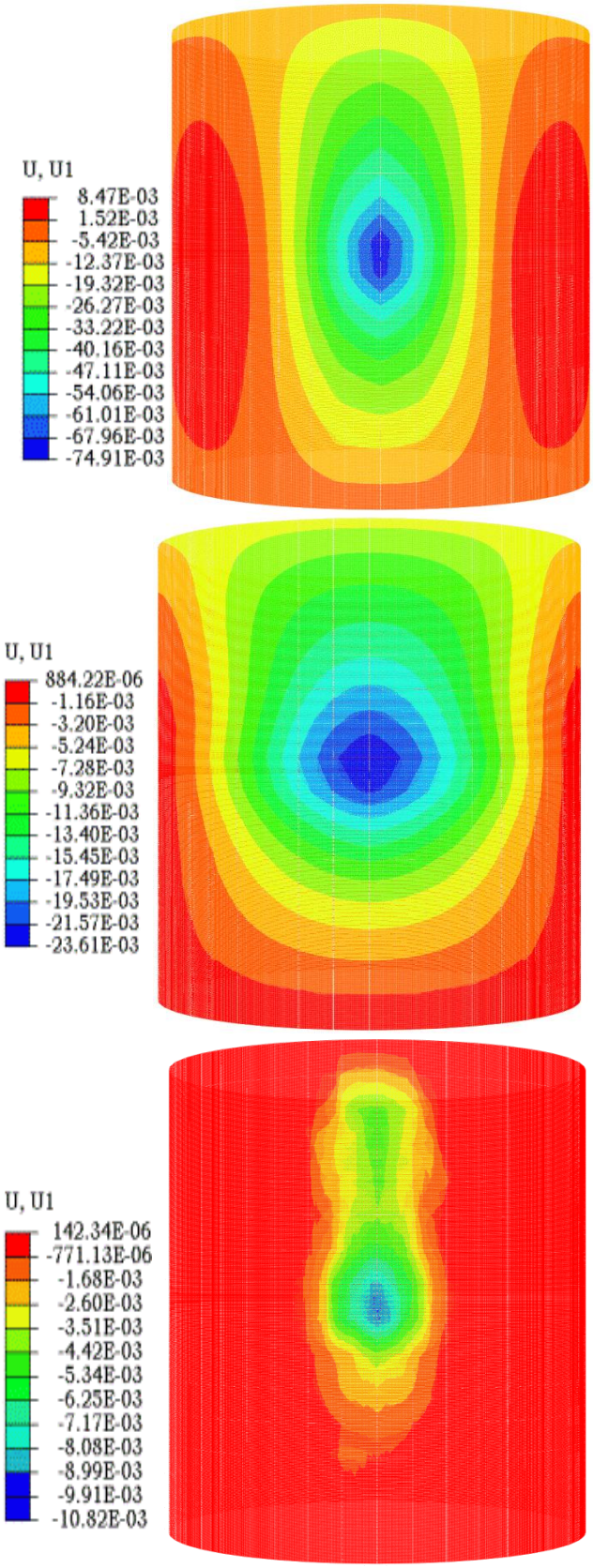

Fig. 5.25 Deformation contour of inner reinforcement against Boeing 707-320 aircraft
(a) Average area (b) Area trifurcation (c) Geometric model

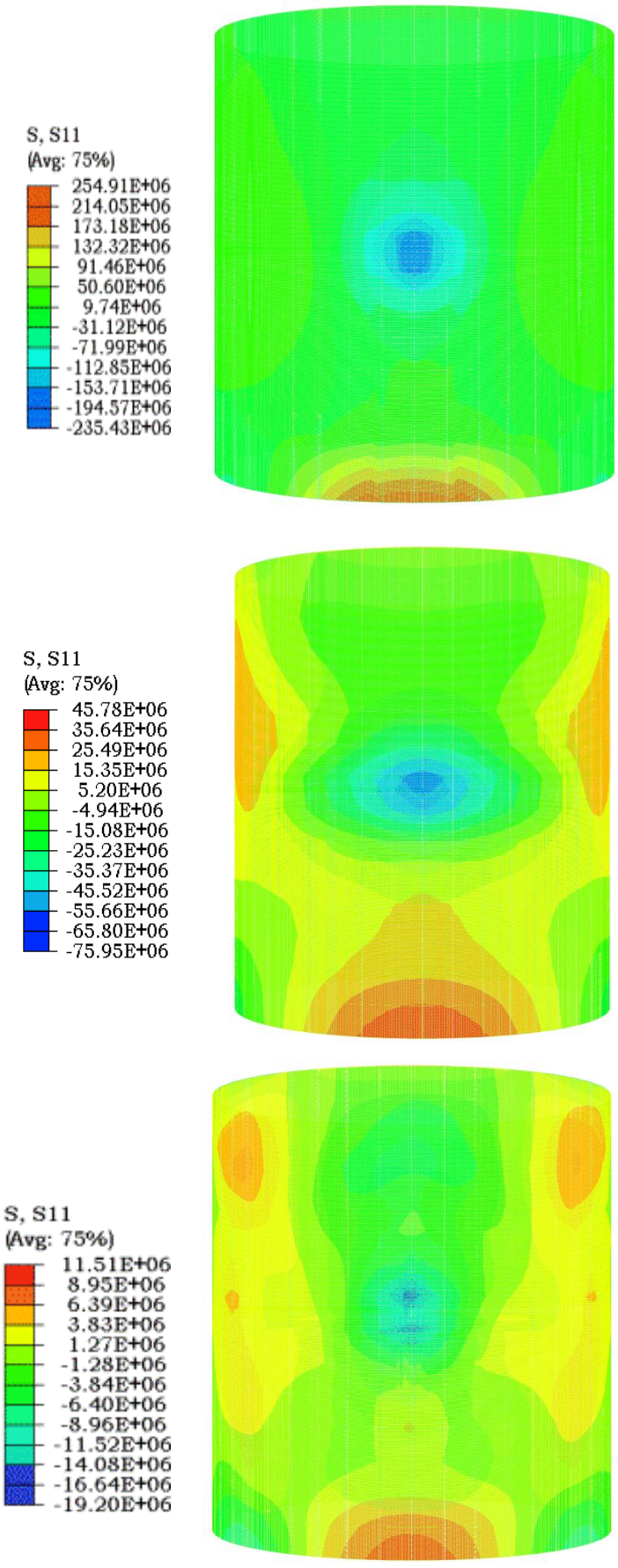

Fig. 5.26 Axial stresses in outer reinforcement against Boeing 707-320 aircraft (a) Average area (b) Area trifurcation (c) Geometric model

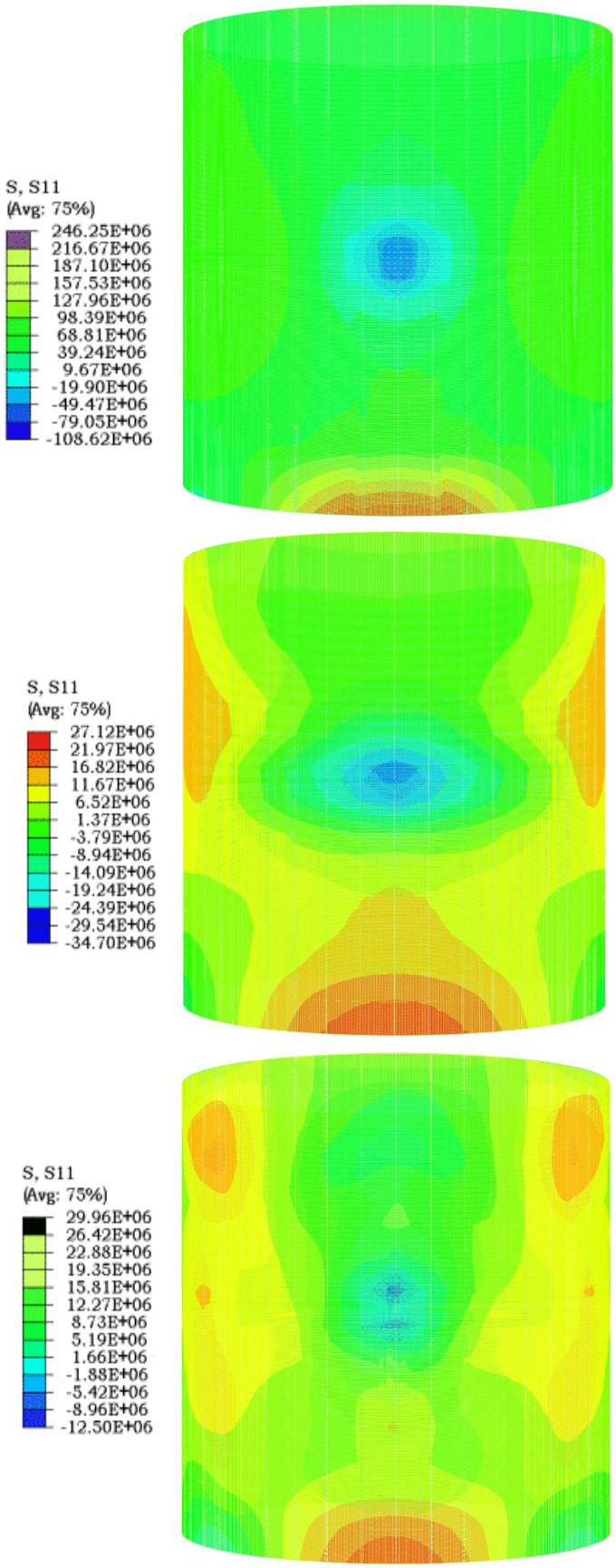

Fig. 5.27 Axial stresses in inner reinforcement against Boeing 707-320 aircraft (a) Average area (b) Area trifurcation (c) Geometric model

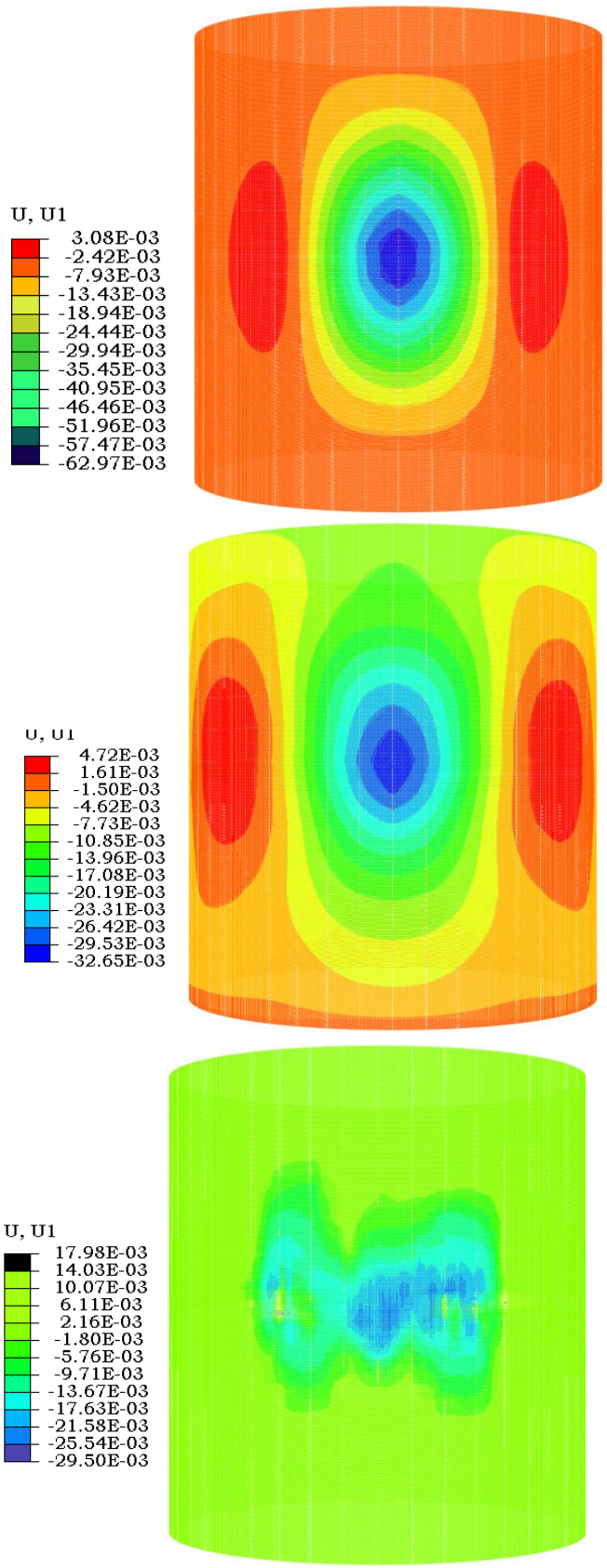

Fig. 5.28 Deformation contour of outer reinforcement against Boeing 747-400 aircraft (a) Average area (b) Area trifurcation (c) Geometric model

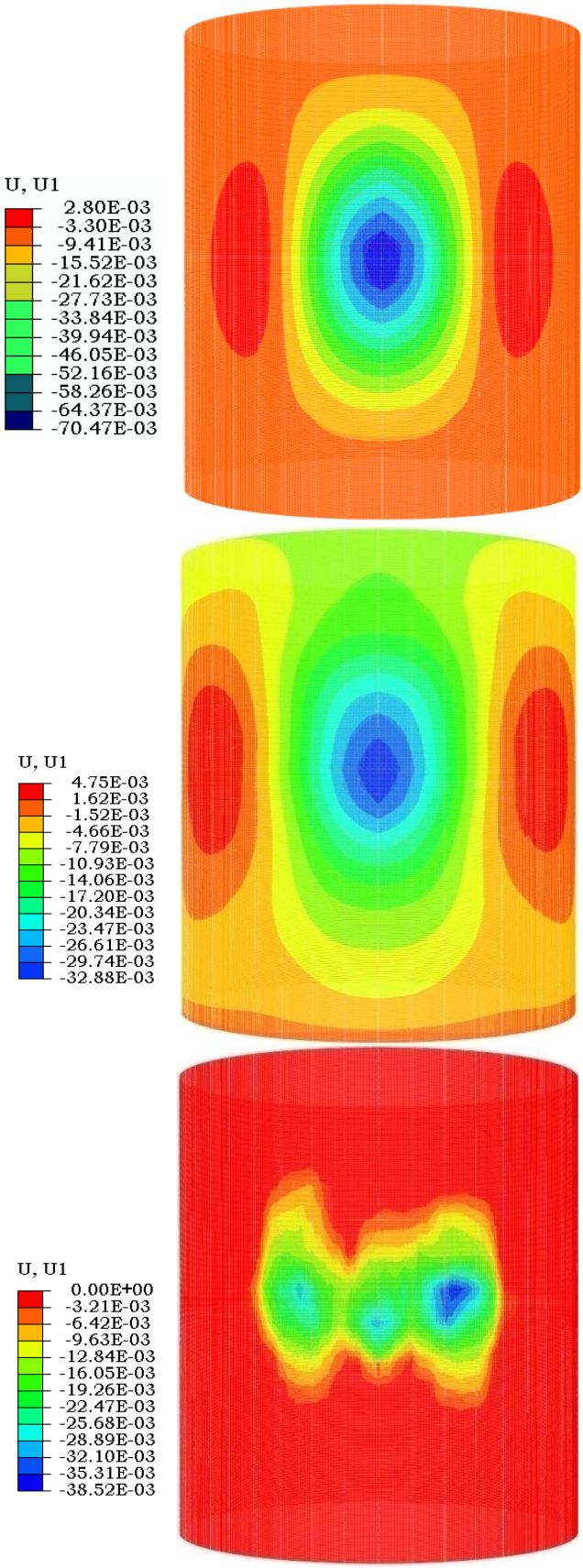

Fig. 5.29 Deformation contour of inner reinforcement against Boeing 747-400 aircraft (a) Average area (b) Area trifurcation (c) Geometric model

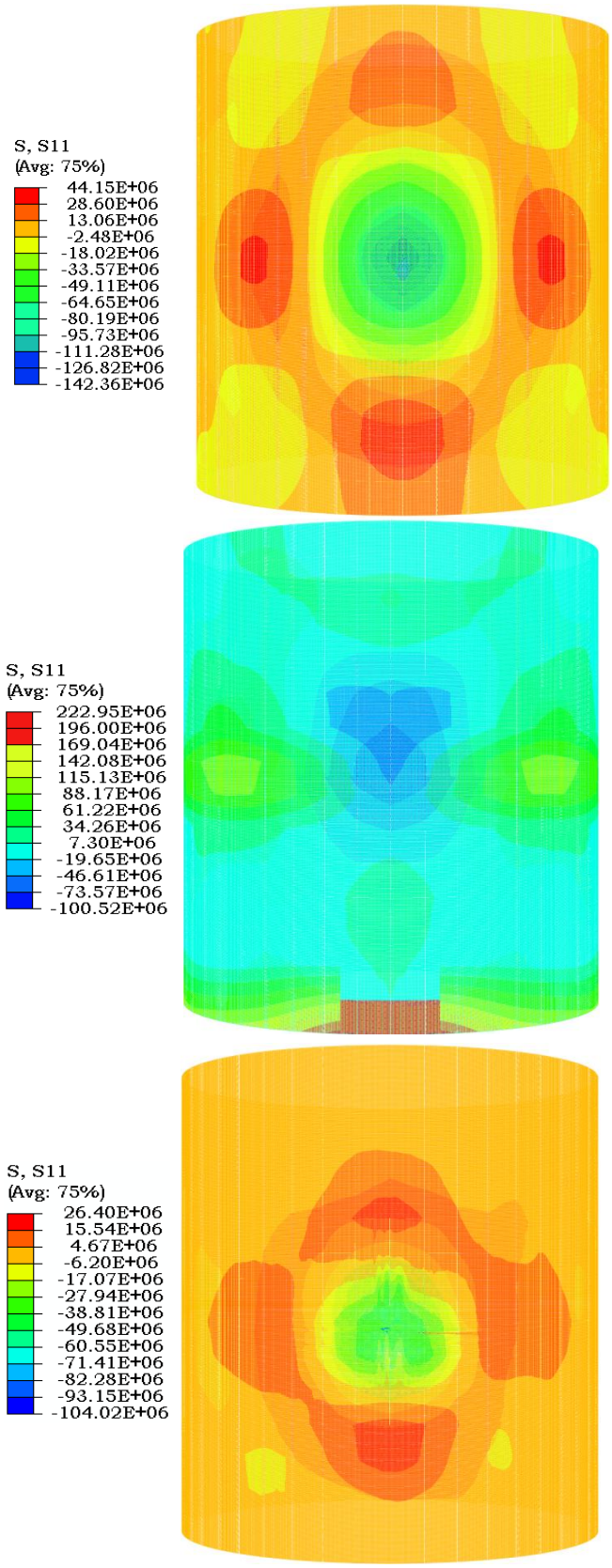

Fig. 5.30 Principal stress in outer reinforcement against Boeing 747-400 aircraft (a) Average area (b) Area trifurcation (c) Geometric model

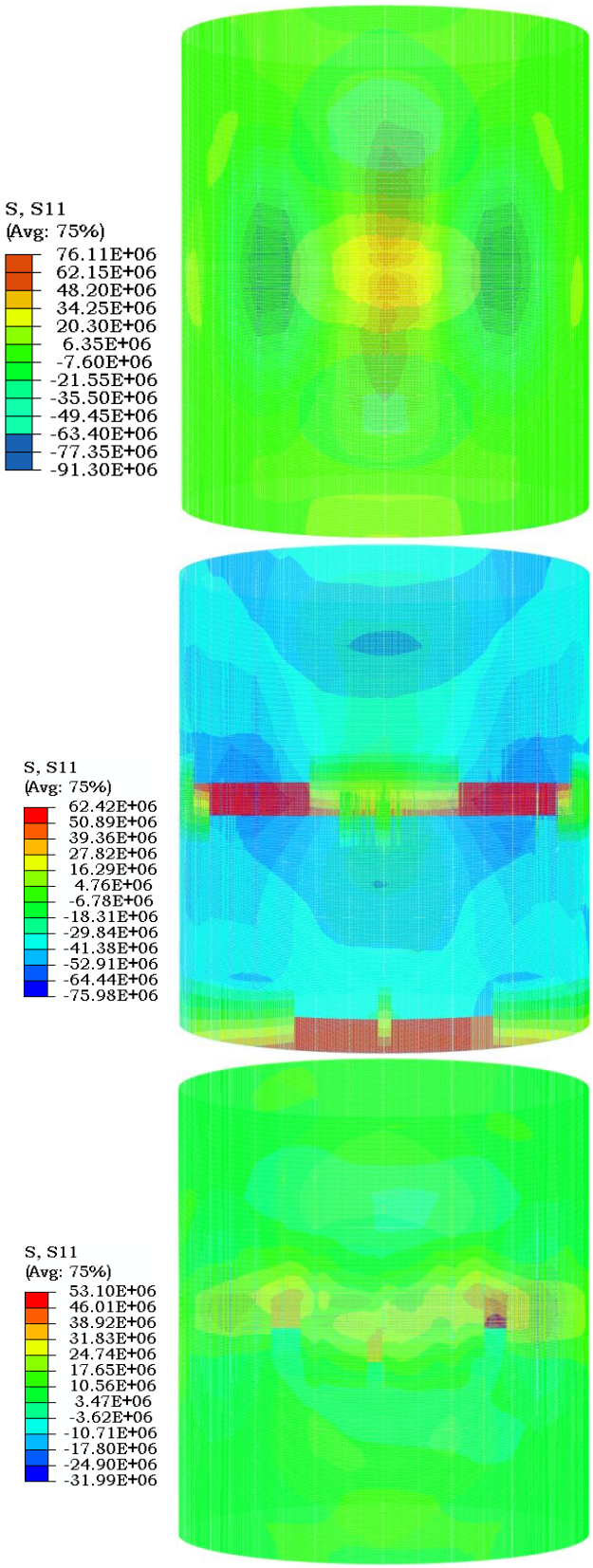

Fig. 5.31 Principal stress in inner reinforcement against Boeing 747-400 aircraft (a)Average area (b) Area trifurcation (c) Geometric model

5.5 CONCLUDING REMARKS

In the present chapter, the effect of target curvature and deformability has been evaluated on the reaction-time curve. The geometric model of aircrafts Boeing 707-320 and Boeing 747-400 were impacted on the rigid and deformable targets of varying curvature (D_{inf}, D100 and D42). The increase in target curvature has been found to delay the peak impact force and reduce its magnitude. The peak of the reaction-time curve obtained against deformable target was lower than that obtained against rigid target of same diameter.

The variation in the contact area with respect to time impact has been obtained analytically as well as numerically. Further, the obtained contact area has been trifurcated corresponding to fuselage, first set of engines and second set of engines, and the loading has been allocated corresponding to time and location of these components. The discretization of containment for different loading methodologies has been done accordingly. The response of containment against the geometric model of aircraft and the reaction-time curve approach with area trifurcation scheme has been found to be in close agreement. This behavior has been observed for both the aircrafts employed in this study i.e., Boeing 707-320 and Boeing 747-400.

Chapter 6

BEHAVIOUR OF NUCLEAR CONTAINMENT UNDER CRASH INDUCED FIRE

6.1 GENERAL

As of now the fire is not considered a design parameter for the nuclear containment structure. Hence, the assessment of fire resistance has not been established yet for nuclear safety related structures. As such the temperature limits have been well established for the normal operation and the shutdown conditions during a test. However, the most sever temperature in case of an internal accident such as loss of coolant and main line break (175 ^{o}C) is significantly lesser than the fire spread due to an aircraft crash. According to Nuclear Energy Institute (2009) guideline both external and internal fires may be erupted as a result of an aircraft crash over a containment structure. The response of the containment structure exposed to the external fire due to an aircraft crash will depends upon the size, velocity and fuel capacity of aircraft as well as the strike location and weather conditions.

Although the fire spread in a containment structure due to aircraft crash has been studied earlier (Contri et al., 2005; Jeon et al., 2005 & 2012) however, a coupled analysis of aircraft crash and the induced fire effect has not been dealt in the literature. The crash induced fire will be ignited as a result of the breach of the fuel tank as soon as the wings come in contact. Therefore, in order to obtain a more realistic response of containment for the crash induced fire the effect of impact loading must be considered. In the present study therefore initially the Boeing 707-320 and Boeing 747-400 aircrafts have been considered to hit the containment at the mid height of the cylindrical wall (23 m from the base) and the fire has been assumed to break out as soon as the wings come in contact. The impact analysis has been carried out using the reaction-time response approach discussed in the previous chapter. The deformed state of the containment obtained through the impact analysis has been considered as the initial state for the thermal stress analysis. Before performing the thermal stress analysis however, the heat transfer analysis has been carried out in order to obtain the nodal temperature variation with respect to time in the containment structure. It should be noted however, that the heat transfer analysis is not supported by the ABAQUS/Explicit. Therefore the impact analysis performed in the previous chapter was repeated using the ABAQUS/Implicit. Thereafter the heat transfer analysis and thermal stress analysis was carried out using ABAQUS/Implicit, see Fig. 6.1(a)

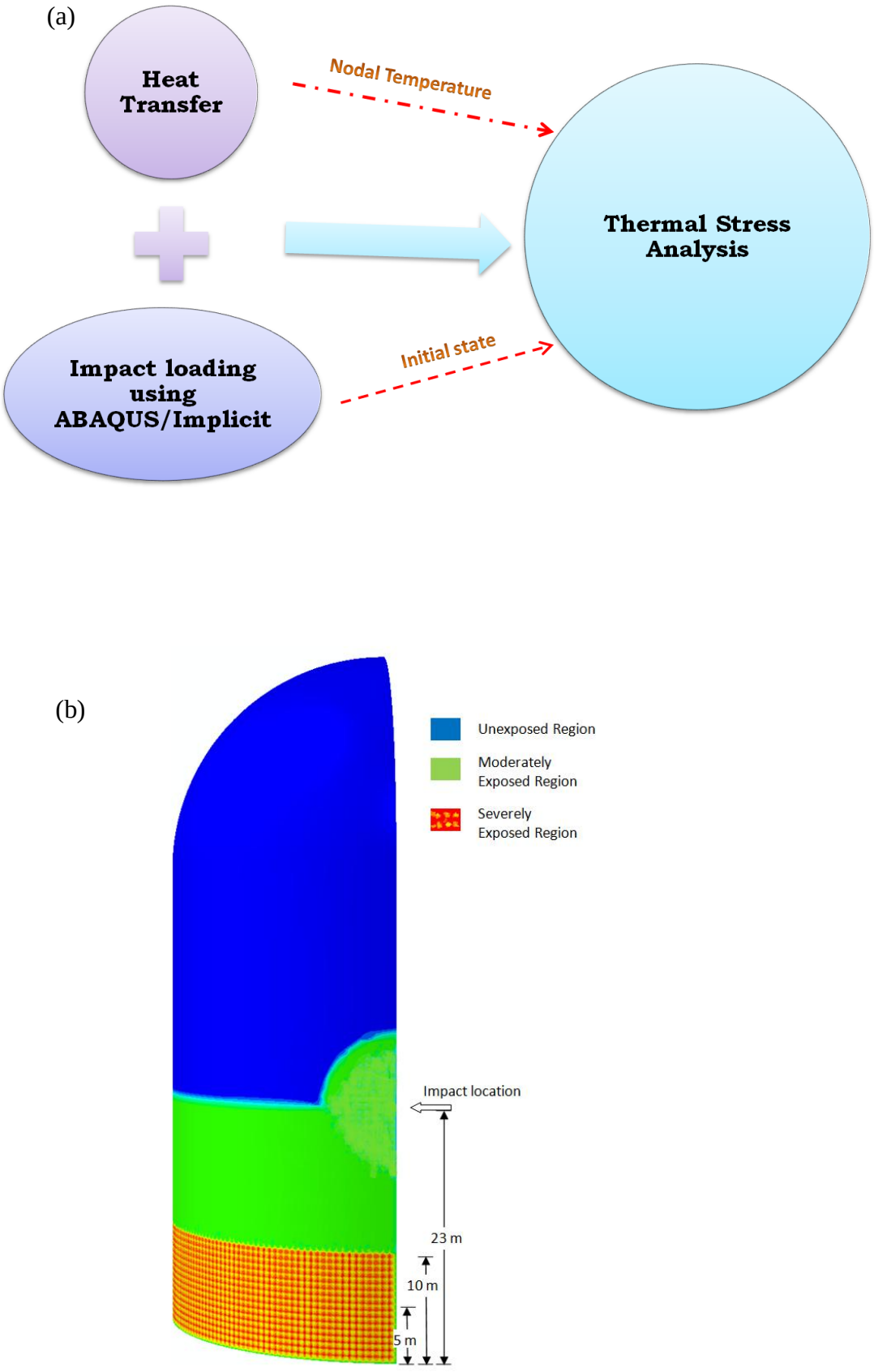

Fig. 6.1 (a) Analysis procedure (b) Containment surface subjected to varying intensity of fire exposure

6.2 HEAT TRANSFER ANALYSIS

The external surface of the containment structure has been categorized based on the intensity of heat exposure. The aircraft fuel scattered on the containment will flow down immediately after the impact. Hence, the impact region will be exposed to intensive fire not more than a few minutes. Therefore the impact location has been considered to be less important in terms of aircraft induced fire analysis, Fig. 6.1(b). On the other hand, the fuel flew down through the wall of the containment will accumulate at the base and result severe inflammation and fire pool effect up to 10 m height. Hence, the wall of the containment up to 10 m height from the base has been assumed to have severe exposure, Fig. 6.1(b).

The intensity and time duration of the fire is another important factor affecting the response of the containment. The ignition of the aircraft fuel (jet fuel) is highly rapid such that the resultant fire immediately attains the peak temperature. The fire curves of Boeing 707-320 and Boeing 747-400 aircraft are shown in Fig. 6.2. The maximum temperature in the jet fuel and hydrocarbon fire is known to be as high as 1300°C in an enclosed space for example inside a tunnel (Promat Tunnel, 2011). However, in open space the maximum temperature will not increase beyond 1100°C due to dissipation of heat. Hence, in the present study the increase in the fire temperature has been assumed to be up to 1100 ºC while the ambient temperature considered 20ºC.

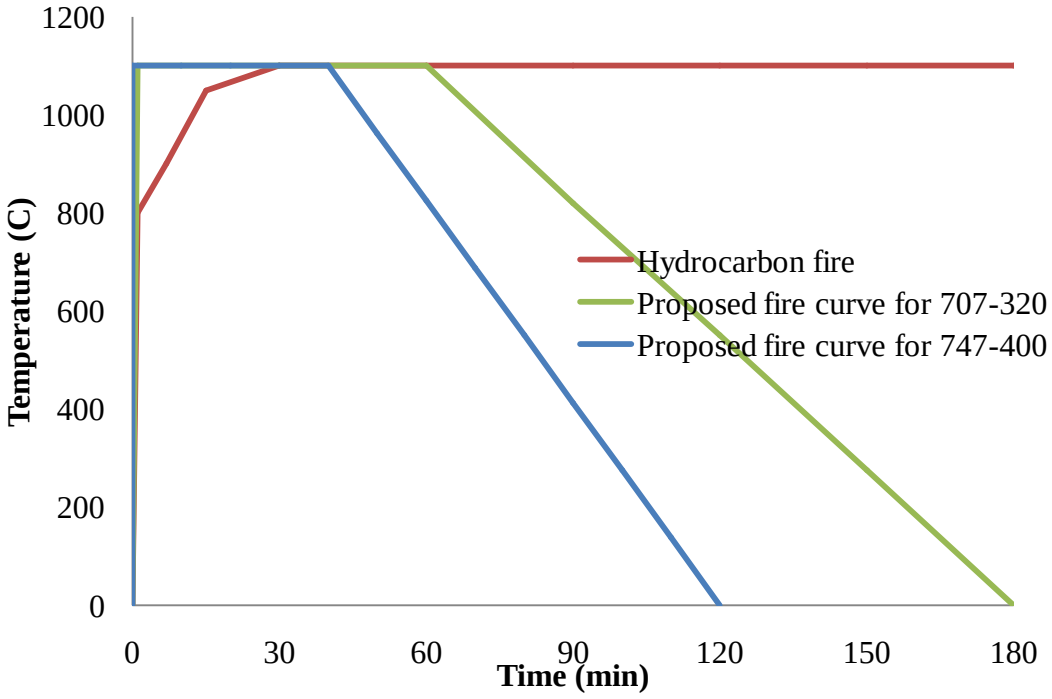

Fig. 6.2 Proposed fire curves

As such the time duration of the induced fire will be dependent up on the pool depth of the jet fuel accumulated at base of the containment. The pool depth on the other hand will be dependent on the fuel capacity of the given aircraft. Generally, irrelevant to the pool depth, 3-4 hours duration may be considered sufficient to start the fire fighting action. Hence, this time duration is often referred to as fire endurance time required for important structures (CES 2002, NRC 2003). The fuel carrying capacity of Boeing 707-320 and Boeing 747-400 is 61000 kg and 164000 kg respectively. For Boeing 767 aircraft, which carries approximately 90,000 kg fuel, Jeon et al., (2012) assumed fire duration of 3 hours. In the present study therefore, the fire duration of 2 and 3 hours respectively has been assumed for Boeing 707-320 and Boeing 747-400 aircrafts, see Fig. 6.2. For simulating the fire at impact region however, these curves have been modified by lowering the fire intensity to 700ºC and reducing the time duration to 15 minutes.

6.2.1 Heat Transfer Analysis for BOEING 707-320 Aircraft

The heat transfer analysis has been performed on the BWR containment for the proposed fire curve of Boeing 707-320 aircraft. In order to plot the thermal gradient across the containment thickness, the path A, B and C have been identified as shown in Fig. 6.3 at 5 m, 10 m and 23 m height from the base respectively. The thermal gradient at "path A" and "path B" has been found to be almost same at different time duration, Fig. 6.4 (a) and (b). However, the magnitude of the nodal temperature at "path A" is slightly higher than that of "path B". Both of these points were lying under severe fire zone, however, the vicinity of moderate fire zone may be the reason of the slightly reduced magnitude at "path B". Moreover, at "path C" the maximum temperature has been found to be very low, 43°C, as a result of the decrease in fire intensity as well as the time duration. It can be noticed from Fig. 6.4 (a) and (b) that after 1 hour time duration the temperature at the exposed face has been found to reduce. In the inside elements however, the temperature has been found to further increase, see the curve corresponding to 2 hours time duration. Similar trend can also be noticed in Fig. 6.4(c), however, in this case the temperature started decreasing just after 30 minutes.

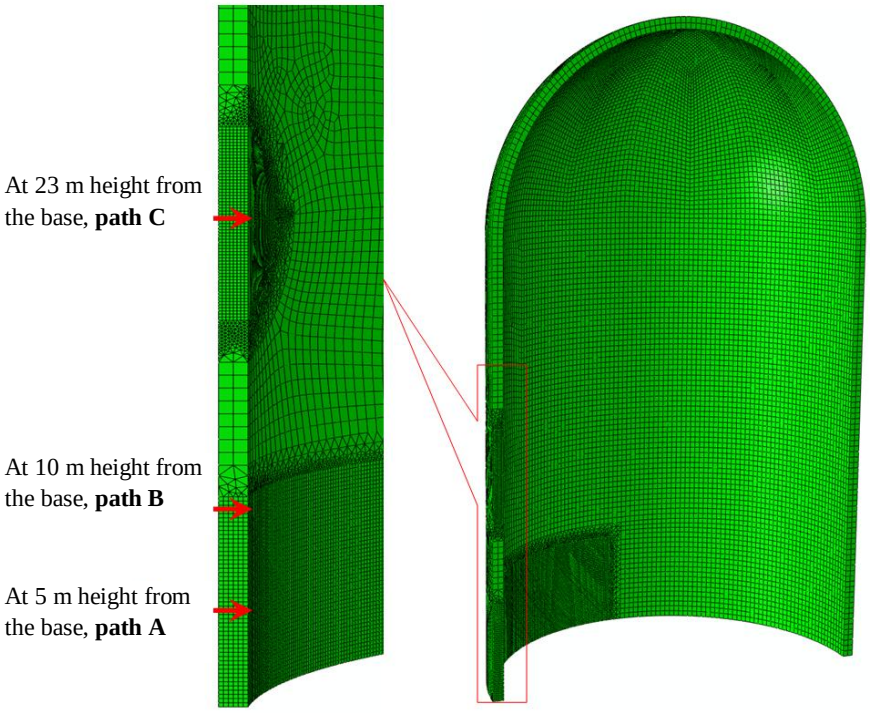

Fig. 6.3 Locations identified for plotting the temperature gradient across the thickness

The thermal profile of the containment, as well as outer and inner reinforcement due to the crash induced fire of aircraft Boeing 707-320 has been plotted at different time intervals in Figs. 6.5 - 6.8. The maximum temperature after 25 sec. was found to be 101ºC, and 48.5ºC in concrete and outer reinforcement respectively, see Figs. 6.5 (a) and (b) respectively. However, no temperature change has been noticed in the inner reinforcement, see Fig. 6.5 (c). After 103 seconds, the maximum temperature in concrete and in outer reinforcement reached 300ºC and 126 ºC respectively, see Figs. 6.6(a) and (b) respectively. Moreover, the temperature in the inner reinforcement increased to 21˚C, see Fig. 6.6(c). The maximum temperature in the concrete reached 1094.24˚C after 1850 seconds and thereafter it started decreasing, Fig. 6.7(a). In the outer set of reinforcement the maximum temperature was found to be 938.70˚C at 2880 sec. and then it decreased, Fig. 6.7(b). Similarly, in the inner set of reinforcement the temperature reach a maximum 31.58˚C at 3240 sec. and subsequently it decreased, Fig. 6.7(c). It can be noticed here that even after the decrement of temperature at the exposed face, the through thickness temperature is continuously increasing. It can also be noticed that the peak temperature is highly localised in the severely exposed region in concrete as well in reinforcement. At the end of 2 hours the residual maximum temperature noted in concrete, outer reinforcement and inner reinforcement was

676°C, 674°C and 28°C respectively, Fig. 6.8. However, the fall in the peak temperature was more significant in the concrete as compared to reinforcement.

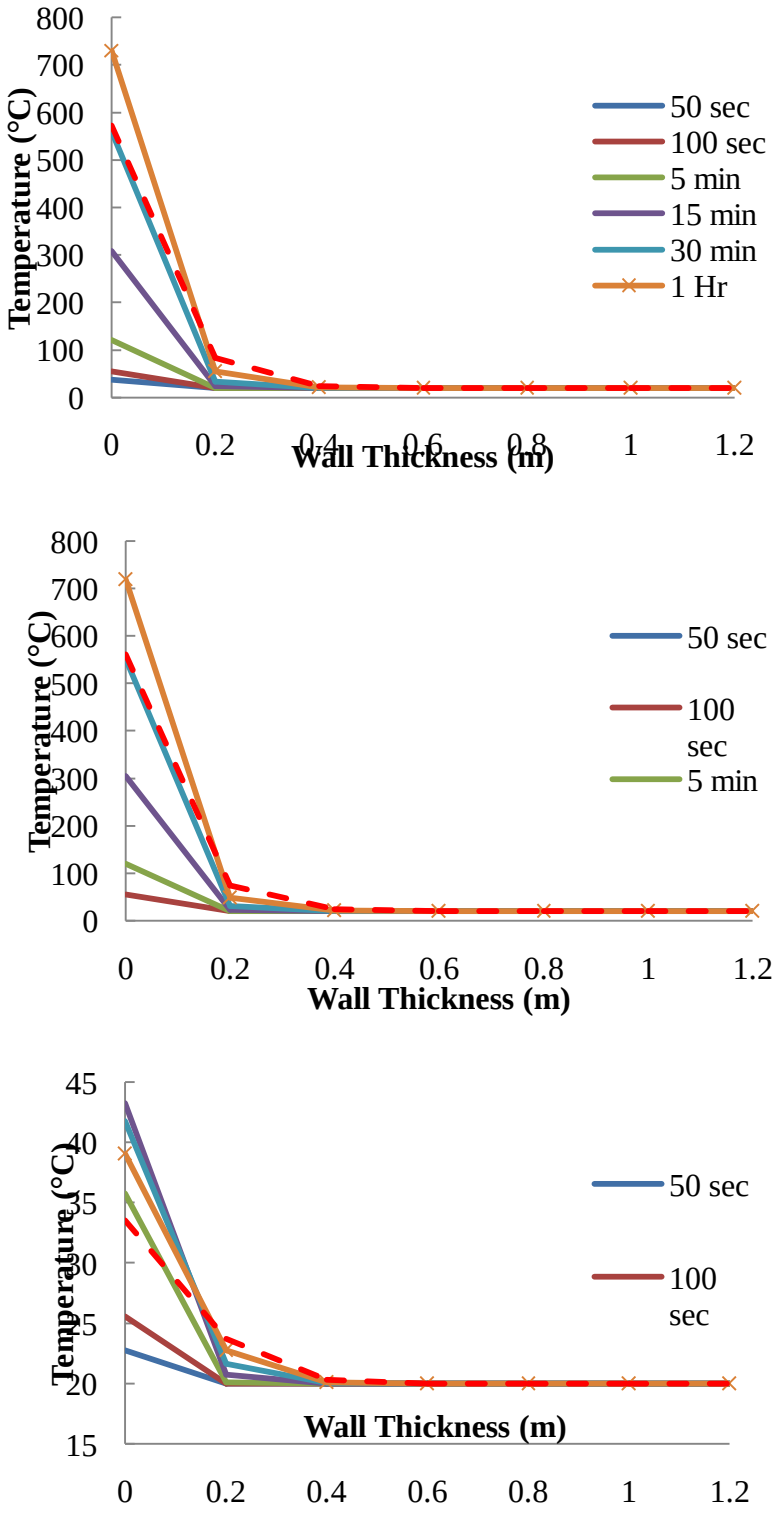

Fig. 6.4 Temperature gradient in concrete across the thickness of containment for Boeing 707-320 aircraft (a) at path A (b) at path B (c) at path C

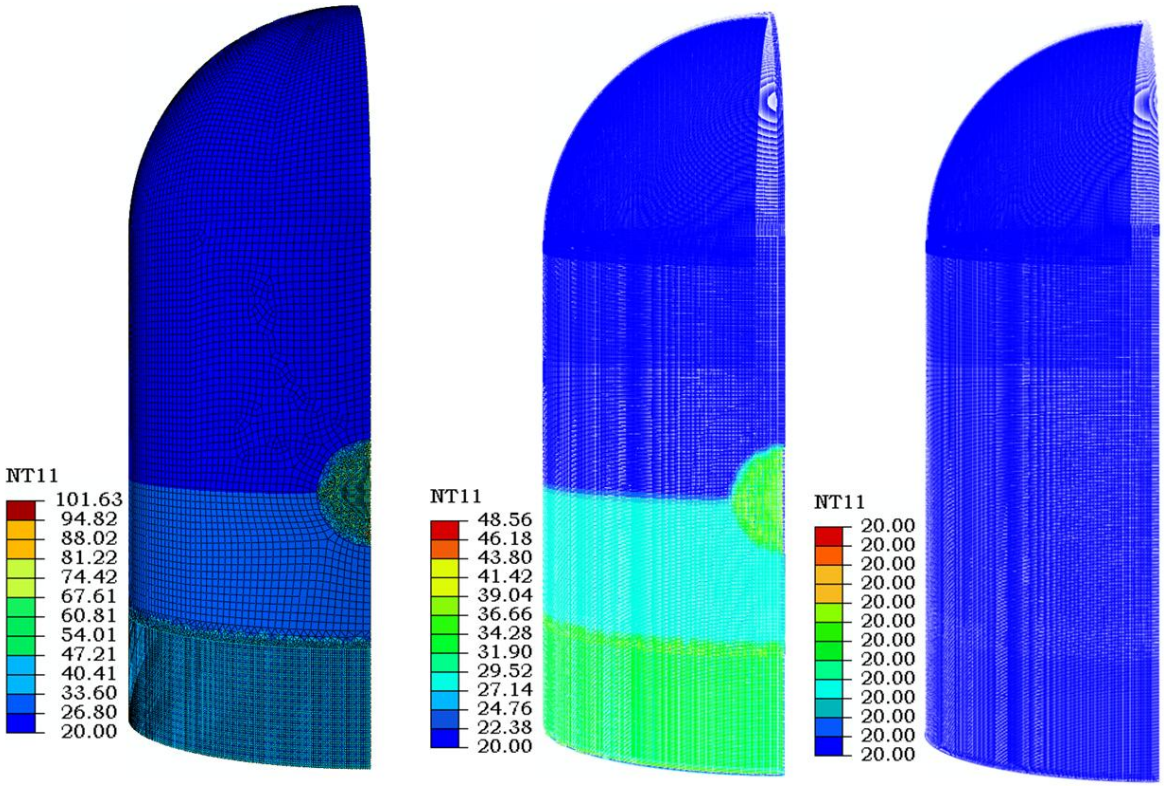

Fig. 6.5 Thermal profile at time t = 25 sec. against Boeing 707-320 aircraft (a) concrete (b) outer reinforcement (c) inner reinforcement

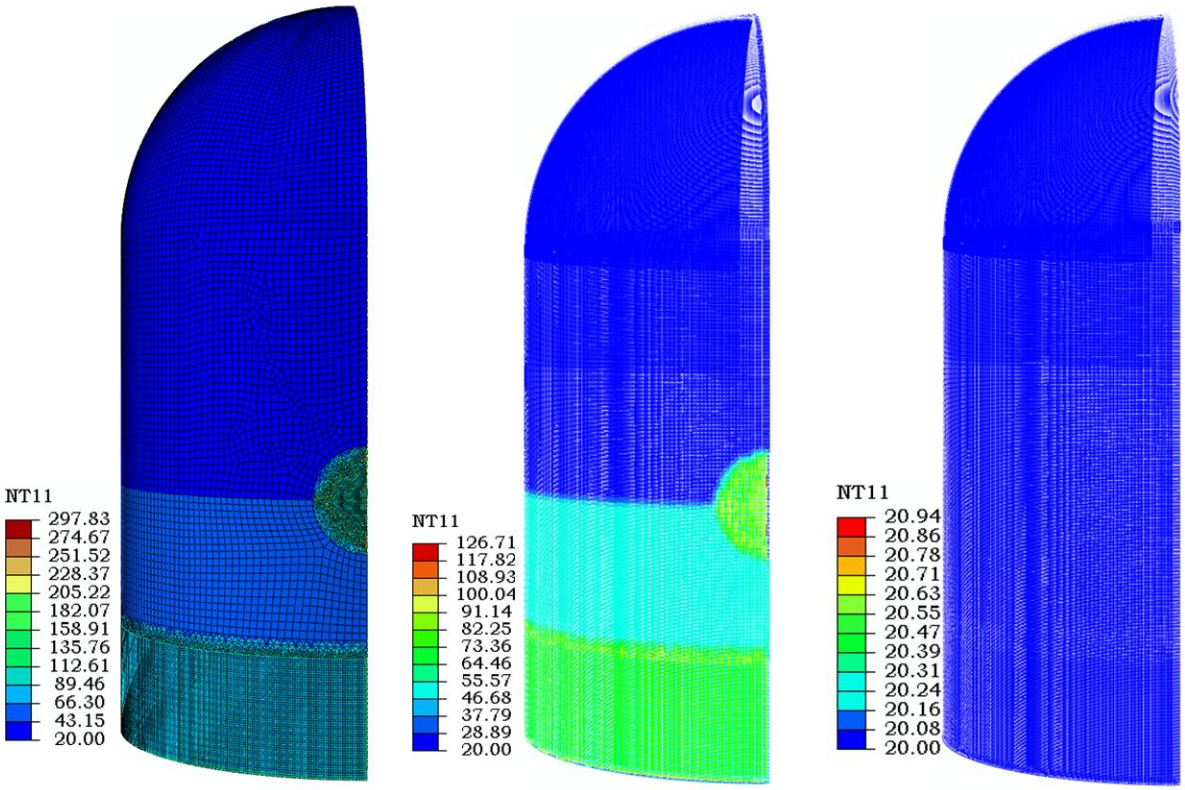

Fig. 6.6 Thermal profile at time t=103 sec against Boeing 707-320 aircraft (a) concrete (b) outer reinforcement (c) inner reinforcement

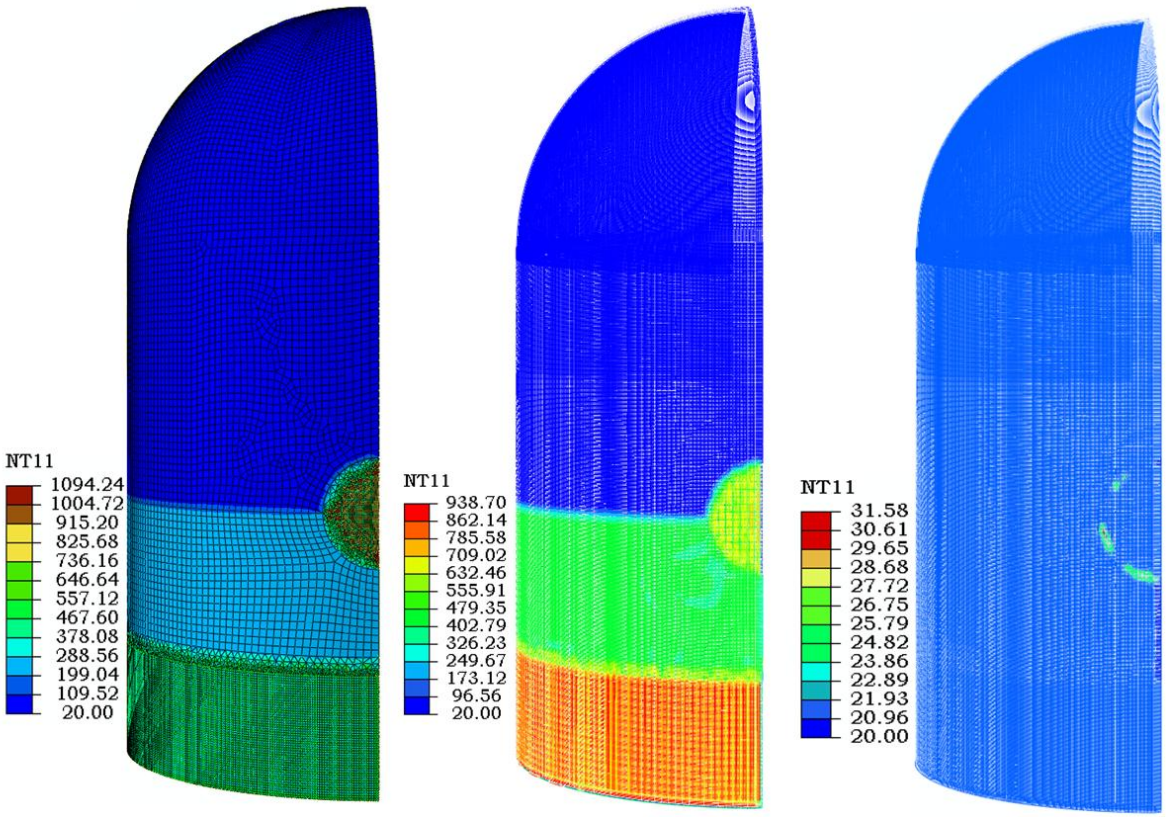

Fig. 6.7 Thermal profile with maximum nodal temperature against Boeing 707-320 aircraft (a) concrete (time t = 1850 sec.), (b) outer reinforcement (t = 2880 sec.) and (c) inner reinforcement (time t = 3240 sec.)

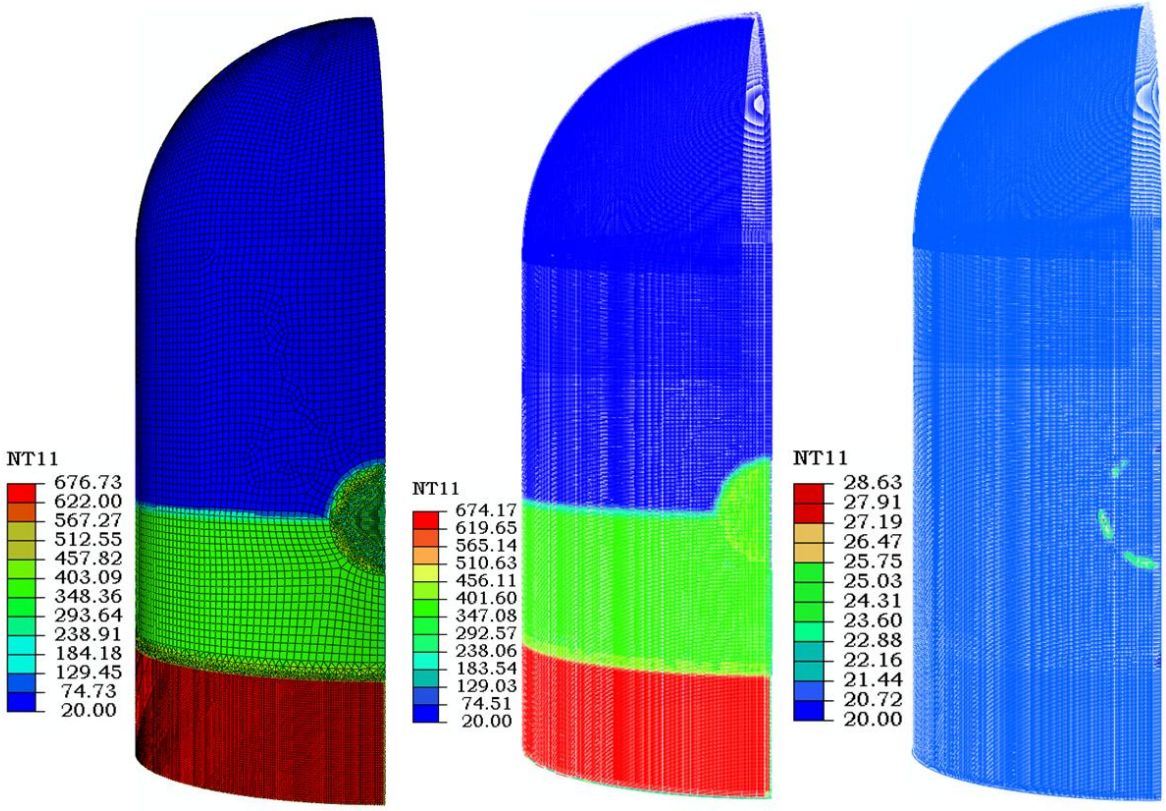

Fig. 6.8 Thermal profile against Boeing 707-320 aircraft after 2 hours time duration (a) concrete (b) outer reinforcement (c) inner reinforcement

6.2.2 Heat Transfer Analysis for BOEING 747-400 Aircraft

In order to study the thermal effects due to Boeing 747-400 aircraft, the heat transfer analysis has been performed assuming 3 hours fire duration, Fig. 6.2. The thermal gradient has been plotted across the thickness of the containment at three different locations identified in Fig. 6.3. The pattern of temperature variation is almost similar to that of Boeing 707-320 aircraft, however the temperature noticed at the front face after 1 hour was about 877°C along "path A" as well as "path B", Fig. 6.9. Thus the temperature in this case is almost 150ºC higher than Boeing 707-320 aircraft. Moreover higher values of temperature can also be noticed in the inner elements than that of fire induced due to Boeing 707-320 aircraft.

The thermal profile of the containment, as well as outer and inner reinforcement after different time duration, due to the crash induced fire of aircraft Boeing 747-400 has been plotted in Fig. 6.10- Fig. 6.13. The maximum temperature in concrete after first 100 sec. of fire was found to be 287°C while in the outer reinforcement it was about 208°C, see Figs. 6.10 (a) and (b) respectively. However, very small temperature change has been noticed at the inner reinforcement, Fig. 6.10 (c). The temperature in concrete reached a maximum 1094.24°C after 3680 sec. and thereafter it decreased, Fig. 6.11(a). In the outer reinforcement the highest temperature reached 1045.71°C after 3870 sec. while in the inner reinforcement it reached maximum 34.07°C at 4190 sec. and subsequently decreased with further increase in time, see Figs. 6.11(b) and (c) respectively. It has been observed that after 30 minutes the surface temperature started decreasing, however, the through thickness temperature has been found to increase consistently. This phenomenon has been found to be more prominent in this case as compared to the fire induced against Boeing 707-400 aircraft. The peak temperature is highly localised in the severely exposed regions of concrete as well in reinforcement. After 2 hours time duration the maximum temperature in concrete reached almost 818°C while in outer reinforcement it was 813°C, see Fig. 6.12(a) and (b) respectively. However, the temperature in the inner reinforcement reduced to 31.6°C, Fig. 6.12(c). After 3 hours duration, the residual maximum temperature noted in concrete, outer reinforcement and inner reinforcement were 605°C, 599°C and 28°C respectively, Fig. 6.13. However, the residual temperature in this case has been found to be higher than Boeing 707-320 aircraft.

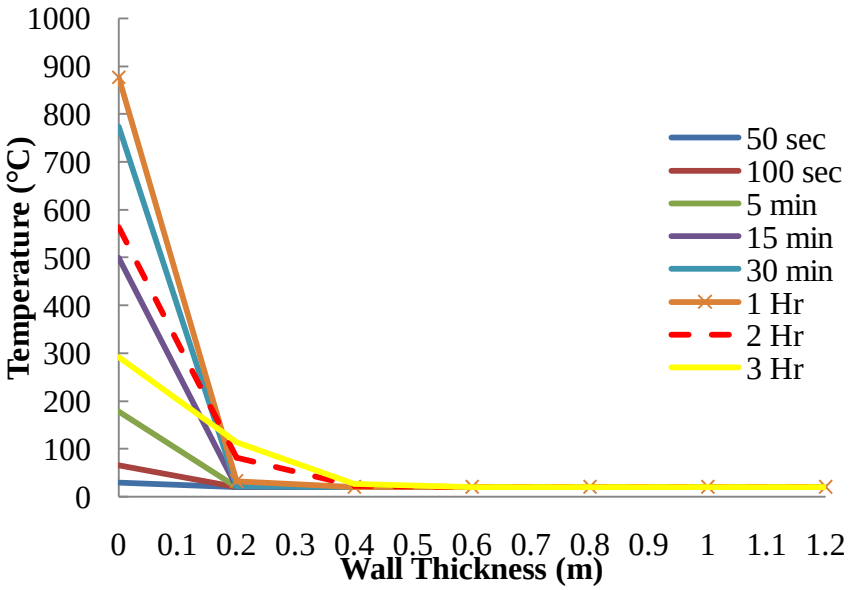

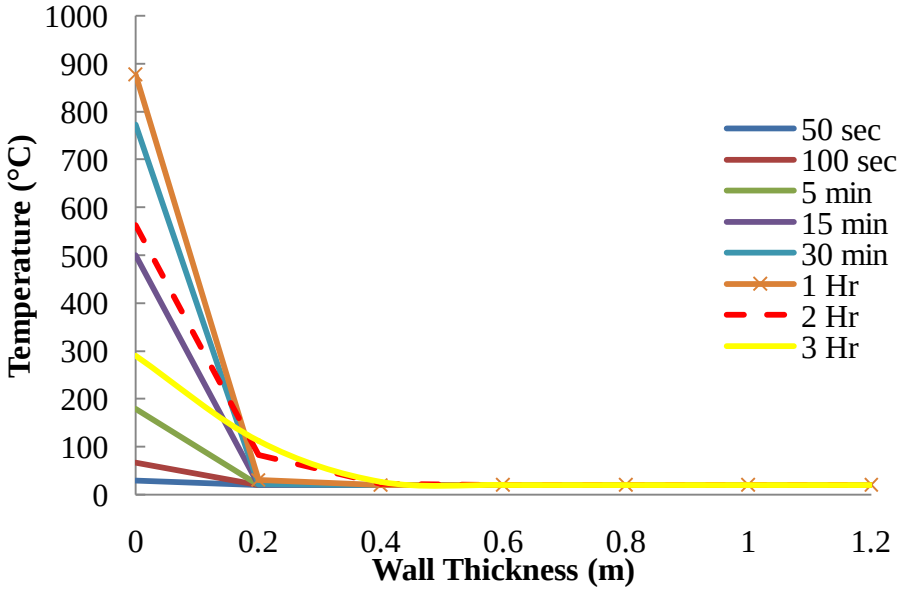

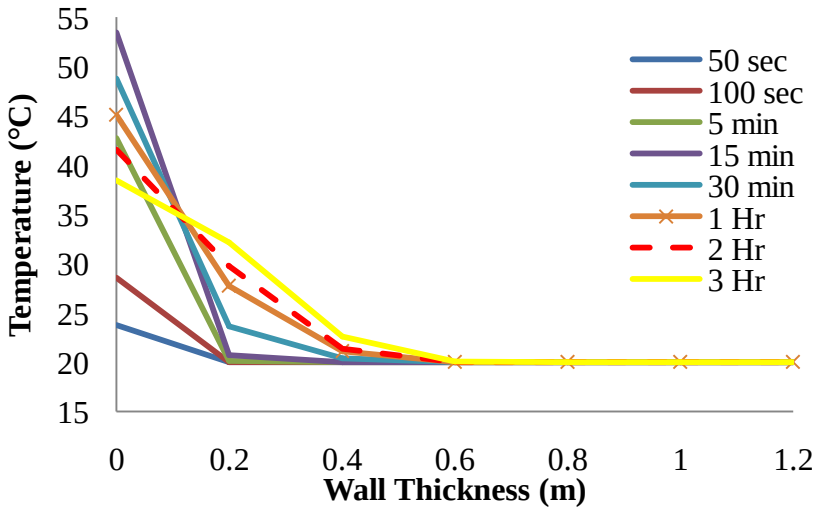

Fig. 6.9 Temperature gradient in concrete across the thickness of containment for Boeing 747-400 aircraft (a) at path A (b) at path B (c) at path C

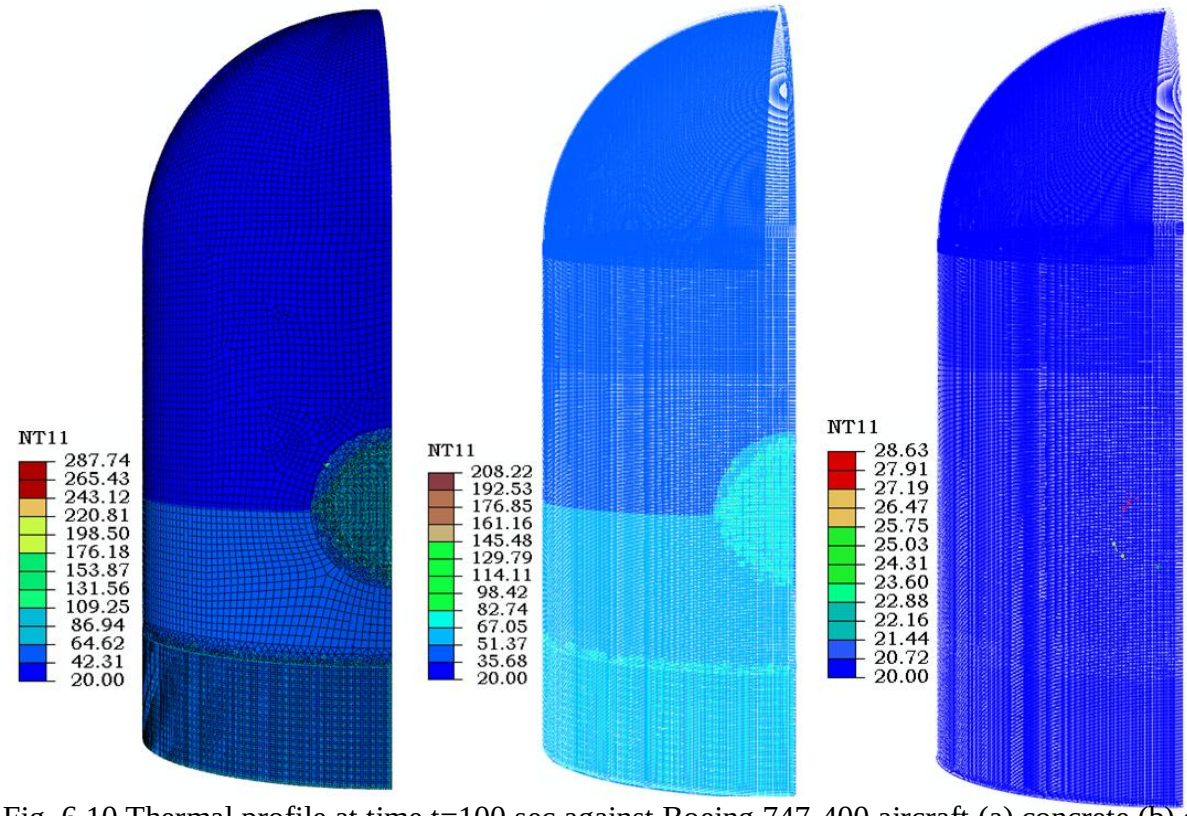

Fig. 6.10 Thermal profile at time t=100 sec against Boeing 747-400 aircraft (a) concrete (b) outer reinforcement (c) inner reinforcement

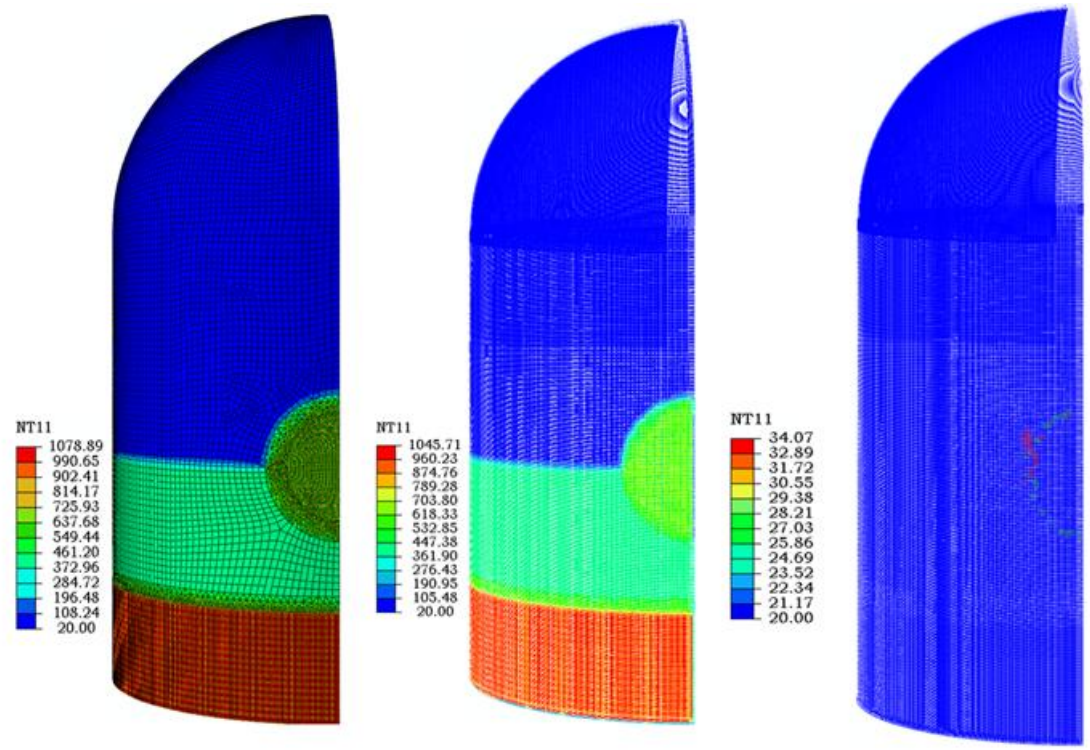

Fig. 6.11 Thermal profile with maximum nodal temperature against Boeing 747-400 (a) concrete (time t= 3680 sec.), (b) outer reinforcement (time t= 3870 sec.) and (c) inner reinforcement (time t = 4190 sec.)

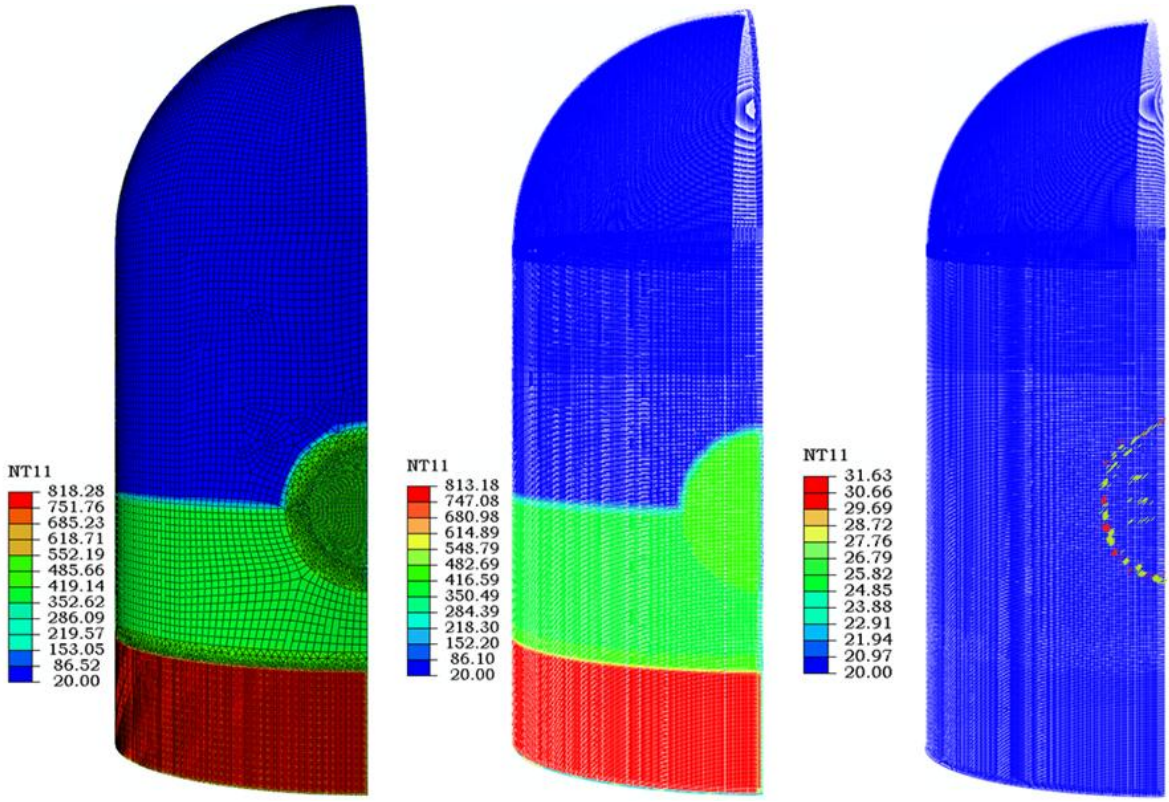

Fig. 6.12 Thermal profile after 2 hours time duration against Boeing 747-400 aircraft (a) concrete (b) outer reinforcement (c) inner reinforcement

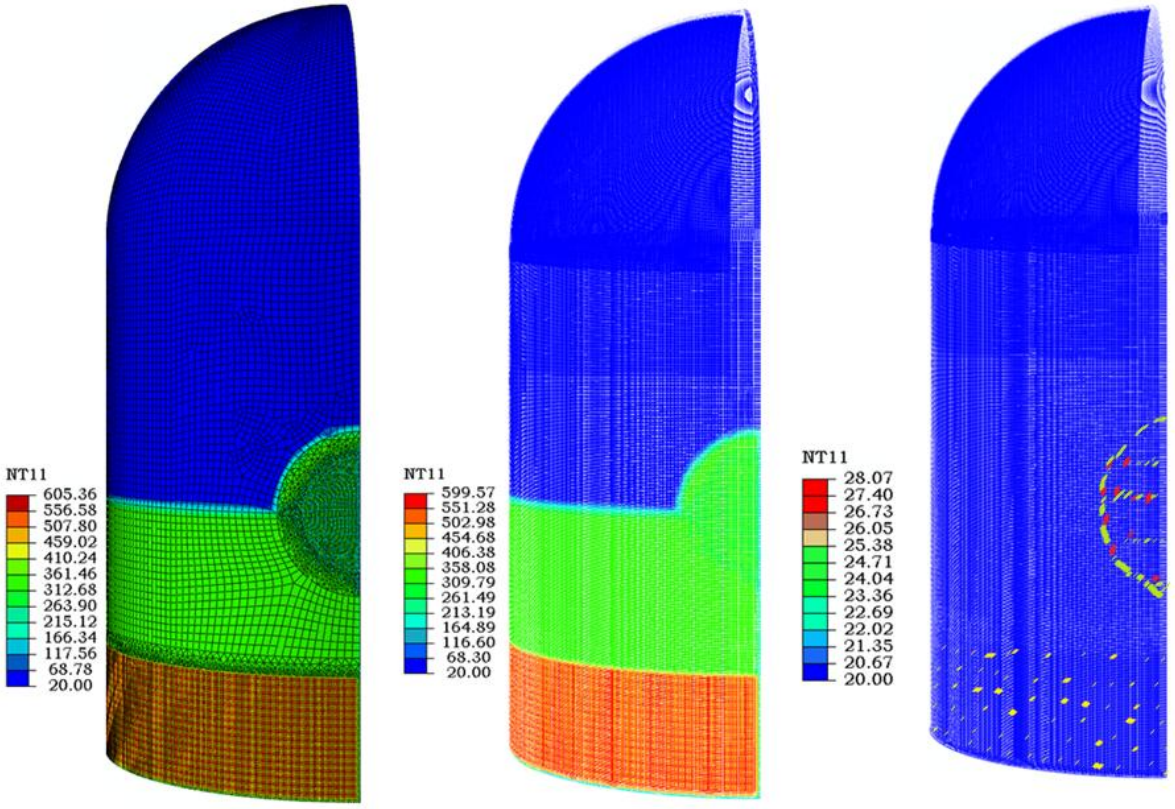

Fig. 6.13 Thermal profile after 3 hours time duration against Boeing 747-400 (a) concrete (b) outer reinforcement (c) inner reinforcement

6.3 IMPACT ANLYSIS

Impact analysis on BWR Mark III containment has been carried out using ABAQUS/Implicit scheme since ABAQUS/Explicit does not support the heat transfer analysis. Hence, the deformed profile of the containment obtained from the impact analysis and the nodal temperature obtained from the heat transfer analysis have been considered input for the thermal stress analysis. However, the constitutive model and the meshing characteristics of the containment have been considered identical to what have been employed in Chapter 4. It should also be noted that the loading has been assigned through the corresponding reaction-time curves of Boeing 707-320 and Boeing 747-400 aircrafts, please see chapter 5. Further, the average area approach has been employed for assigning the loading through the reaction-time curves.

6.3.1 Impact Response Against Boeing 707-320 Aircraft

In general majority of the aircraft fuel is contained in and around the wings (Jeon et al., 2012). Hence, in the present study it has been assumed that the fire will break out as soon as the wings come in contact. The wings of Boeing 707-320 aircraft have been seen to contact the containment after 0.2 sec. of the onset of strike, Fig. 5.17. Hence, the break out of fire has been assumed to occur after 0.2 sec. of initial contact.

The implicit impact analysis has therefore been carried out until 0.2 sec. and the deformation obtained has been considered to be the input for the thermal stress analysis. The maximum deformation in the containment at 0.2 sec. has been found to be 38.35 mm at the impact location, Fig. 6.14(a). A nominal outward bulging has also been noticed on the surface of the containment beyond the impact zone. The maximum displacement in the inner reinforcement has been found to be slightly higher than that of the outer reinforcement. The maximum displacement in the outer and inner reinforcement was 37.31 mm and 37.70 mm respectively, see Fig. 6.14(b) and (c) respectively. A maximum compressive stress in concrete has been found to be 5.9 MPa, Fig. 6.15(a) at the outer face of containment. The concrete at the inner face of containment however, has been found to be under tension. The maximum tension has been noticed to be 7.7 MPa. However this extreme vale of tension has been predicted only in few elements under the impact zone. In general the value of tensile stress at the inner face of containment was found to be about 2 MPa.

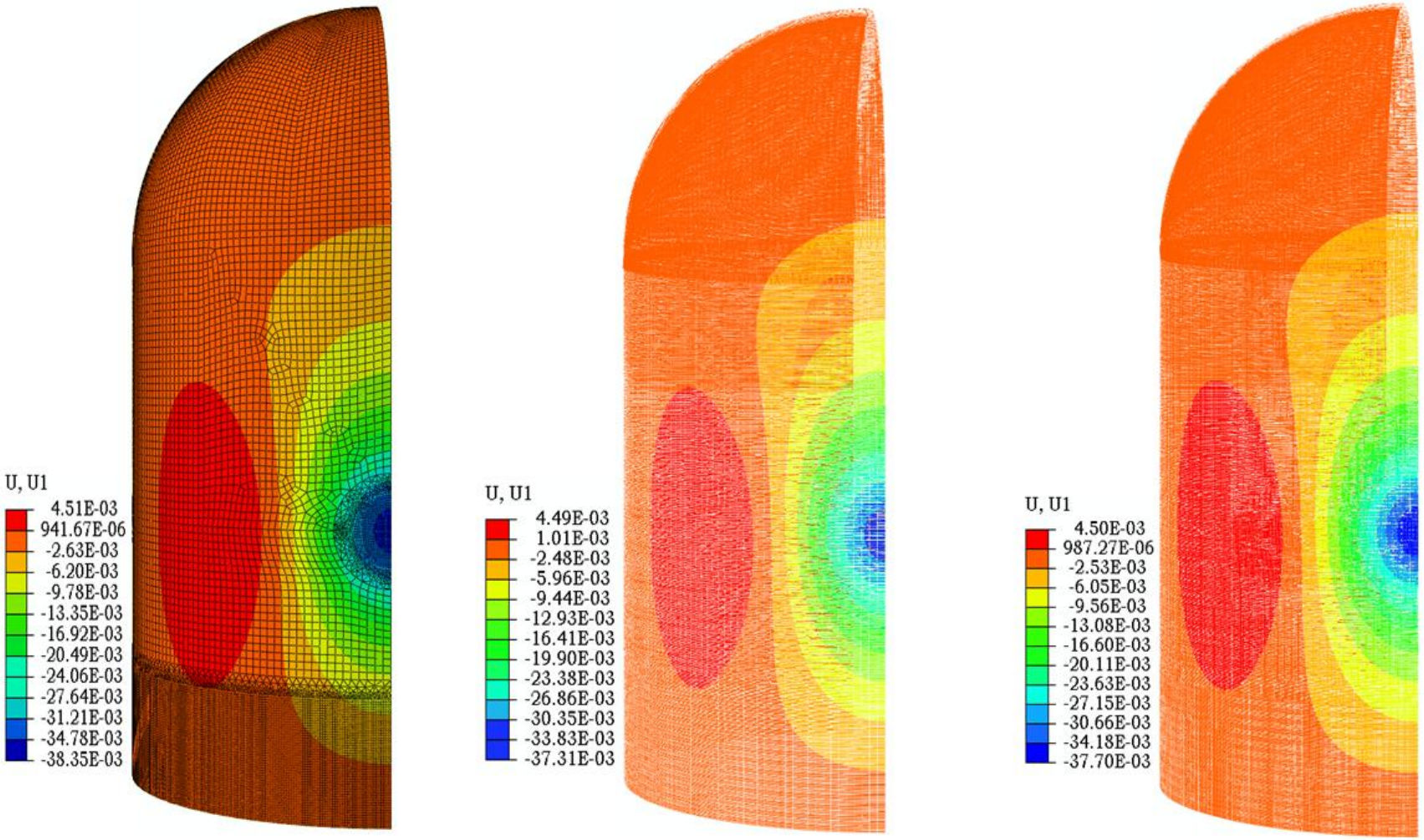

Fig. 6.14 Deformation contour before break out of fire against Boeing 707-320 aircraft (a) concrete (b) outer reinforcement (c) inner reinforcement

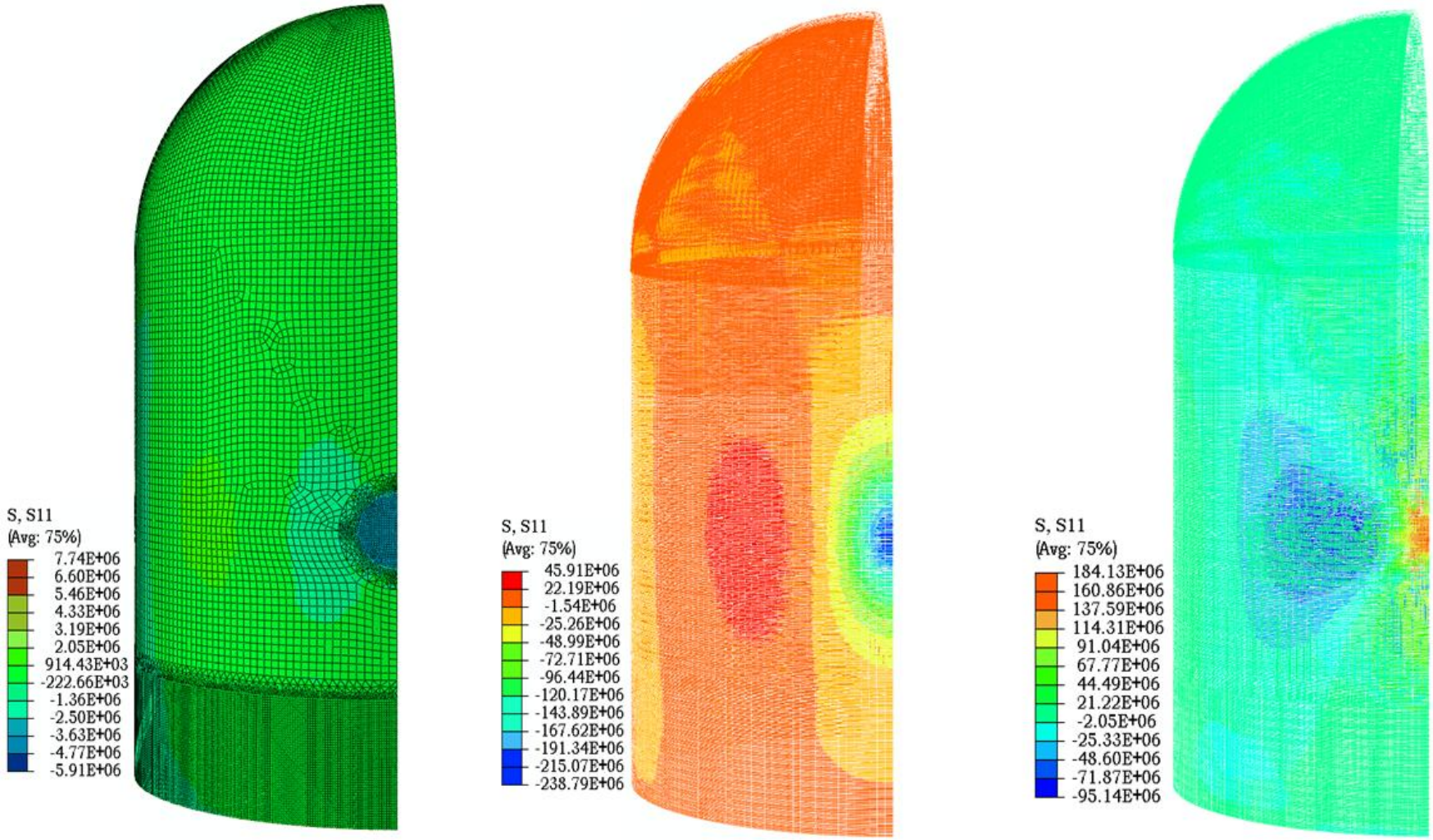

Fig. 6.15 Normal stress (σ_{11}) contour before break out of fire against Boeing 707-320 aircraft (a) concrete (b) outer reinforcement (c) inner reinforcement

The outer set of reinforcement is predominantly under compression particularly at the impact region. The maximum stress has been noticed to be 239 MPa while a nominal tensile stress of 45.9 MPa has also been noticed away from the impact region, Fig. 6.15(b). The inner set of reinforcement has been found to be under predominant tension. The maximum tensile stress of 184 MPa has been found under the impact zone while the maximum compressive stress of 95 MPa has been noticed away from impact region, Fig. 6.15(c).

6.3.2 Impact Response Against Boeing 747-400 Aircraft

In case of Boeing 747-400 aircraft the wings have been found to strike the containment after 0.19 sec. of the onset of strike (Fig. 5.18). Hence, the fire in this case has been assumed to spread at 0.19 sec. The maximum displacement of the containment has been noticed to be 50.47 mm in the impact region, Fig. 6.16(a). The displacement caused due to the impact of Boeing 747-400 was found to be more localised than Boeing 747-400 aircraft. The maximum displacement in the outer and inner reinforcement was 49.9 mm and 50.1 mm respectively, see Figs. 6.16(b) and (c) respectively. However, the deformation in the inner set of reinforcement has been found to be more localised than that of the outer set of reinforcement. The maximum compressive stress in concrete was found to be 8.32 MPa at the outer face of containment in the impact region, Fig. 6.17(a). The inner face has been found to be under tension with a maximum stress 2.9 MPa in the impact region. The compressive stress is found to be dominating in the outer set of reinforcement. The maximum compressive stress has been noticed to be 406 MPa. The tensile stress of 80-120 MPa has also been noticed in the outer set of reinforcement along the circumferential axis away from the impact region, Fig. 6.17(b). In the inner set of reinforcement however, tensile stress of 349.6 MPa has been observed under the impact zone while circumferentially away from the impact zone, the compressive stress of 312 MPa has been developed, Fig. 6.17(c).

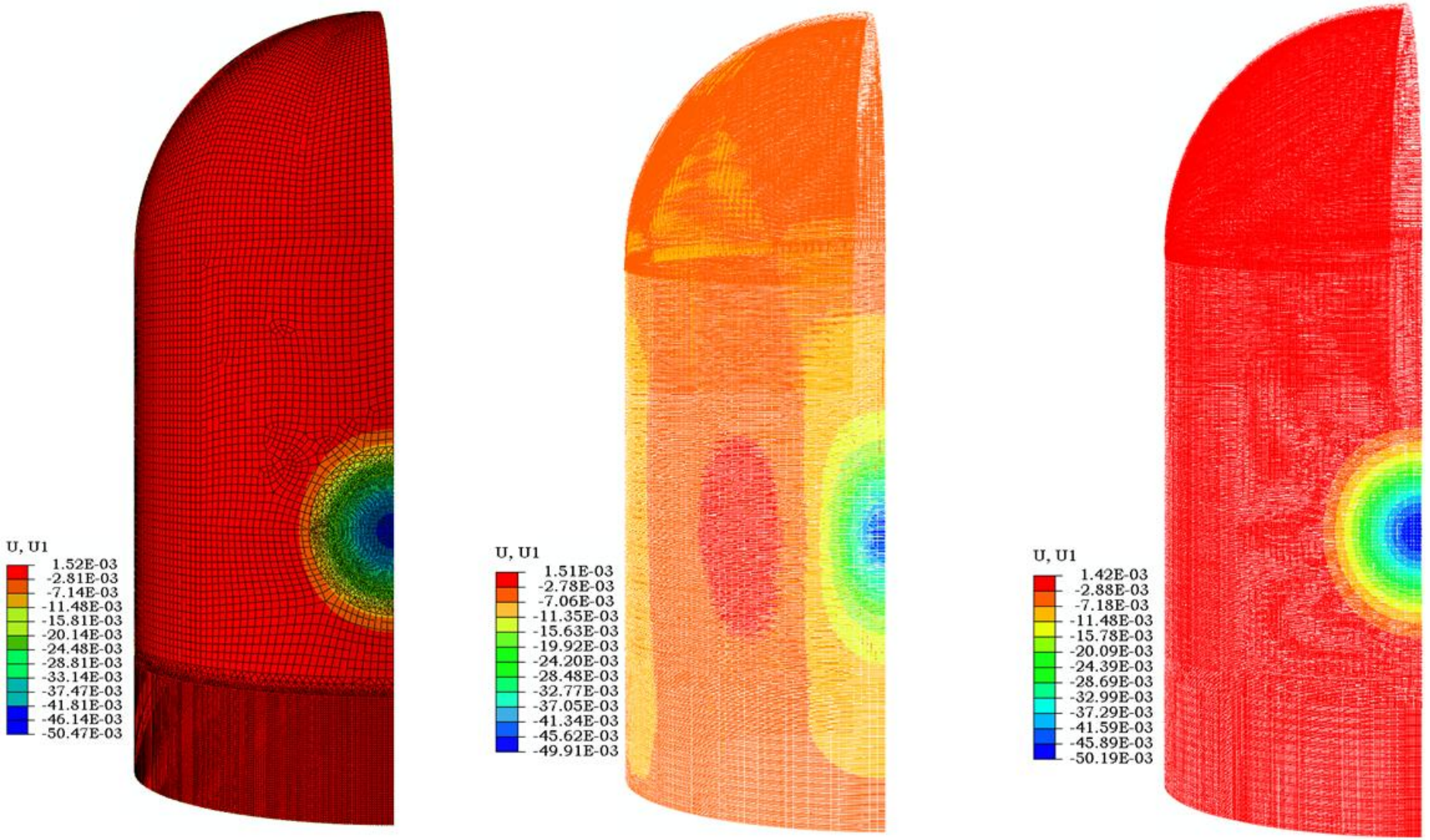

Fig. 6.16 Deformation contour before break out of fire against Boeing 747-400 aircraft (a) concrete (b) outer reinforcement (c) inner reinforcement

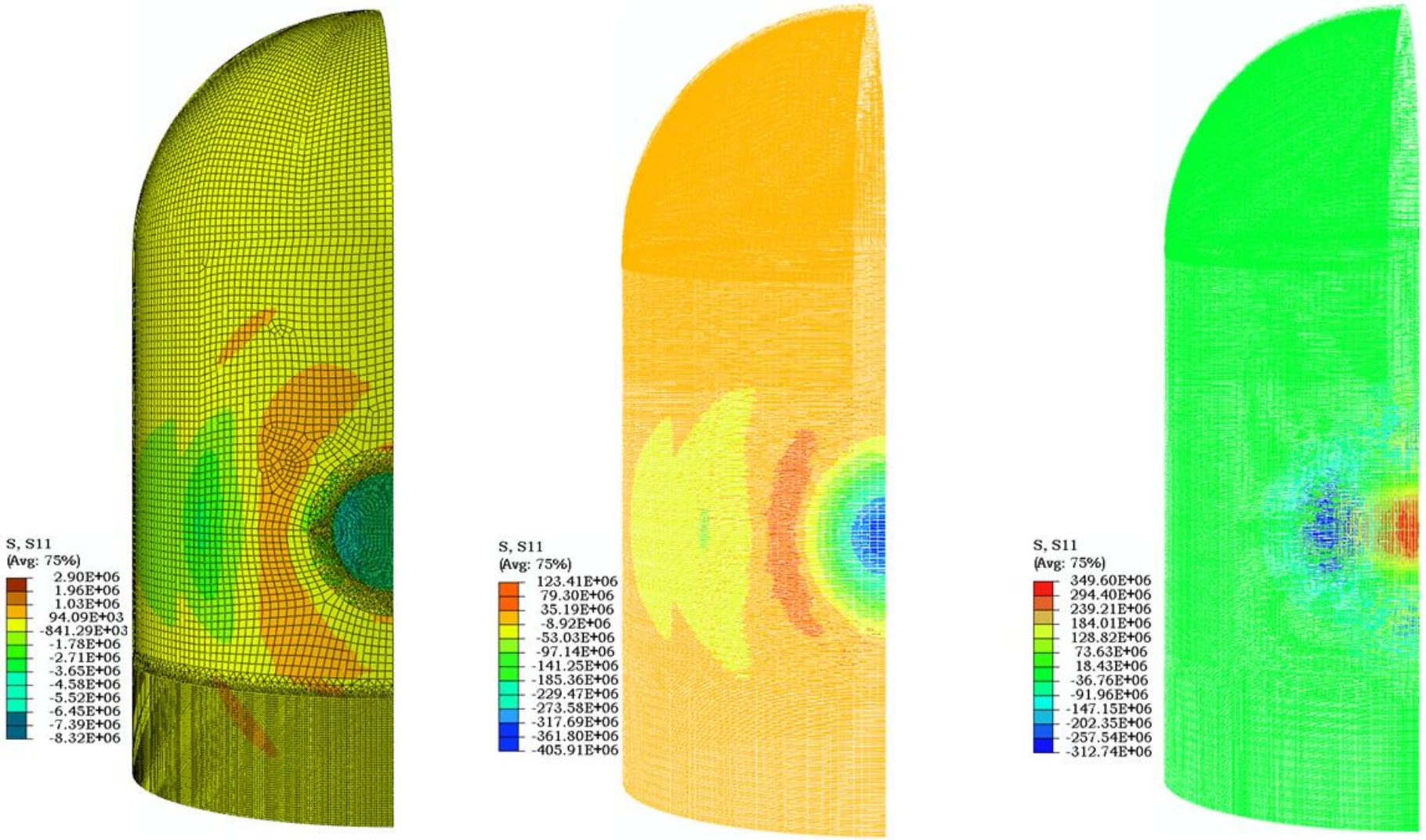

Fig. 6.17 Normal stress (σ_{11}) contour before break out of fire against Boeing 747-400 aircraft (a) concrete (b) outer reinforcement (c) inner reinforcement

6.4 THERMAL STRESS ANALYIS

The thermal stress analysis is the third step of the analysis wherein the impact and the heat transfer responses have been coupled together to obtain the resultant thermal stresses. The deformation and the stresses at the end of impact analysis have been considered as the initial state to evaluate the further damage of the containment due to the induced fire.

6.4.1 Thermal Response against BOEING 707-320 Aircraft

The variation of stresses across the thickness of the containment has been plotted at three different locations identified for plotting the temperature gradients (path A, B and C), Fig. 6.3. The deformation of the containment has also been plotted along path D highlighted Fig. 6.19. Along "path A", the exposed face of the containment was under nominal tension throughout the fire duration, Fig. 6.18(a). However, the elements in the middle of the thickness have been found to be under compression. This behaviour may be due to the fact that the elements at the exposed face had a tendency of expanding while the inner elements are restraining their expansion. The compressive stress has been found to increase with increase in temperature. After 1 hour of fire however, the temperature starts decreasing and hence the stresses. A similar pattern of stress variation has been found along "path B", however, the rate of stress decrement has been was found to be higher at this location, Fig. 6.18(b). After 2 hours the maximum compressive stress was 9.6 MPa and 8.3 MPa along path A and B respectively. The variation of stresses along path A and B during the cooling face may be due to the fact that path B is located near the moderate exposed region. The pattern of stress gradient observed in the present study has a close agreement with the results of Jeon et al. (2012). However, due to the higher wall thickness (1.5 m), Jeon et al. (2012) found negligible stresses at the inner face of the containment.

The stress variation along path C has been plotted in Fig. 6.18 (c). It should be noted that path C is located at the impact region. Before the application of fire the outer face of the containment was under predominant compression while the inner face under predominant tension. A maximum compressive stress of 4 MPa was noticed at the outer face of the containment along path C. At the corresponding inner face along path C, a maximum tension of 1MPa has been noticed. Due to the elastic recovery however, the trend of stresses has been found to have reversed. The complete elastic recovery has occurred within 100 seconds of the analysis. It should be noted that the fire effect in this region is insignificant. However, after half an hour

of fire duration, nominal compressive stresses have been noticed at the front as well as inner face of the containment. The nominal compressive stresses at the front face might have been developed due to the loss of moisture content.

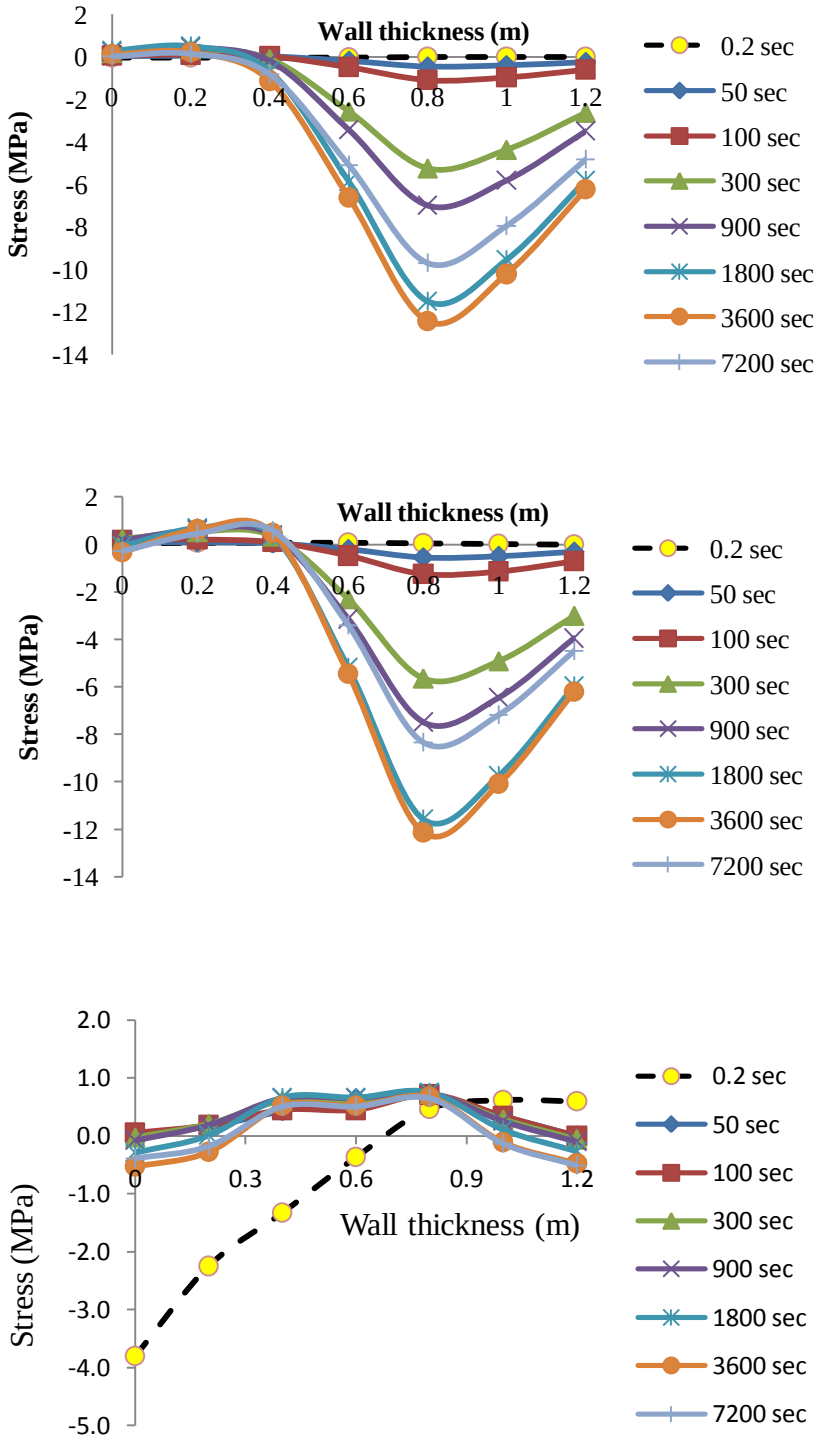

Fig. 6.18 Stress gradient in concrete across the thickness of containment for Boeing 707-320 (a) at path A (b) at path B (c) at path C

At the inner face however, a nominal compressive has been noticed. The elevation of temperature at the front face will cause a overall expansion at the this face, hence the entire opposite inner face will be under nominal compressive stress.

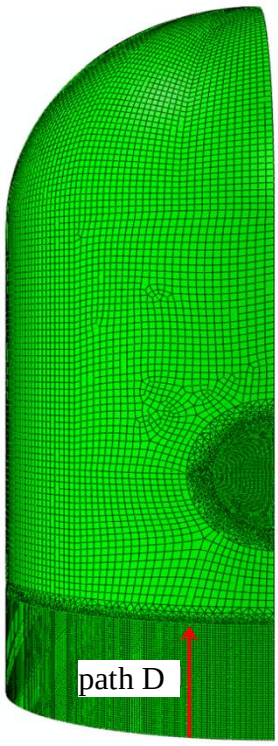

Fig. 6.19 Locations identified for plotting the displacement up to 10 m height from

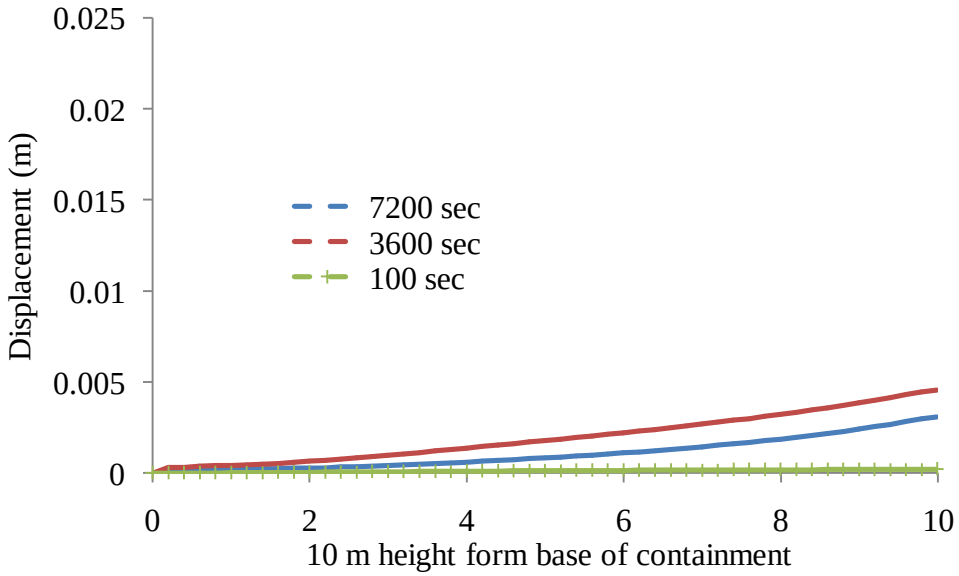

Fig. 6.20 Displacements in concrete along "path D" for Boeing 707-320 aircraft

The nodal displacement along path D has been plotted at selected time intervals in Fig. 6.19. An outside bulging can be noticed when moving up from the base of the containment. The displacement near the base is zero due to the fixidity of the containment. At a height of 10 m from the base a maximum displacement of 4.5 mm has been noticed after 1 hour of fire. Thereafter however, the recovery in deformation has been noticed due to gradual decrease in surface temperature.

6.4.2 Thermal Response against BOEING 747-400 Aircraft

For Boeing 747-400 aircraft, the variation of normal stress across the thickness of the containment has been plotted in Fig. 6.21. The stress variation in this case was similar to that what has been found against Boeing 707-320 aircraft. However, the magnitude of the compressive stress within wall element was found to be higher than that of reported in case of Boeing 707-320 aircraft. Maximum compressive stress was found to be 21.15 MPa, Fig. 6.21 (a). Moreover, according to provisions in Eurocode 2 (2004) concrete has ultimate compressive strength of 4.5 MPa at a temperature of 800°C. Hence, concrete at the exposed face will fail as it cannot bear of tensile stress about 1.3 MPa.

At the "path B" however, the stresses at the exposed face are negligible but there has been high compressive stress at the inner element. At "path C" the initial stress due to impact was 6 MPa compressive at exposed face and 2.2 MPa tensile at the inner face Fig. 6.21 (b) and (c). However, after elastic recovery of the front face the magnitude of compressive stress was a of 1 Mpa till significant rise in temperature. Further 300 seconds an increase in compressive stress was noticed that might be due to loss of moisture content.

The variation of nodal displacement along the "path D" due to crash induced fire of Boeing 747-400 has been highlighted in Fig. 6.22. The pattern of variation is almost similar to that of Boeing 707-320 however; the net displacement is quite higher. The nodal displacement at the height of 10m was approximately 25 mm at peak temperature. After 3 hour the displacement was found to be 15.5 mm and 9.3 mm at respective height of 10m and 5m from the base of containment.

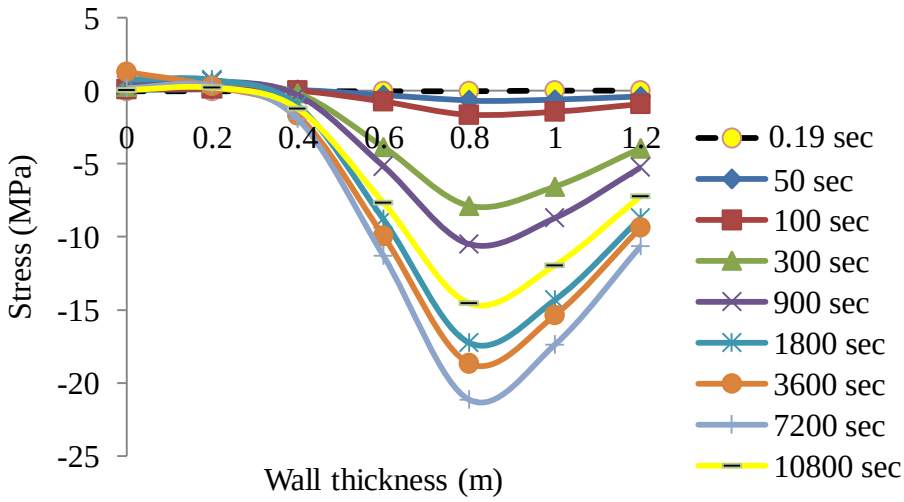

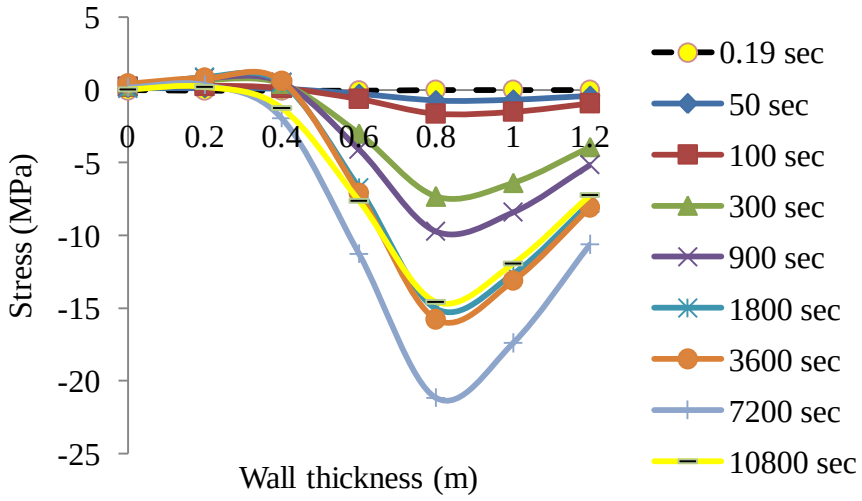

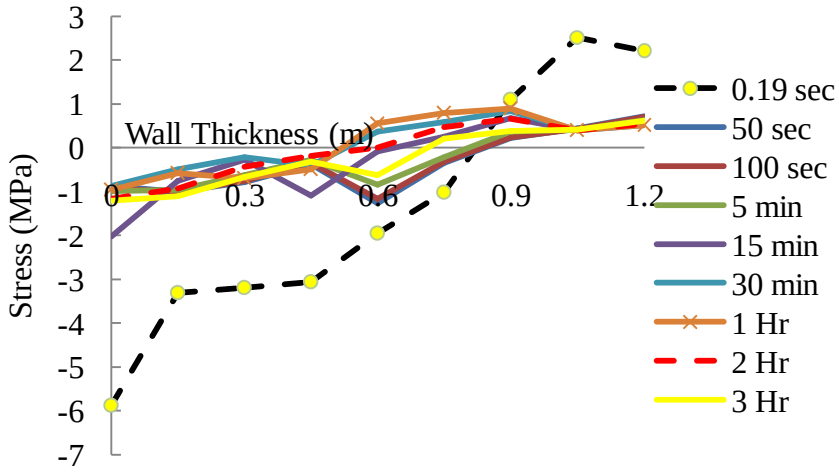

Fig. 6.21 Stress gradient in concrete across the thickness of containment for Boeing 747-400 (a) at path A (b) at path B (c) at path C

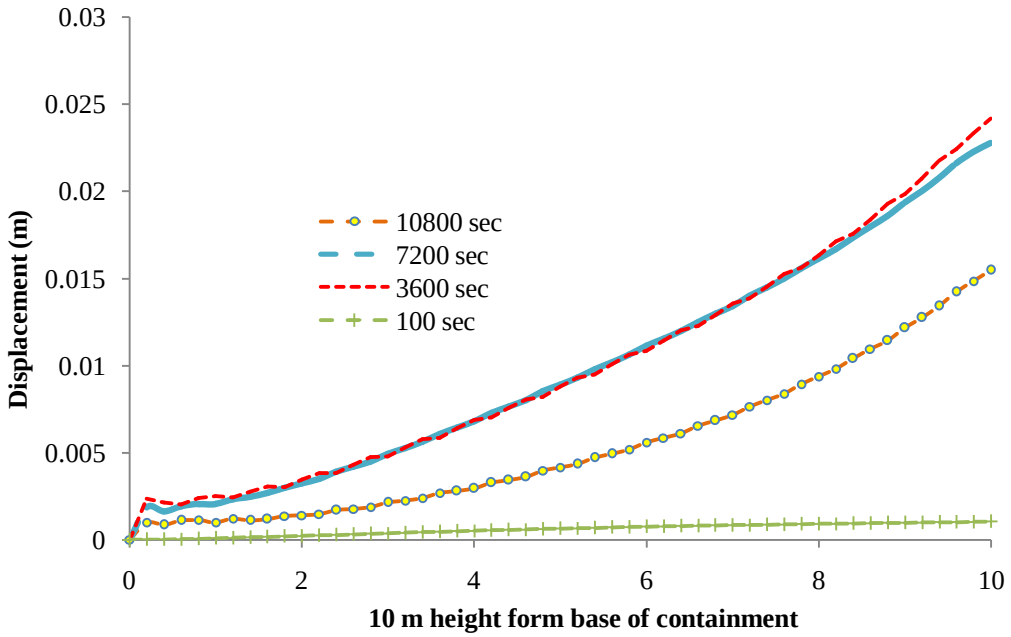

Fig. 6.22 Displacements in concrete along "path D" for Boeing 747-400 aircraft

6.5 CONCLUDING REMARKS

Heat transfer, Impact and thermal stress analyses have been carried out using finite element code ABAQUS/Implicit. The effect of fire induced due to aircraft crash has been studied against Boeing 707-320 and Boeing 747-400 aircrafts. The reaction time curve obtained against curved flexible target was applied on the surface area of the containment based on the average area method discussed in the previous chapter. The impact of aircraft was considered to occur up to the point the engines came in contact with the containment structure. Thereafter the fire was assumed to have spread out since majority of the aircraft fuel is stored in and around the wings. The fire effect was considered to be most severe at the bottom of containment up to 10 m height from the base. At the impact region however, moderate fire effect has been considered. Deeper as well higher temperature penetration has been noticed for fire induced due to Boeing 747-400 aircraft. However, at a depth of 10 cm only temperature was found to be less than 50% of the surface temperature. Hence, due to sharp fall in the thermal gradient across the thickness of the containment, the damage has been limited to few centimeters depth only. Hence, it can be concluded that the containment suffers severe local damage due to the fire resulting in scabbing of the concrete however, the global behaviour of the containment will not be affected.

Chapter 7

SUMMARY, CONCLUSIONS AND SCOPE OF FUTURE RESEARCH

7.1 SUMMARY

The present study addresses the response of the nuclear containment structure subjected to aircraft crash. The outer containment of Boiling Water Reactor (BWR Mark III) nuclear power plant has been impacted to explore the most vulnerable location and the most damaging aircraft. The reaction-time curves of various aircrafts have been determined assuming the deformable and non-deformable targets of varying curvature using numerical and analytical approaches. The reaction-time curves thus obtained have been compared and discussed. The area of containment in contact with that of the aircraft has been found to vary with respect to time and the striking velocity. The variation of the contact area has been studied through the numerical and analytical methods. The reaction-time curves and the corresponding contact area thus obtained have been idealized and employed to seek the response of the containment. The geometric models of the aircrafts, developed numerically, have also been employed to hit the containment structure at the most vulnerable location. The response of the containment has been obtained in terms of local and global deformation, stresses induced in the concrete and reinforcement and the corresponding material degradation. The results thus obtained corresponding to the geometric model and the reaction-time curve have been compared and discussed. The fire induced due to aircraft crash has also been considered to study the further degradation of the structure. A sequentially coupled impact and fire analysis has been carried out to identify the global and local behavior of the containment. The deformed state of the containment after impact analysis has been considered as the initial state for the fire analysis. The fire has been considered to be critical up to 10 m height from the base. The effect of fire has been considered moderate in the impact region. The implicit as well as explicit integration schemes available in ABAQUS finite element code have been employed to carry out the numerical simulation. The Concrete Damaged Plasticity (CDP) model has been employed to simulate the behavior concrete while the Johnson-Cook elasto-viscoplastic material model has been used predict the behavior of the reinforcement as well as the aircrafts.

7.2 CONCLUSIONS

The following conclusions may be drawn based on the results obtained under the present study;

- The strain rate is an important parameter which must be carefully incorporated to predict the material behavior of the containment as well as the aircraft. The material model without strain rate and 290 s^{-1} strain rate predicted very high deformations and the local failure of the containment. However, the deformation was found to be comparatively low for the sophisticated material model wherein the combined effect of strain rate was considered. Moreover, the results of this model were found in agreement with those of the 620 s^{-1} strain rate.

- The mid-height of the containment has been found to be the most vulnerable location followed by junction of dome and cylinder. On the other hand, the crown of the dome has been found to be the safest location. The deformation in the concrete at the mid-height of the containment was at least three times higher than that of the crown of the containment for aircrafts considered in the present study.

- The Boeing 747-400 and Boeing 767-400 aircrafts caused most significant damage to the concrete leading to the global failure of the containment. Phantom F4 on the other hand, caused local damage and expected to perforate if impacted at high incidence velocities. The damage of concrete was found to be critical under tension.

- The curvature and deformability of the target are important parameters affecting the reaction-time response of aircraft. A decrement in the peak reaction force has been noticed with increase in target curvature. Further, the arrival of the peak has also been found to have delayed as the curvature is increased. The peak impact force has been found to decrease by more than 40% in case of non-deformable curved containment comparing to non-deformable flat target. The reaction-offered by the deformable target was lesser in magnitude in comparison to what has been offered by the rigid target of equivalent curvature radius. The peak impact force against deformable target has been found to decrease by approximately 40% as compared to non-deformable target.

- The application of average area scheme overestimated the local deformation while underestimated the global deformation of the containment. However, the magnitude of

deformations predicted by the area trifurcation approach and the geometric model of the aircraft are comparatively low and in close agreement. The deformation with average area scheme was almost three times higher than that of the area trifurcation scheme and geometric model. The trifurcation approach is therefore more accurate and hence represents a more realistic estimate of the contact area of the aircraft.

- Thermal stresses and deformations produced due to crash induced fire may cause scabbing of concrete leading to exposure of reinforcement. However, the induced fire did not impose threat to the global behavior of the containment structure.

7.3 SCOPE OF FUTURE RESEARCH

The following may be considered as the scope of work for the extension of present study in future;

- ❖ The impact and fire may be simultaneously considered near the base of containment to simulate the most critical condition.
- ❖ The aircraft crash may also cause possible explosion of the fuel tanks. Hence, impact blast and fire may be considered as the resultant sequence of the phenomena
- ❖ The neo-developed variant of fighter jets which have higher cruise velocity at lower altitude may perforate the containment. Hence evaluation of reaction time curve of these jets may enhance the effectiveness of the aircraft crash studies.
- ❖ The studies are also required for the refinement of the constitutive modeling in order to handle such complex problems. A robust constitutive model is required to predict the behavior of concrete under high strain rate and temperature.

REFERNCES

1. Abaqus Explicit user manuals Version 6.8.
2. Abbas, H., 1992. Dynamic response of structures subjected to missile impact. Ph.D. thesis, University of Roorkee, India.
3. Abbas, H., Gupta, N.K., Alam, M., 2004. Nonlinear response of concrete beams and plates under impact loading, Int J of Imp Engg 30 1039–1053.
4. Abbas, H., Paul, D.K., Godbole, P.N., Nayak, G.C., 1995. Reaction-time response of aircraft crash. Comp. Struct. 55, 809–17.
5. Abbas, H., Paul, D.K., Godbole, P.N., Nayak, G.C., 1995b. Soft missile impact on rigid targets. Int J Imp Engg. 16(5), 727-37.
6. Abbas, H., Paul, D.K., Godbole, P.N., Nayak, G.C., 1996. Aircraft crash upon outer containment of nuclear power plant. Nucl. Eng. Des. 160, 13-50.
7. Abrams M.S.," Performance of concrete structures exposed to fire", PCA R&D Bulletin RD060.01D, Portland Cement Association, 1977.
8. Anderberg Y., Thelandersson S., "Stress and deformation characteristics of concrete at high temperature, 2. Experimental investigation and material behaviour model."Bulletin 54, Lund Institute of Technology, Lund, Sweden, 1976.
9. Anderberg, Y. (1978)," Analytical fire engineering design of reinforced concrete structures based on real fire conditions," in: Proceeding of the FIR Congress, London, Part I, pp. 112-121.
10. Arioz, O., 2007. Effects of elevated temperatures on properties of concrete Original Research Article, Fire Safety Journal, 42(8), 516-522.
11. Arros, J., Doumbalski, N., 2007. Analysis of aircraft impact to concrete structures, Nucl. Eng. Des. 237 1241–49.
12. Bazant, Z.P., and Cedolin, L., 1983.Finite Element Modeling of Crack Band Propagation, J of Struct Engg, ASCE, Vol. 109, No. STI, pp. 69-92
13. Bignon P.G., Riera, J.D., 1980. Verification of methods of analysis for soft missile impact problems. Nucl. Eng. Des. 60, 311-26.
14. Bingo, A.F., Gul, R. (2009)," Residual bond strength between steel bars and concrete after elevated temperatures", Fire Safety Journal V. 44 pp. 854-859.
15. Boeing Commercial Airplanes.<http://www.boeing.com>. last visited 09/02/2014.

16. Bonet J., Wood, R. D., 2008. Non-linear continnum mechanics foe finite element analysis, cambridge university press.
17. Børvik T, Hopperstad OS, Berstad T, Langseth M. A computational model of visco-plasticity and ductile damage for impact and penetration. Eur J Mech A—Solids 2001;20:685–712.
18. Børvik T, Hopperstad OS, Berstad T. On the influence of stress triaxiality and strain rate on the behaviour of a structural steel. Part II. Numerical simulations. Eur J Mech A—Solids 2002;22:15–32.
19. Børvik T., Hopperstad O. S., Pedersen K. O., 2010. Quasi-brittle fracture during structural impact of AA7075-T651 aluminium plates Int J Imp Engg, 37(5), 537-551
20. Børvik, T., Hopperstad, O.S., Dey, S., Pizzinato, E.V., Langseth, M., Albertini, C. 2005. Strength and ductility of Weldox 460 E steel at high strain rates, elevated temperatures and various stress triaxialities, Engineering Fracture Mechanics 72 (2005) 1071–1087.
21. Buchanan, A H. (2001),"Structural design for fire safety", John Wiley & Sons, 421pp.
22. Cadoni, E., Dotta, M., Forni, D., Tesio, N., Albertini, C., 2013. Mechanical behaviour of quenched and self-tempered reinforcing steel in tension under high strain rate, Materials & Design, 49, 657-666.
23. Cadoni, E., Fenu, L., Forni, D., 2012. Strain rate behaviour in tension of austenitic stainless steel used for reinforcing bars, Construction and Building Materials, 35, 399-407.
24. Carvel, R., Fire protection in Concrete Tunnels, in The Handbook of Tunnel Fire Safety (Eds. Beard, A. & Carvel, R.) Thomas Telform, London, 2005.
25. Cervera, M., Hinton, E., Boner J.,Bicanic N., 1987.Numerical Methods and Software for Dynamic Analysis of Plates and Shells, Pineridge Press, Swansea, UK, 320-504.
26. Chelapati, C.V., Kennedy, R.P.,Wall, I. B., 1972. Probabilistic assessment of aircraft hazard for nuclear power plants. Nucl. Eng. Des. 19, 333–364.
27. Ciria, H., Peraire, J., Bonet, J., 2008, Mesh adaptive computation of upper and lower bounds in limit analysis, Int J for Numerical Methods in Engg., 75(8), 899-944.
28. Dharmaraju, N., Tiwari, R., Talukdar, S., 2004. Identification of an open crack model in a beam based on force-response measurement, Computers and Structures ,82,167 -179.

29. Drittler, K., Gruner, P., 1976. The force resulting from impact of fast-flying military aircraft upon a rigid wall. Nucl. Eng. Des. 37, 245-48
30. Elghazouli, A.Y., Cashell, K.A. and Izzuddin, B.A. (2009)," Experimental evaluation of the mechanical properties of steel reinforcement at elevated temperature", Fire Safety Journal, V.44, pp. 909-919.
31. Eurocode 2 (2004), "Design of concrete structures: Part 1-2: general rules-structural fire design", European Committee for Standardisation, Brussels, BS EN 1992-1-2, 2004.
32. European Nuclear Society, info/encyclopedia/n/nuclear-power-plant-world-wide.htm, www.euronuclear.org
33. Farmer F.R., Siting Criteria - A new Approach, Paper SM-89/34, IAEA Symposium, Containment and Siting, Vienna, April 1967
34. Federal Register notice 2009. June 12, Volume 74 of the Federal Register, page 28111 (74 FR 28111) the U.S. Nuclear Regulatory Commission (NRC) www.nrc.gov.
35. Felicetti, R. Gambarova, P G and , Meda, A. (2009),"Residual behaviour of steel rebars and R/C sections after a fire", Construction and Building Materials 23 3546-3555.
36. Fletcher I., Welch S., Torero J., Carvel, R..O. and Usmani, A.(2007) ," The Behaviour of concrete structures in Fire", Journal o Thermal Science, V. 11(2), pp.33-57.
37. Frano, R.L., Forasassi, G., 2011. Preliminary evaluation of aircraft impact on a near term nuclear power plant. Nucl. Eng. Des. 241, 5245-50.
38. Freskakis, G.N. (1980), " Behaviour of reinforced concrete at elevated temperatures ", Paper 3-4, Second ASCE conf. on Civ. Eng. And nuclear power, Vol. 1, Paper 3-5, pp. 3-5-1 to 3-5-21, Knoxville, Tennessee.
39. Gardner J W, 1984. Calculation of forces acting upon a rigid structure from an aircraft impact. Int J Impact Engg., Vol 2(4), 345-56.
40. Giroldo F. and bailey, C.G. (2008), " Experimental bond behaviour of welded mesh reinforcement at elevated temperatures," Magazine of Concrete Research, 60, No. 1, February, 23-31.
41. Gomathinayagam S., Dharaneepathy M.V., Keshava Rao M.N., 1994. Damage-zones of containment structures under aircraft impact loads. Comp. Struct. 52 N o. 3.pp.581-590,

42. Gupta, N.K., 2013. Plasto-mechanics of large deformation under impact loading. Mechanics Down Under - Proceedings of the 22nd International Congress of Theoretical and Applied Mechanics, ICTAM 2008 PP. 67 - 84.
43. Hao, Y., Hao, H., Li, Z. X., 2013. Influence of end friction confinement on impact tests of concrete material at high strain rate, Int J Imp Engg, 60, 82-106
44. Heckotter C and Sievers J, (2013) Simulation of Impact Tests With Hard, Soft and Liquid Filled Missiles on Reinforced Concrete Structures, J of Applied Mechs.80 031805-1-7.
45. Hillerborg, A., Modeer, M., and Petersson, P.E., 1976. Analysis of Crack Formation and Crack Growth in Concrete by Means of Fracture Mechanics and Finite Elements, Cement and Concrete Research, 6,. 773-782
46. Hopperstad OS, Børvik T, Langseth M, Labibes M, Albertini C. On the influence of stress triaxiality and strain rate on the behaviour of a structural steel. Part I. Experiments. Eur J Mech A—Solids 2003;22:1–13.
47. Hornyik, K., Analytic modeling of the impact of soft missiles on protective walls, 4th SMiRT, USA, 1977 Paper No: J7/3.
48. Hornyik, K., Robinson A. H., Grund J. E., 1973. Evaluation of Aircraft Hazards at the Boardman Nuclear Plant Site, Portland General Company, PGE -2001(5)
49. IAEA, 2007, http://www.iaea.org/Publications/, Internatinal Atomic Energy Agency, last cited 02/2013.
50. Iliev, V., Georgiev K., Serbezov V., 2011. Assessment of impact load curve of Boeing 747- 400. MTM Virtual J. 1(2011), 22-25.
51. Iqbal, M.A., Rai, S., Sadique, M.R., Bhargava, P., 2012. Numerical simulation of aircraft crash on nuclear containment structure.Nucl.Eng. Des. 243, 321-335.
52. Jeon, S., Jin B, Kim, Y., 2012. Assessment of the Fire Resistance of a Nuclear Power Plant Subjected to a Large Commercial Aircraft Crash, Nucl. Eng. Des, 247,11-22
53. Jin, B.M., Lee, Y.S., Jeon, S.J., Kim, Y.J., Lee, Y.H., 2011. Development of finite element model of large civil aircraft engine and application to the localized damage evaluation of concrete wall crashed by large civil aircraft. in: Transactions SMiRT 21 Div-V: Paper ID 862.
54. Johnson G.R., Cook W.H. 1985. Fracture characteristics of three metals subjected to various strains, strain rates, temperatures and pressures. Engg.Fract.Mech. 21(1): 31–48.

55. Johnson G.R., Cook W.H., 1983. A constitutive model and data for metals subjected to large strains, high strain rates and high temperatures. In: Proceedings of the seventh International symposium on Ballistics. The Hague.
56. Kachanov, L.M., 1958. On creep rupture time. Izvestiya Akademii Nauk SSSR, Otdeleniya Tekhnicheskikh I Nauk 8, 26–31.
57. Kaplan, M.F., 1961. Crack Propagation and the Fracture of Concrete, ACI Journal, Vol. 58, No. 11
58. Katayama et al., 2004. Numerical simulation of jumbo jet impacting thick concrete walls-effect of reinforcement and wall thickness, ACHPR-2, Nara, Japan,
59. Khoury G.A., Effect of fire on concrete and concrete structures, Progress in Structural Engineering, 2(2000), 4, pp.429-447
60. Khoury, G.A. and Anderberg, Y.(2000)," Concrete spalling review", Areport on Fire Safety Design, Swedish National Road Administration.
61. Kobayashi, T., 1988. Probability analysis of an aircraft crash to a nuclear power plant. Nucl. Eng. Des. 110 207-211.
62. Koechlin, P., Potapov S., 2009. Classification of Soft and Hard Impacts—Application to Aircraft Crash, Nucl. Eng. Des., 239 613–618.
63. Krutzik, N. J., 1988. Reduction of the Dynamic Response by Aircraft Crash on Building Structures, Nucl. Eng. Des., 110 191-200
64. Kukreja, M., 2005. Damage evaluation of 500 MWe Indian Pressurized Heavy Water Reactor nuclear containment for aircraft impact. Nucl. Eng. Des. 235, 1807–17.
65. Kukreja, M., Singh, R.K., Vaze, K. K., Kushwaha, H.S., 2003.Damage evaluation of 500MWe Indian Pressurized HeavyWater Reactor nuclear containment for aircraft impact.Trans. 17th SMiRT, No. 3, Division J.
66. Lahiri, S. K., Bonet, J., Peraire, J., 2010. A variationally consistent mesh adaptation method for triangular elements in explicit Lagrangian dynamics. Int. J. Numer. Meth. Engng; 82:1073–1113.
67. Law A., Gillie M., 2010, Interaction diagrams for ambient and heated concrete sections. Engineering Structures, 32(6), 1641–1649.
68. Lee J., Fenves G.L.1998. Plastic-damage model for cyclic loading of concrete structures, Journal of Engineering Mechanics, Vol. 124, No. 8, , pp. 892–900.

69. Lie T.T and Irwin R.J., " Method to calculate the fire resistance of reinforced concrete columns with rectangular cross section" ACI Structural Journal Vol. 90, No. 1, 1993, pp. 52-60.
70. Lie T.T. and Kodur V.K., " Thermal properties of fiber reinforced concrete at elevated temperatures", NRC-CNRC, April 1995.
71. Liu Lixian, Reddy D. V., and Sobhan K., " Size effect on fire resistance of reinforced concrete columns and beams", Eighth LACCEI Latin American and Caribbean Conference for Engineering and technology, 2010.
72. Lo Frano R., Forasassi G., 2011. Preliminary evaluation of aircraft impact on a near term nuclear power plant, Nucl. Eng. Des. 241 5245-50.
73. Lu Yong, 2009. Modelling of concrete structures subjected to shock and blast loading: An overview and some recent studies, Struct Engg Mechs, Vol. 32, No. 2 235-249.
74. Lubliner J., Oliver J., Oller S, Oñate E.,1989.A plastic-damage model for concrete, International Journal of Solids and Structures, Vol. 25, 299–329.
75. Luo, M., Wierzbicki, T., Mohr, D., 2011. Anisotropic ductile fracture of AA6260-T6 al-alloy extrusions, ASME International Mechanical Engineering Congress and Exposition, IMECE 2011 8 PP. 403 - 411
76. Lyman, E.S., Nuclear Energy and Human Health, Encyclopedia of Environmental Health, 2011, Pages 185-192,
77. Malhotra, H. L. (1956)," The effect of on the compressive strength of concrete", Magazine of concrete Research (London) 8, pp. 85-94.
78. Martin O., 2010. Comparison of different Constitutive Models for concrete in ABAQUS/ Explicit for Missile Impact Analysis. Safety of present Nuclear Reactor Unit (SPNR) EUR 24151 EN-2010.
79. Matsagar V.A., Jangid, R.S., 2002. Impact response of structures with sliding system, 2nd International Conf. on Structural Stability and Dynamics, Singapore, pp. 907-910,.
80. Matsagar V.A., Jangid, R.S., 2007 Response of seismically isolated shear beam to impact forces, 9th International Symposium on Plasticity and Impact Mechanics (IMPLAST 2007), Bochum, pp. 335-342.

81. Mishraa, B., Jenaa, P.K., Ramakrishnaa, B., Madhua, V., Bhat, T.B., Gupta, N.K., 2012. Effect of tempering temperature, plate thickness and presence of holes on ballistic impact behavior and ASB formation of a high strength steel. Int J Imp Engg 44, 17-28.
82. Muralidhara, S., Raghu Prasad, B.K., Karihaloo, B.L., Singh, R.K., 2011. Size-independent fracture energy in plain concrete beams using tri-linear model, Construction and Building Materials, 25(7), 3051-3058.
83. Muralidhara, S., Raghu Prasad, B.K., Singh, R.K., 2013, Size independent fracture energy from fracture energy release rate in plain concrete beams, Engg Fract Mechs 98 284–295.
84. Murthy, A. R., Karihaloo, B.L., Iyer, N. R., Raghu Prasad, B.K., 2013. Determination of size-independent specific fracture energy of concrete mixes by two methods, Cement and Concrete Research 50, 19–25.
85. Nabold C., Schildknecht P.O., 1977. Material nonlinear analysis of nuclear power plant structures subjected to an aircraft impact, applications using ADINA, Proc. of the ADINA Conference, Aug. 1977, Ed. by K.-J. Bathe, MIT, MA.
86. NEI, 2012, http://www.nei.org/Knowledge-Center/Nuclear-Statistics/World-Statistics, Nuclear Energy Institute, last cited 03/2014.
87. Nuclear Explosions: Weapons, Improvised Nuclear Devices. U.S. Department of Health and Human Services. 2008-02-16. Retrieved 2008-07-03.
88. Paul, D. K., Abbas, H., Godbole, P. N., Nayak, G. C., 1993. Aircraft crash upon a Containment Structure of a Nuclear Power Plant, SMiRT-12, J06/5.
89. Q.M. Li, S.R. Reid, H.M. Wen, A.R. Telford, Local impact effects of hard missiles on concrete targets. Int J of Imp Engg. 32 (2005) 224–284
90. Rabotnov Y.N., 1969. Creep problems in structural members, North-Holland, Amsterdam.
91. Rebora B, Zimmermann T, Wolf J P, 1976. Dynamic rupture analysis of reinforced concrete shells, Nucl. Eng. Des. 37, pp 269-97.
92. Rice, J.S. and Bahar, L.Y. 1978. Simplified derivation of the reaction-time history in aircraft impact on a nuclear power plant, Nucl. Eng. Des. 49, 263-268.
93. Riedel et al 2010. Local damage to Ultra High Performance Concrete structures caused by an impact of aircraft engine missiles Nucl. Eng. Des. 240, 2633–2642.

94. Riera, J.D., 1968. On the stress analysis of structures subjected to aircraft impact forces. Nucl. Eng. Des. 8, 415-26.
95. Riera, J.D., 1980. A critical reappraisal of nuclear power plant safety against accidental aircraft impact. Nucl. Eng. Des. 57, 193-206.
96. Riera, J.D., Zorn NF, Schueller GI, An approach to evaluate the design load time history for normal engine impact taking into account the crash-velocity distribution, Nucl. Eng. Des. 71 311-16. 1982
97. Röben, C., Gillie, M., Torero, J., 2010. Structural behaviour during a vertically travelling fire, Journal of Constructional Steel Research 66, 191-197.
98. Siddiqui, et al., 2003. Reliability analysis of nuclear containment without metallic liners against jet aircraft crash. Nucl. Eng. Design 224 11-21
99. Siefert A. and Henkel, F.O., 2011. Nonlinear analysis of commercial aircraft impact on a reactor building–comparison between integral and decoupled crash simulation. In: Transactions SMiRT 21, Div-III: Paper ID 144.
100. Starke, jr* E. A. and Staleyt,J. T. 1996. Application of modern aluminum alloys to Aircraft, prog. Aerospace sci. 32, pp. 131-172.
101. Sugano, T., Tsubota, H., Kasai, Y., Koshika, N., Orui, S., Riesemann, W.A.V., Bickel, D.C., Parks, M.B., 1993a. Full-scale aircraft impact test for evaluation of impact force, Nucl. Eng. Des. 140, 373-385.
102. Sugano, T., Tsubota, H., Kasai, Y., Koshika, N., Orui, S., Riesemann, W.A.V., Bickel, D.C., Parks, M.B., 1993b. Local damage to reinforced concrete structures caused byimpact of aircraft engine missiles, Part 1. Test program,method, results. Nuclear Engineering and Design 140, 387–405.
103. Sugano, T., Tsubota, H., Kasai, Y., Koshika, N., Orui, S., Riesemann, W.A.V., Bickel, D.C., Parks, M.B., 1993c. Local damage to reinforced concrete structures caused by impact of aircraft engine missiles, Part 2. Evaluation of test results. Nuclear Engineering and Design 140, 407–423.
104. Topcu, I.B. and Karakurt, C. (2008), "Properties of reinforced concrete steel bars exposd to high temperatures", Research letters in Materials Science, (Article ID 814137), pp. 1-4.

105. Trivedi, N., Singh, R.K., 2013. Prediction of impact induced failure modes in reinforced concrete slabs through nonlinear transient dynamic finite element simulation. Annals of Nuclear Energy 56, 109–121.
106. Tu Zhenguo, Lu Yong, 2009, Evaluation of typical concrete material models used in hydrocodes for high dynamic response simulations. Int J of Impact Engg. 36(1), 132–146.
107. Unluoglu, E., Topcu, I.B. and Yalaman, B. (2007)," Concrete cover effect on reinforced concrete bars exposed to high temperatures," Construction and Building Materials, Vol. 21, No. 6, pp. 1155-1160.
108. Usmani, A.S., Rotter, J.M., Lamont, S., Sanad, A.M., Gillie, M., 2001. Fundamental principles of structural behaviour under thermal effects, Fire Safety Journal 36 721–744.
109. Wall I.B., 1969. Probabilistic Assessment of Risk for Reactor Design and Siting, Trans. Am. Nucl. Soc., 12 169.
110. Wierzbicki, T., Bao, Y., Lee, Young-Woong, Bai, Y., 2005. Calibration and evaluation of seven fracture models, Int J of Mech Sci, 47(4–5), 719–743.
111. WNA, 2013, http://world-nuclear.org/info/Facts-and-Figures/, World Nuclear Assosiation, last cited 02/2013.
112. Wolf, J.P., Bucher, K.M., Skrikerud, P.E., 1978. Response of equipment to aircraft impact. Nucl. Eng. Des. 47, 169-193.
113. Xue, L., Wierzbicki, T., 2008. Ductile fracture initiation and propagation modeling using damage plasticity theory, Engineering Fracture Mechanics, 75(11) 2008, 3276–3293.
114. Yang, H.T.Y., Godfrey D.A., 1970. Structural Analysis of Aircraft Impact on a Nuclear Containment Vessel and Associated Structures, Nucl. Eng. Des. 11 295-307.
115. Z P Bazant and P A Pfeiffer (1987) Determination of fracture energy from size effect and brittleness number, ACI Material Journal, 84-M41, 463-80.
116. Zerna W., Schnellenbach G. and Stangenberg F., 1976. Optimized reinforcement of nuclear power plant structures for aircraft impact forces, Nucl. Eng. Des. 37 313-320.
117. Zhao C.F., Chen J.Y., Wang Y., Lu S.J., 2012. Damage Mechanism and Response of Reinforced Concrete Containment Structure under Internal Blast Loading, Theoretical and Applied Fracture Mechanics, 61 12–20.
118. Zorn, N.F., Schueller, G. I., 1986. On the Failure Probability of the Containment under Accidental Aircraft impact, Nuclear Engineering and Design, 91, 277-86.

LIST OF PUBLICATIONS

(a) Papers publication in International Journals

1 M.A. Iqbal, S. Rai, **M.R.Sadique**, P. Bhargava
Numerical simulation of aircraft crash on nuclear containment structure
Nuclear Engineering and Design, 243,2012, 321-335

2 **M.R. Sadique**, M.A. Iqbal, P.Bhargava ,
Nuclear containment structure subjected to commercial and fighter Aircraft crash
Nuclear Engineering and Design, 260,2013, 30-46

3 M.A Iqbal, **M.R. Sadique** P. Bhargava, N. M. Bhandari Damage Assessment of Nuclear Containment Against Aircraft Crash
Nuclear Engineering and Design, *Under Review*

4 Crash analysis of military aircraft on nuclear containment,
M.R. Sadique, M.A Iqbal, P. Bhargava
Structural Engineering and Mechanics, *Under Review*

(b) Papers publication in International Conferences

1 M.A. Iqbal, P. Bhargava, S. Rai, **M. R. Sadique**
Response of Nuclear Containment Structure to Aircraft Crash IMAC XXX Conference and Exposition on Structural dynamics,
Florida, Jan 30 - Feb 2, 2012.

2 **M, R. Sadique**, I. Ahmad, M. A. Iqbal, P. Bhargava
Analysis of Concrete Structures Against Aircraft Crash ICCABE 2012 : International Conference on Civil, Architectural and Building Engineering,
Paris, June 27-28, 2012.

3 **M.R. Sadique,** M.A. Iqbal, P. Bhargava
Evaluation of Nuclear Containment Building Against Crash of Boeing 767 Aircraft
International conference on Challenges in Disaster Mitigation and Management,
Roorkee,15 - 17 February 2013.

4 **M.R. Sadique,** M.A. Iqbal, P. Bhargava
Response of Nuclear Power Plants against Crash of Commercial Aircrafts
UKIERI Concrete Congress, Innovations in Concrete Construction,
Jalandhar, 5 - 8 March 2013.

5 **M.R. Sadique,** M.A. Iqbal, P. Bhargava Factors Affecting the Reaction Time Response of Aircraft, SMiRT-22,
San Francisco,18-24 August 2013.

6 **M.R. Sadique,** M.A. Iqbal, P. Bhargava
Assessment of Structural Strength of BWR Containment Vessel against Aircraft Impact
1st Saudi International Conference on Crisis and Disaster Management
Riyad,8-9 September, 2013.